EFFECTS OF PHENOLATE IONS ON CATIONIC MICELLAR GROWTH

KHALISANNI KHALID

FACULTY OF SCIENCE
UNIVERSITY OF MALAYA
KUALA LUMPUR

2017

EFFECTS OF PHENOLATE IONS ON CATIONIC MICELLAR GROWTH

KHALISANNI KHALID

THESIS SUBMITTED IN FULFILMENT OF THE REQUIREMENTS FOR THE DEGREE OF DOCTOR OF PHILOSOPHY

DEPARTMENT OF CHEMISTRY
FACULTY OF SCIENCE
UNIVERSITY OF MALAYA
KUALA LUMPUR

2017

UNIVERSITY OF MALAYA
ORIGINAL LITERARY WORK DECLARATION

Name of Candidate: KHALISANNI BIN KHALID [redacted]

Matric No: SHC 130030

Name of Degree: DOCTOR OF PHILOSOPHY (PhD)

Title of Project Paper/Research Report/Dissertation/Thesis ("this Work"):

EFFECTS OF PHENOLATE IONS ON CATIONIC MICELLAR GROWTH

Field of Study: PHYSICAL ORGANIC CHEMISTRY

I do solemnly and sincerely declare that:

(1) I am the sole author/writer of this Work;
(2) This Work is original;
(3) Any use of any work in which copyright exists was done by way of fair dealing and for permitted purposes and any excerpt or extract from, or reference to or reproduction of any copyright work has been disclosed expressly and sufficiently and the title of the Work and its authorship have been acknowledged in this Work;
(4) I do not have any actual knowledge nor do I ought reasonably to know that the making of this work constitutes an infringement of any copyright work;
(5) I hereby assign all and every rights in the copyright to this Work to the University of Malaya ("UM"), who henceforth shall be owner of the copyright in this Work and that any reproduction or use in any form or by any means whatsoever is prohibited without the written consent of UM having been first had and obtained;
(6) I am fully aware that if in the course of making this Work I have infringed any copyright whether intentionally or otherwise, I may be subject to legal action or any other action as may be determined by UM.

[redacted]

Date: 30/3/2017

Subscribed and solemnly declared before,

[redacted]

Witness's Signature Date: 30/3/2017

Name: PROFESSOR DR. MOHAMMAD NIYAZ KHAN

Designation: LECTURER, DEPARTMENT OF CHEMISTRY, FACULTY OF SCIENCE, UNIVERSITY OF MALAYA, 50603 KUALA LUMPUR, MALAYSIA

Witness's Signat [redacted] Date: 30/3/2017

Name: PROFESSOR DR. SHARIFUDDIN MD. ZATN

Designation: LECTURER, DEPARTMENT OF CHEMISTRY, FACULTY OF SCIENCE, UNIVERSITY OF MALAYA, 50603 KUALA LUMPUR, MALAYSIA

ABSTRACT

In this study, the effects of phenolate and its substituted ions on cationic micellar growth involving different alkyl substituted phenolate salts, MX and CTABr micelles in aqueous system were determined with the interest of investigating the relationship of ion-exchange constant to the micellar aggregation behavior by using rheological technique and microscopy analysis. By the use of psedophase micellar model, the value of micellar binding constant, (K_S) of PSa^- or PS^- was determined in the absence and presence of inert salt. The non-linear least squares calculated value of K_S^0 (K_S in the absence of inert salt) was found to be 6748 ± 435 M^{-1}. This is the first study which describes the use of PSa^- as a probe molecule to determine the values of R_X^{Br} or K_X^{Br} by using a semi-emperical spectrophotometric (SESp) method. The use of R_X^{Br} refers to the relative binding constant value where the K_{Br} value of spherical micelles is used as a reference (denominator value is the binding constant of spherical micelles) and K_X^{Br} is refers to ion exchange constant value of nanoparticle aggregates (spherical/ wormlike/ vesicle). Since bromide ion has been considered as a reference counterion to determine binding constant of other counterions, the catalytic effects of CTABr/NaX/H_2O (X=Br, Cl) nanoparticle catalysts on rate constant were investigated at [PS^-] = 0.2 mM, [NaOH] = 30 mM, [Pip] = 100 mM at different [CTABr]. The results revealed that the values of k_{obs} at [NaX]=0 and 6 mM ≤ $[CTABr]_T$ ≤ 10 mM were ten times smaller than the value of k_{obs} at $[CTABr]_T$=[NaX]=0 (X=Br, Cl). The investigation of the effects of substituted phenolate ions on cationic micellar growth were carried out for sodium phenolate (C_6H_5ONa), 2-ethyl sodium phenolate (2-ethyl C_6H_4ONa), 3-ethyl sodium phenolate (3-ethyl C_6H_4ONa), 4-ethyl sodium phenolate (4-ethyl C_6H_4ONa), 2-propyl sodium phenolate (2-propyl C_6H_4ONa), 4-propyl sodium phenolate (4-propyl C_6H_4ONa), 3-isopropyl sodium phenolate (3-isopropyl C_6H_4ONa) and

4-isopropyl sodium phenolate (4-isopropyl C_6H_4ONa) at [PS^-] = 0.2 mM, [NaOH] = 30 mM, [Pip] = 100 mM, [CTABr] = 6, 10 and 15 mM respectively at 35°C. The R_X^{Br} values of counterions were 6.3, 24.0, 24.4, 32.3, 66.3, 145.9, 60.8 and 66.6 for phenolate ions ($C_6H_5O^-$), 2-ethyl phenolate ions (2-etyl $C_6H_4O^-$), 3-ethyl phenolate ions (3-ethyl $C_6H_4O^-$), 4-ethyl phenolate ions (4-ethyl $C_6H_4O^-$), 2-propyl phenolate ions (2-propyl $C_6H_4O^-$), 4-propyl phenolate ions (4-propyl $C_6H_4O^-$), 3-isopropyl phenolate ions (3-isopropyl $C_6H_4O^-$) and 4-isopropyl phenolate ions (4-isopropyl $C_6H_4O^-$) respectively. By means of the correlation between R_X^{Br} values and rheological analysis with the evident of microscopic studies at [CTABr] = 15 mM, the microstructures of micellar self assembly of flexible nanoparticles were found as follows for $C_6H_5O^-$ = spherical, 2-ethyl $C_6H_4O^-$ = spherical, 3-ethyl $C_6H_4O^-$ = spherical, 4-ethyl $C_6H_4O^-$ = wormlike, 2-propyl $C_6H_4O^-$ = vesicle, 4-propyl $C_6H_4O^-$ = rodlike, 3-isopropyl $C_6H_4O^-$ = vesicle and 4-isopropyl $C_6H_4O^-$ = wormlike. The findings revealed the increase of R_X^{Br} values lead to the changes of spherical micelles to wormlike, rodlike or vesicles micelles.

ABSTRAK

Dalam kajian ini, kesan ion fenolat dan terbitannya ke atas pertumbuhan misel kation melibatkan penggantian garam alkil phenol, MX yang berbeza dan misel CTABr ke dalam sistem akueus ditentukan oleh pendekatan semi empirikal dengan kajian khusus mengenai hubungan pemalar penukaran ion dan ciri-ciri pengagregatan misel melalui kaedah analisis mikroskopi and reologi. Kepentingan mengkaji pemalar pengikat penukaran ion, R_X^{Br} atau K_X^{Br} bagi ion fenolat dan terbitannya dimulakan dengan penentuan ciri-ciri fizik-kimia penentu, PSa^- atau PS^-. Dengan menggunakan pendekatan semi emperikal spektrofotometri (SESp), nilai pemalar pengikat misel, (K_S atau K_S^0) ditentukan dalam ketiadaan garam lengai. Penggunaan terma R_X^{Br} adalah merujuk kepada nilai pemalar pengikat ion relatif dimana nilai K_{Br} misel sfera adalah asas rujukan (nilai penyebut adalah pemalar pengikat bagi misel sfera) dan K_X^{Br} adalah merujuk kepada nilai pemalar penukaran ion agregat partikal nano (sfera/ cecacing/ vesikel) sebagai rujukan (nilai penyebut adalah pemalar pengikat bagi agregat). Melalui pengiraan kuasa dua tidak linear, nilai K_S^0 adalah dianggarkan 6748 ± 435 M^{-1}. Kajian pertama yang menyifatkan kepenggunaan PSa^- sebagai penentu dan nilai min R_X^{Br} atau K_X^{Br} didapati 4.8 ± 0.3, setanding dengan nilai yang dilaporkan diperoleh dengan menggunakan kaedah fizikal yang berbeza dan semi emperikal kinetik (SEK). Oleh kerana ion bromida telah dianggap sebagai pemalar penukaran ion rujukan bagi menentukan pemalar pengikat ion yang lain, kesan pemangkin CTABr / NaX / H_2O (X = Br, Cl) nanopartikel pada kadar malar telah diuji pada kepekatan ion fenil salisilat, [PS-] = 0.2 mM, [NaOH] = 30 mM, [Pip] = 100 mM dengan [CTABr] yang berbeza. Hasil kajian menunjukkan nilai-nilai k_{obs} di [NaX] = 0 dan 6 mM ≤ $[CTABr]_T$ ≤10 mM adalah sepuluh kali ganda lebih kecil daripada nilai k_{obs} di $[CTABr]_T$ = [NaX] = 0 (X = Br, Cl). Kajian kesan ion fenolat dan terbitannya ke atas

pertumbuhan misel kation telah dijalankan bagi natrium fenolat (C_6H_5ONa), 2-etil natrium fenolat (2-etil C_6H_4ONa), 3-etil natrium fenolat (3-etil C_6H_4ONa), 4-etil natrium fenolat (4-etil C_6H_4ONa), 2-propil natrium fenolat (2-propil C_6H_4ONa), 4-propil natrium fenolat (4-propil C_6H_4ONa), 3-isopropil natrium fenolat (3-isopropil C_6H_4ONa) dan 4-isopropil natrium fenolat (4-isopropil C_6H_4ONa) pada [PS^-] = 0.2 mM, [NaOH] = 30 mM, [Pip] = 100 mM, [CTABr] = 6, 10 dan 15 mM pada 35°C. Nilai R_X^{Br} bagi ion-ion berlawanan adalah 6.3, 24.0, 24.4, 32.3, 66.3, 145.9, 60.8 dan 66.6 bagi ion fenolat ($C_6H_5O^-$), ion 2-etil fenolat (2-etil $C_6H_4O^-$), ion 3-etil fenolat (3-etil $C_6H_4O^-$), ion 4-etil fenolat (4-etil $C_6H_4O^-$), ion 2-propil fenolat (2-propil $C_6H_4O^-$), ion 4-propil fenolat (4-propil $C_6H_4O^-$), ion 3-isopropil fenolat (3-isopropil $C_6H_4O^-$) dan ion 4-isopropil fenolat (4-isopropil $C_6H_4O^-$). Melalui perkaitan antara nilai-nilai R_X^{Br} dan analisis reologi serta kajian mikroskop pada [CTABr] = 15 mM, mikrostruktur misel adalah didapati seperti berikut; $C_6H_5O^-$ = sfera, 2-etil $C_6H_4O^-$ = sfera, 3-etil $C_6H_4O^-$ = sfera, 4-etil $C_6H_4O^-$ = cecacing, 2-propil $C_6H_4O^-$ = vesikel, 4-propil C_6H_4O- = rod, 3-isopropil C_6H_4O- = vesikel dan 4-isopropil $C_6H_4O^-$ = cecacing. Hasil kajian menunjukkan peningkatan nilai R_X^{Br} membawa kepada perubahan misel sfera kepada struktur lain iaitu cecacing, rod dan vesikel.

ACKNOWLEDGEMENTS

The greatest thanks to Allah The Almighty, for giving me strength to overcome the unprecedented difficulties throughout the completion of my PhD thesis. He is my greatest companion whenever I faced the obstacles. I realized that the sense of "He always believed in me when everybody doesn't" has enormously increased my self-esteem to finish my study.

I would like to express my sincere gratitude to all people who in different ways have contributed to this thesis. I am grateful to you all, and especially:

Prof. Dr. Muhammad Niyaz Khan for guiding me in the area of kinetic and mechanism of micellar catalysis. He has devoting his utmost time with me and his thoughtful ideas will always be remembered. I am also obliged to Prof. Dr. Sharifuddin Md. Zain who always be there and contribute to the knowledge in the area of computational chemistry. I would like to thanks Prof. Dr. Zanariah Abdullah (Dean, Faculty of Science, UM), Prof. Dr. Ismail Yusoff (Deputy Dean, Faculty of Science, UM) and committee members of my viva examination council for giving me positives criticism on my research project.

My parents, Mr. Khalid and Madam Rohani, who giving me the courage when times were rough, telling me to work less when I worked too much and believing me. My sister, Assoc. Prof. Dr. Khalizani Khalid (Abu Dhabi University) and her family for the moral support during the study.

Special thanks to Datuk Dr. Sharif Haron, Director General of Malaysian Agricultural Research and Development Institute (MARDI) for giving me the opportunity to pursue my study under the Bright Spark program. Because of your support, faith and believes, it drives me to be able to graduate on time. Also thanks to MARDI's team,

especially to Hj. Mohd Ghazali Omar, Mr. Sanusi, Mr. Muhammad Najib Othman Ghani, Mdm Faridatul Akmar Mohammed Nuri, Mdm. Ramlah Md. Isa, Mdm Nor Suhayati, Mdm. Zainab, Mr. Badrul Hisyam, Laboratory Management Program staff, Laboratory and Technical Service Centre staff, G77s, MARDI Kuala Linggi staff and all MARDIs who had devoted their trust on me.

Dr. Zaira Zaman Chowdhury who contributes her time and idea for my study; Mr. Muhammad Azri Mohd Noh and Miss Rosalind Kim Pei Theng for being the best lab mate ever; Mr Vicit Rizal Eh Suk for helping the microscopic analysis; Dr. Ruzaina Ishak from University of Lincoln, UK – Management and Science University (MSU) for her moral supports; my mentee Mr. Mohammad Hafiz Hamzah (Administration and Diplomatic Officer- INTAN); Mdm Zura (rheology); Mr. Hamzah (TEM), Mr. Mohd Saimi Abdul Hamid (Postgraduate Section, Faculty of Science) and to all my laboratory members (Ibrahim Isah Fagge, Norazizah Abd. Razak, Wan Hamdah, Idayu).

I'm also thanks to Bright Spark Scholarship for sponsoring this study, especially Bright Spark Scholarship Unit (Mdm Mariati Shakor, Mdm Mazni Sidek, Mdm. Norazwani, Mdm. Nurhasanah, Miss Syairah) and University of Malaya for their kindness.

Last but not least, to all Department of Chemistry, Faculty of Science, University of Malaya staff and students for their commitment in the study.

"*I'm in debt to all of you*"

Thank you…….

KHALISANNI KHALID

850617-08-6061

SHC 130030

TABLE OF CONTENTS

Page

Page

Page

Page

Page

Page

LIST OF FIGURES

LIST OF SCHEMES

LIST OF TABLES

LIST OF SYMBOLS AND ABBREVIATIONS

$[\ ]_T$	total concentration
Å	angstrom
α	degree of counterion dissociation
β	the degree of counterion binding
δ_{app}	apparent molar absorptivity
κ	conductivity
µm	micro meter
η	shear viscosity
$\dot{\gamma}$	shear rate
η_0	zero-shear viscosity
2-ethyl $C_6H_4O^-$	2-ethyl phenolate ion
2-$EtC_6H_4O^-$	2-ethyl phenolate ion
2-ethyl C_6H_4ONa	2-ethyl sodium phenolate
2-EtC_6H_4ONa	2-ethyl sodium phenolate
3-ethyl $C_6H_4O^-$	3-ethyl phenolate ion
3-$EtC_6H_4O^-$	3-ethyl phenolate ion
3-ethyl C_6H_4ONa	3-ethyl sodium phenolate
3-EtC_6H_4ONa	3-ethyl sodium phenolate
4-ethyl $C_6H_4O^-$	4-ethyl phenolate ion
4-$EtC_6H_4O^-$	4-ethyl phenolate ion
4-ethyl C_6H_4ONa	4-ethyl sodium phenolate
4-EtC_6H_4ONa	4-ethyl sodium phenolate
2-propyl $C_6H_4O^-$	2-propyl phenolate ion

2-Prop$C_6H_4O^-$	2-propyl phenolate ion
2- propyl C_6H_4ONa	2-propyl sodium phenolate
2-PropC_6H_4ONa	2-propyl sodium phenolate
4- propyl $C_6H_4O^-$	4-propyl phenolate ion
4-Prop$C_6H_4O^-$	4-propyl phenolate ion
4- propyl C_6H_4ONa	4-propyl sodium phenolate
4-PropC_6H_4ONa	4-propyl sodium phenolate
3-isopropyl $C_6H_4O^-$	3-isopropyl phenolate ion
3-Isoprop$C_6H_4O^-$	3-isopropyl phenolate ion
3-isopropyl C_6H_4ONa	3-isopropyl sodium phenolate
3-IsopropC_6H_4ONa	3-isopropyl sodium phenolate
4-isopropyl $C_6H_4O^-$	4-isopropyl phenolate ion
4-Isoprop$C_6H_4O^-$	4-isopropyl phenolate ion
4-isopropyl C_6H_4ONa	4-isopropyl sodium phenolate
4-IsopropC_6H_4ONa	4-isopropyl sodium phenolate
A_{calc}	calculated absorbance
A_{obs}	observed absorbance
Bz-	$C_6H_4CO_2^-$
BzNa	$C_6H_4CO_2Na$
$C_6H_5O^-$	phenolate ion
C_6H_5ONa	sodium phenolate
$C_8 – C_{20}$	unsaturated hydrocarbon chains
$C_{16}E_{12}$	hexadecyldodecaoxyethylene glycol
cmc	critical micelle concentration/ cmc_1

cmc_2	second critical micelle concentration
CN	cationic nanoparticle
CPC	cetylpyridinium chloride
CTABr	cetyltrimethylammonium bromide
D_n	detergent/ micelle
DLS	dynamic light scattering
E_a^F	flow activation energy
Eq.	equation
ESR	electron spin resonance
FN	flexible nanoparticle
GUV	giant unilamellar vesicle
ISE	ion selective electrode
K	Kelvin
k_{calc}	calculated rate constant
k_M	rate constant for the reaction in micellar phase
K_M	equilibrium constant for micelle formation
K_N	micellar binding constant for piperidine
k_{obs}	observed pseudo-first-order rate constant
K_S	cationic micellar binding constant of PS^- in presence of salts (Br^-)
K_S^0	cationic micellar binding constants of PS^- in absence of salts (Br^-)
k_W	rate constant for the reaction in aqueous phase
K_X^Y	ion-exchange constant for ion-exchange process X^-/Y^-

$K^{X/S}$	binding constants for ion-exchange X^- and ionized phenyl salicylate
M	Molarity
MLV	multi lamellar vesicle
MEUF	Micellar-enhanced ultra filtration
mM	mili molar
mol dm^{-3}	molar
MX	inert organic salt
N_a	Avogadro's number
NaSal	sodium salicylate
nm	nanometer
NMR	nuclear magnetic resonance
PEK	Pre-equilibrium kinetic
PIE	Pseudophase Ion Exchange
Pip	Piperidine
PM	Pseudophase Micellar
PS^-/ PSa^-	ionized phenyl salicylate
$R_4N^+X^-$	quarternary ammonium halides
RE	residual error
R_M	reactant in the micellar pseudophase

R_X^{Br}	represents $K_{X/S}^n/K_{Br/S}^n$ where $K_{X/S}^n$ and $K_{Br/S}^n$ is the normalized kinetic parameters for counterion X^- and reference counterion Br^-, respectively or relative counterions binding constant
s	second
S	substrate/ solubilizate
S$^-$	*N*-(2-Methoxyphenyl)phthalamate ion
SDS	Sodium dodecyl sulfate
SEK	semi-empirical kinetic
SESp	semi-empirical spectrophotometric
SM	spherical/ globular micelles
surf	surfactant
S_W	substrate in the aqueous pseudophase
SWM	short wormlike micelles
TEM	transmission electron microscopy
TTABr	tetradecyltrimethylammonium bromide
ULV	unilamellar vesicle
UV	ultra-violet
V_M	micellar volume
V_S	vesicles
vs.	versus
WM	wormlike micelles
XRD	X-ray diffraction

CHAPTER 1

GENERAL INTRODUCTION

1.1 What are Micelles?

A micelle is an aggregate (or supramolecular assembly) of surfactant molecules either cationic, anionic, zwitterionic or nonionic, dispersed in a liquid colloid (Loppinet & Monteux, 2016). A typical micelle in aqueous solution forms an aggregate structure with the hydrophilic "head" regions in contact with surrounding aqueous, parallel with the hydrophobic single-tail regions in the micelle centre. This phase is caused by the packing behavior of single-tail lipids in a bilayer which is hydrophobic (Papaioannou et al., 2016; Shah et al., 2016; Ferreira et al., 2016; Lebarron & London, 2016; Schindler et al.,2016).

The molecule must have a strong polar "head" and a non-polar hydrocarbon chain "tail". When this type of molecule is added to water, the non-polar tails of the molecules clump into the center of a ball like structure called a micelle, because they are hydrophobic or "water hating". The polar head of the molecule presents itself for interaction with the water molecules on the outside of the micelle. Thus, the micelle is formed when a variety of molecules are added to water (Chen et al., 2016; Jia et al., 2016; Patil et al., 2016). The molecule may be a fatty acid, a salt of a fatty acid (soap), phospholipids, or other similar molecules.

Micelles are approximately spherical or globular in shape (Giorgio et al., 2016; Pottage et al., 2016; Upadhyay et al., 2016; Yang et al., 2016; Zaheer et al., 2016; Jiao et al., 2016). Other structures, including shapes such as wormlike, rodlike and vesicle are also possible (Kusano et al., 2016; Xia et al., 2002; Suárez-Suárez et al., 2016; Tian et al., 2016;

Zhang et al., 2016). The structures of a micelle are a function of the molecular geometry of its surfactant molecules and solution conditions such as surfactant concentration and ionic strength. The process of micellar formation is known as micellisation.

1.2 Why is This Study Carried Out?

Micellar structural transition from spherical to other micellar aggregates formation occurs with either increase in the concentration of micelle-forming surfactants, [surf], in the absence or the presence of a constant concentration of an additive, [additive], or increase in [additive] at a constant value of [surf]. The effect of change of micelle shape (i.e., from spherical to cylindrical and lamellar micelles) and the corresponding change in kinetics must be carefully studied (Arranja et al., 2016; Cognigni et al., 2016; Jan et al., 2015). Most importantly, the kinetics of these complex nonspherical micellar systems must be systematically investigated, as many products are supplied in concentrated form in household and industrial applications to subsequently be diluted by water for their applications (Olkowska et al., 2012; Tyagi & Tyagi 2014; Zhao et al., 2014).

1.3 Objectives of the Study

In search to investigate the effects of phenolate and its substituted ions on the cationic micellar growth, the aims of present studies are:

i. To determine and verify the micellar binding constant, K_S value of the new probe PS^- for the study
ii. To test the ability of phenolate ions and substituted phenolate ions (X^-) to expel another counterion (PS^-) from a cationic micellar to the aqueous pseudophase

iii. To determine the value counter ion exchange constants R_X^{Br} for MX= 2-,3- and 4-alkyl substituted phenols at different values of $[CTABr]_T$ by the use the kinetic technique

iv. To determine the rheological measurements on aqueous solution containing a constant value of [CTABr] and varying values of [MX]

v. To determine the micellar structural transition with either increase in the concentration of micelle-forming surfactants, [surf], in the absence or the presence of a constant concentration of an additive, [additive], or increase in [additive] at a constant value of [surf]

vi. To determine the correlation study between the relationship of R_X^{Br} values and micellar self-assembly structure

vii. To determine the apparent conditions of the FN through turbidity test, particle size analysis and real pictures

viii. To determine microscopic evidence of proposed micellar structure with respect to the relationship of R_X^{Br} values and micellar self-assembly structure

ix. To determine the mechanism of counterion binding to micelles and concentration of counterion [MX] on micellar growth

1.4 Research Highlights

In this thesis, the establishment of a new probe, PS^- for the determination of counterion binding constant, R_X^{Br} or K_X^{Br} is discussed. It was found that the values of R_X^{Br} or K_X^{Br} are independent of the physicochemical characteristics of probe molecules. The mean value of R_X^{Br} or K_X^{Br} is found to be comparable with the reported values obtained by the use of different probe and SEK method as well as different physical methods.

The study is also successfully proven the relationship between R_X^{Br} values and micellar aggregations behavior. The increase of R_X^{Br} values leads to the microstructural changes from spherical micelles to rodlike, wormlike and vesicle micelles. The correlations are supported by the rheological data and microscopic evidences.

1.5 Potential Applications to the Industries

Micellar-enhanced ultra filtration (MEUF) process is a successful concept adapted from these studies (Azizi & Mousavi 2016; Chang et al., 2015; Nguyen et al., 2015; Rafique et al., 2016). The principle of MEUF dictated the micelles are too large to pass through the membranes and retain highly concentrated surfactant micelles containing soluble phenols and its derivatives. In drug delivery system, the micelles have been used as skin permeation enhancers for transdermal drug delivery coordination. (Allijn et al., 2016; Dai et al., 2016; Goswami et al., 2016; Stefani et al., 2016; Zeng & Liu 2016). The colloidal dispersion in essential oil process may adapt the present study to determine the kinetics and mechanism of the separation between solvent and essential oil phase.

1.6 Plan of Thesis

The first chapter contains the general introduction of the studies, problem statements, research objectives, highlights and potential applications to the industries. Chapter 2 reviews the previous literatures and works done related to the present studies. Chapter 3 discussed on the determination of relative counterion binding constant (R_X^{Br} or K_X^{Br}) to cationic micelles by the use of various methods. This chapter described and discussed the uses PSa^- as a probe to determine R_X^{Br} or K_X^{Br} by means of other techniques. The value of R_X^{Br} or K_X^{Br} is found to be comparable with the reported values obtained by the use of different probe and semi empirical kinetic (SEK) method as well as different physical

methods. The application of semi empirical methods in the calculation of the values of R_X^{Br} or K_X^{Br}, involves an inherent assumption that the values of R_X^{Br} or K_X^{Br} should be independent of the physicochemical characteristics of probe molecules.

The bromide ion has been considered as a reference counter ion that is used to determine the aqueous relative CTABr micellar/nanoparticle binding constant of other counter ions (CTABr=cetyltrimethylammonium bromide). Because of this reason, Chapter 4 discussed the catalytic effects of CTABr/NaX/H_2O (X=Br, Cl) nanoparticle catalysts on rate constant, k_{obs} for the nucleophilic substitution reaction of piperidine (Pip) with PSa^-. The results and their plausible mechanistic explanations are also described in this chapter. In Chapter 5, the effect of apparent catalysis at different concentration of FN-piperidine with phenyl salicylate ion for substituted sodium phenolate and its derivatives [MX] $\neq$ 0 at 35°C is discussed. The observed data (k_{obs} *vs*. [MX]) have been discussed quantitatively based on pseudophase micellar (PM) model. Such data treatment gives relative micellar binding constants of counterion X^- and Br^-(R_X^{Br}) with FN.

Chapter 6 discussed the effects of [MX] on the rheological behavior of FN. The k_{obs} have been coherence in terms of the rheological data. The large catalytic effect of FN on the rheological evidence of micellar structure correlate to the relative counterion binding constant, R_X^{Br} are also described. The turbidity, particles size and real picture of FN are rationalized in Chapter 7. Due to the prospective evidences of the correlations of R_X^{Br} to the micellar self-assembly structures in the above-mentioned analysis, Chapter 8 discussed the microscopic evidence of miceller structure for FN-catalyzed piperidinolysis of phenyl salicylate ions, PS^-.

In Chapter 9, the conclusion and recommendations is summarized in details. It is noteworthy that semi empirical technique gives a presumption for the aggregation behaviors of FN. However, for the validation of data obtained, it is advisable for these

techniques preeminently followed by different experimental analysis. It is also a relative option for robust and low cost method to estimate the presence of identical micelles representing the entire system without repudiating the capabilities and accuracies of the microscopic technique (cryo-TEM) since the respective instruments is barely available in the country.

CHAPTER 2

LITERATURE REVIEW

2.1 Surfactants

A surfactant is briefly defined as a material that can greatly reduce the surface tension of water when used in very low concentrations. Surfactants are usually organic compounds and abundant in nature (Song et al., 2014; Mondal et al., 2015). Surfactants that are owned by nature are commonly termed as polar lipids which can be found in all living organisms (Dowhan et al., 2000; Doehlert et al., 2010). Other than that, oleochemicals and petroleum industry also contribute as inexpensive sources for synthetic surfactants (Foley et al., 2012). Since the discovery of the "natural" alkali soaps as surfactants to be used in a wide variety of cleaning process and personal hygiene more than 2000 years ago (Willcox, 2000), the utilization of surfactant has advanced and broaden to almost all aspects of science and industry (Holmberg et al., 2002; Karsa, 2006). The increased needs of surfactant as product and process additives with the demands from the economy worldwide has been a major factor for numerous applications of surfactants in science and industry. The applications of surfactant encompass:

a) Households products (detergents and cleaners)
b) Cosmetics and personal care products (soaps, wash mouth)
c) Textiles and fibers (dyes)
d) Leather and furs
e) Paints, lacquers, and other coating products
f) Paper and cellulose products
g) Mining and ore flotation

h) Plant protection and pest control

i) Foods and food packaging

j) The chemical industry

k) Oilfield chemicals and petroleum production

l) Plastics and composite materials

m) Pharmaceuticals

n) Medicine and biochemical research

The applicability of surfactant roles in numerous applications either in science or industry benefited the humanities because of the dualistic properties in their molecular structure which possessed both hydrophilic (lyophilic or solvent-loving) and hydrophobic (lyophobic or solvent-hating) characteristics. The dualistic behavior exhibited by the surfactants that it is sometimes also called as amphiphilic molecules which comes from the *Greek* word *amphi*, meaning both (Myers, 2006; Holmberg et al., 2002; Karsa, 2006). These interesting features of surfactants are depicted in Figure 2.1 where the headgroup of a surfactant is hydrophilic in nature while the tail of a surfactant is hydrophobic in nature.

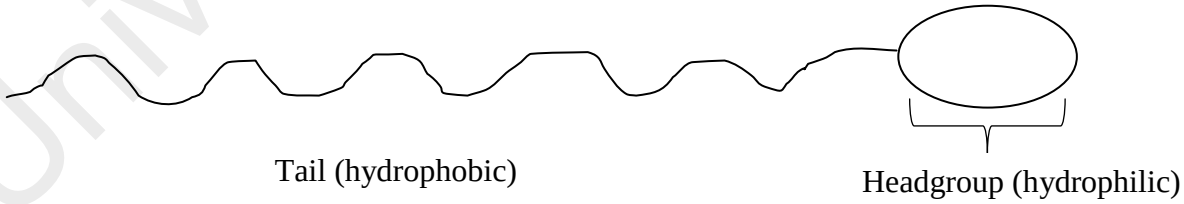

Figure 2.1 Illustration of a surfactant molecule.

2.2 Types of Surfactant

Surfactants were classified based on the physical properties of the polar headgroup which can be divided into four basic classes (Cullum, 1994):

i. Anionic – the headgroup is a negatively charged group. Examples of polar headgroup in anionic surfactants are carboxyl group, sulfonate, sulfate or phosphate.

ii. Cationic – the polar headgroup holds a positive charge. Almost all cationic surfactants headgroup bears nitrogen atom carrying positive charge. Common headgroups of cationic surfactants are amine (in protonated state) and quarternary ammonium halides ($R_4N^+X^-$).

iii. Nonionic – the hydrophilic headgroup contains no charge which could be either polyether or a polyhydroxyl unit.

iv. Zwitterionic – the smallest surfactant class where the hydrophilic part of the surfactant possessed both negative and positive signs. The sources for negative charges are commonly carboxylate though it may vary whereas ammonium is the main source for positive charge.

Even though hydrophilic headgroup determined the surfactant classes, however, the hydrophobic group could provide a wide variety of surfactants. The hydrophobic part of a surfactant may be a long linear or branched saturated and/or unsaturated hydrocarbon chain which can be ranged from C_8 – C_{20} (Clint, 2012; Khan, 2006). Furthermore, the hydrophobic tail may also consist of fluoroalkyl groups (Park et al., 2007), alkylbenzenes (Abdel-Raouf et al., 2011), alkylnapthalenes (Sadegh et al., 2015) and polydimethylsiloxanes (Sigoillot & Nguyen, 1992). Other than that, the apolar group of surfactant might as well come from the derivatives of natural and synthetic polymers (Foley

et al., 2012; Myers, 2006). Looking at the uniqueness and varieties of surfactants, it is not surprising that surfactants were found in almost all aspects of science and industry. On top of that, it is remarkable that it has breakthrough into the developing field of nanoscience and nanotechnology (Deda & Araki, 2015; Moghassemi & Hadjizadeh, 2014; Otzen, 2015)

2.3 Micelles

The aggregation of surfactants to form micelles in water are driven by the expulsion of hydrocarbon tails of the surfactants from the aqueous phase and into the interior non-polar region of the micelles where the hydrophobic interactions are maximum to minimize contacts from the water, and the electrostatic repulsion (as the case for ionic surfactant) between the headgroups as they move into close proximity at the micelle's surface (Evans, 1988; Patist et al., 2001). Typically, micelles are comprised of clusters with an average 30-200 monomeric units of whereas the size of a micelle can vary from 5 to 60 nm depending on the type of headgroups and length of the alkyl chains (Schramm et al., 2003; Kellermann et al., 2004). Micelles are usually spherical but it may also exist in the form of tubular or ellipsoidal micelles (Langevin, 1992; Iyer & Blankschtein, 2012). In micelles, the hydrophilic and hydrophobic regions are separated and the existence of interface occurred from the interactions between the polar headgroups and surrounding water. Furthermore, the surface of micelles are highly flexible and porous (Magid & Li, 2000; Menger & Bonicamp, 1981). These dynamic properties of micelles make them a suitable model for biological membrane system which is important in understanding related applications such as micellar decomposition and drug deliveries (Aoun et al., 2015).

The uniqueness of micelles has become the subject of interest in researchers to study the dynamics of formation and structure of the micelles (Rosen, 2004, Khan, 2006;

Vincent, 2014). Up to date, reports on the structures of micelles have been massively published using various instruments (Holmberg et al., 2002; Khan, 2006). Yet, the exact interpretation on the true nature of the micelles aggregation which can be universally accepted has never been concluded (Myers, 2006). The search on the complexity of micelles formation and its structure is still being continued even today. The structure of micelles have been studied using numerous experimental techniques such as nuclear magnetic resonance (NMR) (Bjima et al., 1998; Yang et al., 2008), X-ray diffraction (XRD)(Anderson et al., 1998; Briganti et al.,1996), dynamic light scattering (DLS) (Kuperkar et al., 2011), fluorescence spectroscopy (Techen et al., 2012), electron spin resonance (ESR)(Wasserman et al., 2010; Li et al., 2011), neutron scattering (Gibhardt et al., 2014; Sharma et al., 2010) and others (Helgeson et al., 2010; Lipfert et al., 2007).

2.4 Critical Micelle Concentration (CMC) and its Determination

The *critical micelle concentration* (cmc) represents specific total concentration of surfactant at which the surfactant monomers start to assemble among themselves and forming aggregates under specific conditions. The value of cmc plays a vital role in investigating the surfactant physicochemical behaviors in aqueous solutions since the cmc value indicates the measure of stability of surfactant in its micellar form. In addition, the values of cmc are important in determining various characteristic properties of micelles including the binding affinity of solubilizates (Tsujii, 1998). Besides that, the value of cmc signifies a point at which phase transition of surfactant occurs i.e. spherical-to-rodlike (Vermathen et al., 2002; Carpena et al., 2002). In view of this context, it is no doubt that the cmc is one of very important parameter in the studies of micellization.

Until the present day, numerous physicochemical methods have been used to determine the value of cmc and these methods include conductivity (Wu et al., 2014), surface tension (Mata et al., 2004) and fluorescence techniques (Dominguez et al., 1997). It can be seen that these methods are utilized from the fact that the nature of micellar solutions exhibit the physicochemical behavior that are unique and different from those without micelle of the same surfactant (Khan, 2006).

The determination of precise and accurate value of cmc is important in quantitative analysis of studies on kinetics of nanoparticles (micellar) catalyzed reactions. Usual physical methods have been used to determine the cmc values in most of the studies on kinetics of nanoparticles-catalyzed reactions. However, it is practically difficult to obtain values of cmc under reaction kinetic conditions determined by the various physicochemical methods.

A kinetic graphical method has been developed by Broxton (Broxton et al., 1988) to determine the value of cmc under reaction kinetic conditions. This method is performed by plotting a graph of rate constants (k_{obs}) vs. total concentration of surfactant ($[Surf]_T$) within the $[Surf]_T$ range. The value of cmc can be determined from the intersection of two linear plots of k_{obs} vs. $[Surf]_T$. On the other hand, if the inflection point (cmc value) in the plot is not very sharp, then this method does not produce a very reliable cmc values. In this case, a kinetic iterative method (Khan & Arifin, 1996) can be used to provide a more reliable cmc value. The details on the kinetic iterative method have been explained elsewhere (Khan, 2006). Both kinetic graphical method and kinetic iterative method have been used to determine the values of cmc in the studies of kinetics and mechanism of piperidinolysis of ionized phenyl salicylate in the presence of cationic micelles and the cmc values obtained from both techniques are appreciably almost the same under different reaction conditions.

Therefore, these methods have been used to determine the value of cmc in the present study.

2.4.1 Factors Affecting CMC

It is clear that the value of cmc could provide valuable information regarding the physicochemical characteristic of aqueous solution containing micelles. Hence, it is important to understand the factors affecting the value of cmc. The value of cmc depends on the chemical structure of the micelle-forming surfactants. Generally, non-ionic surfactants will have a much lower cmc value than that of ionic surfactants whereas anionic surfactants have a slightly lower cmc value than cationic surfactants (Holmberg et al., 2002). For example, the cmc of cationic surfactant, hexadecyltrimethylammonium bromide (CTABr) is ~1.0 mM (Bahri et al., 2006; Javadian et al., 2013) whereas the cmc of non-ionic surfactant with the same alkyl chain length, hexadecyldodecaoxyethylene glycol ($C_{16}E_{12}$) is equal to 0.0023 mM (Holmberg et al., 2002). Moreover, increasing the alkyl chain length of the surfactant will decrease the value of cmc (Lin et al., 1974).

Effects of four different amine additives on cmc of CTABr and SDS in buffered aqueous solutions show a decrease in cmc with increase of amine concentrations. The decreasing effect on cmc of an amine is almost the same for CTABr and SDS surfactant (Broxton et al., 1994).

2.5 Micellar Growth

Micellization is a unique and spontaneous process involving the self-assembly of surfactant monomer to form micelles that occur in the conditions above the cmc and Kraft temperature (Holmberg et al., 2002; Khan, 2006. Kraft temperature or Kraft point is

defined as the lowest temperature for the micellization to start to occur (Schramm et al., 2003)

From the general perspective, the micelle formed above the cmc is in spherical form. It is widely known that increasing the concentration of micelle-forming surfactants will increase the size of the micelle. Thus, if the concentrations of surfactant were further increased until, above a second critical concentration, known as the *second critical micelle concentration* (cmc_2) the micelles will start to grow in size and form rodlike, cylindrical or even vesicles aggregates (Myers, 2006; Khan, 2006). **Figure 2.2** illustrates the growth of micelles with increase in surfactant concentrations. The second cmc (cmc_2) were also referred as the sphere-to-rodlike transition.

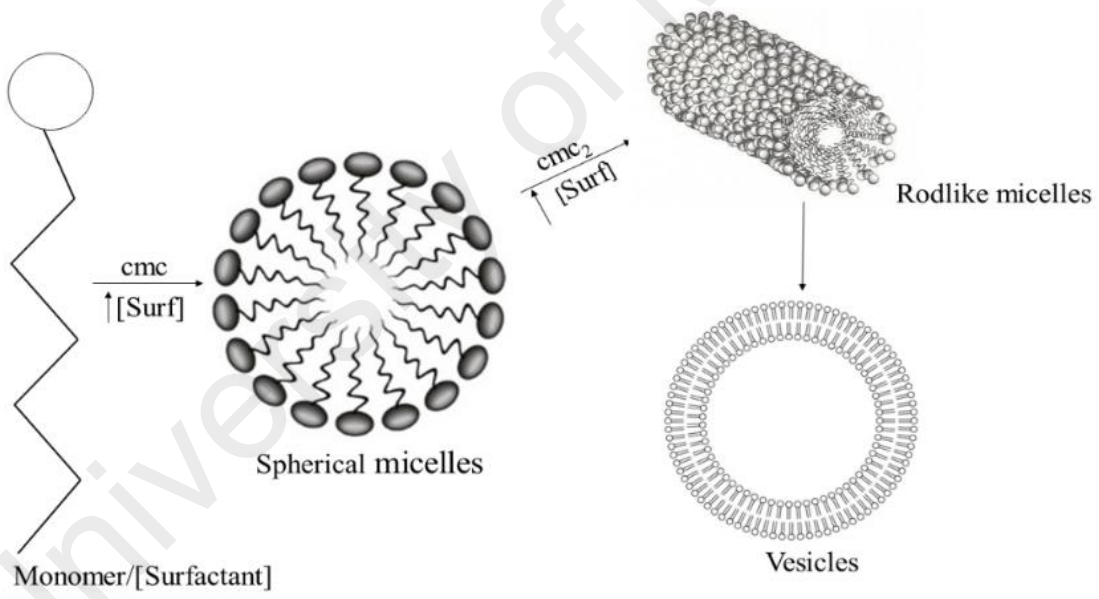

Figure 2.2 Micellar growth with increase in surfactant concentrations.

Bellare and co-workers (Khan, 2006) reported that the spherical micelles could grow with the increase of surfactant concentration to form aggregates such as rodlike micelles through cryo-TEM technique. However, the growth of such micellar solutions can be induced by the addition of some specific counterions in a dilute aqueous solution of surfactant (Rao et

al., 1987; Rehage & Hoffmann, 1991). Iyer and co-workers (Rao et al., 1987) have studied the effects of sodium salicylate on the micellization of CTABr micelles. It was found that, the cationic surfactant, CTABr formed spherical micelles at $[CTABr]_T$ = 0.8 mM and the spherical-to-rodlike transition were observed at $[CTABr]_T$ = 270 mM. Nevertheless, the presence of equivalent molar ratio of sodium salicylate with CTABr ([NaSal] = $[CTABr]_T$ = 0.15 mM) causes a direct transition from monomer to rodlike/wormlike micelles and transition from monomer to spherical was no longer observed. This phenomenon occurs because of relatively strong binding affinity of salicylate ions to CTABr micelles which results in micellar solutions with viscoelastic properties. Other than salicylate ions, the rodlike/wormlike transition of cationic surfactants were also induced by a number of organic anions as reported in a few studies (Hassan et al., 2003; Kumar et al., 2002; Lindemuth et al., 1993). This finding has become a trigger for increasing interest in induced micellar growth studies and its effect on the micellar-catalyzed rate of reactions.

2.6 Nanoparticle (Micellar) Catalysis

A catalyst is defined as a chemical species that catalyze or inhibit the rate of reactions without being consumed throughout the course of reaction (Khan, 2006). Catalysis is very important in modern science and industrial application with broad range from the petroleum chemical process to small-scale biochemical processes (Maite et al., 2005; Fan et al., 2011). Moreover, it provides an economical and green reactions media for selective production of chemical products (Roschat et al., 2016).

It is prominent that the presence of surfactant nanoparticles (micelles) in a chemical reaction in solution could alter the reaction rates by dragging the reaction center into the surfactant aggregates environment leading to kinetic medium effect (Romsted, 1977). Thus,

providing the reaction with two different phases which is the micellar pseudophase and bulk aqueous phase (Khan, 2006). In this perspective, nanoparticles (micelles) act as a catalyst since it can either increase or decrease the rate of reactions and act as a reaction medium. Besides, from a certain point of view, the behavior of micelles is similar to enzymes, separating species from the bulk solvent, playing some roles at a time like improving solubilization of organic reagents in water, favoring compartmentalization of reagents with enhancement of the local concentration and reactivity (Romsted, 1977).

The first reported systematic studies on the effect of micelles on the rate of reactions turn up in 1959 (Duynstee & Grunwald, 1959). Since then, the catalytic effects of micelles on the rate of reactions have been massively studied (Handa, et al., 2015; Bunton, 1979; Bunton, 1997; Bunton & Robinson, 1968; Bunton et al., 1981). In conjunction to that, micellar catalysis has been found useful in numerous applications (La Sorella et al., 2015). The presence of micelles could directly improve the yield of a product of chemical reactions such as dehydration reaction (Manabe et al., 2002), oxidations (Bahrami et al., 2012), C-C bond forming reactions (Friedel-Crafts acylation of aromatics) (Reddy et al., 2013) and C-heteroatom bond forming reactions (Nairoukh et al., 2013). Other than that, incorporation/solubilization of metal catalysts in micelles also provides yield improvement for metal catalyzed reactions (Gogoi et al., 2005). Moreover, product selectivity such as regioselectivity (Dey et al., 2013) and enantioselectivity (Sato et al., 2004) can also be improved through the use of micellar catalysis.

2.7 Pre-equilibrium Kinetic Model of the Micelle

Until the mid-1960s, the kinetic data on the rates of micellar-catalyzed reactions have been explained only qualitatively since there is lack of an acceptable kinetic micellar

model (Khan, 2006). In 1967, Menger and Portnoy proposed a reaction mechanism (**Scheme 2.1**) based on their observations (Menger & Portnoy, 1967). Nowadays, this mechanism is referred as Menger's phase-separation model, enzyme-kinetic-type model or preequilibrium kinetic (PEK) model for micellar-catalyzed reactions and it has been used to explained unimolecular reactions quantitatively (Menger & Portnoy, 1967; Khan, 2006)

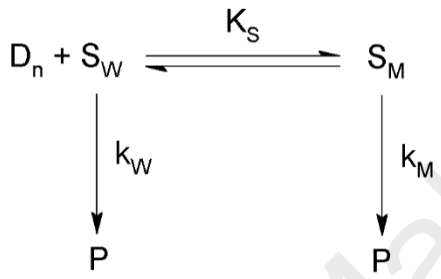

Scheme 2.1 Schematic representation of the reaction steps of unimolecular reaction in terms of PEK model of micelles.

In **Scheme 2.1**, K_S is the micellar binding constant of substrate S, subscripts W and M represent aqueous phase and micellar pseudophase, respectively, k_W and k_M are pseudo-first-order rate constants for unimolecular reactions occurring in respective aqueous phase and micellar pseudophase and $[D_n] = [Surf]_T$ – cmc with $[Surf]_T$ and cmc representing total concentration of surfactant and critical micelle concentration of surfactant, respectively. The PEK model are strict with a few assumptions which are (i) substrate does not complex with surfactant monomer, (ii) substrate does not perturb micellization (ii) substrate associates with the micelles in a 1:1 stoichiometry (iv) micellization occurs exactly at the cmc rather than over a small concentration range and (v) the relationship $[D_n] = \{[Surf]_T$ – cmc$\}/n$ is valid (Khan, 2006; Khan, 2010).

2.8 Pseudophase Micellar Model

When an aqueous solution of surfactant was put under UV-visible radiation at $[Surf]_T$ less and greater than cmc, it remains transparent to the radiation and thus is defined as a single homogenous phase. Hence, micelles cannot be considered as a real phase but technically represent a *pseudophase* which is the reason for the emergence of Pseudophase Micellar (PM) model. The PM model, by retaining all the assumptions introduced in PEK model, considers several assumptions which includes (Bunton et al., 1980; Khan, 2006; Khan, 2010): (i) micelles and bulk aqueous solvents are regarded as distinct reaction regions, (ii) micellar effects on reaction rates and equilibria are insensitive to changes in the size and shape of micelle, (iii) $k_S >> k_W$ and $k_{-S} >> k_M$ where k_S and k_{-S} represent rate constants for micellar incorporation and micellar exit, respectively, of substrate S, hence $k_S/k_{-S} = K_S$ (**Scheme 2.1**), (iv) equilibrium processes or equilibrium constants for micellar incorporation/solubilization of different solubilizates are independent of each other, i.e. there is no cross-interaction between equilibrium constants of micellar incorporation of different solubilizates, (v) equilibrium constant, K_M, for the formation of micelles as expressed by **Eq. 2.1**, is independent of equilibrium constants, K_S, for micellar solubilization of different solubilizates and rate constants, k_M, for micellar-mediated reactions i.e. in other words, the rates of formation and disintegration of micelle are independent of the corresponding rates of micellar intake and exit of a solubilizate $k_f^M >> k_W$ and $k_d^M >> k_M$ where k_f^M and k_d^M represent rate constants for micelle formation and micelle disintegration, respectively, and therefore $k_f^M/k_d^M = K_M$.

$$\{ (n - N) / N_A \} \text{ monomers} \underset{}{\overset{K_M}{\rightleftharpoons}} (N / rN_A) \text{ micelles} \tag{2.1}$$

In **Eq. 2.1**, n represents total number of surfactant molecules, N is the total number of surfactant molecules used up in the formation of number of micelles (N/r), r signifies the mean aggregation number of a micelle and N_A is Avogadro's number. (vi) for a bimolecular reaction, the reaction between a reactant (R_M) in the micellar pseudophase and the other reactant (S_W) in the aqueous pseudophase does not occur, i.e. the cross-interface reactions such as between R_M and S_W or R_W and S_M does not take place and (vii) for a bimolecular reaction between R and S, the equilibrium constants, K_S and K_R for micellar solubilization of both reactants are independent of each other.

2.9 Pseudophase Ion Exchange Model

When one or more of the reactants of a bimolecular reaction are ionic, the kinetic analysis of such reactions are rather more complicated. Especially in the case when the ionic reactants are not identical to the counterions of the ionic surfactant, estimation of the concentrations of reactive ions in the interfacial region requires a refinement of the model. The theoretical interpretation of kinetic data on micellar-catalyzed reactions that involves the competition between counterion (X) and another ion (Y) of similar charge (ion exchange occurrence) for ionic micellar surface was not established, only until Romsted and co-workers developed theoretical model known as the pseudophase ion-exchange (PIE) model in order to gives quantitative or semiquantitative interpretation of the kinetics of micellar catalysis for ionic or semi-ionic (i.e. one of the reactants being ionic) bimolecular reactions (Romsted, 1984; Quina & Chaimovich, 1979)

The PIE model is basically an extension of PM model and thus comprises all the assumptions involved in the PM model with the addition of a few more assumptions listed below which has been described in details elsewhere (Khan, 2006; Khan, 2010):

1) The degree of counterion ionization remains constant (i.e. there is a strictly 1:1 ion exchange) irrespective of ion type or concentration or surfactant concentration.
2) The micellar surface region can be thought of as an ion-exchange resin in which ion exchange processes occur in the same was as for a resin.

Effects of inert salt (=KBr) on pseudo first-order rate constant (k_{obs}) on alkaline hydrolysis of moderately hydrophobic anionic esters (Vera & Rodenas, 1986) and imide (Khan, 1997) in the presence of flexible micelles/FN, have been analyzed in terms of PIE model by considering HO^-/Br^- ion exchange coupled with an empirical **Eq. 2.2**:

$$K_S = K_S^0 - L[KBr] \tag{2.2}$$

where K_S is flexible micellar/FN binding constant of anionic reactant (S^-) in the presence of KBr and L is an empirical constant. The magnitude of L measures the ability of Br^- to expel S^- from the pseudophase of FN to the bulk aqueous phase.

Even though PIE model is an extension of PM model, it does not give a better data fit than the PM model due to the fact that PIE model which include ion exchange occurrence, involves more assumptions than PM model. It is a common perception that confidence in the general utility of a theoretical model decreases with an increase in the number of assumptions. Thus, if the ion exchange cannot be detected kinetically, then the PP model is more reliable than the PIE model. Some more weaknesses of PIE model have been discussed in details in a few reports (Germani et al., 1993).

2.10 Rheology of Micelles

Wormlike micelles are elongated and semiflexible aggregates resulting from the self-assembly of surfactant molecules in aqueous solutions. In the general context of complex fluids, wormlike micelles have received considerable attention from theoreticians and

experimentalists during the past decade (Walker, 2001; Yang, 2002). One reason for this interest is due to their remarkable rheological properties where wormlike or rodlike micelles show the presence of shear thinning and spherical micelles and vesicles show the absence of shear thinning. When micelles grow and become wormlike, the aggregates are much like polymers, and as polymers they entangle above a critical concentration. The aqueous solutions then become viscoelastic. Quantitative rheological measurements show that this viscoelasticity is characterized by a single relaxation time, a property which is rather unusual for fluids with complex microstructures. This rule is indeed so general that it is now admitted that a single relaxation time in the linear mechanical response is a strong indication of the wormlike character of self-assembled structures. Wormlike micelles are also considered as models for polymers because of their nonlinear rheological properties. When submitted to steady shear, these viscoelastic fluids undergo a shear banding transition, which is associated with a plateau in the stress versus shear rate curve. The shear banding transition is a transition between the homogeneous and a non homogeneous state of flow, the latter being characterized by a "separation" of the fluid into macroscopic regions (bands) of different shear rates. Zero shear viscosity is the viscosity measured in shear deformation at a shear rate approaching to zero. The phase transition temperature is called the consolute temperature. The consolute temperature of a given mixture can be determined by first measuring the storage (G') and loss (G") moduli of the material versus temperature, and then plotting log G' versus log G".

2.11 Turbidity of Micelles

Above the cmc, the number of micelles will increase as the total surfactant concentration increases. This results in increases in solution turbidity and solubilization with increased

surfactant concentration. Once the cmc is reached the change in surface tension with surfactant concentration is significantly reduced or eliminated with further increase in surfactant. The occurance of the turbidity may results on the formation of wormlike micelles and vesicles (Razak & Khan, 2013)

2.12 Particle Size Analysis of Micelles

Surfactant micelles are used in a wide variety of applications, from personal care products to pharmaceutical formulations. Dynamic light scattering can be used to characterize micelle size and charge, determine the critical micelle concentration, and study the influence of surfactant concentration and dispersant conditions on micelle size. Dynamic light scattering (DLS) such as Zetasizer is a technique used for particle sizing of samples, typically in the sub-micron range. The technique measures the time-dependent fluctuations in the intensity of scattered light from a suspension of particles undergoing random, Brownian motion. Analysis of these intensity fluctuations allows for the determination of the diffusion coefficients, which in turn yield the particle. (Eh Suk & Misni, 2017).

2.13 Transmission Electron Microspy

The transmission electron microscope is a very powerful tool for material science. A high energy beam of electrons is shone through a very thin sample, and the interactions between the electrons and the atoms can be used to observe features such as the crystal structure and features in the structure like dislocations and grain boundaries. Chemical analysis can also be performed. TEM can be used to study the growth of layers, their composition and defects in semiconductors. High resolution can be used to analyze the quality, shape, size and density of quantum wells, wires and dots. The TEM operates on the same basic

principles as the light microscope but uses electrons instead of light. Because the wavelength of electrons is much smaller than that of light, the optimal resolution attainable for TEM images is many orders of magnitude is better to determine the microstructural of micelles (Tan & Misni, 2013).

CHAPTER 3

THE STUDY OF RELATIVE COUNTERION BINDING CONSTANT (R_X^{Br}) TO CATIONIC MICELLES BY THE USE OF SEMI EMPERICAL TECHNIQUES

3.1 Introduction

Induced micellar growth has been one of the major areas of interest in research (Khan, 2006, Agarwal et al., 2006; Singh, 2012). This is due to the fact that these micelles could grow and exhibit viscoelastic properties even at a low concentration of surfactant solution co-micellized with organic anions and some additives (Mishra et al., 1993; Vermathen et al., 2002; Rakitin & Pack, 2005). It is believed that the viscoelastic properties exhibited by ionic micelles are due to by the transition of the spherical to wormlike micelle which could further transform into an entangled wormlike micelle. Despite that, the induced cationic micellar growth also exhibits some other remarkable properties such as micellar catalysis (Khan, 2006; Sen & Chaterjee, 2015; Singh, 2012), drag reduction in turbulent flow (Lu et al., 1998; Ulmius et al., 1979), streaming birefringence (Mishra et al., 1993; Aiello et al., 2010), drug deliveries (Aiello et al., 2010; Techen et al., 2012), and nano-emulsions (Xin et al., 2013).

Since the discovery of the surfactant aggregates in aqueous solution suggested by McBain (McBain, 1944) in the early 20th century, his theory has been accepted today eventhough scientists doubted it in the beginning. Despite that, this significant discovery by Mc Bain has introduced the world into the colloidal and surface chemistry that has massively contributed to the field of surface science and engineering.

As defined by Dominguez and co-workers, surfactants are amphiphilic compounds that possessed both hydrophobic (apolar tail), and hydrophilic (polar headgroup)

characteristics (Dominguez et al., 1997). These surfactant molecules can be categorized as cationic, anionic, zwitterionic (ampholitic), or nonionic based on the chemical structure of the headgroups. These surfactants, which come from the word abbreviation of surface active agents are one of the most diverse and versatile chemicals available. In polar solvents, for example water; increase in the concentration of the surfactants shows an abrupt change in various aqueous surfactant solution properties such as specific conductivity, surface tension, turbidity, magnetic resonance, self-diffusion and reaction rates (Figure 3.1).

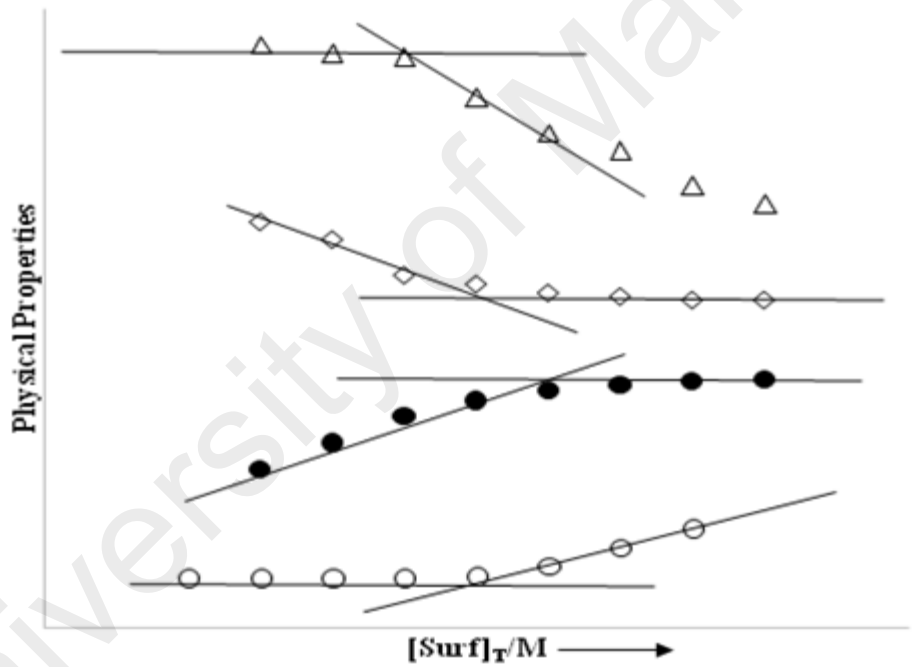

Figure 3.1: Clear sudden changes in micellar aqueous solutions physical properties at a certain total surfactant concentration, $[Surf]_T$ (where $[Surf]_T = [CTABr]_T$). The intersection point of two linear lines represents the critical micelle concentration (cmc) (Khan, 2006).

These changes in various physical properties of aqueous solution are described by the formation of aggregates above a critical surfactant concentration which is termed as *critical micelle concentration* (cmc) (Khan, 2006). In 1913, McBain (McBain, 1913) has suggested that when the concentration of a particular aqueous surfactant solution is

increased above the cmc, the surfactant monomer start to assemble among themselves into organized and thermodynamically stable molecular aggregates known as *micelles* (Figure 3.2). This remarkable discovery by McBain has lead Hartley (Hartley, 1936) to introduced the first model of a spherical micelle.

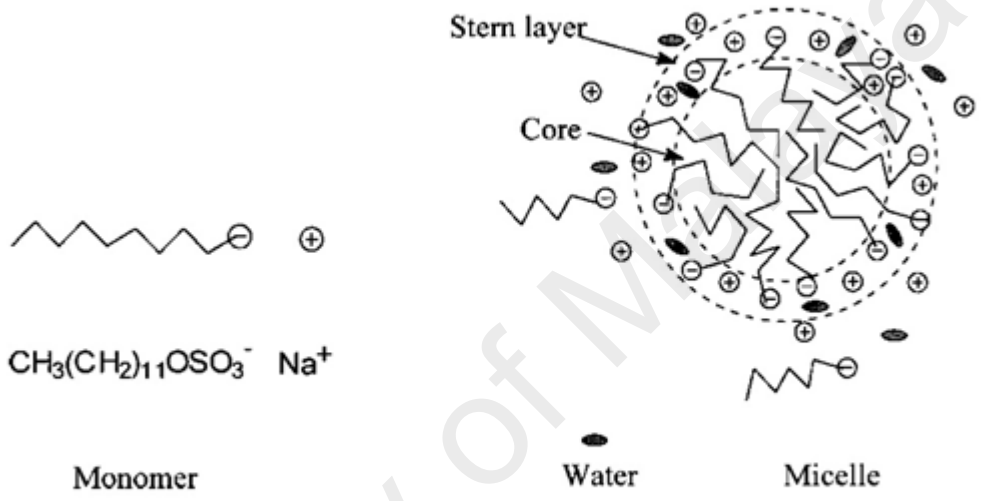

Figure 3.2: Spherical micelle model of sodium dodecyl sulfate (Dominguez et al., 1997).

These changes of physicochemical behavior have helped the scientists to study in more details on the chemical and physical properties of the aqueous surfactant solutions. In the last few decades, numerous studies on the various physicochemical behaviors of aqueous surfactant solutions show that the cmc of a surfactant is a very important parameter in view of its importance in the determination and optimization of various characteristic properties of micelles, such as micellar stability and binding affinity of a solubilizate (Tsujii, 1998). Moreover, cmc value also represents the formation or phase transition of surfactant such as monomer-spherical, spherical-wormlike, wormlike-vesicle etc. Ruiz and

co-workers (Carpena et al., 2002) have mentioned the significance of cmc as a parameter in the studies of micellization. The thermodynamic of micellization studies can be exploited from the cmc value of surfactant since its value measures the stability of the surfactant in its micellar form.

The addition of anions (organic or inorganic counterions) such as benzoate and salicylate into the cationic surfactant systems decreases the cmc (Vermathen et al., 2002; Bijma et al., 1998; Bijma & Engberts, 1997; Bachofer & Simonis, 1996; Sepúldeva et al., 1980; Maiti et al., 2009). These results show that the association of anions to cationic micelles stabilizes micellar aggregates system (decreasing the Gibbs free energy of micellization, ΔG_m^0). The counterion associations to the micellar aggregate promote the formation of other shape of aggregates (rodlike, wormlike, vesicle, etc.). Counter ion association helps the assembling of the surfactant monomers by both electrostatic and hydrophobic interaction between surfactant and counter ion thus decreasing the cmc (Rao et al., 1987). Bachofer (Bachofer & Simonis, 1996) and Sepúldeva (Sepúldeva et al., 1980) have suggested that there is a competitive activity between the counter ions at the micellar interface and they used the ion exchange constant to quantitatively explain the extent of counter ion binding towards the micelles.

Many techniques that has been used in order to determine the cmc, counter ion binding and ultimately to investigate the interesting features of cationic micellar growth in aqueous solution. In 1996, Bachofer and Simonis (Bachofer & Simonis, 1996) have addressed the various methodologies to study the extent of counter ion binding to cationic micellar interface in two categories namely:

(a) Conductivity, ion selective electrode (ISE) and potentiometry to determine the fractional ionization constant, α of the micelle;

(b) ISEs, light scattering, ^{1}H-NMR, UV-vis spectroscopy, ultrafiltration, and fluorescence quenching to determine the fraction of counter ion competition with another inorganic anion for binding to the micellar interface.

Perhaps, it is noteworthy that the most common methods used are conductivity, surface tension, and ^{1}H-NMR spectroscopy technique or the combination of these methods. Herein this review paper, we would like to compare and analyze these methods with method(s) SEK and SESp in terms values of K_X^{Br} or R_X^{Br}obtained.

3.2 Common Methods to Determine Counterion Binding Constant, R_X^{Br} or K_X^{Br}

3.2.1 Conductivity Method

Studies on micellar systems by means of conductivity method have begun in the early 19 centuries until now (McBain, 1913; McBain & Taylor, 1910; McBain & Taylor, 1911; McBain & Salmon, 1920; Briggs, 1928). The use of conductivity method to determine cmc of ionic micellar systems involves the plot of conductivity (κ) versus concentration of the ionic surfactant solution and the point of curvature represents the critical micelle concentration (cmc) (see Figure 3.3). The point of curvature or cmc was determined from the intersection of the fitting lines of the curves above and below the break point. Generally, behavior of micellar system in aqueous solution is studied by plotting conductivity-concentration graph at different temperatures and/or chemical compositions (stoichiometry). These plots will give a detail explanation on the temperature-dependence of micellar behavior. The line below the singular point break of curvature (cmc) is the premicellar region in which each of the surfactant monomer starts to aggregate among themselves to form micelles and the line above the cmc is the postmicellar region in which each of the surfactant monomer has fully aggregated to micelle (generally spherical micelle as this is the first transition phase of aqueous surfactant). Nevertheless, Zana and

others (Zana & Lévy, 1997; De Lisi et al., 1997) made an assumption based on calculation that the degree of counterion dissociation of micelles (α) is related to the ratio between the slopes of the premicellar region and the postmicellar region. Since degree of counterion dissociation (α) can be calculated from conducitivity, thus one might as well determine the degree of counterion binding (β) (Bijma et al., 1998; Bijma & Engberts, 1997) because α + β = 1.

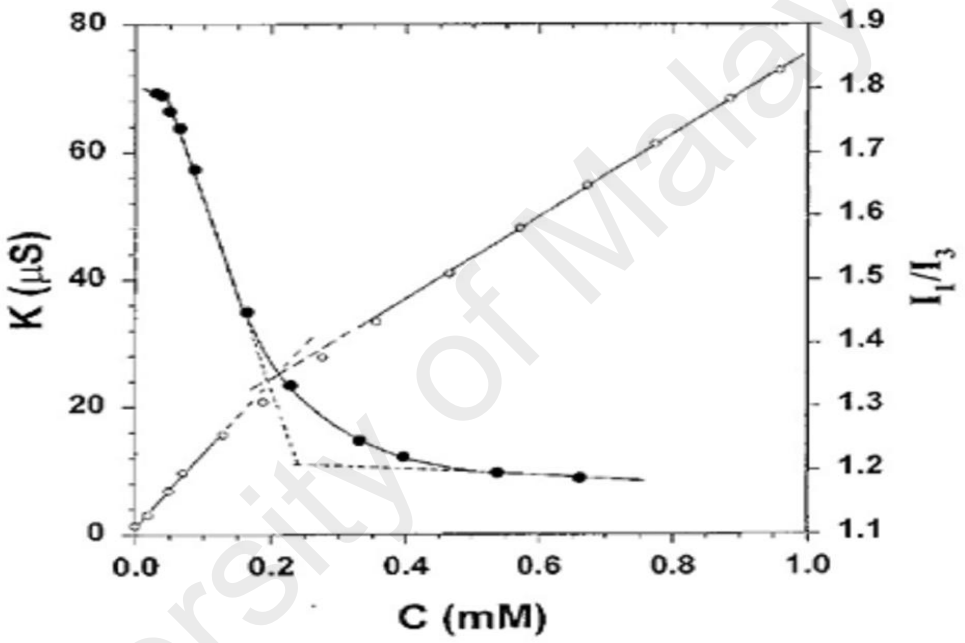

Figure 3.3: Disodium 1,11-didecyl-3,6,9-trioxaundecane-1,11-disulfate: variation of the conductivity κ(◦) and the ratio of I_1/I_3(•) with the CTABr concentration at 25°C (Zana & Levy, 1997).

Other than that, conductivity method can act as a probe to monitor the growth of micelles such as from monomer to spherical and spherical to rodlike micelles. This has been done by Vermathenet and co-workers (Vermathen et al., 2002) for TTA^+/*ortho*-benzoate sytems which exhibit growth to spherical micelles even at high concentration of TTA^+ whereas TTA^+/*meta*- and *para*-benzoate sytems exhibits growth from spherical to rodlike micelles at high concentration of TTA^+. These observations by both TTA^+/*meta*-

and *para*-benzoate systems are designated by the second cmc in the conductivity-concentration plot (Figure 3.4). Investigations on benzyldimethyltridecylazanium chloride cationic surfactant in aqueous solution by Savarogluet and co-workers (Savaroglu & Yurt, 2011) using conductivity measurement method also reveals the two breaks in the conductivity-concentration plot whereby the first breaks corresponds to cmc and the second less distinct breaks at higher concentration corresponds to the second cmc. Savarogluet and co-workers also described that the spherical micelles will transform into rodlike micelles if the concentration of the solutions exceed the cmc by 2-10 times. Regardless of the capability of conductivity technique to determine the cmc and degree of counterion dissociation to describe the micellar systems behavior, this technique seems not to be flawless as pointed out by Carpena and co-workers (Carpena et al., 2002). It was mentioned that it is not easy to determine the specific break point that denotes the value of cmc obtained from empirical graphical procedures especially when determining the cmc of surfactants with low aggregation numbers. This is because not all, but some of the conductivity-concentration plot produced displays of a weak curvature (see Figure 3.5) making the determination of the intersection of two straight lines less accurate. In this case, the cmc determination will be very difficult to carry out and as a result, it produced a great uncertainty in the cmc. Consequently, this uncertainty will affect the value of degree of counterion dissiociation.

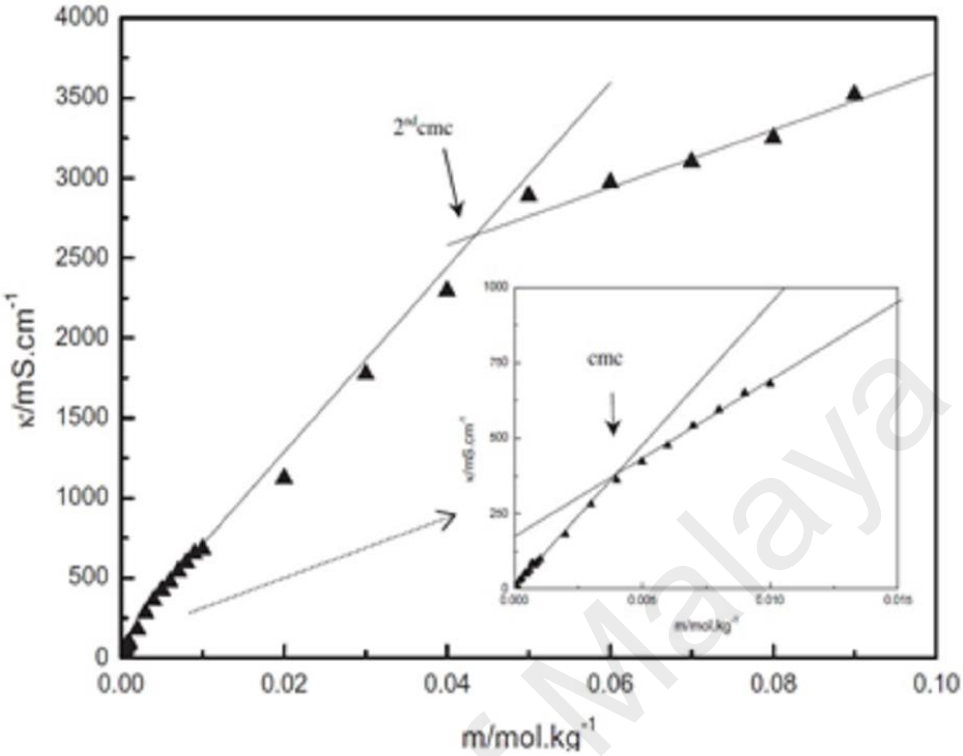

Figure 3.4: Plot of conductivity κ of benzyldimethyltridecylazanium chloride as a function of concentration at T = 293.15 K. The arrows denote the cmc and the second cmc (2nd cmc) (Vermathen et al., 2002).

3.2.2 NMR Spectroscopic Technique

Nuclear magnetic resonance (NMR) spectroscopic technique has been applied to study various micelles structures in surfactant systems since 1960s (Lawson & Flautt, 1965; Muller & Birkhahn, 1967; Muller & Birkhahn, 1968; Bailey & Cady, 1969; Clifford & Pethica, 1964). Numerous reports on the structures of micelles and behavior in surfactant systems by using NMR spectroscopic technique as a probe have been published since then. Other than that, this NMR spectroscopic technique also has been utilized to the study of various complex lipids micelles (Clifford & Pethica, 1964; Chapman & Morrison, 1966; Haque et al., 1972). It is worth mentioning that NMR spectroscopy is one of the powerful tools to study the micellar related systems.

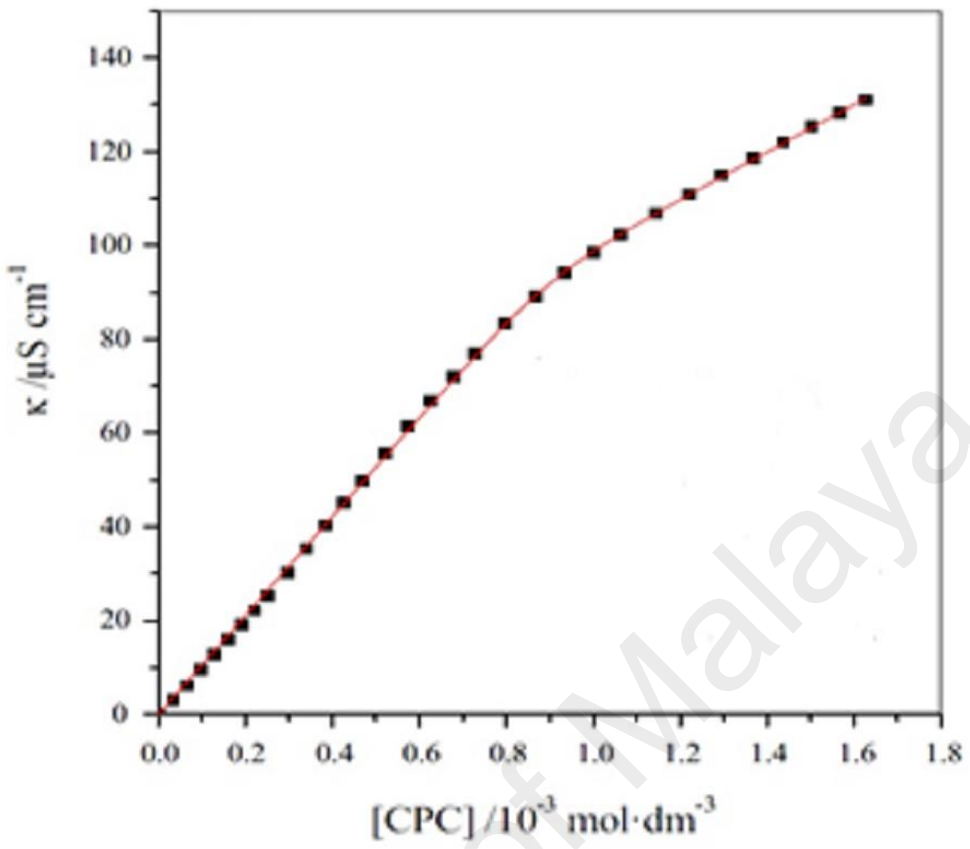

Figure 3.5: Plot of conductivity κ versus cetylpyridinium chloride (CPC) concentration obtained in 0.05 mol dm^{-3} aqueous-glycine media at 303 K that's shows a weak curvature (Koya et al., 2015).

Basically, study of micellar systems by NMR technique is construed through a few NMR parameters (Wong, 2006): (i) chemical shifts, (ii) linewidth, (iii) spin-spin coupling constants (iv) nuclear spin relaxation and (v) measurement of self-diffusion. Chemical shifts obtained from NMR which was determined involving weaker forces such as hydrogen-bonding, ring current effects, etc. give remarkable information on the molecules aggregation, location of molecules and interaction between molecules to micelles whereby linewidth of an NMR signal regularly used to monitor changes in phases and aggregation qualitatively. By using the different values of coupling constant in the monomer and micellar forms, one can determine the micellar formation via spin-spin coupling constants while analysis of the dynamic information of the micellar system can be obtained from

nuclear spin relaxation. However, the analysis is strictly applied only to spherical micelles (Khan, 2006).

NMR technique is often applied to obtain the quantitative information regarding the size, shape and inner structure of micelles. NMR can reveal information on the effect of counterions and hydrophobicity towards the micellization and describe the penetration as well as the orientation of the counterion inside the micellar systems. Sabatino and co-workers (Sabatino et al., 2010) proposed that at neutral pH, both phenol counterion and cetyltrimethylammonium (CTA^+) micelles are in vicinity. However, as the pH increased which give rise to the ion pairing pushes the phenol deeper into the micelles in which the negatively charged oxygen interacts with the positively charged nitrogen and the aromatic rings resides in the upper part of the hydrophobic region. This hypothesis was made through chemical shift basis and supported through NOESY experiments. Chemical shifts changes observed in the ^{1}H-NMR spectrum when CTAB solutions was added to the sodium salicylate, NaSal solution indicates that in the presence of micelles, the ortho proton of NaSal stay in the vicinity of micellar-water interface whereby meta and para proton are shifted to a more nonpolar region of the micelle (Rao et al., 1987). This observation shows that the chemical shifts changes obtained in NMR measurements, clearly revealed the location and orientation of a certain molecule and/or with respect to the micellar interface. As mentioned before, linewidth changes measured from NMR sprectrum could reveal the set point in which the monomer surfactant start to aggregates among themselves and transformed to micelles. The trend in NMR spectrum observed by Bachofer (Vermathen et al., 2002; Bachofer & Simonis, 1996) and Bijma (Bijma & Engberts, 1997) noticeably revealed that below the cmc, the linewidths of the spectrum is narrow, but, as the concentration of the surfactant increases, the linewidth becomes broader which represents

the phase transition occurred in the micellar systems eg. monomer to spherical micelles or spherical to rodlike micelles. Apart from that, chemical shift changes measured from NMR spectrum has allowed Majid and co-workers (Kreke et al., 1996) and Iijima and co-researchers (Iijima & Kato, 2000) to determine the degree of counterion binding which led to a deeper details study on the micellar systems.

Despite the advantage and versatility of NMR spectroscopy technique, the determination of degree of counterion binding at micellar-water interface is seldom not carried via NMR technique alone, but with the combination of other technique such as conductivity (Šarac et al., 2013; Sehgal et al., 2007), surface tension (Javadian et al., 2013; Pan et al., 2014), etc.

3.3 Semi Empirical Technique

It is now well known that the presence of counterion (X) which is either moderately hydrophobic or hydrophilic could induce the micellar growth from spherical, rod/ wormlikes to vesicles. The binding of these counterions with the micellar interface is critically important as it enhances and/or promotes the micellar formation. The efficiency of counterion affinity towards the ionic micelles were often described in terms of the degree of counterion binding (β_X) to ionic micelles or the conventional ion exchange constants, K_X^{Br} or R_X^{Br}. However, recent report reveals that the values of K_X^{Br} or R_X^{Br} seem to be in better agreement than those of β_X with counterion-induced micellar structural growth for different moderately hydrophobic counterion (Khan, 2010). Thus, both semi-empirical kinetic as well as semi empirical spectrophotometric methods were developed to determine the values of K_X^{Br} or R_X^{Br} in order to have a deep understanding on the X-induced micellar growth.

3.3.1 Semi Empirical Kinetic (SEK) Technique

The relative counterion binding constant for ion exchange process of counterions (organic/inorganic) at the cationic micellar surface were determined by applying the SEK approach (Khan, 2010; Yusof & Khan, 2010; Yusof et al., 2013). Basically, this method uses a specific kinetic probe (e.g. piperidinolysis of ionized phenyl salicylate, PSa^-, and alkaline hydrolysis of a few imides and ester) which measures the effects of varying concentrations of inert inorganic or organic salts on rate constant, k_{obs} for the reaction of piperidine with PSa^- (Khan, 2010; Yusof & Khan, 2010; Yusof et al., 2013). It is important to note that the characteristic observations of the kinetic probe for SEK method are as follows: (a) The rate constant, k_{obs} shows 10 to 20-fold increase when the probe molecules transfer from micellar to aqueous phase (k_W/k_M = 10 to 20-fold) (b) The addition of counterion (inert salts) at different concentration in the reaction medium in the presence of anionic probe shows catalytic behaviour (increase or decrease) in terms of pseudo-first order rate constant, k_{obs}, hence giving a nonlinear curve of k_{obs} *vs*. salts concentration. This method has been used since last nearly more than ten years. The values of K_X^{Br} or R_X^{Br} for several anionic counterions (X) have been published in research articles and book (Khan, 2006; Khan, 2010). However, this method has evolved to another technique called semi-empirical spectrophotometric (SESp) method (Khan et al., 2013)

3.3.2 Determination of Relative Counterion Binding Constant by the Use of Semi – Empirical Spectrophotometric (SESp) Method in the Presence of Cationic Micelles

The semi-empirical spectrophotometric (SESp) method has been applied for the indirect determination of ion exchange constants (K_X^{Br}) of ion exchange processes occurring between counterions (X^- and Br^-) at the cationic micellar surface (Khan et al., 2013). It is

relevant to note that the present SESp techniques can be used to determine both K_X^{Br} and R_X^{Br}. On the other hand, almost all conventional technique can be used to determine only K^X_{Br}. The use of R_X^{Br} refers to the counterion binding constant value where the binding constant value of spherical micelles is used as a reference (denominator value is the binding constant of spherical micelles) and K_X^{Br} is refers to the experimental aggregates (spherical/ wormlike/ vesicle) binding constant value as reference (denominator value is the binding constant of aggregates).

Basically, this method uses an anionic spectrophotometric probe molecule which measures the effects of varying concentrations of inert inorganic or organic salts on absorbance of sample containing the anionic probe molecule, NaOH and cationic micelles at particular wavelength. The counterionic probe molecule should exhibit maximum absorbance changes when the probe molecules have high affinity to ionic micellar surface (Figure 3.6). It is important to note that a very fundamental requirement of a typically anionic probe molecule needs to be met for SESp pmethod which is as follows: (a) It must be fully anionic and nonreactive/inert during the entire period of spectrophotometric measurements. (b) It should be moderately hydrophobic so that almost entire anionic probe molecules remain in the cationic micellar pseudophase at ≥ 5 mM of CTABr in the absence of any inert salt.

Theoretical basis of both SESp and SEK methods involve an empirical (Eq. (3.1))

$$K_S = \frac{K_S^0}{1 + K_{X/S}\,[MX]} \tag{3.1}$$

where K_S and K_S^0 represent cationic micellar binding constants of S (with S representing spectrophotometric and kinetic probe anionic molecule for respective SESp and SEK method in the presence and absence of counterionic salt = MX, respectively. In Eq. (3.1),

$K_{X/S}$ represents an empirical constant where subscript, X/S, signifies that the decrease in K_S with the increase of [MX] at constant concentration of cationic micelles and S^- is caused by the expulsion of cationic micelle-bound anionic S by the increase in $[X^-]$ through the ion exchange process X^-/S^- at the cationic surface of micelles. The values of $K_{X/S}$ for X=X and X=Y can lead to the calculation of the relative value of counterion binding constant, R_X^Y, where $R_X^Y = K_X/K_Y$ with K_X and K_Y representing cationic micellar binding constant of respective counterions X and Y in the presence of nonspherical micelles (such as rodlike or vesicles) and spherical micelle (Khan, 2010).

3.3.2.1 Determination of R_X^{Br} or K_X^{Br} Values by the Use of Sodium *N*-(2-Methoxyphenyl) phthalamate (*S*$^-$) as SESp Probe

The value of molar extinction coefficient of ***S***$^-$ at 310 nm is significantly higher in the presence of cetyltrimethylammonium bromide (CTABr) micelles than that in the pure bulk water solvent. The molecular structure of sodium *N*-(2-methoxyphenyl) phthalamate is shown in Scheme 3.1. The value of CTABr micellar binding constant, K_S of ***S***$^-$ is 4530 M^{-1} at 35°C and the value of hydroxide ion-catalyzed second-order rate constant, k_{OH}, for hydrolysis of **S**$^-$ at 35°C is 2.2×10^{-7} $M^{-1}s^{-1}$ (Khan et al., 2013). These characteristic physicochemical properties of **S**$^-$ are necessary and sufficient requirements for ***S***$^-$ to act as reliable SESp probe for the determination of R_X^{Br} or K_X^{Br}.

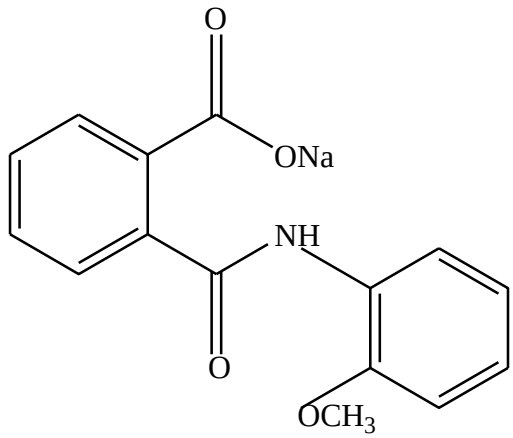

Scheme 3.1: Schematic diagram of sodium *N*-(2-methoxyphenyl) phthalamate

In the use of SESp method for the determination of R_X^{Br} or K_X^{Br}, the magnitude of an essential parameter needed is the empirical constant $K_{X/S}$ of Eq. (3.1). The value of $K_{X/S}$ can be determined from Eq. (3.1) if the experimental feasibility allows one to determine the values of K_S, in the absence and presence of the constant concentration of MX within a reasonable [MX] range. The value of $K_{X/S}$ can be also determined from another empirical equation

$$A_{ob}^{cor} = \frac{A_{ob}^{0} + \theta(K^{X/S})([MX]-[MX]_0^{op})}{1+(K^{X/S})([MX]-[MX]_0^{op})} \quad (3.2)$$

(Eq. (3.2)), where empirical constant $K^{X/S}$ is a function of $K_{X/S}$, K_S^0 and concentration of cationic micelles ($[D_n]$) (Khan et al., 2013) A_{ob}^{cor} represents initial corrected absorbance in the presence of both CTABr and MX, θ represents empirical constant, $[MX]_0^{op}$ represents optimum [MX] required for the micelles to form spherical and other symbols are explained in detail elsewhere (Khan et al., 2013).

3.3.2.2 Determination of R_X^{Br} or K_X^{Br} for Various Inert Counterionic Salts, M_VX (V=1,2) Using *S*$^-$ as SESp Probe

The unknown parameters, θ and $K^{X/S}$, were calculated from Eq. (3.2) for various MX of differing CTABr micellar affinity by Khan and his co-workers (Khan et al., 2013). Theoretical details that led to the derivation of Eq. (3.2) give θ and $K^{X/S}$ as expressed by Eq. (3.3) and (3.4), respectively (Khan et al., 2013).

$$(A_{ob}^0 - \theta) = F_{X/S}\,(A_{ob}^0 - A_0^0) \tag{3.3}$$

where $A_0^0 = A_{ob}$ at $[CTABr]_T = [M_VX] = 0$ and $F_{X/S}$ is an empirical constant whose presence is explained in some detail elsewhere (Khan et al., 2013)

$$K^{X/S} = K_{X/S} / (1 + K_S^0\,[D_n]_T) \tag{3.4}$$

where $[D_n] = [CTABr]_T - CMC$ with CMC representing critical micelle concentration of CTABr. The value of $K_{X/S}$ is calculated from Eq. (3.4) with experimentally determined values of $K^{X/S}$ and K_S^0 at a constant known value of $[D_n]$. The normalized $K_{X/S}^n$ value is then calculated with the relationship: $K_{X/S}^n = F_{X/S}K_{X/S}$ where $F_{X/S}$ value is obtained from Eq. (3.3). It has been concluded in earlier publications (Khan, 2010; Khan et al., 2013) that the values of $K_{X/S}^n$ and $K_{Br/S}^n$, obtained in the presence [CTABr]/[MX]/[H_2O] and [CTABr]/[MBr]/[H_2O] aggregates of the same structural features such as spherical or rodlike micelles or vesicles, can lead to the relationship expressed by Eq. (3.5)

$${}^{sp}K_{X/S}^n / {}^{sp}K_{Br/S}^n = {}^{sp}K_X / {}^{sp}K_{Br} = K_X^{Br} \tag{3.5}$$

where superscript sp stands for spherical micelles, K_X^{Br} represents conventional ion exchange constant for ion exchange process X^-/Br^- at the cationic micellar surface. Perhaps,

it is worth mentioning that the mean value of ${}^{sp}K^{n}_{Br/S}$ (=112 M^{-1} at $[CTAB]_T$ range of > 6 mM - ≤ 15 mM) is obtained in the presence of spherical micelles. But some of the values of $K^{n}_{X/S}$ were also obtained in the presence of nonspherical micelles such as short and long rodlike micelles. Under such conditions, Eq. (3.5) is changed to Eq. (3.6)

$$ {}^{nsp}K^{n}_{X/S} / {}^{sp}K^{n}_{Br/S} = {}^{nsp}K_{X} / {}^{sp}K_{Br} = R^{Br}_{X} \quad (3.6) $$

where superscript nsp represents nonspherical micelles. Since the value of ${}^{nsp}K_X$ is expected to be larger than that of ${}^{sp}K_X$ for some counterions, X, it is obvious that R^{Br}_{X} > K^{Br}_{X} for these X.

The values of R^{Br}_{X} or K^{Br}_{X} have been determined for various X of differing apparent hydrophobicity by the use of Eq. (3.5) or Eq. (3.6) where $\boldsymbol{S}^{-}$ represents *N*-(2-methoxyphenyl)phthalamate ion (Khan et al., 2013).

It is evident from Eq. (3.4) that ${}^{n}K^{X/S} = K^{n}_{X/S}/(1 + K^{0}_{S}[D_n])$ where ${}^{n}K^{X/S} = F_{X/S}K^{X/S}$. Similarly, ${}^{n}K^{Br/S} = K^{n}_{Br/S} / (1 + K^{0}_{S}[D_n])$. These relationships and Eq. (3.6) reveal that

$$ {}^{n}K^{X/S} / {}^{n}K^{Br/S} = R^{Br}_{X} \text{ or } K^{Br}_{X} \quad (3.7) $$

The values of R^{Br}_{X} or K^{Br}_{X}, obtained from Eq. (3.5) or (3.6), must be similar to one obtained from Eq. (3.7) for the same X. For comparison purpose, a typical set of partial data for X=2-$FC_6H_4CO_2^-$, reported in Ref. (Khan et al., 2013) have been used to calculate the values of K^{Br}_{X} by the use of Eq. (3.7). These results, obtained at 5,7,10 and 15 mM CTABr, are summarized in Table 3.1. These calculated values of K^{Br}_{X} are comparable with the corresponding values of K^{Br}_{X} calculated from Eq. (11) of Ref. (Khan et al., 2013). The use of Eq. (3.7) for the calculation of R^{Br}_{X} or K^{Br}_{X} does not require the values of K^{0}_{S} and cmc of CTABr. But, the values of K^{0}_{S} and cmc are required if Eq. (3.5) or Eq. (3.6) is used to calculate R^{Br}_{X} or K^{Br}_{X}.

Table 3.1: Calculated Values of K_X^{Br} by the Use of Eq. (3.7) for X = 2-$Cl_2C_6H_3CO_2^-$ [a]

[CTABr]T mM	$K^{Br/S}$ M^{-1}	$F_{Br/S}$	$K^{X/S}$ M^{-1}	$F_{X/S}$	${}^nK^{Br/S}$ M^{-1}	${}^nK^{X/S}$ M^{-1}	K_X^{Br}	K_X^{Br}
5	6.46	0.78	20.5	0.91	5.04 [b]	18.7 [c]	3.7 [d]	3.9 [e]
7	5.05	0.67	16.5	0.94	3.38	15.5	4.6	4.5
10	3.48	0.67	11.5	0.89	2.33	10.2	4.4	4.2
15	3.09	0.51	8.18	0.88	1.58	7.2	4.6	4.4

[a] Partial data are obtained from Ref. (Khan et al., 2013).
[b] ${}^nK^{Br/S} = F_{Br/S} \times K^{Br/S}$. [c] ${}^nK^{X/S} = F_{X/S} \times K^{X/S}$. [d] $K_X^{Br} = {}^nK^{X/S} / {}^nK^{Br/S}$.
[e] $K_X^{Br} = K_{X/S}^n / K_{Br/S}^n$ (Khan et al., 2013).

3.3.2.3 Determination of K_X^{Br} for X = 2,6-Dichlorobenzoate Using Phenylsalicylate (PSa^-) as a New SESp Probe.

One of the assumptions involved in the theoretical aspects of SESp method predicts that the value of R_X^{Br} or K_X^{Br} must be independent of the physicochemical characteristics of the probe molecule. In order to test this prediction or the validity of the theory of SESp method, the value of K_X^{Br} for X = 2,6-dichlorobenzoate ion has been determined by the use of SESp method using a new probe (PSa^-) (Scheme 3.2). The choice of 2,6-dichlorobenzoate as X is based upon the reasons that the value of K_X^{Br} for this counterion has already been determined by SESp method (Khan et al., 2013) using *N*-(2-methoxyphenyl)phthalamate as a probe as well as by other physical methods such as ^1H NMR, floatation and ion selective electrode methods (Magid et al., 1997) in the presence of CTABr micelles. The details of the determination of K_X^{Br} for X = 2,6-dichlorobenzoate ion by the use of PSa^- as SESp probe are described below.

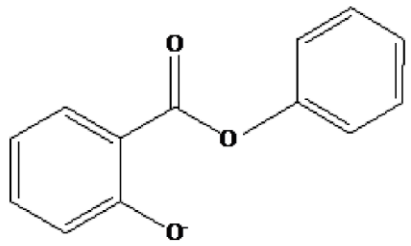

Phenyl salicylate ion

Scheme 3.2: Molecular structure of phenyl salicylate ion

3.4 Materials

Reagent-grade chemicals such as cetyltrimethylammonium bromide, (CTABr), phenyl salicylate (PSaH), 2,6-dichlorobenzoic acids (2,6-$Cl_2C_6H_3CO_2H$) and other common chemicals were the commercial products of the highest available purity. The stock solutions of 2,6-$Cl_2C_6H_3CO_2Na$ (w M) were prepared by adding (w+0.05) M NaOH to the corresponding w M solutions of 2,6-$Cl_2C_6H_3CO_2H$. Water solubility of PSaH is very low and consequently the stock solutions (0.01M) of PSaH were prepared in acetonitrile.

3.5 Spectrophotometric Measurements

Although PSa^- absorbs more strongly at 360 nm compared to that at 370 nm (Figure 3.6), the wavelength lower than 370 nm cannot be chosen because of the increasing background absorption due to especially inert counterionic salt. The values of A_{ob} obtained from the plots of Figure 3.6 at 370 nm, and [NaX] = 0 in the absence and presence of 15 mM CTABr are 0.372 nm and 0.757 nm respectively. The difference in the absorptions at [CTABr] = 15 mM and [CTABr] = 0 turns out to be 0.385 which is a reasonable number to make PSa^- as an appropriate SESp probe.

The initial absorbance (A_{ob}^{ini}) of samples containing constant 0.2 mM PSaH, 30 mM NaOH, 6 mM CTABr and inert counterionic salt, [NaX] (X= 2,6-$C_6H_3CO_2^-$) were obtained

by monitoring the change in A_{ob} at 370 nm and 35°C. In a typical aqueous sample of a total volume of 4.9cm^3 containing all the chemical ingredients except PSaH was equilibrated at 35°C for 10-15 min. Desired amount of PSaH (0.1cm^3 of 0.01M PSaH) was added to the temperature-equilibrated 4.9 cm^3 sample solution. An aliquot of ~ 2.5cm^3 was then quickly transferred to a 3 cm^3 quartz cuvette kept in the thermostated cell compartment of the UV-vis double beam spectrophotometer and the value of A_{ob} was recorded at 370 nm. The value A_{ob} should reduce slowly with time because the time period required for 1% alkaline hydrolysis of PSaH, under such conditions, is < 30 minutes (Khan, 2006).

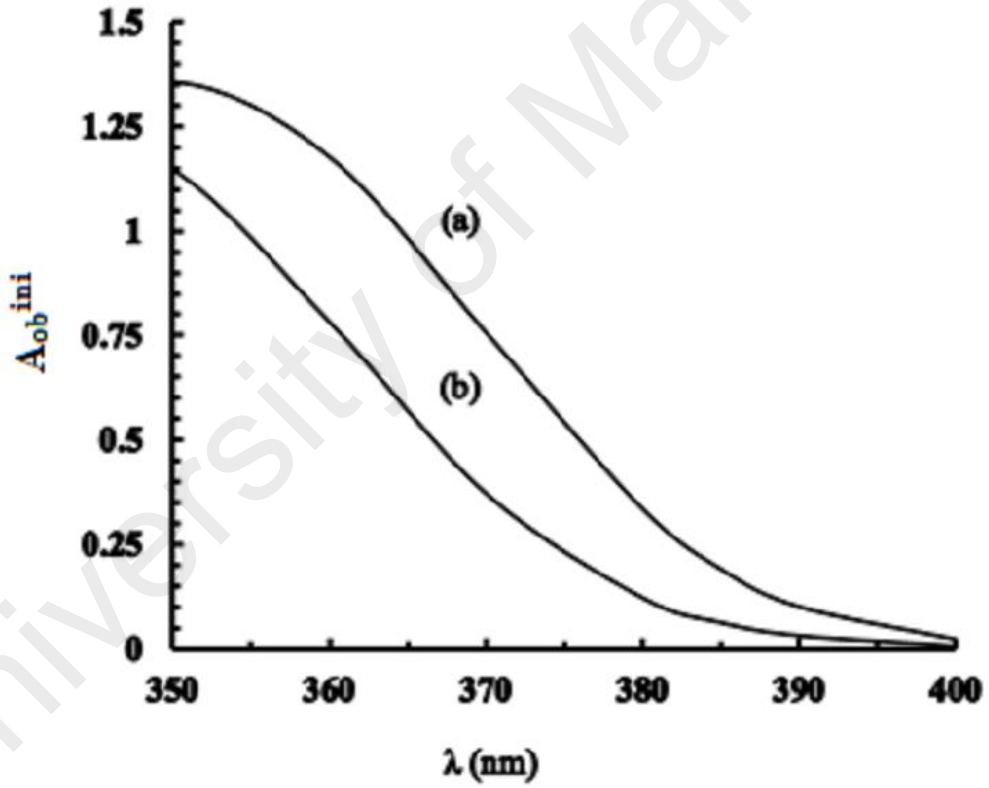

Figure 3.6: Plots showing the UV absorption spectra (absorbance, A_{ob}^{ini}, *vs.* wavelength, λ) of aqueous solutions containing 0.2 mM PSaH, 30 mM NaOH, 2% v/v CH_3CN at 35°C and in the presence (a) and absence (b) of 0.015M CTABr.

3.6 Results and Discussions

3.6.1 Determination of CTABr Micellar Binding Constants (K_S or K_S^0) of PSa^- in the Absence of an Inert Salt

The value of K_S^0(with S=PSa^-) is required in the use of SESp method for the determination of K_X^{Br} or R_X^{Br}at 35°C. The values of A_{ob}^0, of several samples containing 0.2 mM PSa^-, 30 mM NaOH and varying values of $[CTABr]_T$ (0 to 0.03 M) were obtained at 370 nm and in mixed H_2O-CH_3CN solvent containing 2% v/v CH_3CN. The values of A_{ob}^0 were almost independent of $[CTABr]_T$ within its range 0 -≤ 0.08 mM followed by a monotonic increase with increasing values of $[CTABr]_T$ until ~ 3.0 mM CTABr and then again become almost independent of $[CTABr]_T$ until its value becomes 30.0 mM (Fig. 3.7).

The observed data exhibited by the plot of Figure 3.7, have been found to fit Eq. (3.8)

$$A_{ob}^0 = \frac{A_0^0 + A_M K_S [D_n]}{1 + K_S [D_n]} \tag{3.8}$$

Where symbols A_{ob}^0, A_0^0, A_M are the same as A_{ob}, A_W and A_M, respectively as appeared in Eq. (3) of reference published elsewhere (Khan et al., 2013) and K_S^0 represents CTABr micellar binding constant of PSa^- in the absence of counterionic salt. The details of the derivation of Eq. (3.8) are described elsewhere (Khan et al., 2013). The nonlinear least squares calculated values of A_M and K_S^0 for a duplicate data set are summarized in Table 3.2. The effects of K_S in the presence of $[NaBr]_T$ (Figure 3.8) is also found to fit Eq. (3.8) for all range of $[NaBr]_T$ (Table 3.2).

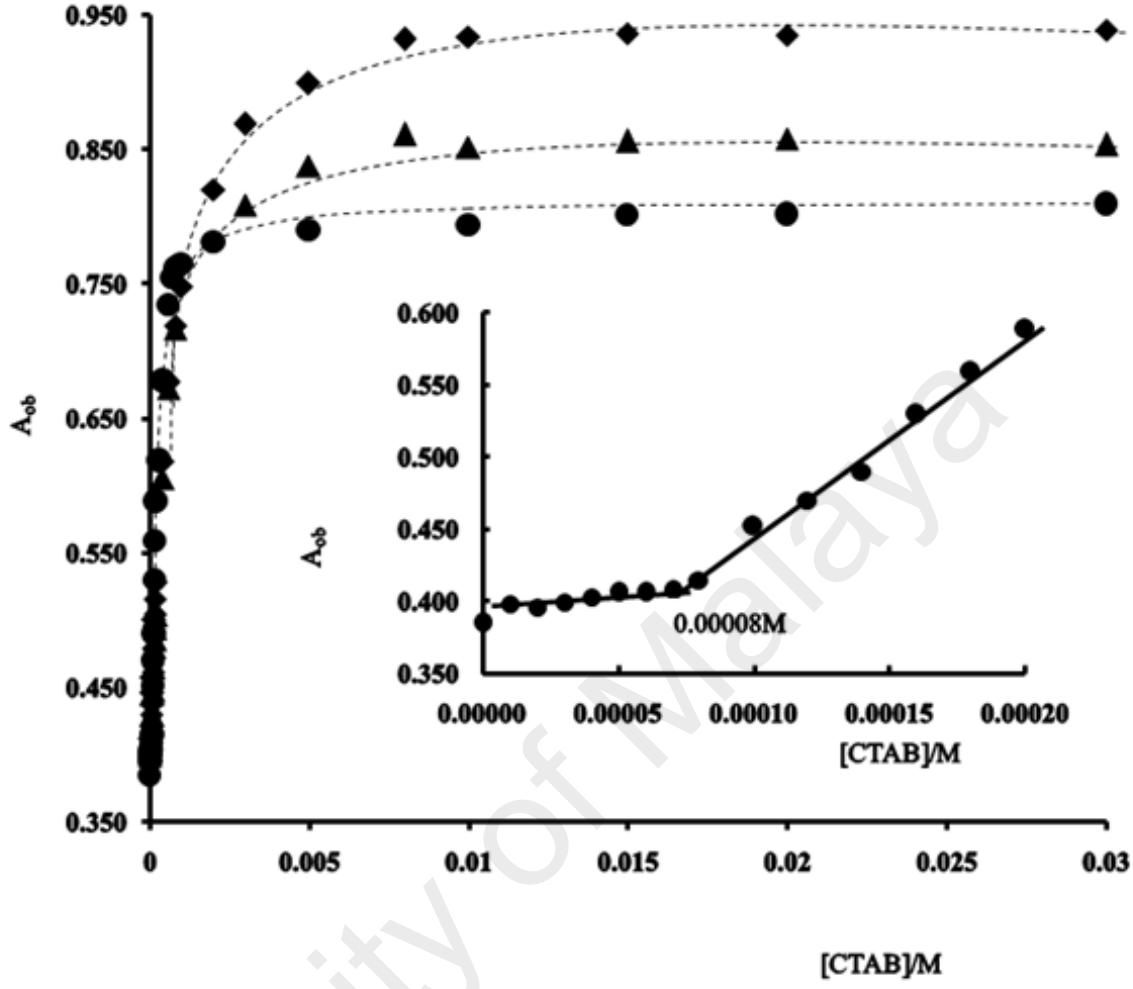

Figure 3.7: Plots showing the monotonic increase of A_{ob} with increasing values of $[CTABr]_T$ at 370 nm where (●) = 0.0, (▲) = 0.1 and (♦) = 0.3 M CTABr.

The calculated valued of K_S at different [NaBr] were found to fit reasonably well to Eq. (3.1). The nonlinear least squares calculated values of K_S^0 and $K_{X/S}$ were found to be 6748 ± 435 M^{-1} and 26 ± 6 M^{-1} respectively. The extend of the fitting of calculated data, K_S *vs*. [NaBr], is evident from the standard deviations associated with the calculated parameters K_S^0 and $K_{X/S}$ from the plot of Figure 3.9 where solid line is drawn through least square calculated data points.

3.6.2 Effects of [NaX] (X= 2,6–$Cl_2C_6H_3CO_2^-$) on A_{ob} of Samples Containing Constant Concentrations of PSa^-, NaOH and CTABr at 35°C and 370 nm

The values of initial absorbance (A_{ob}) of several samples, containing 0.2 mM PSaH, 30 mM NaOH, 6.0 mM CTABr and different values of [NaX], within its range 0.0- 0.5 M for NaX=2,6- $Cl_2C_6H_3CO_2Na$ were obtained at 370 nm and 35°C. Similar results were obtained at 7.0 and 10.0 mM CTABr. These observations are shown graphically as the plots of A_{ob}^{cor} *vs*. [NaX] of Figure 3.10.

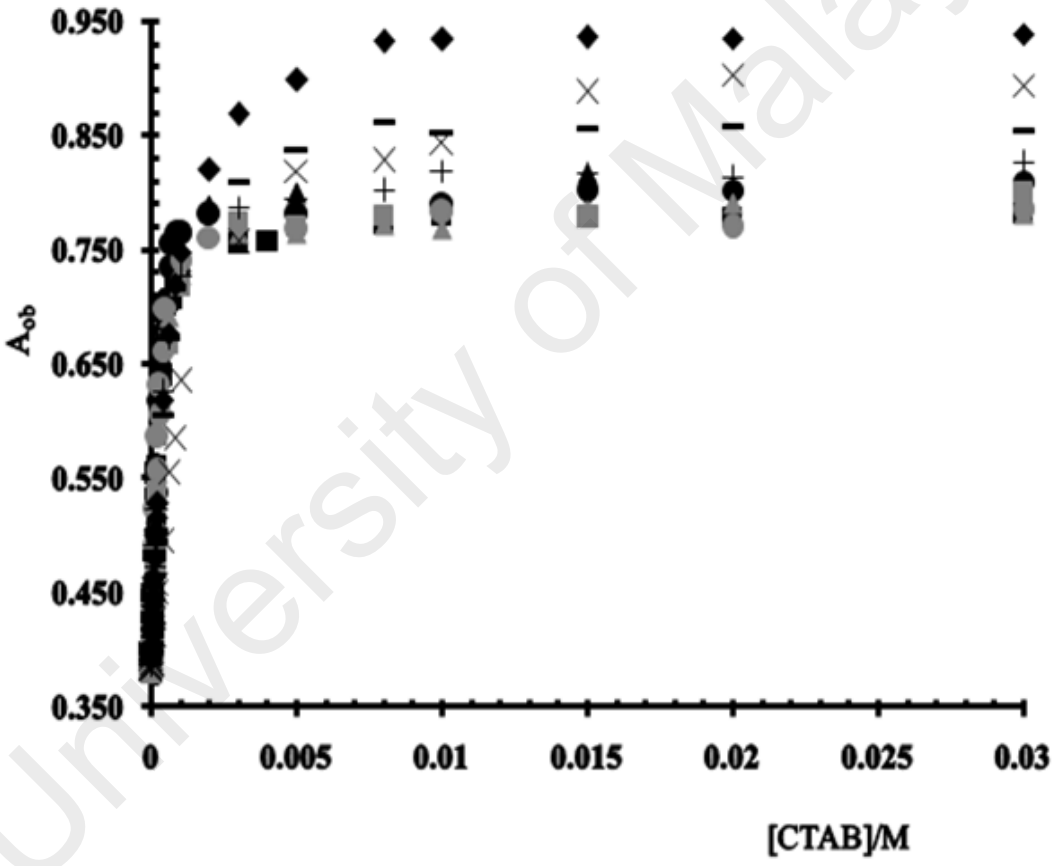

Figure 3.8: Plots showing the monotonic increase of A_{ob} with increasing values of $[CTABr]_T$ at 370nm for [NaBr] = 0.000 M (●), 0.002 M (▲), 0.005 M (■), 0.010 M (●), 0.020 M (▲), 0.030 M (■), 0.050 M (+), 0.100 M (-), 0.300 M (♦) and 0.500 M (×)

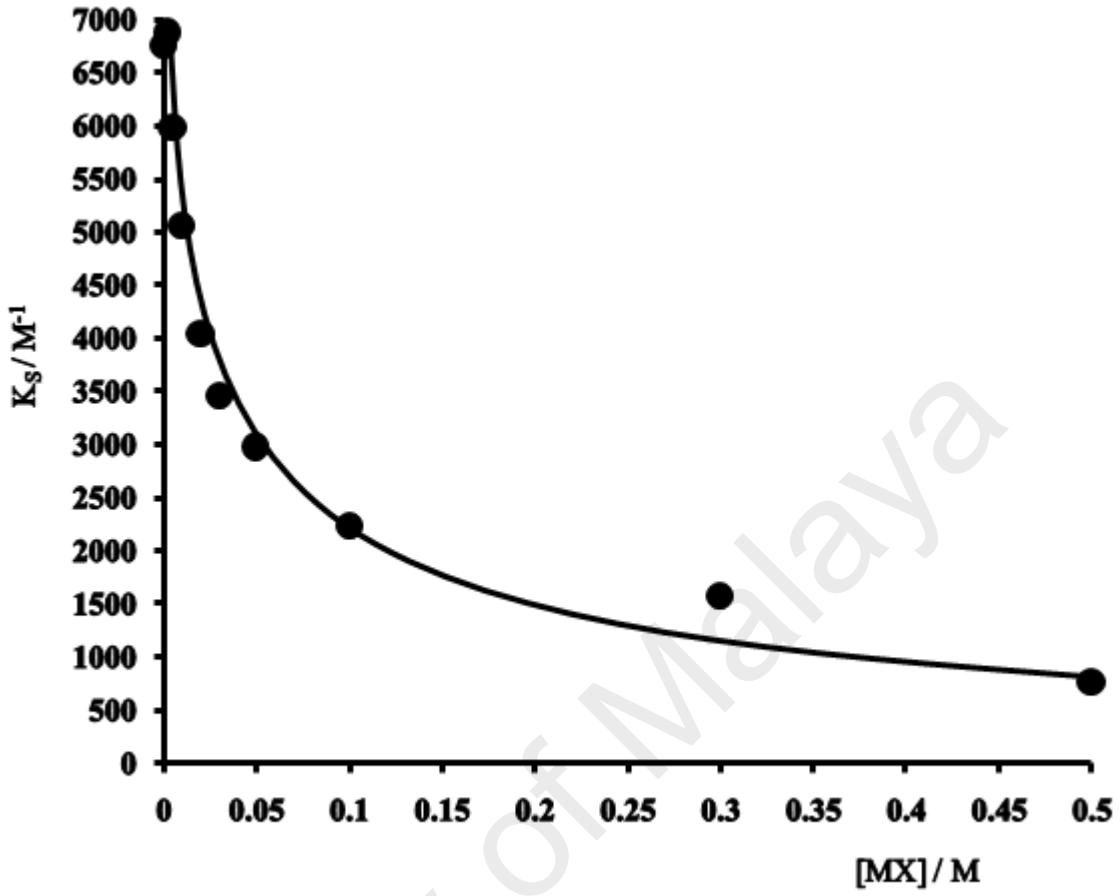

Figure 3.9: Plot of K_S *vs.* $[MX]_T$ (MX = NaBr) where solid line is drawn through the calculated data points.

The nonlinear decrease in A_{ob}^{cor} of Psa^- at 370 nm due to increase in [NaX] (X^- = 2,6-$Cl_2C_6H_3CO_2^-$) at a constant $[CTABr]_T$ may be attributed to the transfer of micelle-bound S^- (i.e. PSa^-_M) to the bulk water phase through ion exchange X^-/S^- since the value of A_{ob}^{cor} is slightly more than 2-fold larger in CTABr micellar psudophase than that in the bulk water phase (Figure 3.7).

Table 3.2: Values of parameters, A_M and K_S, calculated from Eq. (3.8) at 370nm[a]

MX	NaBr [M]	10^5 cmc_{calcd} [M]	10^5 cmc_{exp} [M]	A^0_0	A_{ob}^0	$K_{S\ exp}$ [M^{-1}]	$K_{S\ calcd}$ [b] [M^{-1}]	$CTABr_T$ [M]
NaBr[b]	0.000	8.0	8.0	0.385	0.8120 ± 0.008	6750 ± 740	-	0 – 0.03
	0.000	8.0	8.0	0.371	0.8000 ± 0.010	7220 ± 970	-	0 – 0.03
	0.002	6.8	6.7	0.380	0.8116 ± 0.006	6869 ± 300	6414	0 – 0.03
	0.005	6.4	6.0	0.381	0.7876 ± 0.009	5980 ± 542	5970	0 – 0.03
	0.010	4.3	4.8	0.383	0.8034 ± 0.011	5055 ± 381	5350	0 – 0.03
	0.020	5.4	5.4	0.382	0.7937 ± 0.007	4037 ± 275	4437	0 – 0.03
	0.030	3.4	3.4	0.381	0.8007 ± 0.008	3447 ± 351	3788	0 – 0.03
	0.050	3.2	2.5	0.383	0.8293 ± 0.004	2972 ± 116	2931	0 – 0.03
	0.100	2.7	2.6	0.383	0.8746 ± 0.004	2230 ± 86	1872	0 – 0.03
	0.300	2.0	2.1	0.393	0.9574 ± 0.002	1765 ± 25	766	0 – 0.03
	0.500	0.0	0.0	0.381	0.9215 ± 0.006	759 ± 33	481	0 – 0.03

[a] [phenyl salicylate] = 2 x 10^{-4}mol/dm^3, [NaOH]= 0.03 mol/dm^3, 35°C, reaction mixture for each measurement contains 2% v/v CH_3CN. [b]calculated values of K_S by the use of Eq. (3.1) with K_S^0 = 6748 ± 435 M^{-1} and $K_{X/S}$ = 26 ± 6 M^{-1}

Table 3.3: Values of the empirical constants θ and $K^{X/S}$, calculated from Eq. (3.2)

[CTABr]T/ Mm	A_W	A_M	$10^2\theta$ [s^{-1}]	$K^{X/S}$ [M^{-1}]	$K_{X/S}$ [a] [M^{-1}]	$F_{X/S}$ [b]	$K_{X/S}^n$ [c] [M^{-1}]	$10^4\Sigma di^2$	%RE	R_X^{Br} [d]	R_X^{Br} [e]	R_X^{Br} [f]
6	0.296	0.806	31.6 ±2.9	3.2± 0.4	137.6	0.96	132.1	9.439	1.8	5.07	4.08	5.00
7	0.267	0.763	31.2 ±2.1	2.5± 0.2	125.4	0.91	113.9	3.837	1.1	4.56	4.00	-
10	0.268	0.718	29.7 ±3.9	1.7± 0.2	124.1	0.94	116.1	2.155	1.3	4.64	4.83	-

[a] $K_{X/S} = K^{X/S}(1+K_S^0[CTABr]_T)$ where K_S^0 = 7000 M^{-1}. [b] $F_{X/S} = (A_M - \theta)/(A_M - A_W)$. [c] $K_{X/S}^n = (F_{X/S})(K_{X/S})$. [d] The value of R_X^{Br} obtained experimentally from SESp technique where $R_X^{Br} = K_{X/S}^n / K_{Br/S}$ with $K_{Br/S}$ = 26 M^{-1}. [e] Ref (Yusof et al., 2013). [f] Ref (Magid et al., 1997)

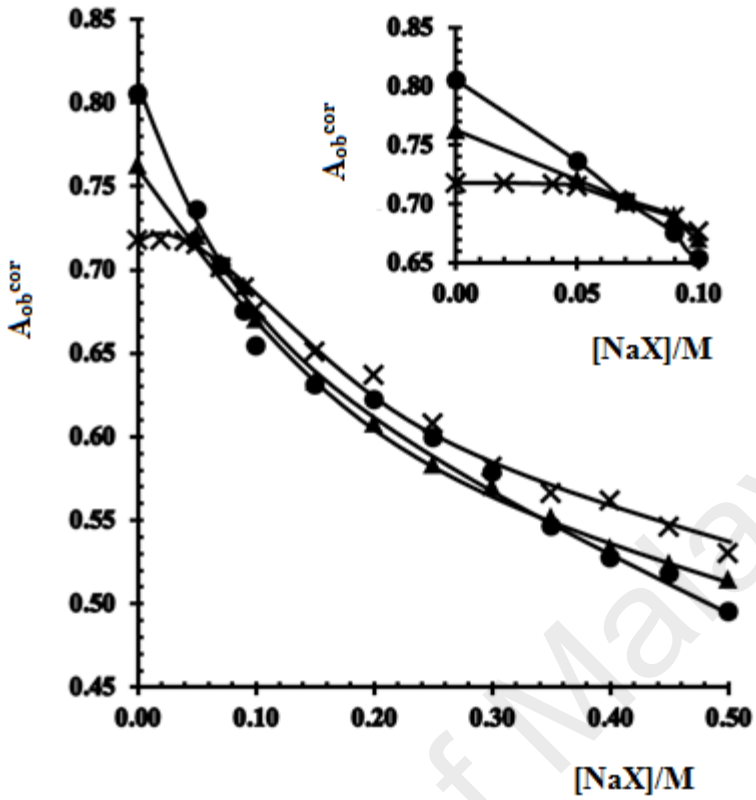

Figure 3.10: Effects of [NaX] (X^- = 2,6-$Cl_2C_6H_3CO_2^-$) on A_{ob}^{cor} (corrected initial absorbance due to Psa^- at 370 nm and 35°C) of aqueous mixtures containing 2% v/v CH_3CN, 0.2 Mm PsaH**,** 30 Mm NaOH and $[CTABr]_T$/Mm= 6.0 (●), 7.0 (▲) and 10.0 (×). The solid lines are drawn through the calculated data points using Eq. (3.2) with parameters (θ, $K^{X/S}$), listed in Table 3.3**.**

It is perhaps pertinent to mention that the experimentally determined mean value of K_S^0 (=6.99 × 10^3 M^{-1}) may be used to calculate the fraction of $[S^-]$ bound to CTABr micelles (f_{SM} = $[Psa^-_M]/[Psa^-]_T$ where subscript M stands for micelles) at a constant $[CTABr]_T$. Such calculated values of f_{SM} are 0.98, 0.98 and 0.99 at 6.0, 7.0 and 10.0 Mm CTABr, respectively. Experimentally determined data, A_{ob}^{cor} *vs*. [NaX], with X^-= 2,6-$Cl_2C_6H_3CO_2^-$, at a constant 6.0 Mm CTABr were found to fit to Eq. (3.2) reasonably well with $[MX]_0^{op}$ = 0. The nonlinear least-squares calculated values of unknown parameters, θ and $K^{X/S}$, are shown in Table 3.3. The observed data, A_{ob}^{cor} *vs*. [NaX], obtained at 7.0 and 10.0 Mm CTABr were also fit to Eq. (3.2) satisfactorily with

nonlinear least-squares calculated values of θ and $K^{X/S}$ as summarized in Table 3.3. The extent of reliability of the observed data fit to Eq. (3.2) is evident from the standard deviations associated with the calculated values of θ and $K^{X/S}$ as well as from the maximum % residual errors as shown in Table 3.3.

CHAPTER 4

CATALYTIC EFFECT OF FLEXIBLE NANOPARTICLE, FN (CTABr/NaX/H_2O; X= Cl, Br) ON THE PIPERIDINOLYSIS OF PSa^-

4.1 Introduction

Wilhelm Ostwald was the first to emphasize the effects of a catalyst on the rate of a chemical reaction, and his famous definition of a catalyst was "a catalyst is a substance that changes the velocity of a chemical reaction without itself appearing in the end products" (Khan, 2006). Research on nanoparticles/nanomaterials has now become a cutting-edge area of chemical research (Stang, 2012). Mono- and bilayer aqueous surfactant aggregates are cationic nanoparticles (CNs) that have been known for their characteristic physicochemical properties for more than 100 years (Menger, 1979). Studies on the catalytic effects of mono- and bilayer aqueous surfactant aggregates/nanoparticles on reaction rates started only nearly six decades ago (Fendler & Fendler, 1975; Fendler, 1982; Khan, 2006). These studies have revealed very complex mechanistic aspects of micellar/nanoparticle catalysis on reaction rates (Fendler, 1982; Khan, 2006; Bunton & Savelli, 1987).

Effects of inert counter ionic salts on pseudo-first-order rate constants (k_{obs}) for ionic surfactant nanoparticle catalyzed semi-ionic bimolecular reactions, in which the ionic reactant is also a counter ion, have been explained quantitatively by use of the pseudophase ion-exchange micellar model (Romsted, 1984). However, some inherent weaknesses of this model have also been realized (Germani et al., 1993; Khan, 2002). An increase in [MX] from 0.0 to 0.3 M (MX=3-FBzNa and 4-FBzNa, $Bz^-=C_6H_4CO_2^-$) causes more than a tenfold nonlinear increase in k_{obs} for the piperidinolysis of anionic phenyl salicylate (PSa^-) at a constant concentration of the cationic micelles (Yusof & Khan, 2010). However, the values of k_{obs} remain independent of [MX] within the 0.0-0.3 M range in the absence of cationic micelles/nanoparticles (Yusof & Khan, 2010). Thus, cationic surfactant/MX/H_2O nanoparticles act as a catalyst. The value of k_{obs} is more than tenfold larger for the reaction in the bulk aqueous phase than in the

pseudophase of surfactant/MX/H_2O FNs. Thus, it is apparent in terms of mechanistic details of this catalytic reaction (Yusof & Khan, 2010) that the source of catalysis is the transfer of PSa^- from the pseudophase of the CNs to the aqueous phase through X^-/PSa^- ion exchange at the surface of the CN catalyst. The significant catalytic effects of cationic surfactant/MX/H_2O nanoparticles (with different MX) have not been emphasized or discussed in earlier reports (Khan, 2006; Khan, 2002; Yusof & Khan, 2010; Khan, 2010). The bromide ion has been considered as reference counter ion that is used to determine the aqueous relative CTABr micellar/nanoparticle binding constant of other counter ions (CTABr=cetyltrimethylammonium bromide) (Khan, 2010). Because of this reason, the catalytic effects of CTABr/NaX/H_2O (X=Br, Cl) nanoparticle catalysts on k_{obs} for the nucleophilic substitution reaction of piperidine (Pip) with PSa^- were studied, for the first time, in the present study. The results and their plausible mechanistic explanations are described.

4.2 Materials and Methods

4.2.1 Reagents

Reagent-grade chemicals such as cetyltrimethylammonium bromide ($C_{16}H_{33}NMe_3Br$, CTABr), phenyl salicylate (PSaH), and piperidine (Pip) were commercial products of highest available purity. All other common chemicals used were of reagent grade. Because of low aqueous solubility, stock solutions (0.01M) of PSaH were prepared in acetonitrile.

4.2.2 Kinetic Measurements

Kinetic measurement of the reaction rates for the nucleophilic substitution reaction between Pip and ionized phenyl salicylate (PSa^-) were performed at 35°C. The rate of disappearance of PSa^- as a function of reaction time (t) was monitored at λ=370 nm by using a Shimadzu double beam UV/Vis spectrophotometer (Model UV-1650) equipped with an electronically controlled thermostatic cell compartment set at 35°C.

In a typical kinetic run, the reaction mixture (of total volume 4.9 mL) containing 30 mM NaOH, 100 mM Pip, a constant value of $[CTABr]_T$ (6, 7, or 10 mM), and a constant value of [NaX] (NaX=NaBr, NaCl) was equilibrated at 35°C (by using a thermostated water bath) for a few minutes. The reaction was then initiated by adding 10 mM PSaH in MeCN (0.1 mL, added by using a 100 μL Hamilton syringe). Nearly 2.5 mL of the temperature-equilibrated mixture was then quickly transferred to a quartz cuvette and kept in an electronically controlled thermostatic cell compartment set at a constant temperature. The total volume of the mixture, in each kinetic run, was 5.0 mL, which contained 2 and 98% *v*/*v* acetonitrile and water, respectively. The values of [NaX] were varied within the 0.0 - ≤ 2.0 M range for $X^- = Br^-$ and within the 0.0 - ≤ 3.0 M range for $X^- = Cl^-$. The absorbance values (A_{ob}) at different reaction times, *t*, were found to fit to Equation (4.1) for about eight half-lives of the reactions.

$$A_{ob}=[R_0]\delta_{ap}\exp(-k_{obs}t)+A_\infty \tag{4.1}$$

in which $[R_0]$ represents the initial concentration of PSaH, δ_{ap} is the apparent molar absorptivity of the mixture, k_{obs} is the pseudo-first-order rate constant, and $A_\infty=A_{ob}$ at $t=\infty$. The nonlinear least-squares fitting of the observed data (A_{ob} vs. *t*) to Equation (4.1) was found to be satisfactory in terms of percent residual error [$RE=100\times(A_{obi}-A_{caldi})/A_{obi}$, in which A_{obi} and A_{caldi} represent respective observed and least-squares calculated values of absorbance at the *i*-th reaction time] and standard deviations associated with the calculated values of kinetic parameters k_{obs}, δ_{ap}, and A_∞. The products of the reaction of Pip with PSa^- were sodium *N*-piperidinyl salicylate and phenol.

4.2.3 Rheological Measurements

Samples with a total volume of 10 mL for each sample in the steady-shear rheological measurements were prepared by mixing a desired amount of sodium hydroxide, piperidine, cetyltrimethylammonium bromide (CTABr), phenyl salicylate, and MX (=NaBr). The concentrations of MX were varied within the 0.05-2.0 M range. The rheological measurements were performed with an Anton Paar MCR301 rheometer

by using a double gap cylinder, DG26.7/T200/SS (internal diameter 24.656 mm, external diameter 26.661 mm) at 35°C. The sample solution was left in the double gap cylinder coated with a Peltier temperature control unit until a constant temperature of 35°C was achieved. Test modes employed were the step rate/start-up flow test and flow curve test. In the step rate test, a constant shear rate, $\dot{\gamma}$ (range 0.01-5 s^{-1}) was applied for a maximum time of 300 s for each sample. This test showed that the stress growth coefficient leveled off at 10-20 s to the steady shear viscosity (η). In the flow curve test, the values of η were measured over a wide range of shear rates (0.01 - 1000 s^{-1}). In this test, the logarithmic preset for the flow test profile was chosen and the duration of the variable logarithmic measuring points was preset, beginning at t = 100 s and ending at t=10s. For every repeat measurement, a new sample was used.

4.3 Results and Discussion

4.3.1 Effects of [NaX] (X=Br, Cl) on k_{obs} of the Reaction of Piperidine with PSa^- at Constant $[CTABr]_T$ and at $[CTABr]_T$=0 and 35°C

A series of kinetic runs were performed within the 0 ≤ [NaBr] ≤ 2.0 M range at constant $[CTABr]_T$ (within 6-10 mM), 0.2 mM PSaH, 0.1 M Pip, and 30 mM NaOH. The results are shown graphically as k_{obs} *vs*. [NaBr] plots at 6, 7, and 10 mM CTABr (Figure 4.1). Similar observations were obtained with NaCl, and the results of this reaction system are shown in Figure 4.2. The plots of Figure 4.1 reveal an approximate threefold nonlinear increase in k_{obs} with an increase in [NaBr] from 0.0 to 2.0 M. To find out if such an effect of [NaBr] on k_{obs} is merely due to salt effects/ionic strength effects, a few kinetic runs were performed at different [NaBr] within the 0.0-2.0 M range at 0.2 mM PSaH, 0.1 M Pip, and 30 mM NaOH. A mild negative salt effect of the values of k_{obs} was observed. These result clearly demonstrate that aqueous nanoparticles ($[CTABr]_T$/NaX/H_2O) for X=Br and Cl act as nanoparticle catalysts. It is also relevant to note that the values of k_{obs} at [NaX]=0 and 6 mM ≤ $[CTABr]_T$ ≤ 10 mM were more than about tenfold smaller than the value of k_{obs} at $[CTABr]_T$=[NaX]=0 (X=Br, Cl).

The reported values of cmc_1 (critical aqueous concentration of CTABr at which spherical micelles begin to form) and cmc_2 (critical aqueous concentration of CTABr at which rodlike/cylindrical micelles begin to form) are 0.8 (Kunitake et al., 1980) and 100 mM (Geng et al., 2006) in the absence of any additive, respectively. The value of cmc_1 dropped to 0.2 mM in the presence of 0.2 mM PSa^- and 30 mM NaOH (Khan & Arifin, 1996). Rheological measurements on aqueous samples containing 6, 7, or 10 mM CTABr; 0.2 mM PSaH; 30 mM NaOH; 0.1 M Pip; and varying values of [NaBr] within the 0.05-2.0 M range at 35°C revealed a Newtonian fluid system within the shear rate range of $1\text{-}10^3$ s^{-1}. The shear viscosity of all samples remained similar to that of pure water. In view of these observations, the structure of the nanoparticles (CTAB/NaBr/H_2O) is essentially spherical within the $[CTABr]_T$ range of 6 to 10 mM and the [NaBr] range of 0.0 to ≤ 2.0 M at 35°C.

The experimental data (k_{obs} *vs*. [NaX]), exhibited by the plots in Figures 4.1 and 4.2, were found to fit to empirical Equation (4.2) (with $[NaX]_0^{op}=0$ for X=Br and $[NaX]_0^{op}\neq 0$ for X=Cl)

$$k_{obs} = \frac{k_0 + k_X([NaX]-[NaX]_0^{op})}{1+K^{X/S}([NaX]-[NaX]_0^{op})} \tag{4.2}$$

in which $k_0=k_{obs}$ at $[NaX]-[NaX]_0^{op}=0$ and $[NaX]_0^{op}$ represents the optimum concentration of [NaX] below which the values of k_{obs} are independent of [NaX]. The kinetic parameters k_X and $K^{X/S}$ represent empirical constants.

The empirical constant k_X is the nanoparticle ([CTAB]/[NaX]/[H_2O])-catalyzed apparent pseudo-second-order rate constant for the nucleophilic reaction of Pip with PSa^-. This is evident from the fact that under limiting conditions for which $1 \gg K^{X/S}\times([NaX]-[NaX]_0^{op})$ (which may be correct at very low values of [NaX] and $K^{X/S}$), Equation (4.2) reduces to Equation (4.3):

$$k_{obs} = k_0 + k_X\left([NaX]-[NaX]_0^{op}\right) \tag{4.3}$$

which may also be used to calculate the value of k_X. The values of $[NaX]_0^{op}$ were calculated by using an iterative technique as described elsewhere (Yusof & Khan, 2010).

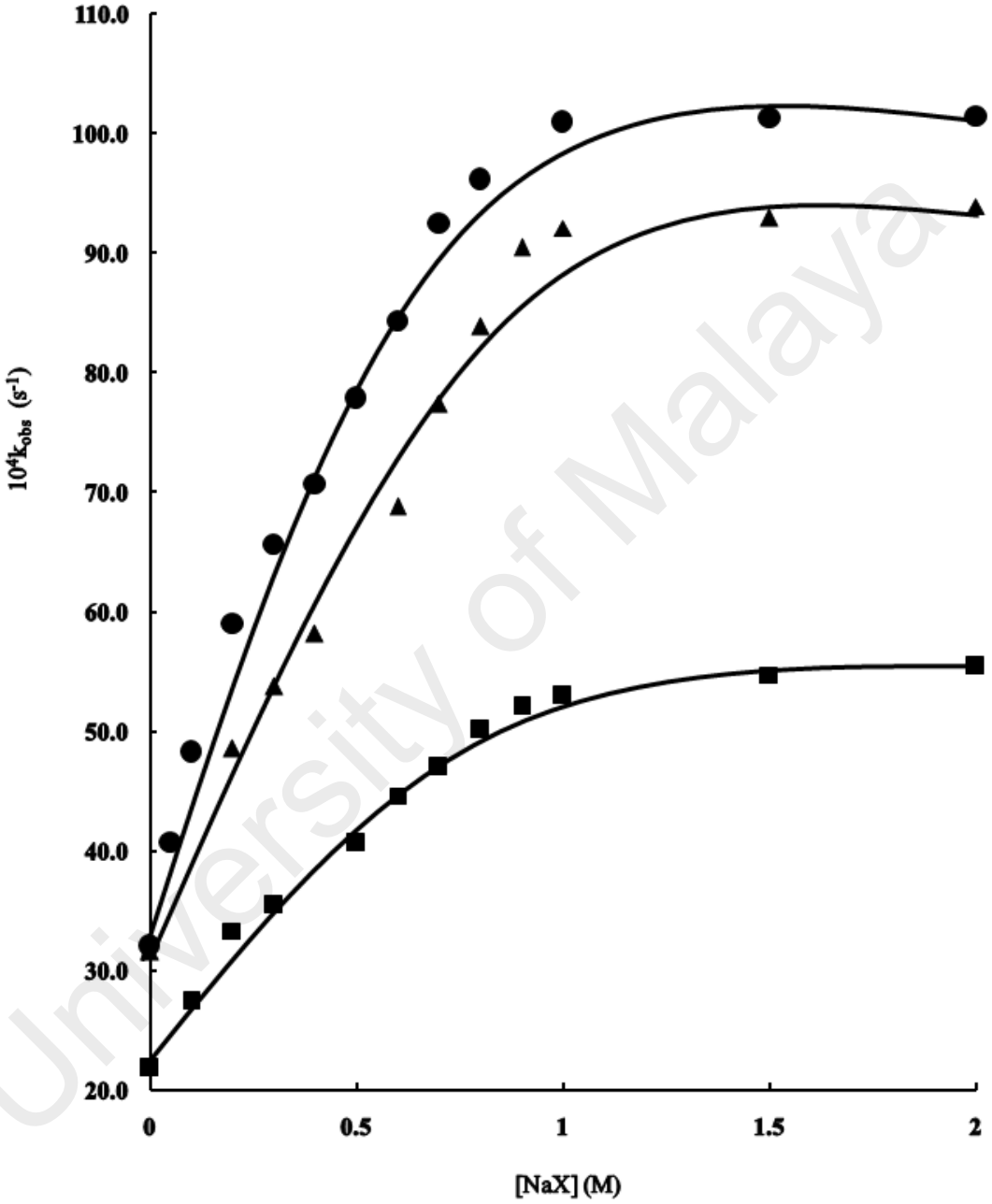

Figure 4.1: Plots showing the effects of nanoparticles, ($CTABr/NaX/H_2O$) with X=Br, on k_{obs} for the piperidinolysis of PSa^- in aqueous mixtures containing 2% *v*/*v* CH_3CN, 0.2 mM PSaH, 30 mM NaOH, 0.1 M piperidine, and $[CTABr]_T$=6 (•), 7 (▲), and 10 mM (▪).

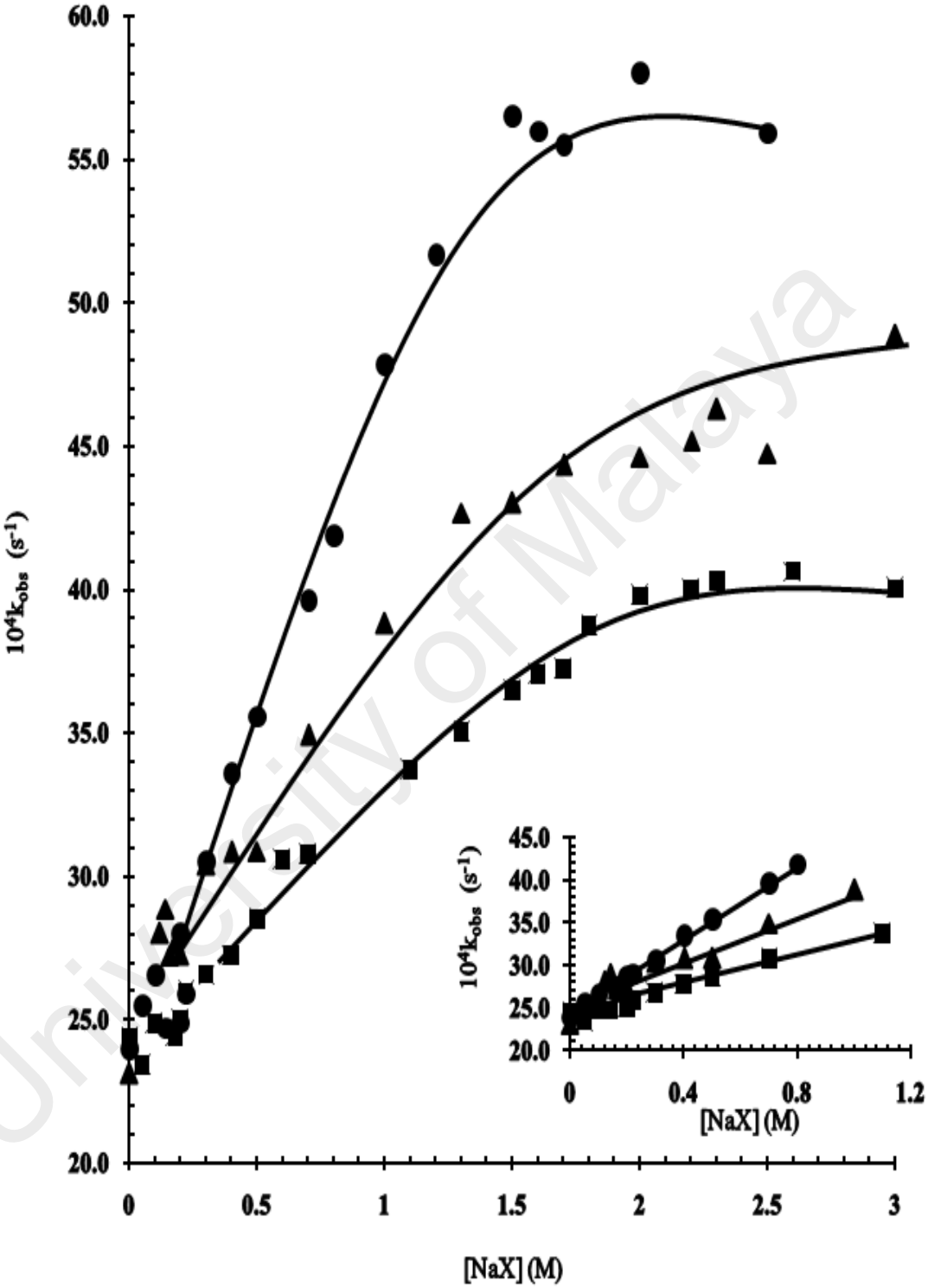

Figure 4.2 Plots showing the effects of nanoparticles, (CTABr/NaX/H_2O) with X=Cl, on k_{obs} for the piperidinolysis of PSa^- in aqueous mixtures containing 2% *v*/*v* CH_3CN, 0.2 mM PSaH, 30 mM NaOH, 0.1 M piperidine, and $[CTABr]_T$=6 (•), 7 (▲) and 10 mM (▪).

As described in detail elsewhere (Yusof & Khan, 2010; Khan, 2010), the value of $[NaX]_0^{op}$ represents the optimum value of [NaX] required for the occurrence of an ion-exchange process of the type X^-/HO^- or X^-/Br^- if $X^- = Cl^-$ and only X^-/HO^- if $X^-=Br^-$. The nonlinear least-squares technique was used to calculate the values of k_X and $K^{X/S}$ from Equation (4.2) by considering k_0 as a known parameter. The values of k_0 were obtained experimentally by performing kinetic runs at [NaX]=0 and $[CTABr]_T \neq 0$. The calculated values of k_0, k_X, and $K^{X/S}$ at different $[CTABr]_T$, for X=Br and Cl, are summarized in Table 4.1.

The extent of reliability of the observed data fit to Equation (4.2) is evident from the plots of Figures 4.1 and 4.2 in which solid lines are drawn through the least-squares calculated data points. The standard deviations, associated with the calculated values of k_X and $K^{X/S}$, also reflect the extent of reliability of the observed data fit to Equation (4.2).

The observed data (k_{obs} *vs*. [NaX]), obtained for the present and related probe reaction systems by using different inert counter ionic salts (NaX), were explained quantitatively by using Equation (4.2) by replacing the empirical constant k_X with $\theta \times K^{X/S}$, in which θ represents an empirical constant. The values of k_{obs} *vs*. [NaX], exhibited by Figures 4.1 and 4.2, were also used to calculate θ and $K^{X/S}$ from Equation (4.2) by replacing k_X with $\theta \times K^{X/S}$ by using the nonlinear least-squares technique. The calculated values θ and $K^{X/S}$ at different $[CTABr]_T$ are shown in Table 4.1 for X=Br and Cl. Notably, the values of $K^{X/S}$ and k_{cald} (at each observed data point) remained unchanged upon replacement of k_X by $\theta \times K^{X/S}$ in Equation (4.2). Similar observations were found in a recent related study (Razak et al., 2014).

4.3.2 Catalytic Mechanism of Nanoparticle ([CTABr]/[NaX]/[H_2O])-Catalyzed Piperidinolysis of PSa^-, in which X=Br, Cl

The values of k_{obs} ($=k_0$) at different $[CTABr]_T$ (within the 6-10 mM range and at [NaX]=0, Table 4.1) are about ten fold smaller than those of k_{obs} ($=k_W$) at $[CTABr]_T$=[NaX]=0[10]. The nonlinear increase in k_{obs} with an increase in [NaX] at

constant $[CTABr]_T$ (Figure 4.1, 4.2) cannot be attributed to ionic strength or specific salt effects for the reason that the effects of [NaX] on k_{obs} at $[CTABr]_T$=0 are only moderate negative salt effects, as mentioned above. Similarly, the values of pseudo-first-order rate constant (k_M) for the nucleophilic reaction of Pip with PSa^- in CTABr micellar pseudophase or inside a nanoparticle (CTABr/NaX/H_2O) spheroidal structural phase for X=Br were essentially unaffected with an increase in [NaX] from 0.04 to 0.50 M (Khan et al., 2000). Thus, the clearest source for positive nanoparticle (CTABr/NaX/H_2O) catalysis (Figures 4.1 and 4.2) is the transfer of nanoparticle-trapped or nanoparticle-bound PSa^- ions (i.e. PSa^-_M ions) to the bulk aqueous phase through the occurrence of a X^-/PSa^- ion-exchange process because the value of k_{obs} is more than tenfold larger in the aqueous phase than in the nanoparticle spheroidal structural phase. All plausible ion-exchange processes, in the nanoparticle-catalyzed reaction system, are X^-/PSa^-, X^-/HO^-, HO^-/PSa^-, and X^-/Br^- (if X=Cl). However, in view of the explanation described elsewhere (Yusof & Khan, 2010; Khan, 2010) the most effective ion-exchange process that could significantly affect k_{obs} is X^-/PSa^- under the experimental conditions of this study.

Table 4.1 Values of empirical constants, k_X, and $K^{X/S}$ at 35°C in the presence of CTABr/NaX/H_2O nanoparticles.[a]

$[Sur]_T$ [mM]	$[NaX]_0^{op}$ [M]	10^3 k_W[b] [s^{-1}]	10^4 k_0[c] [s^{-1}]	10^3 k_X [M^{-1} s^{-1}]	$K^{X/S}$ [M^{-1}]	103 θ [s^{-1}]	$F_{X/S}$[d]	${}^nK^{X/S}$ [M^{-1}]	$K_{X/S}$[e] [M^{-1}]	$K^n_{X/S}$[f] [M^{-1}]	Structure[g]	K^{Cl}_{Br}
NaX; X = Br												
6	0	32.0	32.1±1.7[h]	18.9±1.5[h]	1.18±0.17[h]	16.2±1.0[h]	0.50	0.590	50.7	25.4	SM	2.3[i]
7	0	32.0	31.6±0.9	15.9±3.1	1.24±0.36	12.8±1.2	0.40	0.496	62.0	24.8	SM	2.4
10	0	32.0	21.9±0.5	11.1±1.1	1.59±0.26	6.92±0.33	0.22	0.350	113	24.8	SM	3.3
NaX; X = Cl												
6	0.23	30.2	23.9±0.4	8.40±0.94	1.12±0.17	7.50±0.3	0.25	0.280	48.1	11.9	-	2.1[j]
7	0.18	30.3	23.1±0.4	6.64±0.72	1.21±0.16	5.50±0.2	0.18	0.218	60.4	11.0	-	2.3
10	0.19	30.1	24.3±0.2	3.40±0.33	0.674±0.085	5.00±0.2	0.17	0.114	47.9	8.0	-	3.1

[a] [PSaH]=0.2 mM, λ=370 nm, 30 mM NaOH, 100 mM Pip, aqueous mixture for each kinetic run contained 2% *v*/*v* CH_3CN, Sur=CTABr, and [NaX] range for X=Br at 6, 7, and 10 mM $[CTABr]_T$ was 0.0-2.0 M and for X=Cl at 6 mM CTABr range was 0.0-2.5 M, whereas at 7 and 10 M CTABr, [NaX] range was 0.0-3.0 M. [b] The value of k_W is the mean value of k_{obs} obtained within the [NaBr] range for which the k_{obs} values remained independent of [NaBr] at $[CTABr]_T$=0. [c] The value of k_0 is the mean value of the k_{obs} values obtained within the [NaX] range 0.0-≤$[NaX]_0^{op}$ at $[CTABr]_T \neq 0$. [d] $F_{X/S}=k_X/(k_W \times K^{X/S})$. [e] $K_{X/S}=K^{X/S}\times(1+K_S^0[CTABr]_T)$, for which $K_S^0=7\times10^3 M^{-1}$. [f] $K^n_{X/S}=K_{X/S}\times F_{X/S}$. [g] Structure of CTABr/NaX/H_2O, SM=spherical micelles. [h] Error limits are standard deviations. [i] $K^{Cl}_{Br}=k_{Br}/k_{Cl}$. [j] $K^{Cl}_{Br}=K^n_{Br/S}/K^n_{Cl/S}$.

The occurrence of the X^-/S^- (S^-=PSa^-) ion-exchange process in related reaction systems was found to decrease the nanoparticle (CTAB/NaX/H_2O) binding constant (K_S) of PSa^- with an increase in [NaX] through the empirical relationship shown in Equation (4.4):

$$K_S = \frac{K_S^0}{(1 + K_{X/S}[NaX])} \tag{4.4}$$

in which K_S^0=K_S at [NaX]=0 (Khan, 2006; Yusof & Khan, 2010; Khan et al., 2000). The magnitude of the empirical constant $K_{X/S}$ is the measure of the ability of the X^- counter ion to expel another S^- counter ion from the structural phase of the cationic nanoparticles (CTAB/NaX/H_2O) to the bulk aqueous phase through the occurrence of the X^-/S^- ion-exchange process at the cationic nanoparticle surface. It can be easily shown that the reaction mechanism for the nucleophilic reaction of Pip with PSa^-, expressed in terms of the pseudophase micellar (PM) model, and Equation (4.3), with replacement of X by Br, can lead to Equation (4.2) (Khan, 2010) with k_X and $K^{X/S}$ expressed by Equations (4.5) and (4.6), respectively. In Equation (4.5), k_W=k_{obs} at [NaX]=$[CTABr]_T$=0 and $F_{X/S}$ (=θ/k_W)

$$k_X = F_{X/S} k_W K^{X/S} \tag{4.5}$$

$$K^{X/S} = \frac{K_{X/S}}{(1 + K_S^0[CTABr]_T)} \tag{4.6}$$

is an empirical constant, the magnitude of $F_{X/S}$ should vary in the range of >0.0 to ≤1.0 (Khan, 2010). Equation (4.6) is valid only under the experimental conditions of $[CTABr]_T$-cmc1≈$[CTABr]_T$. Notably, the value of cmc1 for CTABr, at 0.2 mM PSa^- and [NaX]=0, was kinetically determined to be 0.09 mM, and this value changed to 0.04 mM at 0.1 M NaBr. The value of cmc1 became about 0 at ≥ 0.5 M NaBr (Khan et al., 2000). These observations demonstrate that the value of cmc1 is negligible compared to $[CTABr]_T$ at its value of ≥5 mM.

The value $F_{X/S}$ measures the fraction of the nanoparticle-bound counter ions (PSa^-_M) transferred to the aqueous phase by the optimum concentration of NaX through X^-/PSa^- ion exchange (Khan, 2010). The values of $F_{X/S}$ were calculated from Equation (4.5) by using

the listed values of k_W, k_X, and $K^{X/S}$ in Table 4.1, and these values of $F_{X/S}$ are also listed in Table 4.1. The values of $K_{X/S}$ were calculated from Equation (4.6) with the reported value of K_S^0(=7×10^3 M^{-1}) (Bunton & Savelli, 1987; Khan; 2002). The calculated values of $K_{X/S}$ for NaX are also listed in Table 4.1. Equations (4.5) and (4.6) or Equation (4.6) can lead to Equation (4.7):

$$^{n}K^{X/S} = \frac{K^{n}_{X/S}}{\left(1 + K^{0}_{S}\left[\text{CTABr}\right]_{T}\right)} \qquad (4.7)$$

in which $K^{n}_{X/S}$ =$F_{X/S}K_{X/S}$. The values of $K^{n}_{X/S}$ were calculated from Equation (4.7) with the reported value of K_S^0(=7×10^{3}M^{-1}) (Khan, 2006; Yusof & Khan, 2010). The calculated values of $^{n}K^{X/S}$ (=$F_{X/S}K^{X/S}$) and $K^{n}_{X/S}$, at different [CTABr]$_T$, are shown in Table 4.1. As expected in view of Equation (4.7), the values of $^{n}K^{X/S}$ show a decrease with an increase in [CTABr]$_T$, whereas the values of $K^{n}_{X/S}$ are almost independent of [CTABr]$_T$. The mean value of $K^{n}_{X/S}$ (=24.8±0.1 M^{-1} for X=Br) is similar to that obtained earlier by the use of Equation (4.4) (with replacement of X by Br) by using observed data (K_S vs. [NaBr]) (Khan et al., 2000).

The apparent nanoparticle (CTABr/NaX/H_2O) catalytic efficiency or rate enhancement (μ) for the piperidinolysis of PSa$^-$ may be expressed by the relationship μ=k_X/k_0, in which k_0=k_{obs} at [NaX]=0 and constant [CTABr]$_T$≫cmc1. Such calculated values of μ for X=Br at 35°C are 6, 6, and 5 M^{-1} at 6, 7, and 10 mM CTABr, respectively. The values of μ for X=Cl are about 2.5-fold smaller than the corresponding values of μ for X=Br. The values of μ for X=3-O$^-$Bz$^-$, 4-O$^-$Bz$^-$, and Bz'$^-$(Bz$^-$ =$C_6H_4CO_2^-$, Bz'$^-$=$C_6H_5C0_2^-$) are 5.3-, 3.4-, and 12.8-fold larger than μ for X=Br$^-$(Razak et al., 2014; Khan et al., 2010; Khan & Ismail 2010). These observations reveal that electrostatic interaction appears to be less effective than the hydrophobic interaction between X$^-$ and cationic headgroups of nanoparticles (CTABr/NaX/H_2O) in affecting the values of k_X and μ.

It was concluded elsewhere (Khan, 2006; Khan, 2010) that the normalized values of $K^{n}_{X/S}$ should represent the relationship $K^{n}_{X/S} = \Omega_S K_X / K_S$, in which Ω_S represents the

proportionality constant and K_X and K_S are cationic nanoparticle (CTABr/NaX/H_2O) binding constants of X^- and S^- (=PSa^-), respectively. The magnitude of Ω_S is assumed to depend only on the molecular characteristics of the counter ion (S^-). The magnitude of Ω_S is also assumed to be independent of the molecular characteristics of the X^- counter ion. Thus, the ratio $K^n_{Br/S}/K^n_{Cl/S}$= K_{Br}/K_{Cl}, in which $K_{Br/}$ and K_{Cl} represent cationic nanoparticles binding constants of the Br^- and Cl^- counter ions, respectively. The $K_{Br/}/K_{Cl}$ ratio is known as the ion-exchange constant and is usually represented by K_{Br}^{Cl}. The values of $K^n_{Br/S}$ and $K^n_{Cl/S}$ (Table 4.1) were used to calculate the value of K_{Br}^{Cl} at 6, 7, and 10 mM CTABr, and these values are shown in Table 4.1. The mean value of these calculated values of K^{Cl}_{Br} is 2.5±0.5. The values of K^{Cl}_{Br} were determined by using different physicochemical techniques including semiempirical kinetic (Khan et al., 2010) and spectrophotometric (Khan & Ismail, 2010) methods by using different reaction probes. The reported values of K^{Cl}_{Br} are 1.9, 3.0, 2.2, 2.9, 1.6 (Romsted, 1984), 2.3(Khan, 2002), 2.7 (Khan et al., 2010), 2.3 (Khan & Ismail, 2010), 1.7 (Khan et al., 2008), 2.7 (Cuccovia et al., 1997), 5.0 (Bartet et al., 1980) and 3.1 (Morgan et al., 1994). The value of K^{Cl}_{Br} (=2.5) obtained in the present study is comparable to most of these reported values of K^{Cl}_{Br}.

4.3.3 Empirical Correlation Between the Magnitudes of k_X and the Counter ion (X^-) Binding Constant with Cationic Nanoparticles (CTABr/NaX/H_2O)

The values of k_X (Table 4.2), calculated from the relationship $k_X=\theta\times K^{X/Br}$, for a few different counter ions (X), X=3-O^-Bz^-, 4-O^-Bz^-, 2-$O^-Bz'^-$ (Khan et al., 2010), 2,3-$Cl_2Bz''^-$, 3,5-$Cl_2Bz'''^-$($Bz'''^-=C_6H_3CO_2^-$) (Razak et al., 2014) and Bz^{r-} (Khan & Ismail, 2010) at constant $[CTABr]_T$ within the 5-15 mM range were found to fit to empirical Equation (4.8):

$$k_X=k_{RC}\times R_X^{RC} \qquad (4.8)$$

in which k_{RC} represents an empirical constant and RC represents the Br^- reference counter ion. The magnitude of k_{RC} measures the sensitivity of the values of k_X to the values of R_X^{Br} for the CTABr/NaX/H_2O nanoparticle catalyzed piperidinolysis of PSa^- at constant

$[CTABr]_T$ and 0.1 M Pip. $R_X^{Br} = K_X/K_{Br}$, in which K_X and K_{Br} represent cationic nanoparticle ($CTABr/NaX/H_2O$) structural binding constants of the X and Br counteranions, respectively. Notably, the values of K_X and K_{Br} were derived from the kinetic parameters ($K_{X/S}^n$ and $K_{Br/S}^n$) determined in the presence of nonspherical and spherical micelles/nanoparticles, respectively. Thus, $R_X^{Br} = K_X^{Br}$ if the value of $K_{X/S}^n$ was determined in the presence of spherical micelles.

The values of k_{RC} were calculated from Equation (4.2) by using k_X *vs*. R_X^{Br} data at constant $[CTABr]_T$. These calculated values of k_{RC}, at different $[CTABr]_T$, are shown in Table 4.2. The reliability of data fit to Equation (4.8) is evident from the values of k_X^{cald} (Table 4.2) and from the standard deviations associated with the calculated values of k_{RC} at different $[CTABr]_T$ within the 5-15 mM range. The calculated values of k_{RC} at 6, 7, and 10 mM CTABr (Table 4.2) are not significantly different from the corresponding values of k_X for X=Br determined experimentally, as summarized in Table 4.1. These results indirectly imply that the nanoparticle catalytic reaction mechanism remains unchanged in the presence of all these $CTABr/Na_vX/H_2O$ (v=1, 2) nanoparticles, the structures of which change from spherical/spheroidal-to-short to long wormlike shapes. Under such circumstances, Equation (4.8) can also be used to calculate the value of R_X^{Br}, provided that the k_X value was determined at 35°C, 0.1 M Pip, 0.2 mM PSaH, 30 mM NaOH, and constant $[CTABr]_T$ within the 5-15 mM range. The calculated values of k_X for X=Br and Cl, listed in Table 4.1, were used to calculate the values of R_{Br}^{Cl} (=k_{Br}/k_{Cl}), and these values of R_{Br}^{Cl} are also summarized in Table 4.1. As mentioned above, the structure of the $CTABr/NaX/H_2O$ nanoparticle remains spherical/spheroidal under the experimental conditions for which the values of k_X for X=Br and Cl were determined. Thus, under such conditions, $R_{Br}^{Cl} = K_{Br}^{Cl}$. The mean value of K_{Br}^{Cl} (=2.7±0.6) is similar to the value of K_{Br}^{Cl} (=2.5±0.5) obtained from the relationship $K_{Br}^{Cl} = K_{Br/S}^n / K_{Cl/S}^n$.

Table 4.2. Pseudo-second-order rate constants (k_X) for piperidinolysis of PSa^- in the presence of CTABr and different NaX[a]

$10^3[CTABr]_T$/ mM	5			6			7			10			15		
10^3 k_0/ $[s^{-1}]$	2.87 ± 0.24			2.79 ± 0.30			2.69 ± 0.26			2.56 ± 0.18			2.48 ± 0.20		
MX	10^3k_X $[M^{-1}s^{-1}]$	$10^3k_X^{cald}$ $[M^{-1}s^{-1}]$	R_X^{Br}	10^3k_X $[M^{-1}s^{-1}]$	$10^3k_X^{cald}$ $[M^{-1}s^{-1}]$	R_X^{Br}	10^3k_X $[M^{-1}s^{-1}]$	$10^3k_X^{cald}$ $[M^{-1}s^{-1}]$	R_X^{Br}	10^3k_X $[M^{-1}s^{-1}]$	$10^3k_X^{cald}$ $[M^{-1}s^{-1}]$	R_X^{Br}	10^3k_X $[M^{-1}s^{-1}]$	10^3 k_X^{cald} $[M^{-1}s^{-1}]$	R_X^{Br}
4-NaOBzNa	61.5[b] (21)[d]	59.5[c]	2.6[b]	47.9[b] (17)[d]	45.7[c]	2.4[b]	65.6[b] (24)[d]	61.6[c]	3.8[b]	25.0[b] (10)[d]	27.3[c]	2.5[b]	-	-	-
3-NaOBzNa	99.3 (35)	99.8	4.4	81.0 (29)	81.8	4.3	78.6 (29)	81.1	6.0	53.4 (21)	50.2	4.6	41.8[b] (17)	41.5[c]	5.4[b]
2-NaOBzNa	1221 (425)	1225	54	839 (301)	837	44	716 (286)	714	44	437 (171)	481	44	269 (108)	269	35
2,3-Cl_2Bz"Na	522[e] (182)	544	24[e]	478[e] (171)	495	26[e]	401[e] (149)	422	26[e]	298[e] (116)	295	27[e]	175[e] (71)	176	23[e]
3,5-Cl_2Bz"Na	4713 (1642)	4696	207	3968 (1422)	3977	209	3421 (1272)	3390	209	2377 (929)	2352	206	1544 (822)	1546	201
3-FBzNa	325[f] (113)	324	14.3[f]	231[f] (83)	232	12.2[f]	197[f] (73)	196	12.1[f]	148[f] (58)	141	12.9[f]	95.9[f] (39)	95.3	12.4[f]
$10^3k_{RC}/M^1s^{-1}$	22.7 ± 0.6;			19.0 ± 0.5			16.2 ± 0.6			10.9 ± 0.8			7.69 ± 0.05		

[a] Values of k_X were calculated from the relationship: $k_X = \theta \times K^{X/S}$ where the values of θ and $K^{X/S}$ were obtained from references published elsewhere (Yusof & Khan, 2010; Razak et al., 2014; Khan & Ismail, 2010), Bz = $C_6H_4CO_2^-$, and Bz" = $C_6H_3CO_2^-$. [b] Ref (Khan et al., 2000) [c] Calculated from Eq. (4.8) with the values of k_{RC} and R_X^{Br} listed in Table 4.2. [d] Parenthesized values represent for μ as mentioned in the text. [e] Ref. (Razak et al., 2014) [f] Ref. (Yusof & Khan, 2010)

CHAPTER 5

KINETIC DATA FOR FLEXIBLE NANOPARTICLE CATALYSIS IN THE REACTION OF PIPERIDINE WITH PS^-

5. 1 Introduction

The applications of flexible nanoparticles (FN) or surfactants in the industries encompass wetting and drying agent, laundry detergent, emulsion drilling fluid, asphalt and oil spill emulsion (Clare & Bert, 2015; Jungwirth & Tobias, 2006; Shweta & Santosh 2014; Naskar et al., 2013; Alessandro, 2001). Due to its importance, much research has been pre-established since 1890s to study the chemical and engineering aspects of micelles (Romsted, 2007; Leng et al., 2009). This includes the effects of salts on the micellar/ FN structure (Yusof & Khan, 2010; Yusof et al., 2013; Meenakshi et al., 1999). In late 1890s, Hofmeister had performed an experiment where he added different types of salts in the egg to determine the effect of salts to the egg white solution. The result leads to the findings of Hofmeister series representing the ability of anions and cations to precipitate proteins (Khan & Sinasamy, 2011; Khan & Gambo, 1985).

Menger and Portnoy in 1967 using pre-equilibrium kinetic (PEK) model with proposed concept of micellar phase. But due to the definition which does not seem fit very well with its real representative phase, many researchers suggested the concept of Psudophase Micellar (PM) model to define the entire micellar system and retain with an addition of PEK model assumptions (Codari et al., 2012; Dong-June et al., 2011). However, in 1970s, due to lack of kinetic model to explain quantitatively the kinetic data obtained for semi-ionic bimolecular reactions, Bunton and some others researchers suggested Pseudphase Ion-Exchange Model (PIE) which leads to quantitative and semi-quantitative interpretations of ion exchange phenomenon in micellar system (Antheunis et

al., 2010; Khan, 2010). Due to the importance of the study, many researchers begin to study the effect of salts on counterion binding constant (K_X^{Br}) (Khan, 2006; Bunton, 1991; Bunton, 2006). The catalysis reaction by cationic micelles was also reported in the study of the hydrolysis of 1,3-benzoxazine-2,4-dione and its derivatives (Khan & Ismail, 2009).

This chapter reported the R_X^{Br} values and catalytic constant (k_{cat}) of FN on the rate of piperidinolysis of phenyl salicylate ions with the existence of sodium phenolate, sodium 2-, 3-, 4-ethyl, 2-, 4-propyl and 3-, 4-isopropyl phenolate. In the relation to the above mentioned significance and importance of the research, the objectives of the study are to determine the counterion binding constant (R_X^{Br}) and catalytic constant (k_{cat}) of CNP between reaction of piperidine and phenyl salicylate ions in the presence of sodium phenolates and its substitutes.

5.2 Experimental

5.2.1 Chemicals

Commercial products of highest available purity such as cetyltrimethylammonium bromide, $C_{16}H_{33}NMe_3Br$, (CTABr/ Flexible nanoparticle), phenyl salicylate acid, C_6H_5OH, 2-ethyl C_6H_4OH, 3-ethyl C_6H_4OH, 4-ethyl C_6H_4OH, 2-propyl C_6H_4OH, 4-propyl C_6H_4OH, 3-isopropyl C_6H_4OH, 4-isopropyl C_6H_4OH, piperidine (Pip) and all other common chemicals used were reagent grade. The stock solutions of PSaH=0.01M were prepared in acetonitrile because of its low aqueous solubility. The stock solutions (w M) of nonionic substituted phenols were prepared by adding (w + 0.05 M) sodium hydroxide so that wM XH solutions become wM NaX. 3-propyl C_6H_4OH and 2-isopropyl C_6H_4OH were opted due to the expensive prices of chemicals and the unavailability in the country.

5.2.2 Measurements for the Kinetic Part

The measurements of the kinetic part of the ionized phenyl salicylate (PS^-) were studied at 35°C and the rate of desertion of ionized nanoparticles or substrate (PS^-) as a function of time (t) was determined at the wavelength of 370 nm. UV-vis spectrophotometer (Shimadzu) Model 1650 was used for this experiment. It was set with an electronically monitored thermostatic cell section at 35°C (Yusof et al., 2013). The absorbance values obtained from the experimental were found to fit Eq. (5.1)

$$A_{ob} = [R_0]\delta_{ap}\exp(-k_{obs}t) + A_{\infty} \quad (5.1)$$

In Eq.(5.1), $[R_0]$ represents the initial concentration of phenyl salicylate acid and all other symbols are defined elsewhere (Yusof et al., 2013). It was found that the nonlinear Σdi^2 relationship between absorbance (A_{ob}) *vs*. time (t) and Eq. (5.1) is satisfactory in terms of RE% (RE= $100\times(A_{obi}-A_{caldi})/A_{obi}$ where A_{obi} and A_{caldi} represent respective observed and, Σdi^2 represent the calculated values of the series of A_{ob} to the function of time (t) (Yusof & Khan, 2010). The reaction products of piperidine with phenyl salicylate ion are sodium *N*-piperidinyl salicylate and phenol (Yusof & Khan, 2010; Yusof et al., 2013; Meenakshi et al., 1999).

5.3 Results and Discussion

5.3.1 [MX] Effects on Rate Constant, k_{obs} for the Reation on Piperidine with Phenyl salicylate ion in [CTABr] = 0 at 35°C

The use of SEK method involves an empirical equation to rationalize the kinetically determined data, k_{obs} *vs*. [MX], obtained at a constant $[CTABr]_T$ and temperature. The nature of this empirical equation is apparently different with or without of significant MX

salt effect on k_{obs} obtained at the same temperature but in the absence of CTABr (Yusof & Khan, 2010).

A number of kinetic runs at 0.1M Pip, 0.2 mM phenyl salicylate and different values of [C_6H_5ONa], [2-ethyl C_6H_4ONa], [3-ethyl C_6H_4ONa], [4-ethyl C_6H_4ONa], [2-propyl C_6H_4ONa], [4-propyl C_6H_4ONa], [3-isopropyl C_6H_4ONa], [4-isopropyl C_6H_4ONa] were performed in order to find out probable salt effect on k_{obs}. The values of rate constants for each concentrations of respective salts [MX] is nearly independent of each other within the range of 0.0 – 0.35 M for MX = C_6H_5ONa, 0.0 – 0.25 M for MX = 2-ethyl C_6H_4ONa, 0.0 – 0.30 M for MX = 3-ethyl C_6H_4ONa, 0.0 – 0.30 M for 4-ethyl C_6H_4ONa, 0.0 – 0.25 M for MX = 2-propyl C_6H_4ONa, 0.0 – 0.25 M for MX = 4-propyl C_6H_4ONa, 0.0 – 0.30 M for MX = 3-isopropyl C_6H_4ONa and 0.0 – 0.25 M for MX = 4-isopropyl C_6H_4ONa respectively.

5.3.2 Effects of Sodium Phenolate Substituted Salts, (MX) at 35°C with MX = C_6H_5ONa, 2-ethyl C_6H_4ONa, 3-ethyl C_6H_4ONa, 4-ethyl C_6H_4ONa, 2-propyl C_6H_4ONa, 4-propyl C_6H_4ONa, 3-isopropyl C_6H_4ONa and 4-isopropyl C_6H_4ONa

A series of kinetic runs was carried out at various [MX] (=C_6H_5ONa, 2-ethyl C_6H_4ONa, 3-ethyl C_6H_4ONa, 4-ethyl C_6H_4ONa, 2-propyl C_6H_4ONa, 4-propyl C_6H_4ONa, 2-isopropyl C_6H_4ONa and 3-isopropyl C_6H_4ONa) within [MX] range 0.0 to 0.35 M at [CTABr] = 0.006M, [Pip] = 0.1M and 0.2 mM phenyl salicylate and [NaOH] = 0.03 M. Figures 5.1, 5.2, 5.3 and 5.4 shows the values of k_{obs} for different [MX] = C_6H_5ONa, 2-ethyl C_6H_4ONa, 3-ethyl C_6H_4ONa and 4-ethyl C_6H_4ONa respectively. The values of k_{obs} for [MX] = 2-propyl C_6H_4ONa, 4-propyl C_6H_4ONa, 3-isopropyl C_6H_4ONa and 4-isopropyl C_6H_4ONa are shown in Figures 5.5, 5.6, 5.7, and 5.8. Instead, 10 and 15 mM CTABr also shows similar

observations. The values of k_{obs} at various concentration of salt and cetyltrimethylammonium bromide are depicted in Figures 5.1, 5.2, 5.3, 5.4, 5.5, 5.6, 5.7, and 5.8 for MX = C_6H_5ONa, 2-ethyl C_6H_4ONa, 3-ethyl C_6H_4ONa, 4-ethyl C_6H_4ONa, 2-propyl C_6H_4ONa, 4-propyl C_6H_4ONa, 3-isopropyl C_6H_4ONa and 4-isopropyl C_6H_4ONa, respectively.

5.3.3 Determination of R_X^{Br} for X = $C_6H_5O^-$, 2-ethyl $C_6H_4O^-$, 3-ethyl $C_6H_4O^-$, 4-ethyl $C_6H_4O^-$, 2-propyl $C_6H_4O^-$, 4-propyl $C_6H_4O^-$, 3-isopropyl $C_6H_4O^-$ and 4-isopropyl $C_6H_4O^-$

The hydrolysis rate is considered negligible under the experimental conditions of entire kinetic runs (Yusof et al., 2013; Meenakshi et al., 1999; Khan & Sinasamy, 2011; Khan & Gambo, 1985; Codari et al., 2012; Dong-June et al., 2011; Antheunis et al., 2010). Cetyltrimethylammonium bromide concentration effects on the k_{obs} of Piperidine with PS^-, in the absence and the presence of a constant [MX], have been defined in terms of PM model (Codari et al., 2012).

Pseudophase Micellar (PM) model representing an aqueous solution of surfactant was put under UV-visible radiation at $[Surf]_T$ less and greater than cmc where it remains transparent to the radiation and thus is defined as a single homogenous phase. The micelles cannot be considered as a real phase but technically represent a *pseudophase* which is the reason for the emergence of. PM model retaining all the assumptions introduced in PEK model and considers several assumptions which has been discussed in Chapter 2 in the present thesis.

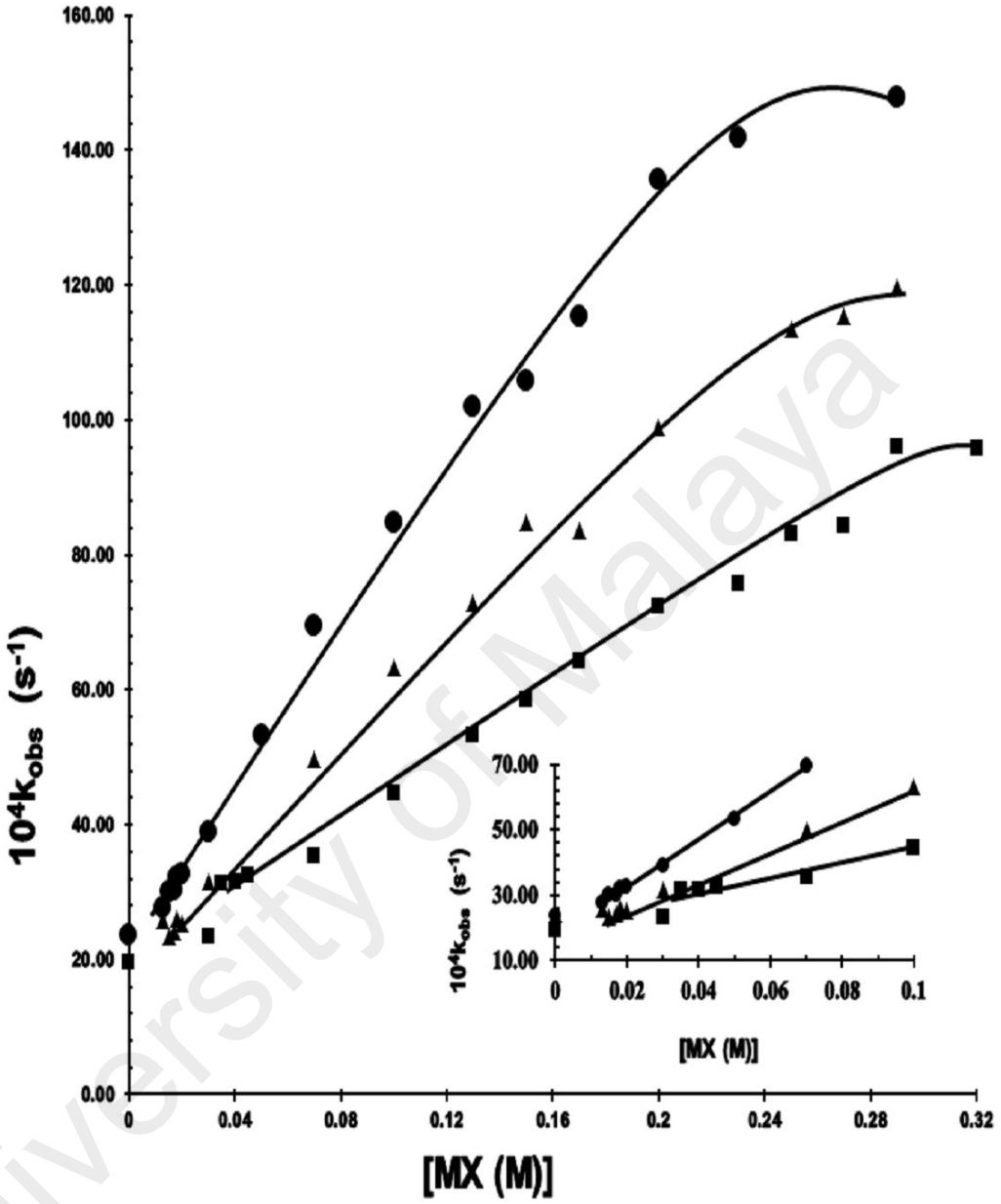

Figure 5.1 The plot of k_{obs} *vs*. [MX] (MX = C_6H_5ONa) at PS^- = 0.2 mM, Piperidine = 100 mM, NaOH = 30 mM at 35°C and $[CTABr]_T$= 6 mM (●), 10 mM (▲) and 15 mM (■). The lines are corresponded to the results listed in Table 5.1, where $[MX]_0^{op}$ = 0.018 M (●), 0.016 M (▲) and 0.043 M (■). Magnification: The plot shows the lowest values of salt concentrations.

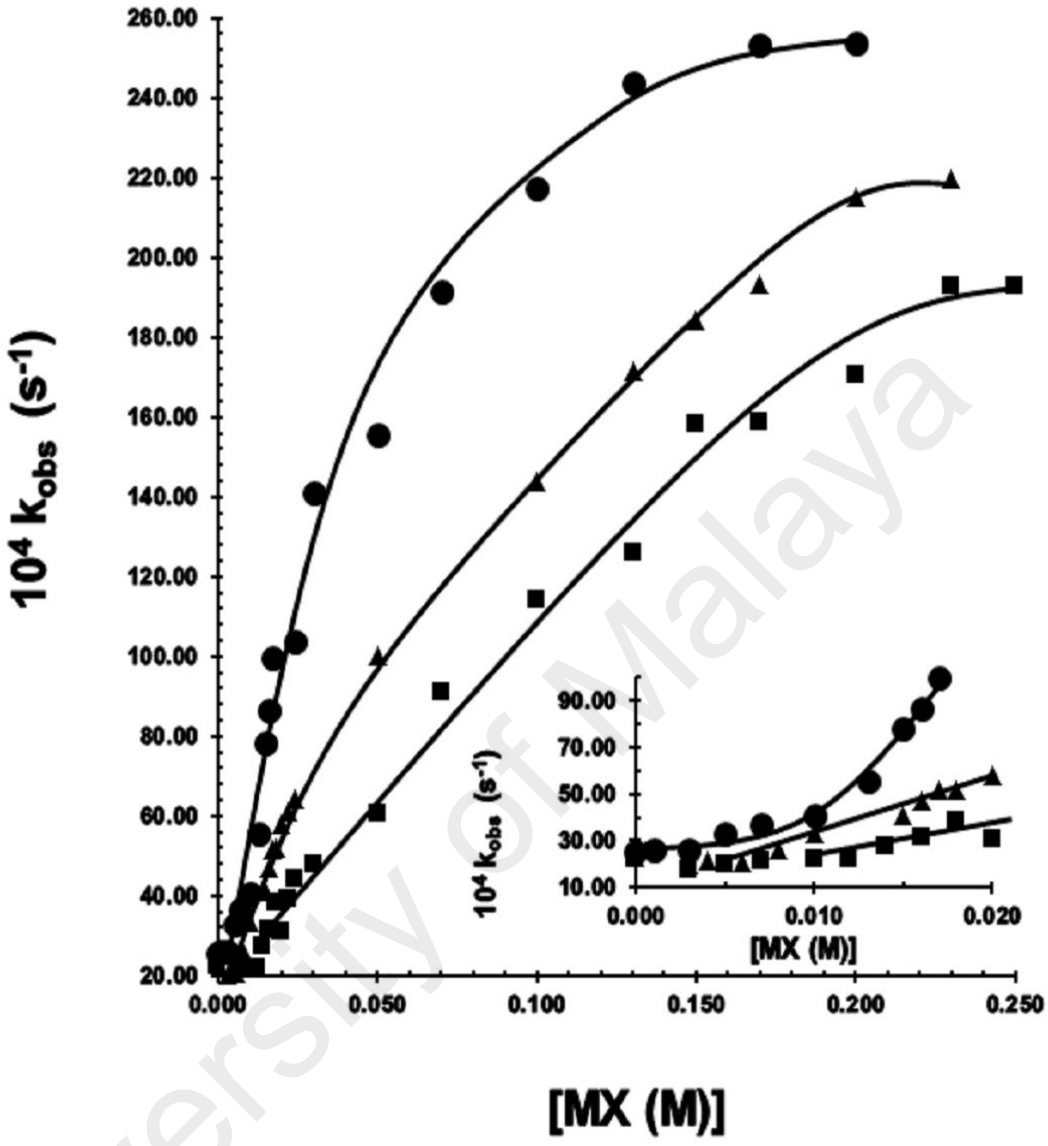

Figure 5.2 The plot of k_{obs} *vs*. [MX] (MX = 2-ethyl C_6H_4ONa) at PS^- = 0.2 mM, Piperidine = 100 mM, NaOH = 30 mM at 35°C and $[CTABr]_T$= 6 mM (●), 10 mM (▲) and 15 mM (■).The lines are corresponded to the results listed in Table 5.1, where $[MX]_0^{op}$ = 0.002 M (●), 0.006 M (▲) and 0.013 M (■). Magnification: The plot shows the lowest values of salt concentrations.

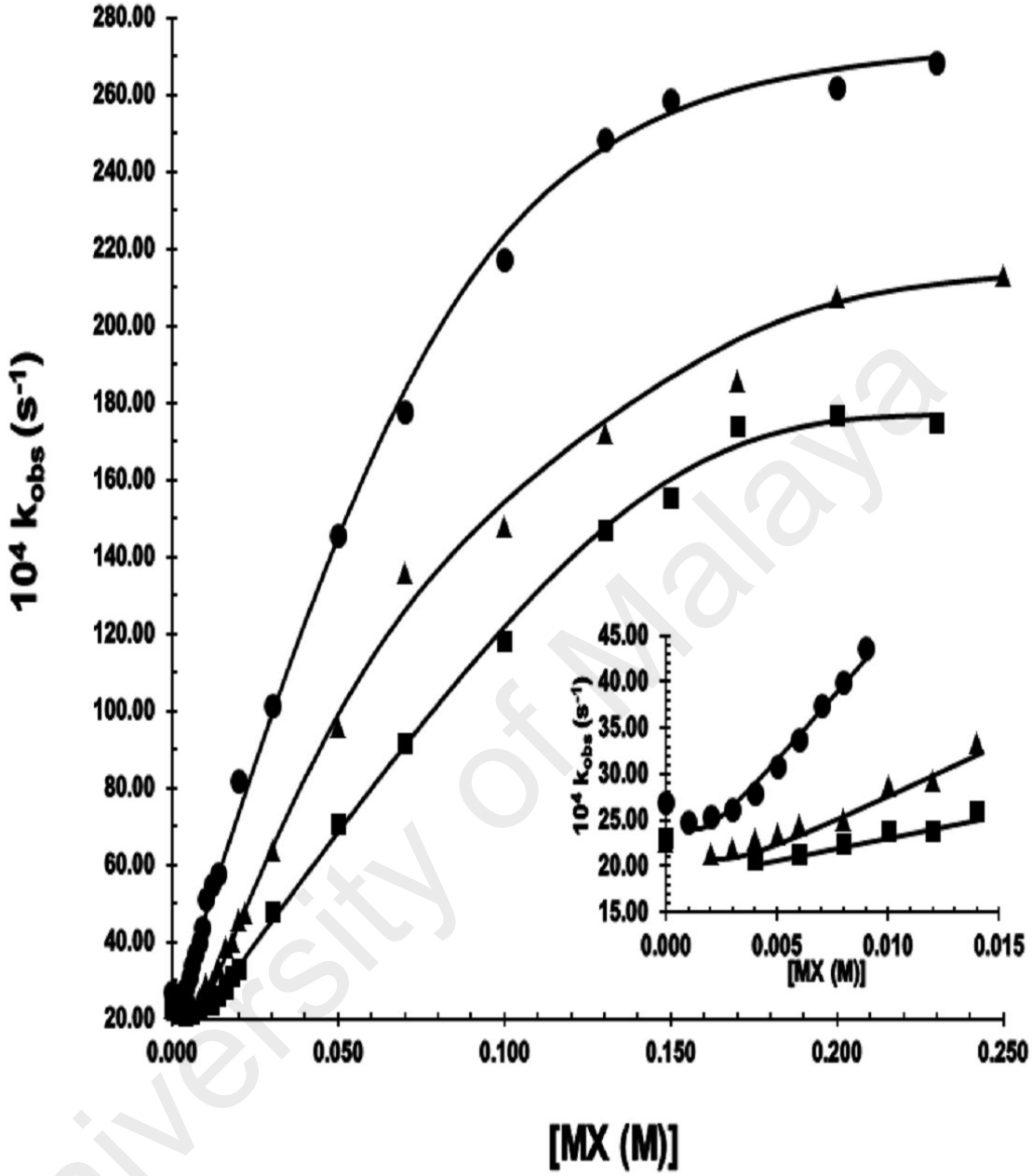

Figure 5.3 The plot of k_{obs} *vs*. [MX] (MX = 3-ethyl C_6H_4ONa) at PS^- = 0.2 mM, Piperidine = 100 mM, NaOH = 30 mM at 35°C and $[CTABr]_T$= 6 mM (●), 10 mM (▲) and 15 mM (■).The lines are corresponded to the results listed in Table 5.1, where $[MX]_0^{op}$ =0.005 M (●), 0.010 M (▲) and 0.014 M (■) .Magnification: The plot shows the lowest values of salt concentrations.

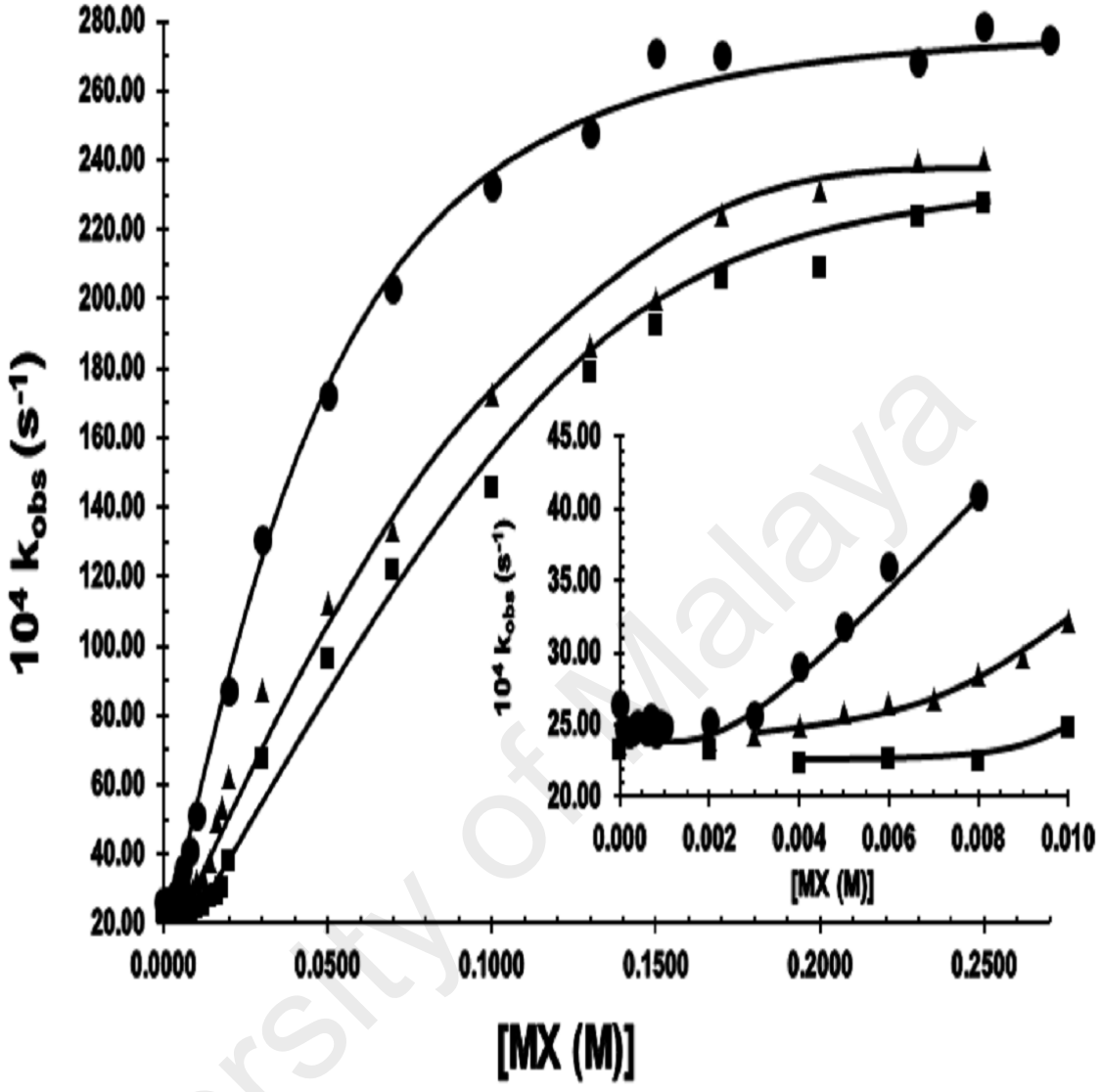

Figure 5.4 The plot of k_{obs} *vs*. [MX] (MX = 4-ethyl C_6H_4ONa) at PS^- = 0.2 mM, Piperidine = 100 mM, NaOH = 30 mM at 35°C $[CTABr]_T$= 6 mM (●), 10 mM (▲) and 15 mM (■).The lines are corresponded to the results listed in Table 5.1, where $[MX]_0^{op}$ =0.003 M (●), 0.004 M (▲) and 0.009 M (■). Magnification: The plot shows the lowest values of salt concentrations.

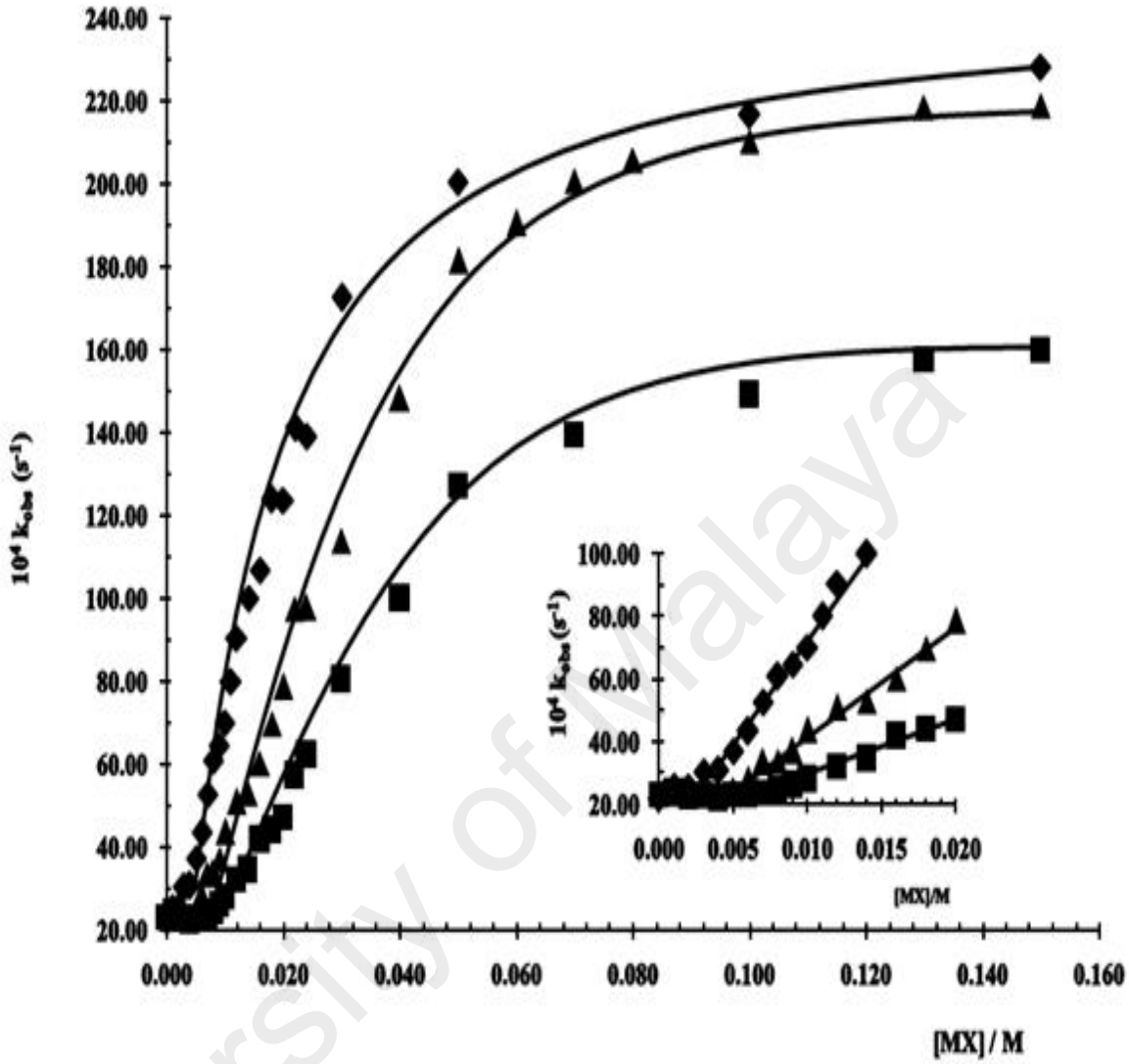

Figure 5.5 The nonlinear correlation of k_{obs} *vs*. [MX] (MX = 2-propyl C_6H_4ONa) at $[PS^-]$ = 0. 2 mM, [Pip] = 0.1 M, [NaOH] = 30 mM, T = 35°C and $[CTABr]_T$= 6 mM (♦), 10 mM (▲) and 15 mM (■) respectively. Inset: The lowest values of salt concentrations correspond to the results tabulated in Table 5.1, where $[MX]_0^{op}$ = 0.004 M (♦), 0.005 M (▲) and 0.010 M (■).

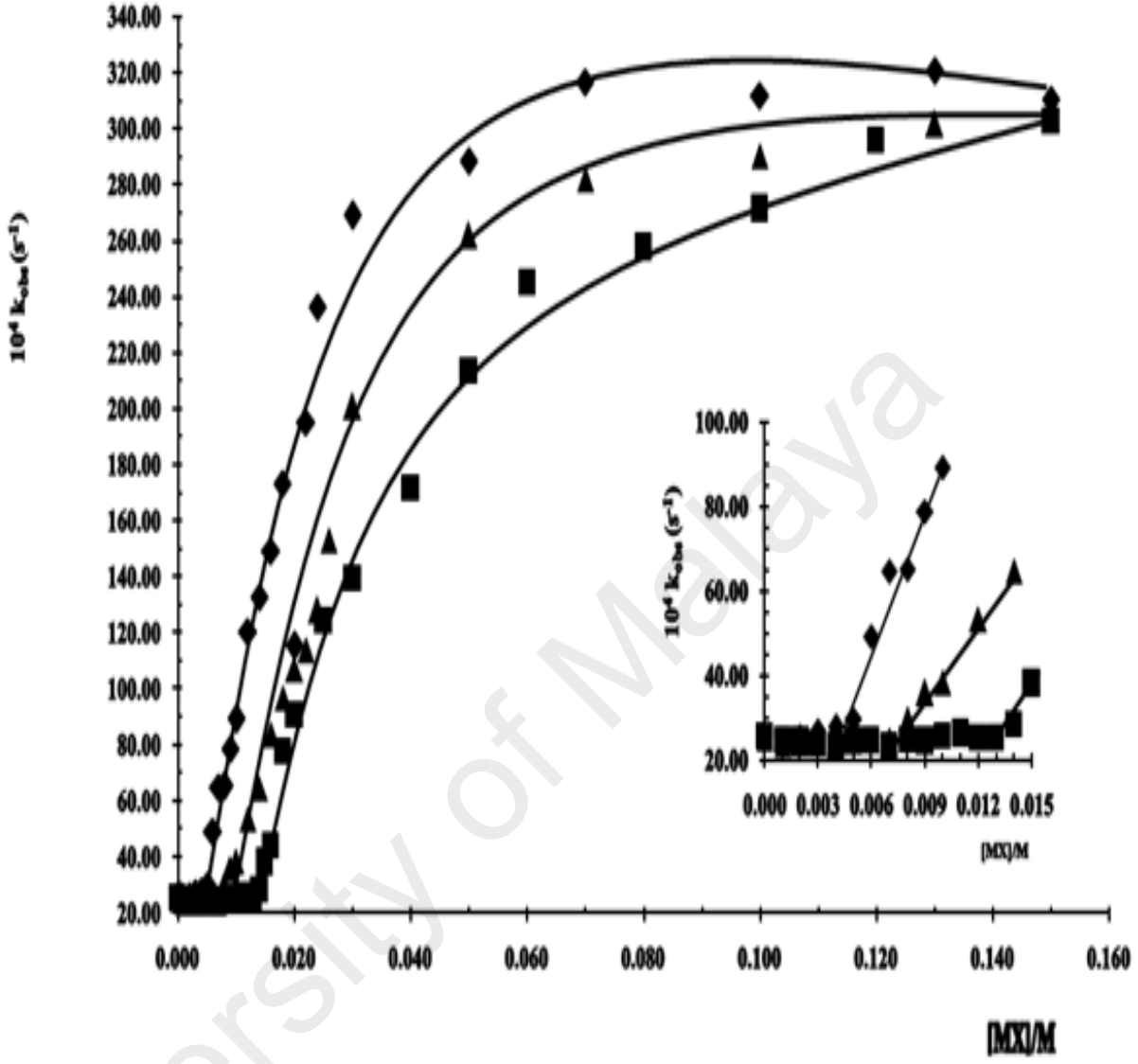

Figure 5.6 The nonlinear correlation of k_{obs} *vs*. [MX] (MX = 4-propyl C_6H_4ONa) at $[PS^-]$ = 0. 2 mM, [Pip] = 0.1 M, [NaOH] = 30 mM, T = 35°C and $[CTABr]_T$= 6 mM (♦), 10 mM (▲) and 15 mM (■) respectively. Inset: The lowest values of salt concentrations correspond to the results tabulated in Table 5.1, where $[MX]_0^{op}$ = 0.005 M (♦), 0.007 M (▲) and 0.013 M (■).

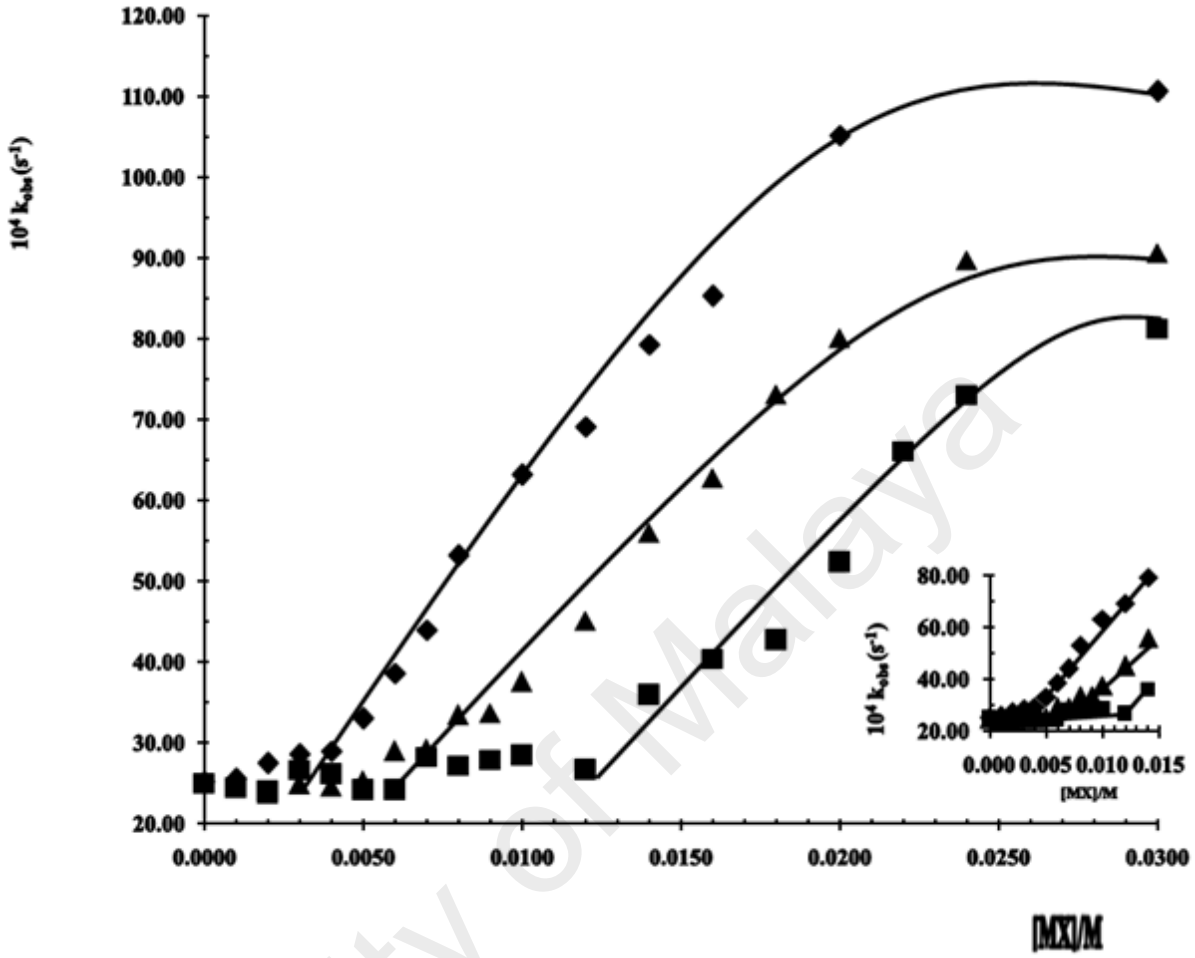

Figure 5.7 The nonlinear correlation of k_{obs} *vs*. [MX] (MX = 3-isopropyl C_6H_4ONa) at $[PS^-]$ = 0. 2 mM, [Pip] = 0.1 M, [NaOH] = 30 mM, T = 35°C and $[CTABr]_T$= 6 mM (♦), 10 mM (▲) and 15 mM (■) respectively. Inset: The lowest values of salt concentrations correspond to the results tabulated in Table 5.1, where $[MX]_0^{op}$ = 0.004 M (♦), 0.007 M (▲) and 0.012 M (■).

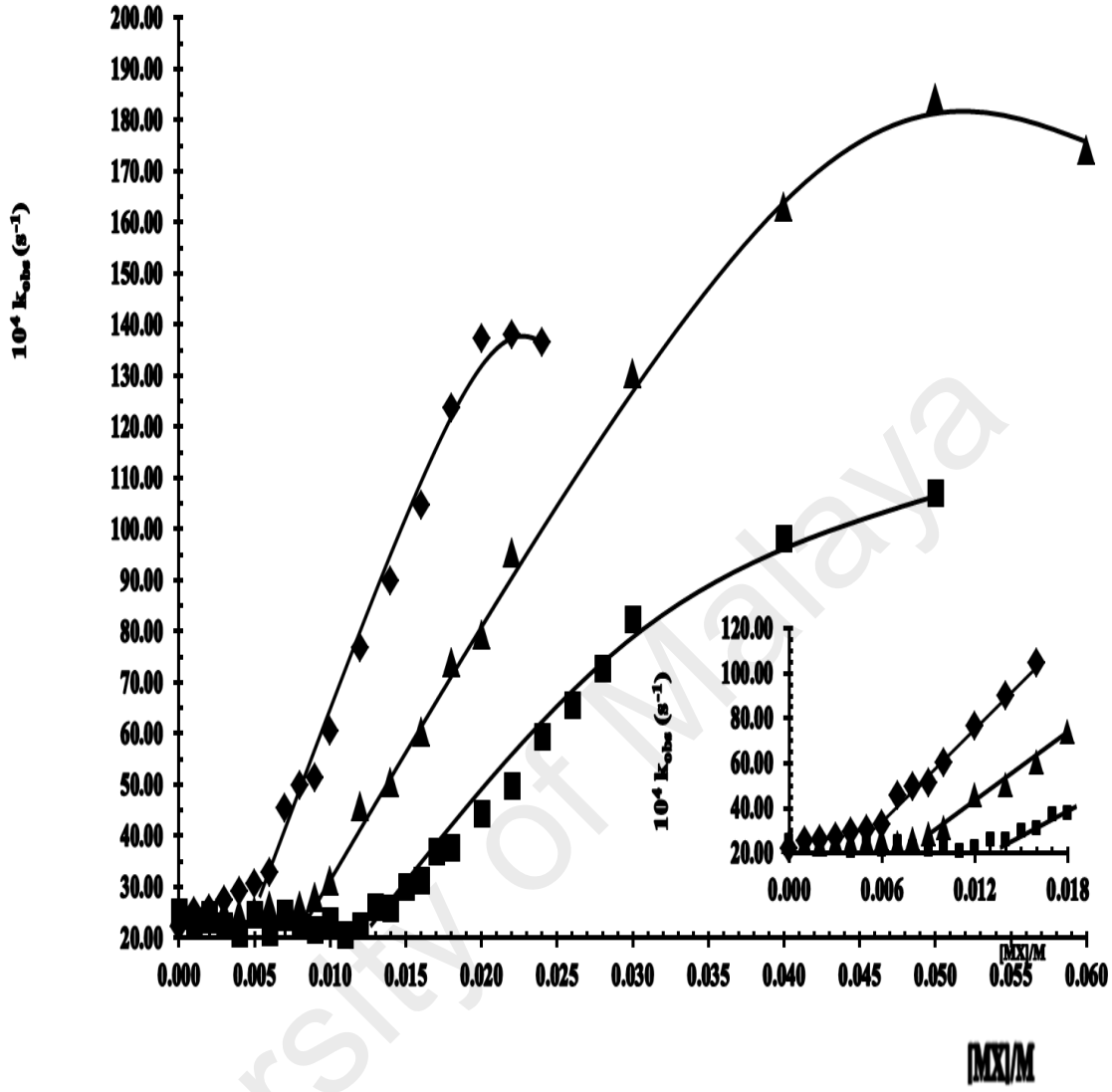

Figure 5.8 The nonlinear correlation of k_{obs} *vs.* [MX] (MX = 4-isopropyl C_6H_4ONa) at $[PS^-]$ = 0. 2 mM, [Pip] = 0.1 M, [NaOH] = 30 mM, T = 35°C and $[CTABr]_T$= 6 mM (♦), 10 mM (▲) and 15 mM (■) respectively. Inset: The lowest values of salt concentrations correspond to the results tabulated in Table 5.1, where $[MX]_0^{op}$ = 0.006 M (♦), 0.009 M (▲) and 0.013 M (■).

The mechanistic reaction for cetyltrimethylammonium bromide micellar catalysis for the reaction of piperidine with PS^- may be expressed by Scheme 5.1 where all other symbols have their usual meanings (Khan, 2010):

$$PS^-_W + D_n \underset{}{\overset{K_S}{\rightleftharpoons}} PS^-_M$$

$$Pip_W + D_n \overset{K_{Pip}}{\rightleftharpoons} Pip_M$$

$$PS^-_W + Pip_W \xrightarrow{k^2_W} P_1 + P_2$$

$$PS^-_M + Pip_M \xrightarrow{k^2_M} P_1 + P_2$$

Scheme 5.1: Mechanistic reaction for cetyltrimethylammonium bromide micellar catalysis for the reaction of piperidine with PS^-

The pseudo-first-order rate constant (Khan, 2006) and Scheme 5.1 can lead to Eq. (5.2)

$$k_{obs} = \frac{k_W + k_M K_S [CTABr]_T}{1 + K_S [CTABr]_T} \tag{5.2}$$

where $k_W = k^2_W [Pip]_T$, $k_M = k^{mr}_M K_{Pip} [Pip]_T$, $k^{mr}_M = k^2_M/V_M$ [36] with V_M representing micellar molar volume in M^{-1} for the reaction of micellar catalysis and all symbols related are defined elsewhere (Khan, 2010; Khan, 2006). The values of k_{obs} (= k_0) at various concentration of cetyltrimethylammonium bromide (within cetyltrimethylammonium bromide concentrations range of 6-15 mM) and [MX] = 0 (Table 5.1) are more than 10-fold smaller than k_{obs} for the reaction of Piperidine with ionized phenyl salicylate at [Pip] = 100 mM and $[CTABr]_T$ = 0 (Khan, 2006). The nonlinear plots of Figure 5.1- 5.8 cannot be discussed in terms of the ionic effect (the strength of ion and specific ionic effect) because the effects of $[C_6H_5ONa]$ on k_{obs} in the absence of cetyltrimethylammonium bromide

concentration showed the negative salt effect. The values of rate constant for the reaction of probe with substrate in micellar phase were not giving any effect with the addition of sodium bromide concentrations from 0.04 to 0.50 M (Bunton, 1991; Bunton, 2006). The major noticeable source for the nonlinear plots of Figures 5.1- 5.8 is the ion exchange process, X^-/PS^- because the value of k_{obs} is > 10 to 20 fold larger in aqueous phase than that in flexible nanoparticle pseudophase (Khan & Ismail, 2009; Lu et al., 1998).

The effects of counterion X^- to expel substrate counterion (PS^-) is found to decrease the flexible nanoparticle binding constant (Yusof & Khan, 2010), K_S with the increase of salt concentration (Khan, 2006; Bunton, 1991; Bunton, 2006) through an empirical relationship Eq. (5.3)

$$K_S = K_S^0 / (1 + K_{X/S}\,[MX]) \tag{5.3}$$

where $K_S^0 = K_S$ at [MX] = 0 [8]. It can be proven that Eqs. (5.2) and (5.3) can lead to Eq. (5.4) (Khan, 2010)

$$k_{obs} = \frac{k_0 + \theta K^{X/S}([MX]-[MX]_0^{op})}{1 + K^{X/S}([MX]-[MX]_0^{op})} \tag{5.4}$$

where $[MX]_0^{op}$ represents the optimum concentration of [MX] below which the values of k_{obs} are independent of [MX] with k_0, θ and $K^{X/S}$ expressed by Eq. (5.5), (5.6) and (5.7), respectively

$$k_0 = \frac{k_W + k_M K_S^0 [CTABr]_T}{1 + K_S^0 [CTABr]_T} \tag{5.5}$$

where $k_W = k_{obs}$ in the absence of salt and cetyltrimethylammonium bromide. Thus, k_M is presumed to be independent of salt concentrations,

$$\theta = F_{X/S}\, k_W^{MX} \tag{5.6}$$

where $k_W^{MX} = k_{obs}$ at a representative value of [MX] and also in the absence of cetyltrimethylammonium bromide, $1 >> K_N\,[CTABr]_T$[14] and $F_{X/S}$ (Khan, 2010) and

$$K^{X/S} = K_{X/S} / (1 + K_S^0[CTABr\,]) \tag{5.7}$$

The nonlinear plots (k_{obs} *vs*. [MX], shown by Figures 5.1- 5.8) were found to fit Eq. (5.4). This Σdi^2 method was used to determine unknown parameters, θ and $K^{X/S}$, $[MX]_0^{op}$ which in latter steps, the value is calculated using iterative technique (Khan, 2006).

The interesting part of this research is the catalytic constant (k_{cat}) for the piperidinolysis of PS^-, obtained from Eq. (5.4) where $\theta K^{X/S}=k_{cat}$. The calculated values of θ and $K^{X/S}$ as well as k_{cat} and $K^{X/S}$ at different $[CTABr]_T$ are summarized in Table 5.1 for MX = C_6H_5ONa, 2-ethyl C_6H_4ONa, 3-ethyl C_6H_4ONa, 4-ethyl C_6H_4ONa, 2-propyl C_6H_4ONa, 4-propyl C_6H_4ONa, 3-isopropyl C_6H_4ONa and 4-isopropyl C_6H_4ONa.

In this study, the k_{cat} is defined as an empirical constant that measures the ability of counterionic salt to catalyze the rate of piperidinolysis of phenyl salicylate ions in the presence of CTABr/ MX / H_2O nanoparticles. Eq. (5.8) which is obtained from the relationship: $k_{cat} = \theta K^{X/S}$ and Eq. (5.7).

$$k_{cat} = \frac{\theta K_{X/S}}{1 + K_S^0[CTABr]_T} \tag{5.8}$$

Table 5.1 The values of θ, k_{cat} and $K^{X/S}$, obtained from Eq. (5.4) for different MX[a]

$[CTABr]_T$[b] [mM]	$10^4 k_o$[c] [s^{-1}]	$[MX]_o$[op] [mM]	10^4 θ [s^{-1}]	$K^{X/S}$ [M^{-1}]	$K_{X/S}$ [M^{-1}]	$F_{X/S}$	$K_{X/S}$[n] [M^{-1}]	R_X[Br]	$10^3 k_{cat}$[i] [M^{-1}]
				X = $C_6H_5O^-$					
6.0	23.7	18	258 ± 25[d]	4.4 ± 0.8[d]	190[e]	0.89[f]	170[g]	6.8[h]	114 ± 10
10.0	24.3	16	325 ± 30	1.7 ± 0.2	123	1.02	125	5.1	56 ± 3
15.0	19.5	43	188 ± 6	2.8 ± 0.2	300	0.58	174	6.9	53 ± 2
				X = 2-ethyl $C_6H_4O^-$					
6.0	25.6	2	353 ± 20	13.8 ± 1.9	583	1.08	638	25.5	489 ± 42
10.0	22.7	6	330 ± 13	7.7 ± 0.6	551	1.03	570	22.8	257 ± 13
15.0	22.6	13	317 ± 20	5.6 ± 0.7	598	0.99	592	23.7	179 ± 13
				X = 3-ethyl $C_6H_4O^-$					
6.0	27.0	5	358 ± 12	13.3 ± 1.2	575	1.09	632	25.2	478 ± 30
10.0	22.8	10	331 ± 16	8.0 ± 0.9	570	1.03	585	23.4	265 ± 20
15.0	23.1	14	309 ± 26	6.1 ± 1.0	647	0.96	619	24.7	188 ± 17
				4-ethyl $C_6H_4O^-$					
6	26.5	3	340 ± 10	18.5 ±1.8	797	1.05	834	33.3	631 ± 48
10	23.6	7	301 ± 12	12.3± 1.4	870	0.93	806	32.2	369 ± 31
15	23.2	9	356 ± 16	6.9 ± 0.6	734	1.07	734	31.3	246 ± 14

Continue to the next page…

Continue…….

$[CTABr]_T$[b] [mM]	10^4k_o[c] [s^{-1}]	$[MX]_o$[op] [mM]	$10^4\ \theta$ [s^{-1}]	$K^{X/S}$ [M^{-1}]	$K_{X/S}$ [M^{-1}]	$F_{X/S}$	$K_{X/S}{}^n$ [M^{-1}]	$R_X{}^{Br}$	10^3k_{cat}[i] [M^{-1}]
				X = 2-propyl $C_6H_4O^-$					
6.0	22.2	4	271 ± 1[d]	47.7 ± 3.2[d]	2038[e]	0.84[f]	1702[g]	68.1[h]	1286 ± 59
10.0	24.0	5	306 ± 23	22.5 ± 4.3	1597	0.95	1527	61.1	688 ± 81
15.0	23.1	10	219 ± 24	23.0 ± 6.6	2349	0.67	1657	66.3	505 ± 94
				X = 4-propyl $C_6H_4O^-$					
6.0	26.1	5	346 ± 12	85.3 ± 14.6	3666	1.04	3814	152.6	2954 ± 428
10.0	25.0	7	309 ± 37	51.3 ± 22.7	3640	0.96	3484	139.4	1585 ± 549
15.0	25.4	13	364 ± 09	33.41 ± 2.5	3541	1.08	3824	152.9	1219 ± 66
				X = 3-isopropyl $C_6H_4O^-$					
6.0	25.2	4	178 ± 15	54.7 ± 9.8	2354	0.54	1289	51.6	975 ± 92
10.0	24.9	7	293 ± 28	20.0 ± 3.8	1421	0.89	1277	51.1	587 ± 61
15.0	25.0	12	230 ± 2	20.4 ± 0.5	2151	0.71	1518	60.8	471 ± 7
				X = 4-isopropyl $C_6H_4O^-$					
6	22.2	6	295 ± 56	45.2 ± 14.4	1942	0.89	1725	69.0	1336 ± 178
10	24.9	9	331 ± 42	22.8 ± 5.3	1617	0.96	1610	64.4	755 ± 84
15	25.1	13	163 ± 16	32.5 ± 7.1	3449	0.48	1663	66.6	531 ± 68

[a] [MX] = C_6H_5ONa, 2-ethyl C_6H_4ONa, 3-ethyl C_6H_4ONa, 4-ethyl C_6H_4ONa, 2-propyl C_6H_4ONa, 4-propyl C_6H_4ONa, 3-isopropyl C_6H_4ONa and 4-isopropyl C_6H_4ONa. [b] $[FN]_T$. [c] $k_0 = k_{obs}$ at the absence of salt. [d] Error limits are standard deviations. [e] $K_{X/S} = K^{X/S}(1 + K_S{}^o[CTABr]_T)$ where $K_S{}^o = 7000\ M^{-1}$. [f] $F_{X/S} = \theta/k_W$ where $k_W = k_{obs}$ at $[CTABr]_T = 0$ and the value of k_W is independent of salt concentrations, $[Piperidine]_T = 100$ mM and the average value of $k_W = 31.1 \times 10^{-3}\ s^{-1}$ at 35°C. [g] $K_{X/S}{}^n = F_{X/S}K_{X/S}$. [h] $R_X{}^{Br} = K_{X/S}{}^n/K_{Br/S}{}^n$, where $K_{Br/S}{}^n = 25\ M^{-1}$. [i] $\theta K^{X/S} = k_{cat}$

Eq. (5.8) shows that the determined value of k_{cat} should decrease with the increase of cationic surfactant concentrations, $[CTABr]_T$ provided $K_{X/S}^n$ is independent of $[CTABr]_T$. Table 5.1 shows the catalytic constant, k_{cat}, values for salts, MX = C_6H_5ONa, 2-ethyl C_6H_4ONa, 3-ethyl C_6H_4ONa, 4-ethyl C_6H_4ONa, 2-propyl $C_6H_4O^-$, 4-propyl $C_6H_4O^-$, 3-isopropyl $C_6H_4O^-$ and 4-isopropyl $C_6H_4O^-$ at different values of cationic surfactants namely 0.006 M, 0.010 M and 0.015M.

It is proven that the findings are tally with the major assumptions of PM model (Khan, 2006). Eq. (5.6) shows that θ values should be independent of $[CTABr]_T$ because 1 >> K_N $[CTABr]_T$ under the experimental conditions of this study (Bunton, 1991;Bunton, 2006). The calculated values of θ (Table 5.1) are almost independent of flexible nanoparticle concentrations for MX = C_6H_5ONa. The satisfactory observed data fit to Eq. (5.4), show that the value of θ is kinetically independent of [MX] and hence $k_W^{MX} = k_W$ under the reaction conditions of this study. This conclusion is proved from the nonlinear plot, k_{obs} *vs*. [MX] in the absence of cetyltrimethylammonium bromide concentration as described earlier in the text. The values of $F_{X/S}$ were determined from Eq. (5.6) with average value of $k_W = 31.1\times10^{-3}$ s^{-1} at Pip = 0.1 M. These findings are tabulated in Table 5.1. The values of $F_{X/S}$ for MX = C_6H_5ONa, 2-ethyl C_6H_4ONa, 3-ethyl C_6H_4ONa, 4-ethyl C_6H_4ONa, 2-propyl $C_6H_4O^-$, 4-propyl $C_6H_4O^-$, 3-isopropyl $C_6H_4O^-$ and 4-isopropyl C_6H_4O are shown in Table 5.1.

The values of empirical constant, $K_{X/S}$ at different flexible nanoparticle concentrations were calculated from Eq. (5.7) (Khan, 2010) with the reported value of K_S^0 (= 7×10^3 M^{-1}) [29]. These calculated values of $K_{X/S}$, at different $[CTABr]_T$, are shown in Table 5.1 for C_6H_5ONa, 2-ethyl C_6H_4ONa, 3-ethyl C_6H_4ONa, 4-ethyl C_6H_4ONa, 2-propyl $C_6H_4O^-$, 4-propyl $C_6H_4O^-$, 3-isopropyl $C_6H_4O^-$ and 4-isopropyl C_6H_4O and it has been

found that the values of $K_{X/S}$ are almost independent of flexible nanoparticle concentrations, $[CTABr]_T$ = 0.006 M, 0.010 M, 0.015 M (Table 5.1).

However, it has been explained in detail elsewhere that the normalized values of $K_{X/S}$, i.e. $K_{X/S}^n(=F_{X/S}K_{X/S})$, is related with conventional ion exchange constant (K_X^{Br}) by the relationship: $K_X^{Br}= K_{X/S}^n/K_{Br/S}^n$ where the values of $K_{X/S}^n$ and $K_{Br/S}^n$ have been calculated from kinetic parameters (θ and $K^{X/S}$) determined in the presence of same structural features of nanoparticles such as spherical or wormlike or vesicle (Khan, 2010). Its values of $K_{Br/S}^n$ and $K_{X/S}^n$ have been obtained under the presence of spherical micelles and non-spherical micelles then, $K_{X/S}^n/K_{Br/S}^n = R_X^{Br}$ (Khan, 2010). The values of $K_{X/S}^n$ (Table 5.1) and the reported value of 25 M^{-1} for $K_{Br/S}^n$ (Khan, 2010) give the values of R_X^{Br} for X = $C_6H_5O^-$, 2-ethyl $C_6H_4O^-$, 3-ethyl $C_6H_4O^-$, 4-ethyl $C_6H_4O^-$, 2-propyl $C_6H_4O^-$, 4-propyl $C_6H_4O^-$, 3-isopropyl $C_6H_4O^-$ and 4-isopropyl C_6H_4O. These evidences are presented in Table 5.1.

CHAPTER 6

RHEOLOGICAL EFFECTS ON FLEXIBLE NANOPARTICLE IN THE PRESENCE OF PIPERIDINE WITH PS^-

6.1 Introduction

The research on catalytic nanoparticles has become of great attention in this new decade. The world of colloid and surface science has risen to this challenge and initiated to study the effects of specific counterion/ion effects on aqueous interfaces (Jungwirth & Tobias, 2006). Bharadwaj and Sar (Shweta & Santosh, 2014) studied the counterion binding effects on the micellization of bile salts—sodium cholate and sodium deoxycholate in aqueous methanol, ethanol and ethylene glycol mixtures by surface tension and conductivity methods. In 2013, Naskar and co-workers (Naskar et al., 2013) studied the counterion effect on micellization of ionic surfactants which leads to the comprehensive understanding of the interaction NaCl and several flexible nanoparticles.

In organic chemistry, phenols, sometimes called phenolics, are a class of chemical compounds consisting of a hydroxyl group (-OH) bonded directly to an aromatic hydrocarbon group. Phenolic compounds are synthesized industrially; they also are produced by plants and microorganisms, with variation between and within species. As phenols have been known as nano-toxic substance to environment and human being (Alessandro, 2001), there is an intriguing to understand the rheological effects on catalytic studies between phenols and the flexible nanoparticle CTABr│MX│H_2O. Since the previous researcher has proven that the magnitudes (forces) related to the specific ion effects are hard to determine (Romsted, 2007) this chapter will discuss on the rheological effects of inert phenolate ions on the flexible nanoparticle catalysis for the reaction of piperidine with PS^-.

6.2 Experimental Design

6.2.1 Chemicals

Commercial products of highest available purity such as cetyltrimethylammonium bromide, $C_{16}H_{33}NMe_3Br$, (CTABr/ Flexible nanoparticle)-Merck, phenyl salicylate (Merck), C_6H_5OH (Merck), 2-ethyl C_6H_4OH (Sigma Aldrich), 3-ethyl C_6H_4OH (Sigma Aldrich), 4-ethyl C_6H_4OH (Sigma Aldrich), 2-propyl C_6H_4OH (Sigma Aldrich), 4-propyl C_6H_4OH(Sigma Aldrich), 3-isopropyl C_6H_4OH (Sigma Aldrich), 4-isopropyl C_6H_4OH(Sigma Aldrich), piperidine (Pip)-Merck and all other common chemicals used were reagent grade. The stock solutions of PSaH=0.01M were prepared in acetonitrile because of its low aqueous solubility. The stock solutions (w M) of nonionic substituted phenols were prepared by adding (w + 0.05 M) sodium hydroxide so that wM XH solutions become wM NaX.

6.2.2 Rheological Measurements

10mL samples are prepared by mixing a constant desired amount of sodium hydroxide (NaOH), piperidine (Pip), cetyltrimethylammonium bromide (CTABr), phenyl salicylate and MX (=C_6H_5ONa, 2-ethyl C_6H_4ONa, 3-ethyl C_6H_4ONa, 4-ethyl C_6H_4ONa, 2-propyl C_6H_4ONa, 4-propyl C_6H_4ONa, 3-isopropyl C_6H_4ONa, 4-isopropyl C_6H_4ONa) for steady-shear rheological measurements. The values of inert salt concentrations, [MX] were experimentally carried out from 0.005 – 0.29 M. The rheological studies were performed using rheometer (Anton Paar-MCR301) with DG26.7/T200/SS (a double gap cylinder) at 35°C (Yusof et al., 2013).

6.3 Results and Discussions

6.3.1 Effects of Rheological Behaviour for the Flexible Nanoparticle in the Reaction of Piperidine with PS^-

In general, shear viscosity (η) *vs*. shear rate ($\dot{\gamma}$) plot of viscoelastic micellar system reveals the regions of Newtonian, shear thickening (η increases) and shear thinning (η decreases). Flow curves showing only the Newtonian fluid behavior at $\dot{\gamma} < 10^3\ s^{-1}$ with η values similar to η of pure water (1.00 m Pa.s) show the presence of spherical micelles/SM or small unilamellar/multilamellar vesicles (ULV/MLV). On the other hand, flow curves exhibiting Newtonian fluid behavior in the initial lower values of $\dot{\gamma}$ followed by shear thinning (η decreases) at the higher values of $\dot{\gamma}$ reveal the presence of rodlike (RM)/wormlike micelles (WM) or large ULV/MLV (Davies et al., 2006). Shear thickening (η increases) is expected to be due to the further entanglement of the micelles as more shear occurs by the rotational rheometer. The existence of high zero-shear viscosity (η_0) are also good indicators in proving the existence of long and entangled wormlike micelles. The aggregation of wormlike micelles instead of normal spherical micelles is indicated by the visibility of maxima as a function of the concentration of the counterionic salt which has been known to be a characteristic feature of such micellar solution in previous studies (Magid, 1998; Rao et al., 1987). Thus, Figure 6.1 to Figure 6.8 represent the rheograms showing the dependence of shear viscosity (η) upon shear rate ($\dot{\gamma}$) for respective phenolate ions namely $C_6H_5O^-$, 2-ethyl $C_6H_4O^-$, 3-ethyl $C_6H_4O^-$, 4-ethyl $C_6H_4O^-$, 2-propyl $C_6H_4O^-$, 4-propyl $C_6H_4O^-$, 3-isopropyl $C_6H_4O^-$ and 4-isopropyl $C_6H_4O^-$. As mentioned above, the maximum viscosities for FN are determined in Figure 6.9 to Figure 6.16 at 25°C and 35°C respectively.

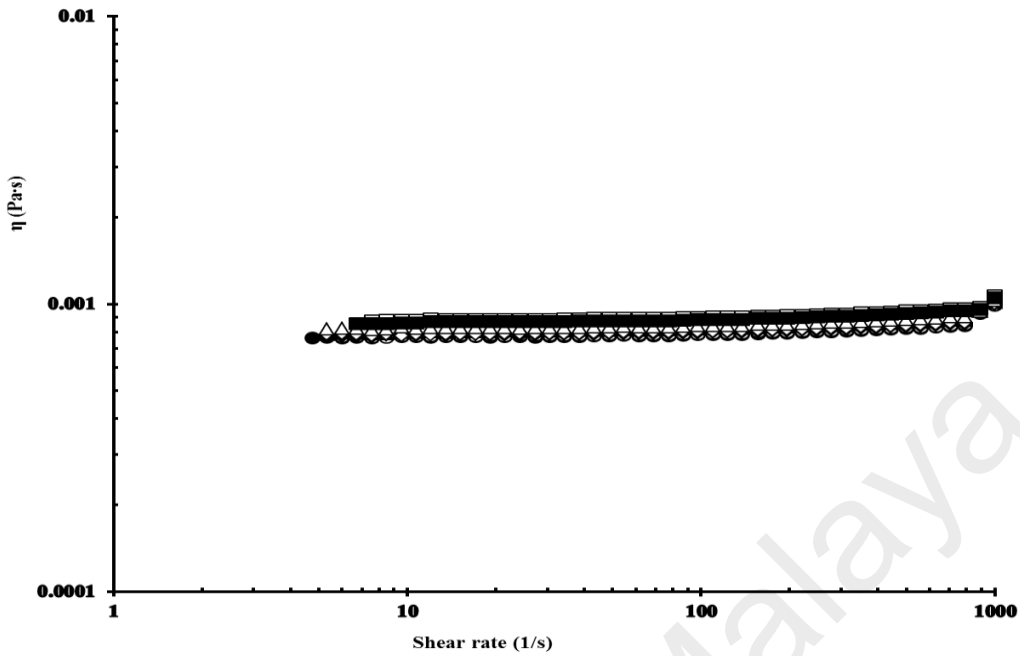

Figure 6.1: Plots showing the dependence of shear viscosity (η) upon shear rate ($\dot{\gamma}$) for MX= C_6H_5ONa where [PSaH] = 2.0×10^{-4} M, [NaOH] = 0.03 M, [Pip] = 0.1 M, [CTABr] = 0.015 M at T = 35°C with and [MX]/M = 0.005 (●), 0.020 (o), 0.030 (♦), 0.050 (◊), 0.100 (▲), 0.150 (Δ), 0.250 (■) and 0.290 (□)

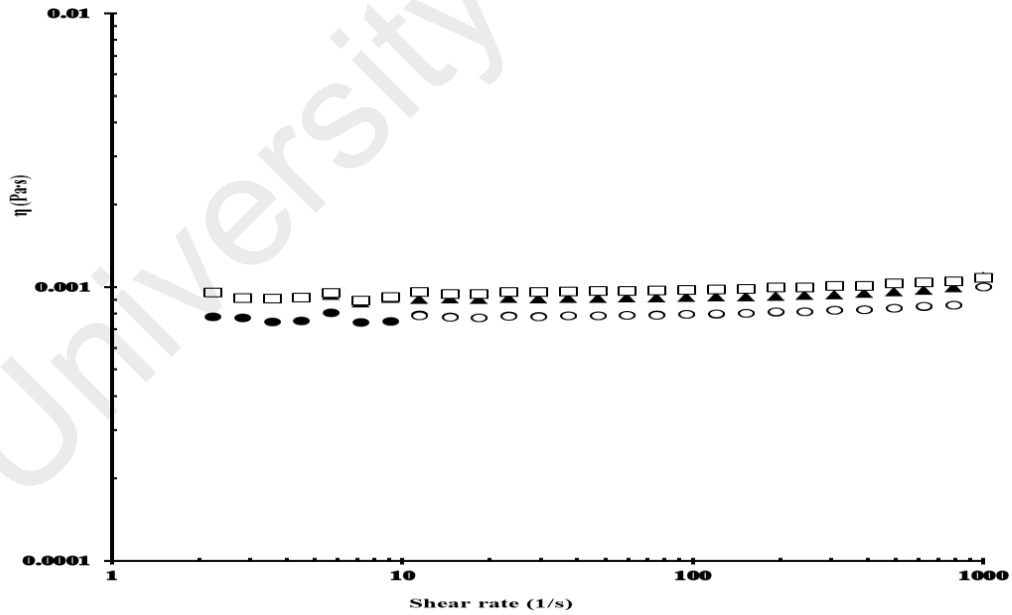

Figure 6.2: Plots showing the dependence of shear viscosity (η) upon shear rate ($\dot{\gamma}$) for MX= 2-ethyl C_6H_4ONa where [PSaH] = 2.0×10^{-4} M, [NaOH] = 0.03 M, [Pip] = 0.1 M, [CTABr] = 0.015 M at T = 35°C with and [MX]/M =0.005 (●), 0.020 (o), 0.030 (♦), 0.050 (◊), 0.100 (▲), 0.150 (Δ), 0.250 (■) and 0.29 (□)

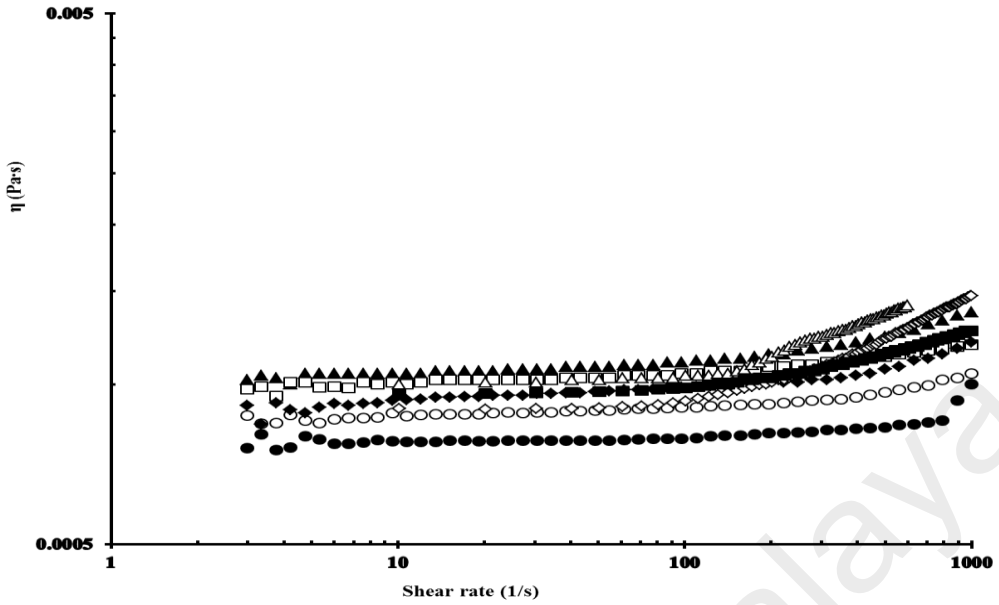

Figure 6.3: Plots showing the dependence of shear viscosity (η) upon shear rate ($\dot{\gamma}$) for MX= 3-ethyl C_6H_4ONa where [PSaH] = 2.0×10^{-4} M, [NaOH] = 0.03 M, [Pip] = 0.1 M, [CTABr] = 0.015 M at T = 35°C with and [MX]/M = 0.005 (●), 0.020 (o), 0.030 (♦), 0.050 (◊), 0.100 (▲), 0.150 (Δ), 0.250 (■) and 0.29 (□)

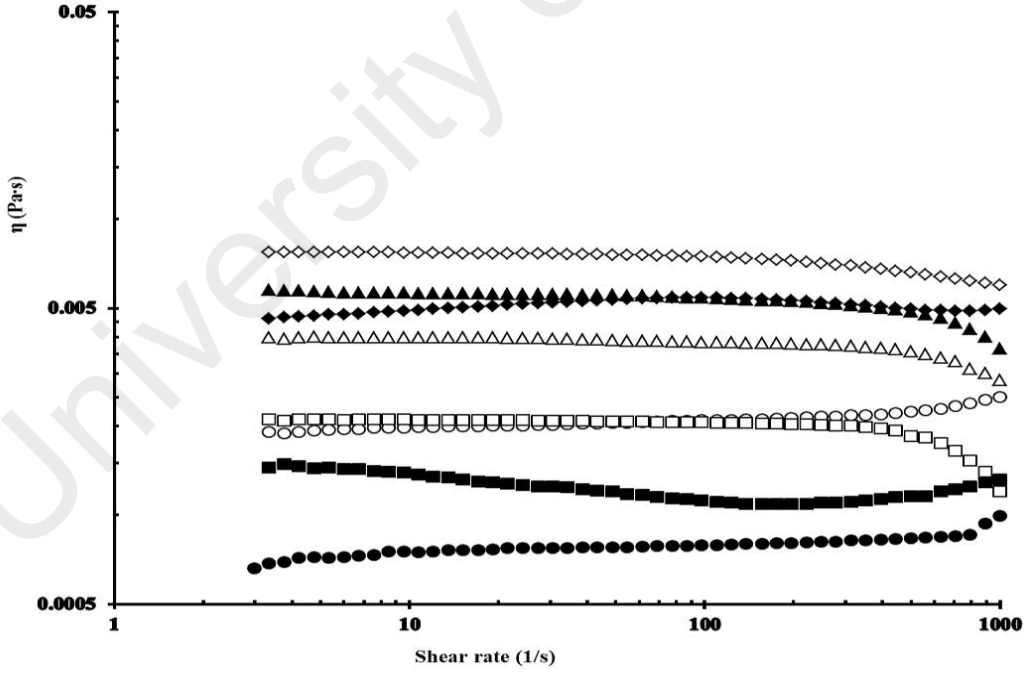

Figure 6.4: Plots showing the dependency of shear viscosity (η) and shear rate ($\dot{\gamma}$) for MX= 4-ethyl C_6H_4ONa where [PSaH] = 2.0×10^{-4} M, [NaOH] = 0.03 M, [Pip] = 0.1 M, [CTABr] = 0.015 M at T = 35°C with and [MX]/M = 0.005 (●), 0.020 (o), 0.030 (♦), 0.050 (◊), 0.100 (▲), 0.150 (Δ), 0.250 (■) and 0.29 (□)

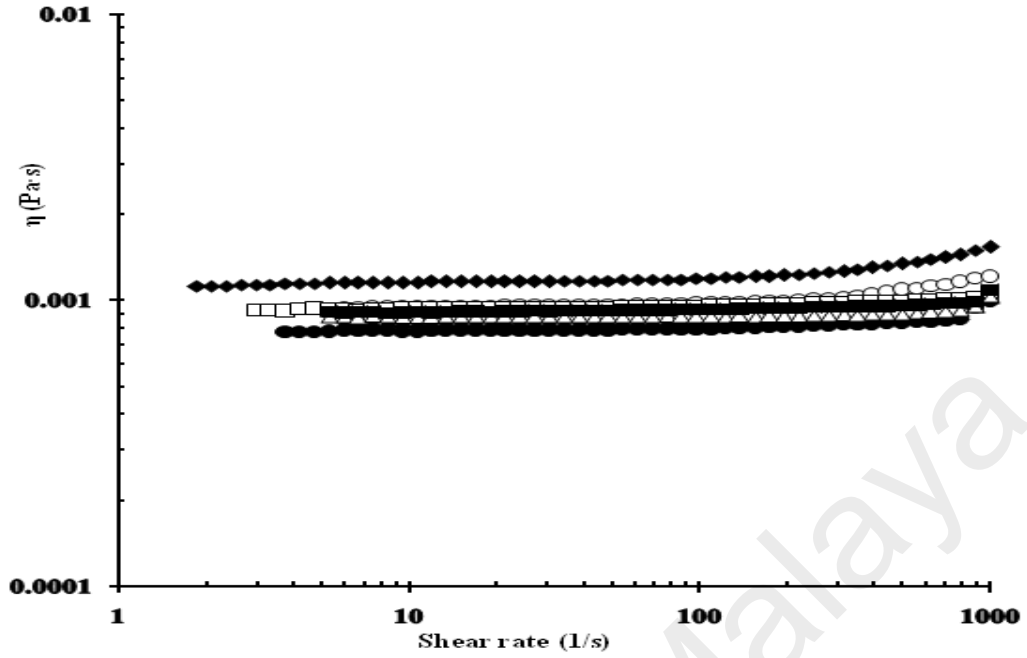

Figure 6.5: Plots showing the dependency of shear viscosity (η) and shear rate ($\dot{\gamma}$) for MX= 2-propyl C_6H_4ONa where [PSaH] = 2.0×10^{-4} M, [NaOH] = 0.03 M, [Pip] = 0.1 M, [CTABr] = 0.015 M at T = 35°C with and [MX]/M = 0.005 (●), 0.020 (o), 0.030 (♦), 0.050 (◊), 0.100 (▲), 0.150 (Δ), 0.250 (■) and 0.29 (□)

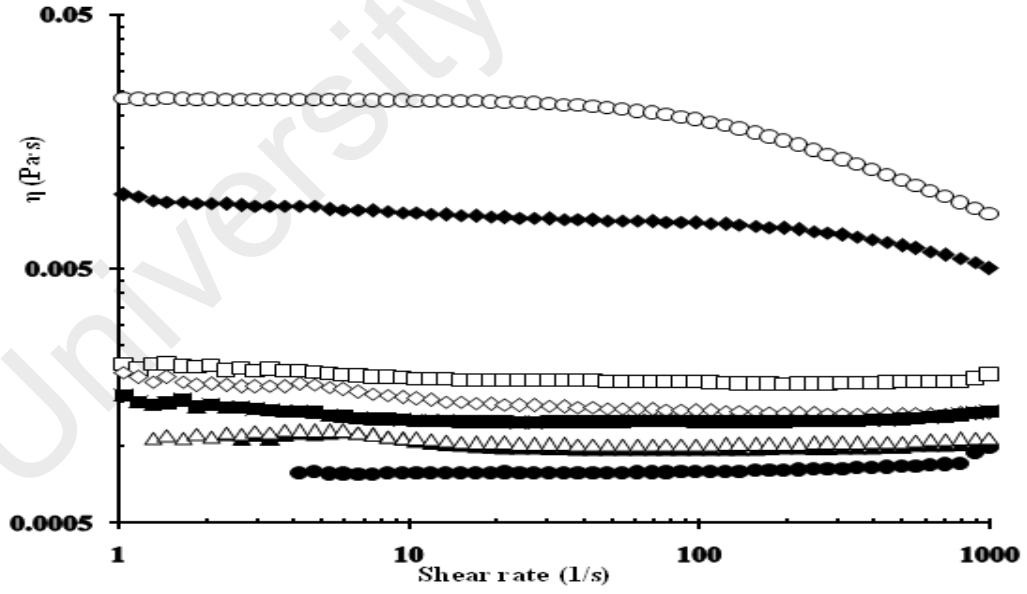

Figure 6.6: Plots showing the dependency of shear viscosity (η) and shear rate ($\dot{\gamma}$) for MX= 4-propyl C_6H_4ONa where [PSaH] = 2.0×10^{-4} M, [NaOH] = 0.03 M, [Pip] = 0.1 M, [CTABr] = 0.015 M at T = 35°C with and [MX]/M = 0.005 (●), 0.020 (o), 0.030 (♦), 0.050 (◊), 0.100 (▲), 0.150 (Δ), 0.250 (■) and 0.29 (□)

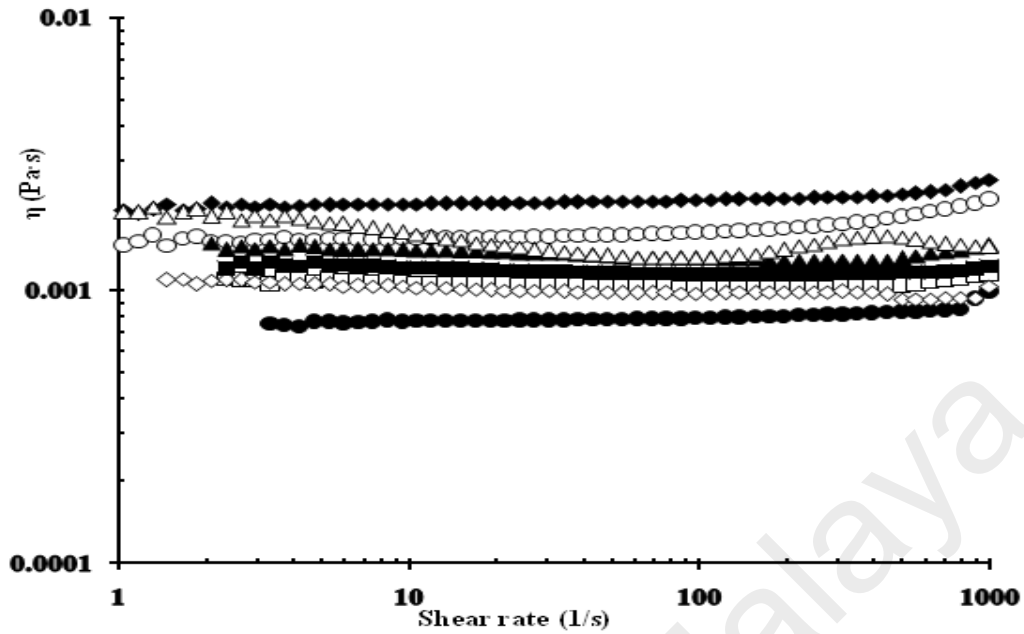

Figure 6.7: Plots showing the dependency of shear viscosity (η) and shear rate ($\dot{\gamma}$) for MX= 3-isopropyl C_6H_4ONa where [PSaH] = 2.0×10^{-4} M, [NaOH] = 0.03 M, [Pip] = 0.1 M, [CTABr] = 0.015 M at T = 35°C with and [MX]/M = 0.005 (●), 0.020 (o), 0.030 (♦), 0.050 (◊), 0.100 (▲), 0.150 (Δ), 0.250 (■) and 0.29 (□)

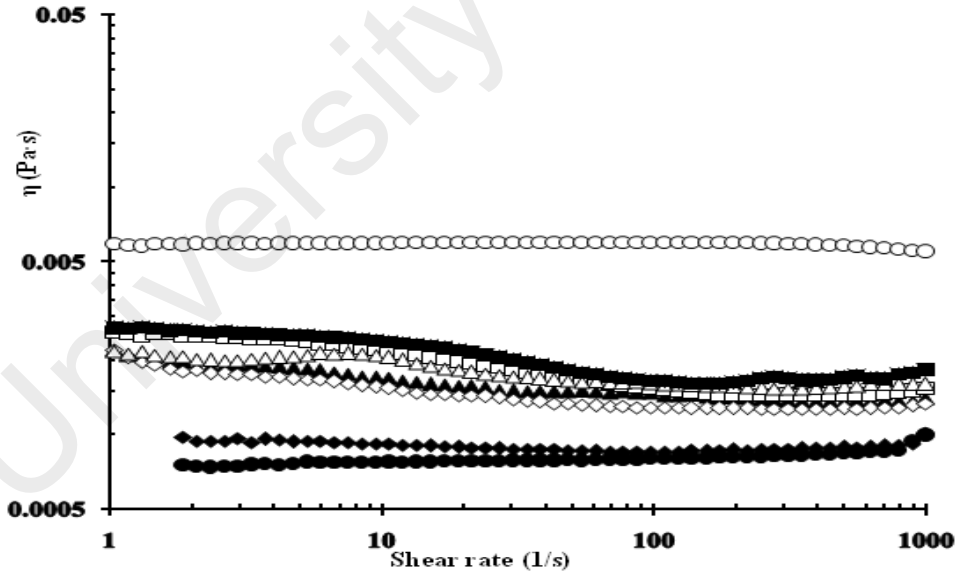

Figure 6.8: Plots showing the dependency of shear viscosity (η) and shear rate ($\dot{\gamma}$) for MX= 4-isopropyl C_6H_4ONa where [PSaH] = 2.0×10^{-4} M, [NaOH] = 0.03 M, [Pip] = 0.1 M, [CTABr] = 0.015 M at T = 35°C with and [MX]/M = 0.005 (●), 0.020 (o), 0.030 (♦), 0.050 (◊), 0.100 (▲), 0.150 (Δ), 0.250 (■) and 0.29 (□)

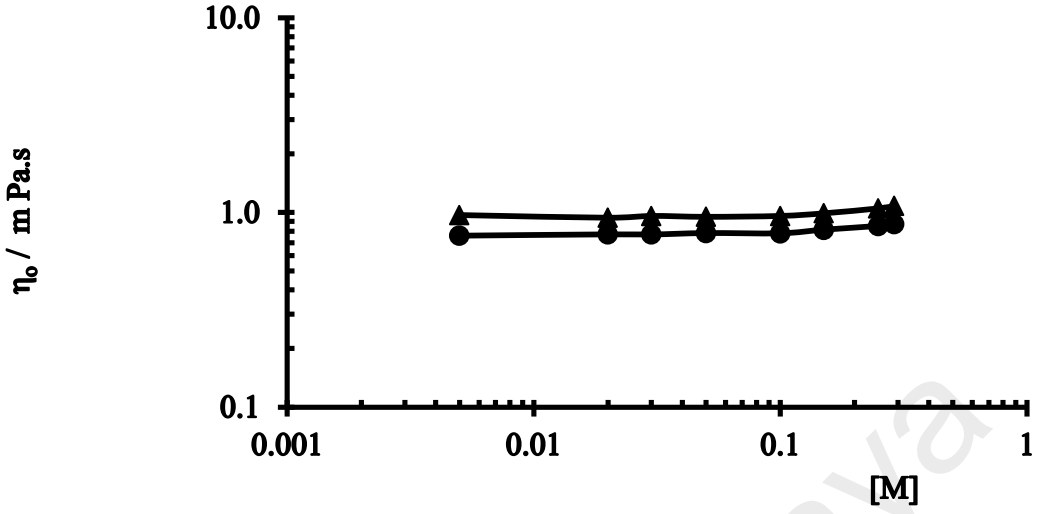

Figure 6.9: Effects of different [MX] upon zero shear viscosity (η_0) for MX = C_6H_5ONa of aqueous solutions containing 15 mM CTABr, 0.2 mM PSaH, 0.1 M Pip, 30 mM NaOH at 25ºC (▲) and 35ºC (●).

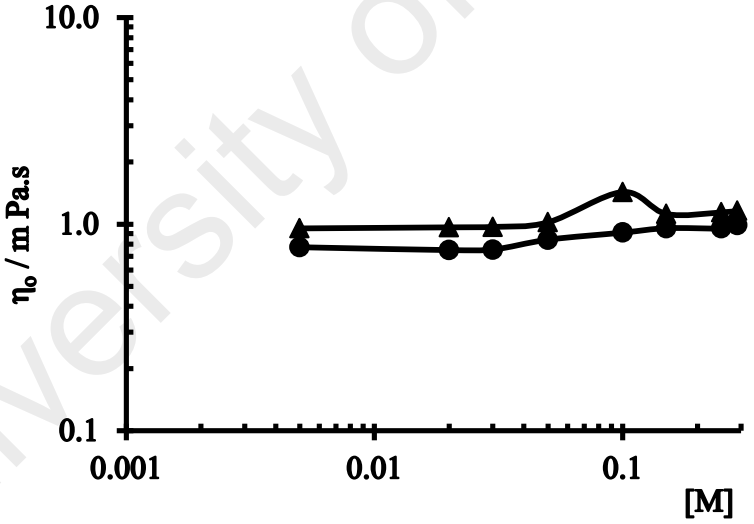

Figure 6.10 Effects of different [MX] upon zero shear viscosity (η_0) for MX = 2-ethyl C_6H_4ONa of aqueous solutions containing 15 mM CTABr, 0.2 mM PSaH, 0.1 M Pip, 30 mM NaOH at 25ºC (▲) and 35ºC (●).

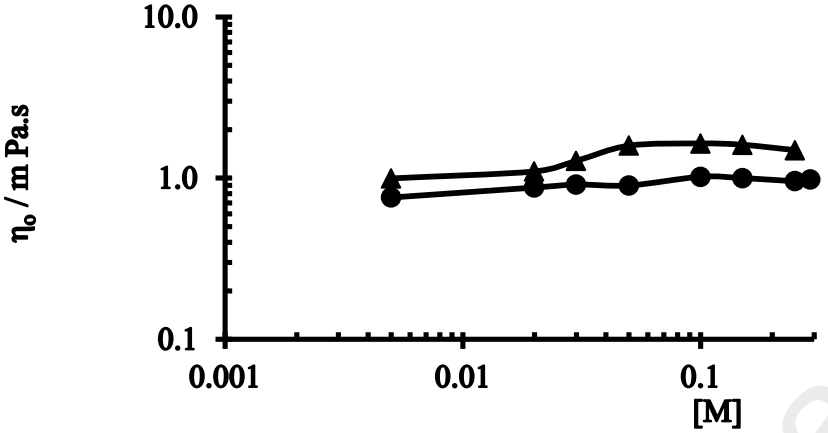

Figure 6.11: Effects of different [MX] upon zero shear viscosity (η_0) for MX = 3-ethyl C_6H_4ONa of aqueous solutions containing 15 mM CTABr, 0.2 mM PSaH, 0.1 M Pip, 30 mM NaOH at 25ºC (▲) and 35ºC (●).

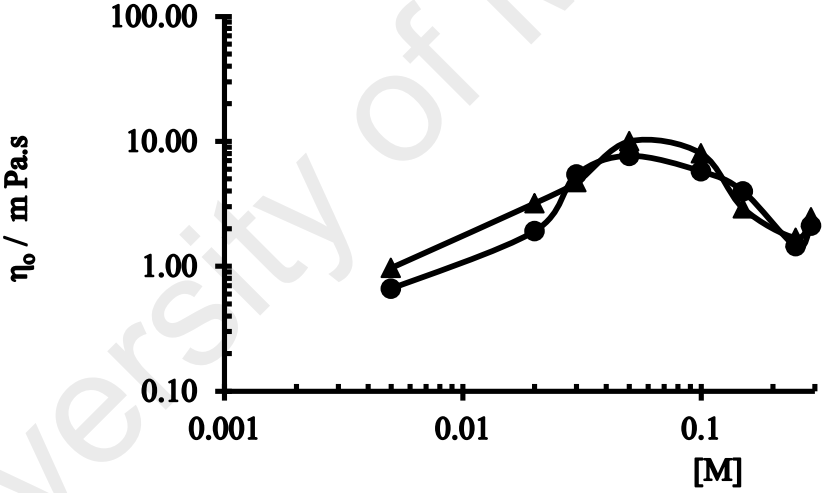

Figure 6.12: Effects of different [MX] upon zero shear viscosity (η_0) for MX = 4-ethyl C_6H_4ONa of aqueous solutions containing 15 mM CTABr, 0.2 mM PSaH, 0.1 M Pip, 30 mM NaOH at 25ºC (▲) and 35ºC (●).

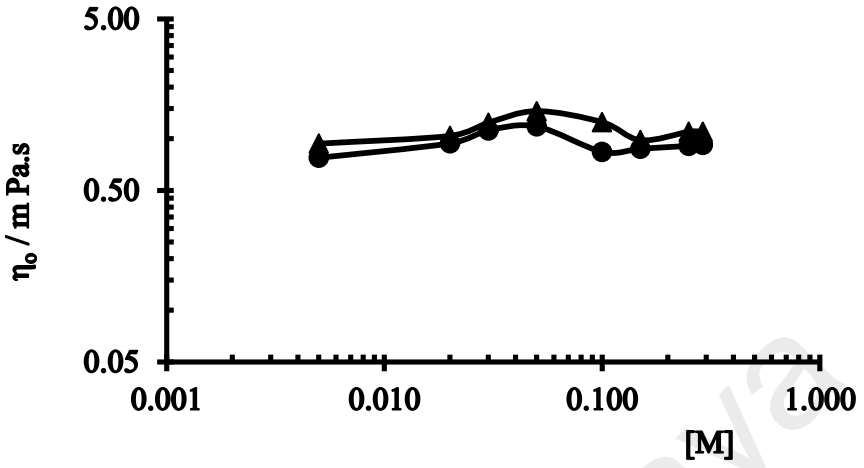

Figure 6.13: Effects of different [MX] upon zero shear viscosity (η_0) for MX = 2-propyl C_6H_4ONa of aqueous solutions containing 15 mM CTABr, 0.2 mM PSaH, 0.1 M Pip, 30 mM NaOH at 25ºC (▲) and 35ºC (●).

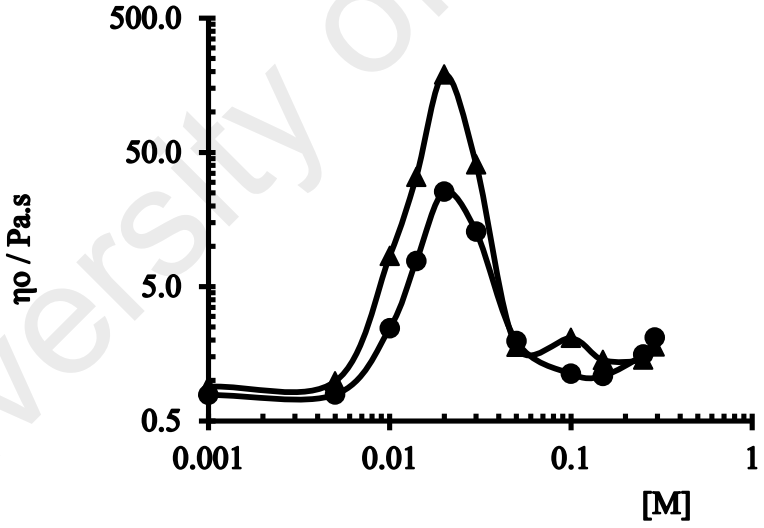

Figure 6.14: Effects of different [MX] upon zero shear viscosity (η_0) for MX = 4-propyl C_6H_4ONa of aqueous solutions containing 15 mM CTABr, 0.2 mM PSaH, 0.1 M Pip, 30 mM NaOH at 25ºC (▲) and 35ºC (●).

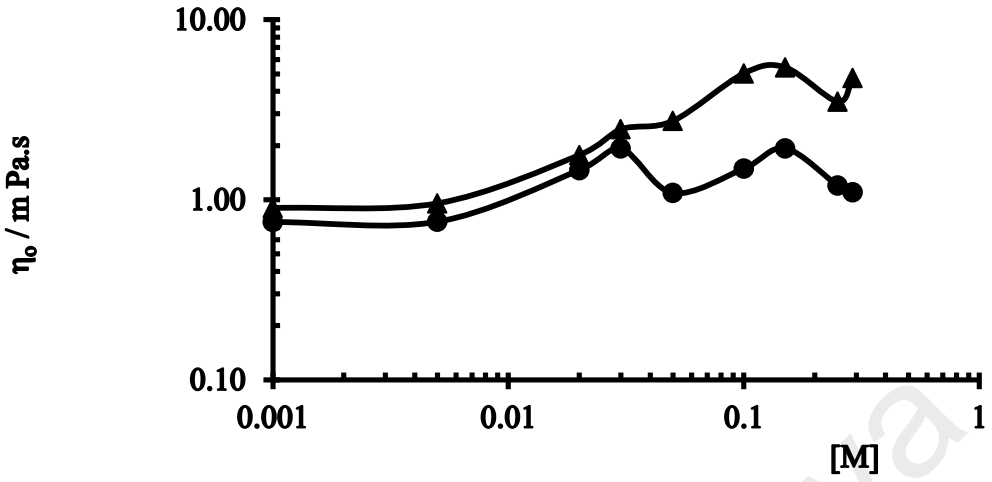

Figure 6.15: Effects of different [MX] upon zero shear viscosity (η_0) for MX = 3-isopropyl C_6H_4ONa of aqueous solutions containing 15 mM CTABr, 0.2 mM PSaH, 0.1 M Pip, 30 mM NaOH at 25ºC (▲) and 35ºC (●).

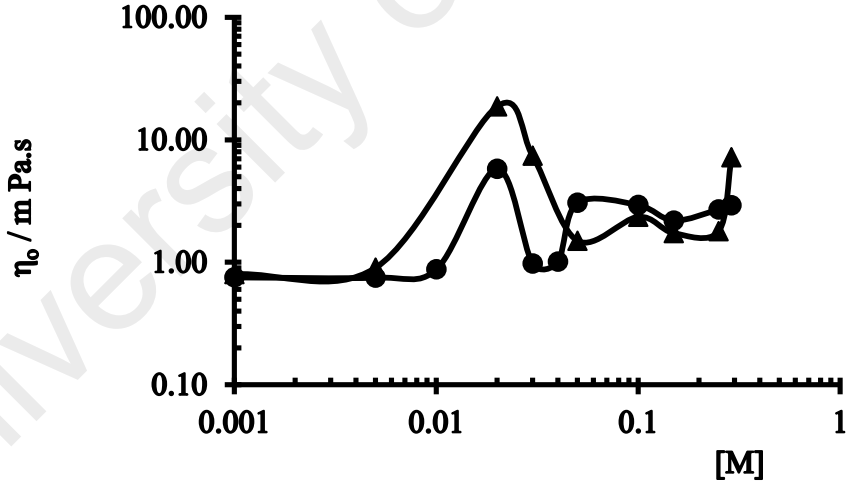

Figure 6.16: Effects of different [MX] upon zero shear viscosity (η_0) for MX = 4-isopropyl C_6H_4ONa of aqueous solutions containing 15 mM CTABr, 0.2 mM PSaH, 0.1 M Pip, 30 mM NaOH at 25ºC (▲) and 35ºC (●).

There were no shear thinning occurred in the rheograms/flow curves showed in Figure 6.1, 6.2, 6.3, 6.5 and 6.7 representing C_6H_5ONa, 2-ethyl C_6H_4ONa, 3-ethyl C_6H_4ONa, 2-propyl C_6H_4ONa and 3-propyl C_6H_4ONa respectively. These pseudoplastic behaviors demonstrate slight changes in zero shear viscosity (η_0) (Baccile et al., 2012) of the flexible nanoparticle in Figure 6.9, 6.10, 6.11, 6.13 and 6.15 representing C_6H_5ONa, 2-ethyl C_6H_4ONa, 3-ethyl C_6H_4ONa, 2-propyl C_6H_4ONa and 3-propyl C_6H_4ONa respectively. The maximum viscosity of solution containing 15mM CTABr and C_6H_5ONa, 2-ethyl C_6H_4ONa, 3-ethyl C_6H_4ONa, 2-propyl C_6H_4ONa and 3-propyl C_6H_4ONa were 0.78 m Pa.s (0.05M), 1.01 m Pa.s (0.10M), 1.02 m Pa.s (0.10M), 1.18 m Pa.s (0.05M) and 1.09 m Pa.s (0.05M) at 35°C respectively. These values are not significantly different from η_0 of water. Thus, the flexible nanoparticle structure is assumed to be spherical (Razak & Khan, 2013).

In contrast of Figure 6.1, 6.2, 6.3, 6.5 and 6.7 representing C_6H_5ONa, 2-ethyl C_6H_4ONa, 3-ethyl C_6H_4ONa, 2-propyl C_6H_4ONa and 3-propyl C_6H_4ONa, Figure 6.4, 6.6 and 6.8 representing 4-ethyl C_6H_4ONa, 4-propyl C_6H_4ONa and 4-isopropyl C_6H_4ONa showed shear thinning at different [NaX]. 4-EtC_6H_4ONa showed shear thinning at [NaX] = 0.03, 0.05, 0.10, 0.15, 0.29 M and giving η_0 = 7.66 m Pa.s at 0.05 M (Figure 6.12) which is higher than that of water. Shear thinning is also observed for 4-propyl C_6H_4ONa (Figure 6.6) at [NaX] = 0.02 M which gives η_0 = 25.5 m Pa.s (Figure 6.14). For 4-isopropyl C_6H_4ONa (Figure 6.8), shear thinning are observed at [NaX] = 0.02 M giving the value of η_0 = 5.8 m Pa.s (Figure 6.16). The maximum plot at 25°C for the effects of different [MX] upon zero shear viscosity (η_0) indicated the concentration on aqueous samples increase when the temperature decrease. The significance of 2 maxima in plot indicates the presence of wormlike and entangled wormlike micelles in the aqueous system.

The zero shear viscosity (η_0) for 4-ethyl C_6H_4ONa, 4-propyl C_6H_4ONa and 4-isopropyl C_6H_4ONa are higher than that of water. Thus, this flexible nanoparticle structure is assumed not spherical micelles. As mentioned in earlier references, it might indicate the presence of rodlike (RM)/wormlike micelles (WM) or large ULV/MLV.

6.3.2 Determination of Flow Activation Energy (E_a^F)

These interesting results of shear thinning at η_0 contribute to the investigation of the flow activation energy, E_a^F. The flow activation energy, E_a^F of a micellar solution represents the energy required to move individual micelles in an environment of surrounding micelles (Razak & Khan, 2013). Hence, the interactions between individual aggregates will affect the value of E_a^F (Fischer & Rehage, 1997). In view of the definitions of E_a^F and micellar contour length, the value of E_a^F should be proportional to the value of micellar contour length. In view to this study, Figure 6.17, 6.18 and 6.19 showing the dependence of shear viscosity (η) upon shear rate ($\dot{\gamma}$) at $[CTABr]_T$ = 15 mM, [PSaH] = 0.2 mM, [Pip] = 0.1 M, [NaOH] = 0.3 mM, T/ºC = 20, 25, 30, 35, 40, 45, 55 for [NaX] = 4-ethyl C_6H_4ONa (50 mM), 4-propyl C_6H_4ONa (20 mM) and 4-isopropyl C_6H_4ONa (20 mM) respectively.

The values of zero shear viscosity, η_0, obtained within the temperature range of 20-55°C at $[CTABr]_T$ = 15 mM and a specific value of [MX] at which viscosity maximum occured in the plot of η_0 *vs*. [MX], are presented graphically in Figure 6.20, 6.21 and 6.22 for MX = 4-ethyl C_6H_4ONa (50 mM), 4-propyl C_6H_4ONa (20 mM) and 4-isopropyl C_6H_4ONa (20 mM). The plots for MX = 4-ethyl C_6H_4ONa and 4-isopropyl C_6H_4ONa appear to be linear, whereas for MX = 4-propyl C_6H_4ONa the plot is nonlinear within the temperature range of 20-55°C. However, the values of η_0 for MX = 4-ethyl C_6H_4ONa, 4-propyl C_6H_4ONa and 4-

isopropyl C_6H_4ONa at different temperature within its range of 20-45°C for as well as 35-55°C were found to fit to an Arrhenius type of empirical equation 6.1:

$$\eta_0 = A \exp (E_a^F / RT) \tag{6.1}$$

where A (pre-exponential factor) and E_a^F represents empirical constants, T is absolute temperature (K), and R is universal gas constant (=8.314 J mol^{-1} K^{-1}).

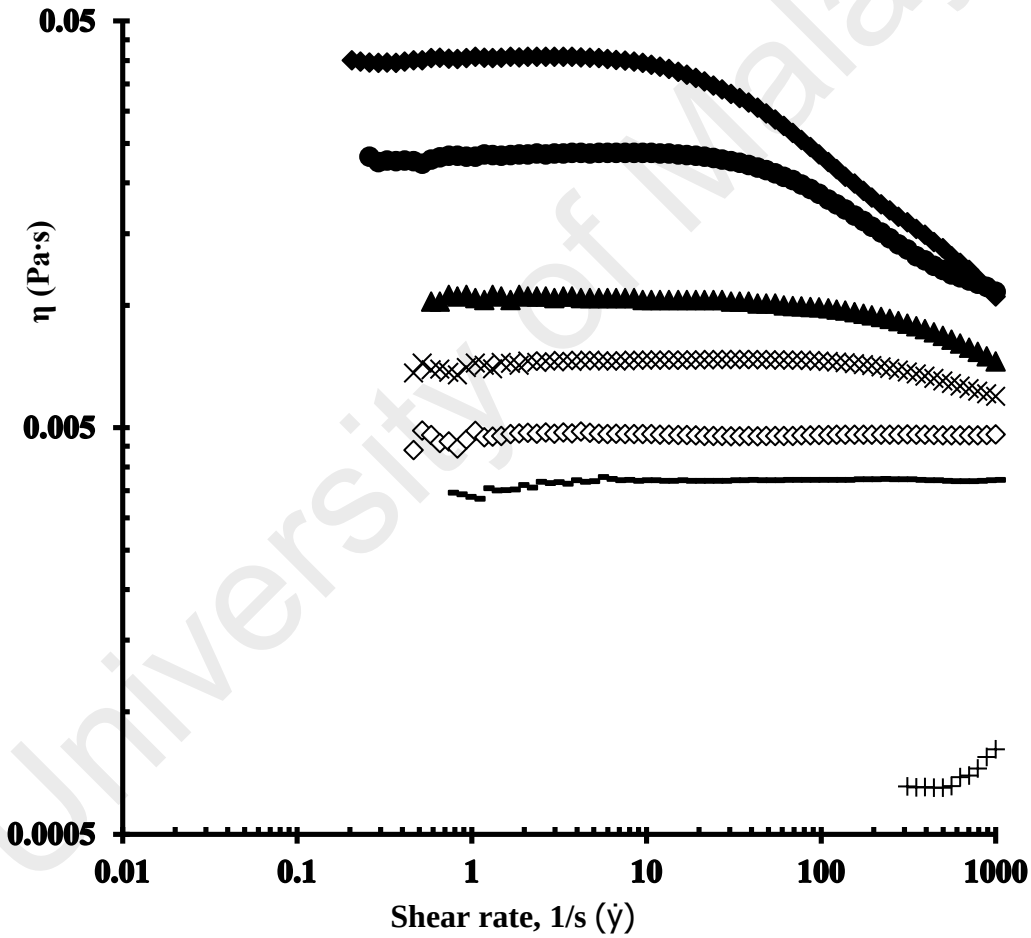

Figure 6.17. Plots showing the dependence of shear viscosity (η) upon shear rate (γ̇) for samples containing $[CTABr]_T$ = 15 mM, [PSaH] = 0.2 mM, [Pip] = 0.1 M, [NaOH] = 0.3 mM and 4-ethylC_6H_4ONa = 50 mM at T/ºC = 20 (♦), 25 (●), 30 (▲), 35 (×), 40 (◊), 45 (-), 55 (+).

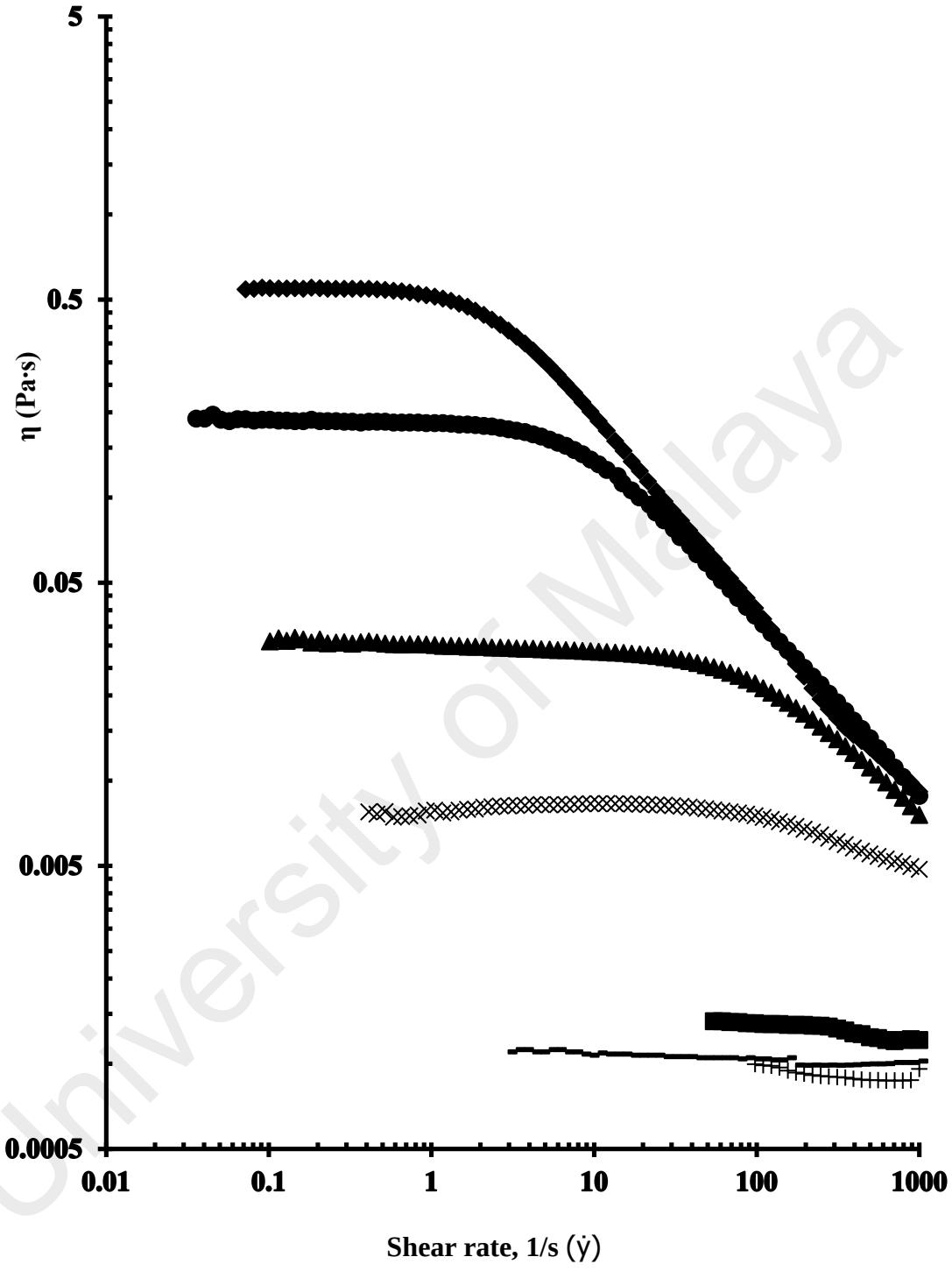

Figure 6.18. Plots showing the dependence of shear viscosity (η) upon shear rate (γ̇) for samples containing $[CTABr]_T$ = 15 mM, [PSaH] = 0.2 mM, [Pip] = 0.1 M, [NaOH] = 0.3 mM and 4-propyl C_6H_4ONa = 20 mM at T/ºC = 20 (♦), 25 (●), 30 (▲), 35 (×), 40 (■), 45 (-), 55 (+).

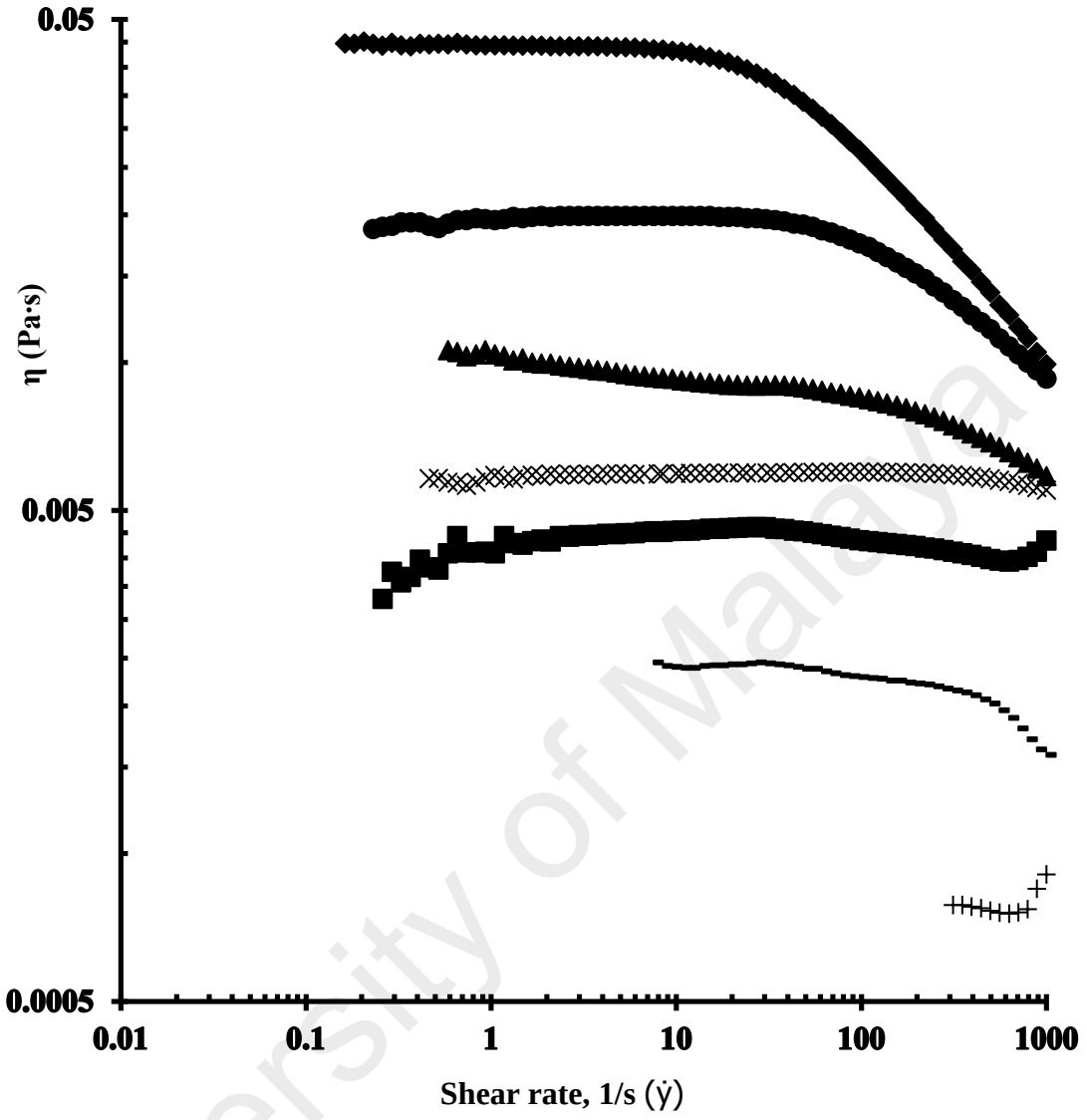

Figure 6.19. Plots showing the dependence of shear viscosity (η) upon shear rate (γ̇) for samples containing $[CTABr]_T$ = 15 mM, [PSaH] = 0.2 mM, [Pip] = 0.1 M, [NaOH] = 0.3 mM and 4-isopropyl C_6H_4ONa = 20 mM at T/ºC = 20 (♦), 25 (●), 30 (▲), 35 (×), 40 (■), 45 (-), 55 (+).

The least-squares calculated values of ln (A) and E_a^F for MX = 4-ethyl C_6H_4ONa, 4-propyl C_6H_4ONa and 4-isopropyl C_6H_4ONa are listed in Table 6.1. The values of η_0 for MX = 4-ethyl C_6H_4ONa, 4-propyl C_6H_4ONa and 4-isopropyl C_6H_4ONa at different temperature within its range 20-55°C were found to fit to Eq 6.1 and the least-squares calculated values

of ln (A) and E_a^F are summarized in Table 6.1. The observed data fit to Eq 6.1 was satisfactory in terms of residual errors (RE = $[\ln(\eta_0) - \ln(\eta_0^{cald})] / \ln(\eta_0)$) and standard deviations associated with the calculated parameter, ln (A) and E_a^F as shown in Table 6.1.

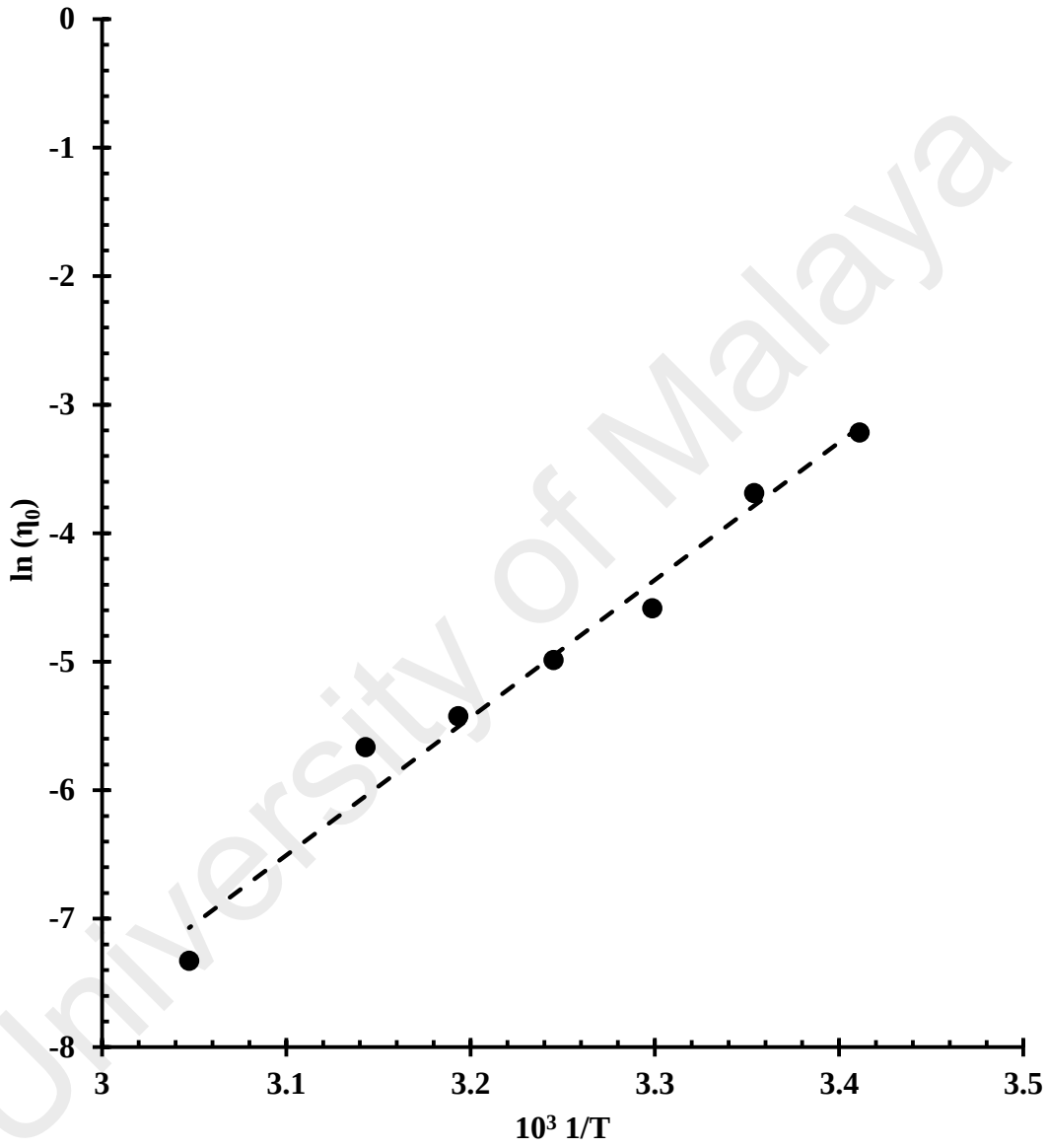

Figure 6.20: Plots showing the dependence of ln η_0 upon 1/T for samples containing $[CTABr]_T$ = 15 mM, [PSaH] = 0.2 mM, [Pip] = 0.1 M, [NaOH] = 30 mM and [MX]/mM = 50 for MX = 4-ethyl C_6H_4ONa (●). Dashed lines are drawn through calculated data points using Eq 6.1 and calculated values of ln (A) and E_a^F obtained within temperature range of 20-55ºC.

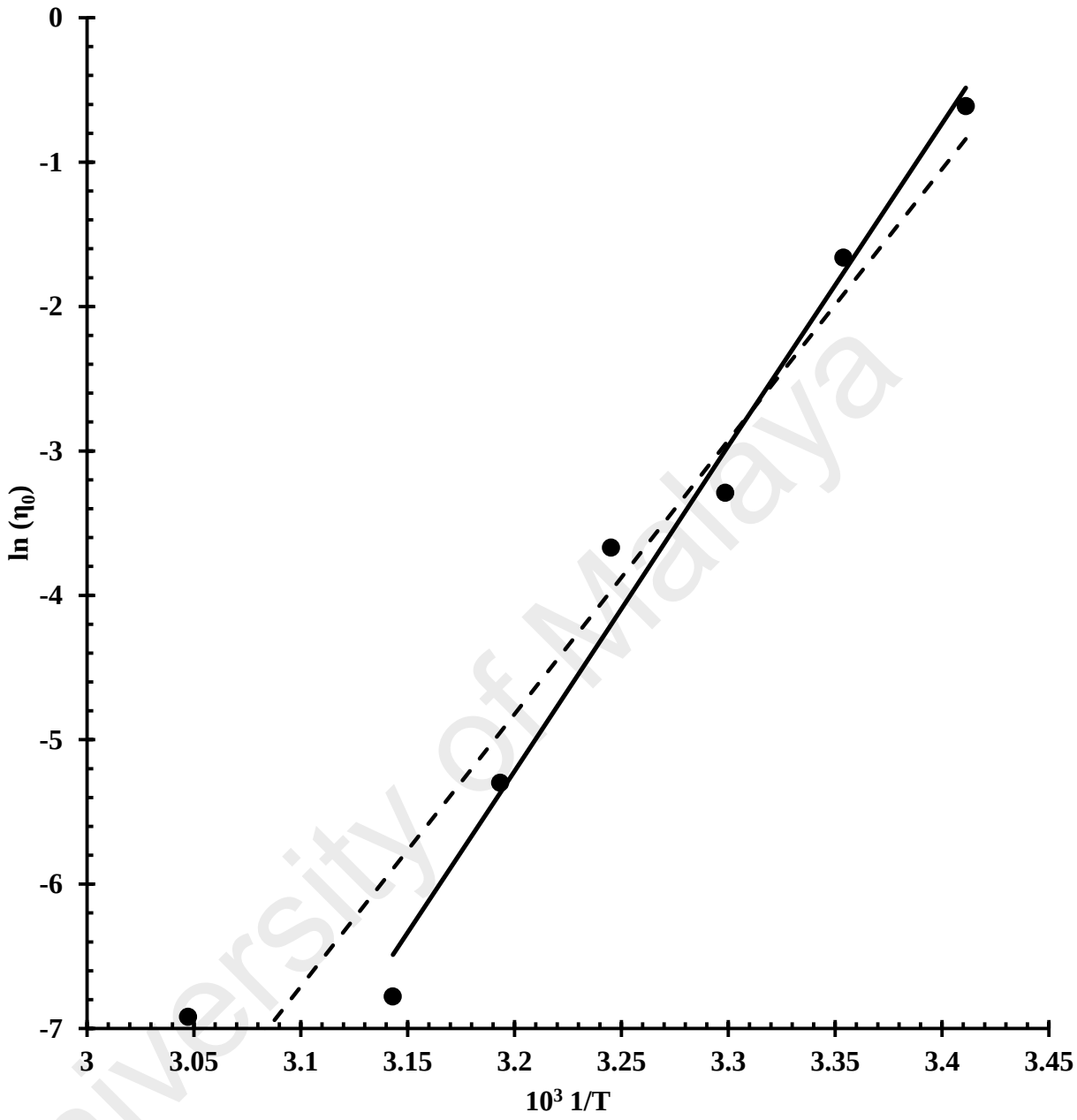

Figure 6.21: Plots showing the dependence of ln η_0 upon 1/T for samples containing $[CTABr]_T$ = 15 mM, [PSaH] = 0.2 mM, [Pip] = 0.1 M, [NaOH] = 30 mM and [MX]/mM = 20 for MX = 4-propyl C_6H_4ONa (●). Solid lines are drawn through the least-squares calculated data points using Eq 6.1 and calculated values of ln (A) and E_a^F listed in Table 6.1 within temperature range of 20-45ºC. Dashed lines are drown through calculated data points using Eq 6.1 and calculated values of ln (A) and E_a^F obtained within temperature range of 20-55ºC.

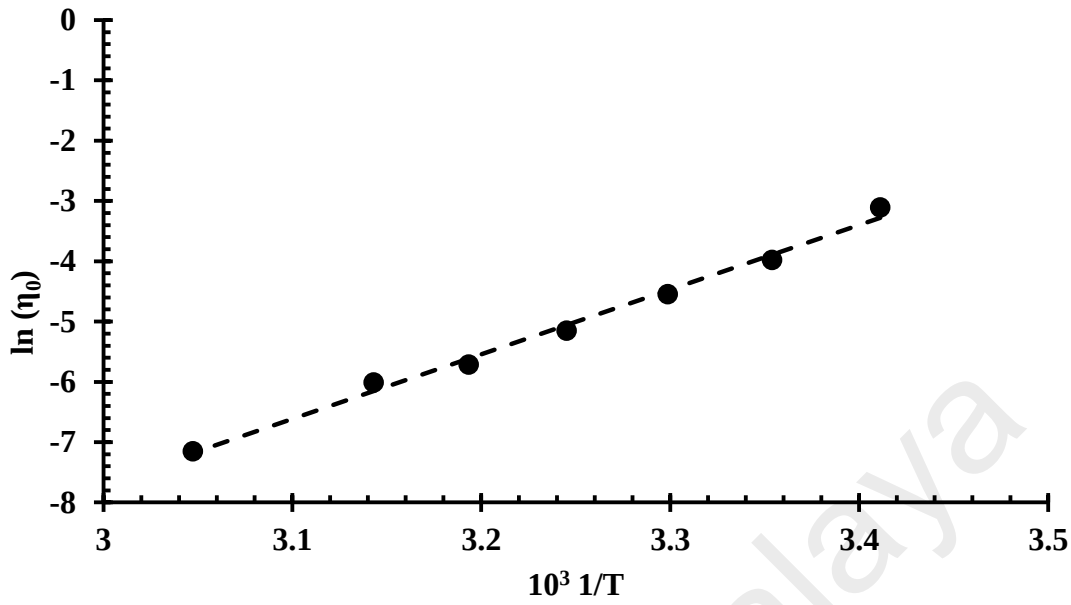

Figure 6.22: Plots showing the dependence of ln η_0 upon 1/T for samples containing $[CTABr]_T$ = 15 mM, [PSaH] = 0.2 mM, [Pip] = 0.1 M, [NaOH] = 30 mM and [MX]/mM = 20 for MX = 4-isopropyl C_6H_4ONa (●). Dashed lines are drown through calculated data points using Eq. 6.1 and calculated values of ln (A) and E_a^F obtained within temperature range of 20-55ºC.

Table 6.1 Values of ln (A) and E_a^F calculated from **Eq. 6.1** in the presence of different MXs.

MX	[MX] [a]	η_0 [b]	- ln (A)	E_a^F	R_X^{Br}	%RE [c]	Temp. range [d]
	mM	mPa s		kJ/mol			°C
4-ethyl C_6H_4ONa	50	7.66	39.73 ± 0.21 [f]	89.1 ± 0.1 [f]	32.5	0.2	20-55
4-isopropC$_6$H$_4$ONa	20	25.5	39.87 ± 1.31	89.2 ± 0.2	66.6	1.7	20-55
4-propyl C_6H_4ONa	20	5.8	65.17 ± 6.38	156.8 ± 0.2	145.7	6.5	20-55
4-propyl C_6H_4ONa	20 [e]	5.8 [e]	76.87 ± 5.09	186.2 ± 0.6	145.7	4.2	20-45

[a] Specific concentration of MX at which first maximum occurs in the plot of η_0 vs. [MX] at 15 CTABr and 35°C.
[b] The value of η_0 at [MX] and 35°C.
[c] %RE = 100 × {[ln(η_0) – ln(η_0^{cald})] / ln(η_0)} where η_0^{cald} represents least-squares calculated value of η_0 using Eq 6.1.
[d] Temperature range used to calculate ln (A) and E_a^F from Eq. 6.1.
[e] Value of [MX] or η_0 corresponding to the plot of η_0 vs. [MX] at 15 mM CTABr and 45°C.
[f] Error limits are standard deviations.

CHAPTER 7

EFFECTS OF TURBIDITY AND PARTICLES SIZE ON FLEXIBLE NANOPARTICLE IN THE PRESENCE OF PIPERIDINE WITH PS^-

7.1 Introduction

Micellar aggregates is due to the self-assembly of surfactant molecules in aqueous solutions (Andreozzi et al., 2010; Chen et al., 2004; Feitosa et al., 2006; Kaler et al., 1989; Kondo et al., 1995). In the general context of complex fluids, micellar aggregates such as vesicles and micelles have received considerable attention from theoreticians and experimentalists for the past decade (Marques et al., 1998; Marques et al., 2003; Tondre & Caillet, 2001). When micelles grow and become vesicle unilamellar, the aggregates are much like liposomes, and as liposomes; they form lipid bilayer. Usually, the sample consisted of vesicle micelles are typically turbid (Razak & Khan, 2013). A lipid bilayer comprised of two layers of phospholipids is arranged end to end with the hydrophobic layered buried between two layers. And as a spherical vesicle, it contains aqueous solution inside the chamber (Velázquez et al., 2007; Fischer et al., 2002; Fuangswasdi et al., 2006a.).

Flexible nanoparticles, FN (CTABr/MX/H_2O)-catalyzed piperidinolysis of ionized phenyl salicylate yield the growth of micellar self-assembly structure. Taking these facts into considerations, we study the turbidity, particle size, optical polarizing microscope (OPM) analysis and the real pictures of FN at different MX.

7.2 Materials And Methods

7.2.1 Chemicals

Commercial products of highest available purity such as cetyltrimethylammonium bromide, $C_{16}H_{33}NMe_3Br$, phenyl salicylate, C_6H_5OH, 2-ethyl C_6H_4OH, 3-ethyl C_6H_4OH, 4-ethyl C_6H_4OH, 2-propyl C_6H_4OH, 4-propyl C_6H_4OH, 3-isopropyl C_6H_4OH, 4-isopropyl C_6H_4OH, piperidine (Pip) and all other common chemicals used were of reagent grade. The stock solutions of PSaH=0.01M were prepared in acetonitrile because of its low aqueous solubility. The stock solutions (w M) of nonionic substituted phenols were prepared by adding (w + 0.05 M) sodium hydroxide so that wM XH solutions become wM MX.

7.2.2 Turbidity

Turbidity measurements for the aqueous samples were carried out spectrophotometrically at a constant wavelength of 600 nm; temperature at 35 °C for solution containing 15 mM CTABr, 0.1 M Pip, 0.03 M NaOH, and 0.2 mM PSaH; and different values of C_6H_5ONa, 2-ethyl C_6H_4ONa, 3-ethyl C_6H_4ONa, 4-ethyl C_6H_4ONa, 2-propyl C_6H_4ONa, 4-propyl C_6H_4ONa, 3-isopropyl C_6H_4ONa and 4-isopropyl C_6H_4ONa. The choice of the wavelength at 600 nm was based upon the visible spectra (scanned within the wavelength range 350–900 nm) of samples containing all chemical ingredients (used for kinetic and rheological measurements) at $[CTABr]_T$ = 0.0 and 15 mM. Turbidity was expressed in absorbance, A_{ob}, units. A_{ob} represents absorbance at 600 nm.

7.2.3 Particle Size

Particle size of the micelles were measured using Zetasizer Nano ZS (Malvern Instruments Ltd., United Kingdom) equipped with a 4mW He-Ne laser at 633 nm by employing dynamic light scattering (DLS) method at a scattering angle of 90°. The four sided clear fluorescent quartz cuvette of 1 cm path length was used for the particle size analysis. All

measurements were carried out in triplicate at 35 ± 1°C ((Tan & Misni, 2013; Eh Suk & Misni, 2017).

7.2.4 Optical Polarizing Microscope (OPM)

The morphology of the micelles prepared was evaluated by employing Leica optical polarizing microscope equipped with image analysis software Leica QWin (Germany). Sample was carefully dropped on the glass slide and covered with a cover slip. A drop of immersion oil was spiked onto the cover slip and micrograph was observed under 100 µm conditions.

7.2.5 Real Pictures

In order to have the clear picture of the samples, sample pictures were taken using phone camera Samsung model GT-18552.

7.3 Results and Discussions

7.3.1 Effects of [MX] on the turbidity

The plots of A_{ob} *vs*. [MX] are shown in Figure 7.1 for C_6H_5ONa, 2-ethyl C_6H_4ONa, 3-ethyl C_6H_4ONa, 4-ethyl C_6H_4ONa, 2-propyl C_6H_4ONa, 4-propyl C_6H_4ONa, 3-isopropyl C_6H_4ONa and 4-isopropyl C_6H_4ONa. The values of A_{ob}^{corr} represent corrected absorbance due to (a) absorbance (A_{MX}^{CTABr}) exhibited by the solutions containing 0.1 M Pip, 0.03 M NaOH, 0.2 mM PSaH, 15 mM CTABr and different values of MX (where $A_{ob}^{CTABr} \leq 0.001$ nm) and (b) absorbance (A_{ob}^{MX}) exhibited by the solution containing 0.1 M Pip, 0.03 M NaOH, 0.2 mM PSaH and different values of MX. The corrected A_{ob} values represent absorbance due to the presence of CTABr/MX aggregates. It is evident from the plots of Figure 7.1 that the turbidity increases with increasing of [MX]. The values of C_6H_5ONa

(●), 2-ethyl C_6H_4ONa (o), 3-ethyl C_6H_4ONa (▲) and 4-ethyl C_6H_4ONa (×) were almost insignificant with clear solutions observed in Figure 7.2, 7.3, 7.4 and 7.5. However, the depicted Figure (Figure 7.1) proved the absence of turbidity of C_6H_5ONa (●), 2-ethyl C_6H_4ONa (o), 3-ethyl C_6H_4ONa (▲) and 4-ethyl C_6H_4ONa (×) that may not be detected through the eyes observation.

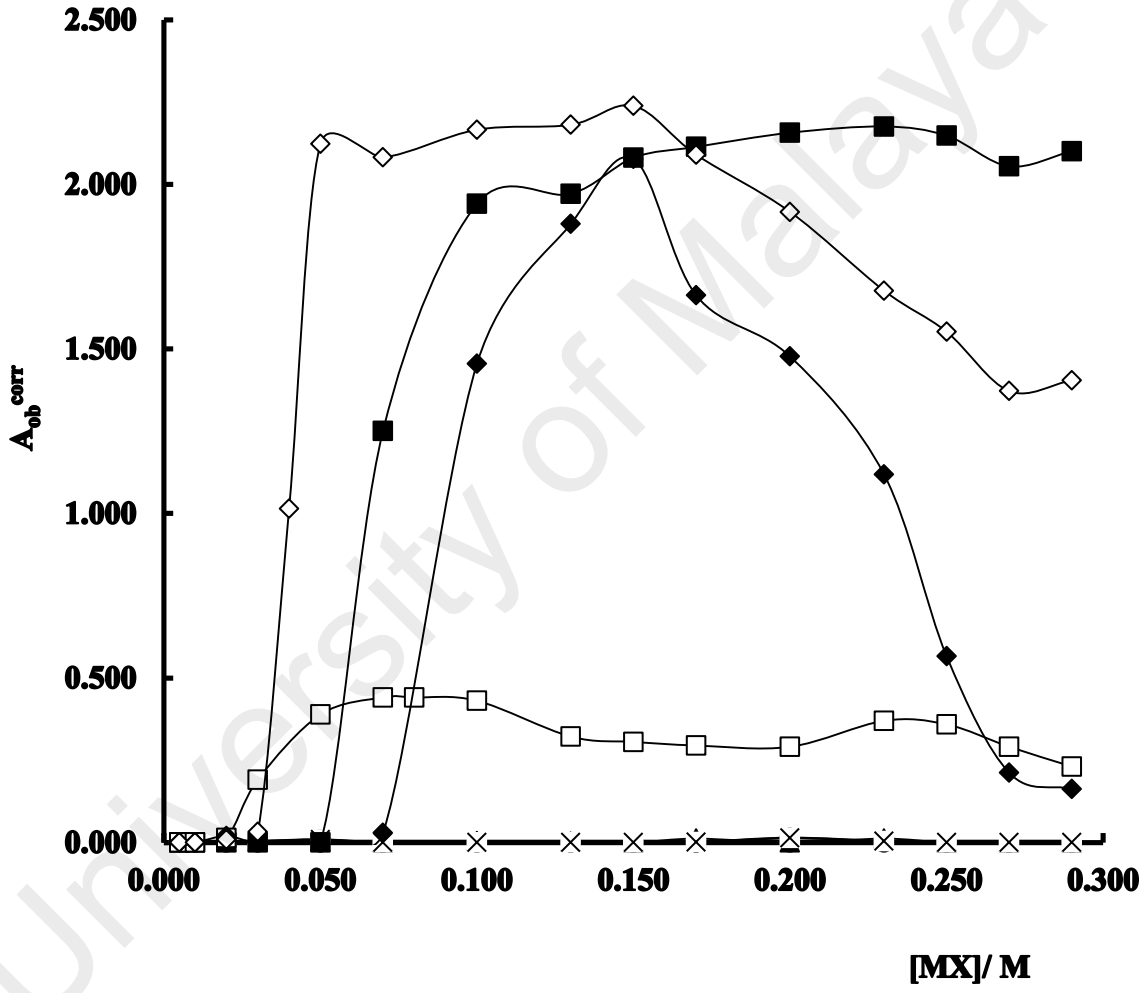

Figure 7.1: Effects of [MX] = C_6H_5ONa (●), 2-ethyl C_6H_4ONa (o), 3- ethyl C_6H_4ONa (▲), 4- ethyl C_6H_4ONa (×), 2-propyl C_6H_4ONa (■), 4- propyl C_6H_4ONa (□), 3-isopropyl C_6H_4ONa (♦) and 4- isopropyl C_6H_4ONa (◊) on corrected absorbance at 600 nm of aqueous containing 15 mM CTABr, 0.1 M Pip, 0.03 M NaOH and 0.2 mM PS^-.

Figures 7.2 - 7.9 represent real pictures of FN where [MX] = C_6H_5ONa, 2-ethyl C_6H_4ONa, 3-ethyl C_6H_4ONa, 4-ethyl C_6H_4ONa, 2-propyl C_6H_4ONa, 4-propyl C_6H_4ONa, 3-isopropyl C_6H_4ONa and 4-isopropyl C_6H_4ONa respectively.

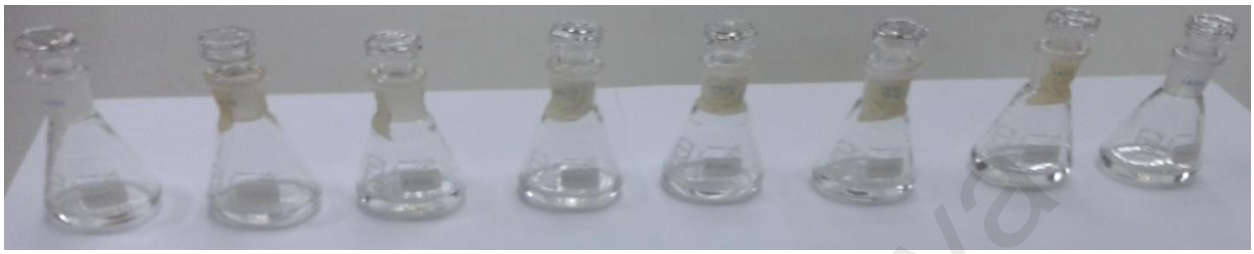

Figure 7.2: FN aqueous solutions where [MX] = C_6H_5ONa containing 15 mM CTABr, 0.1 M Pip, 0.03 M NaOH and 0.2 mM PS^-. The [MX] increases from left to the right handside where [C_6H_5ONa] = 0.005, 0.020, 0.030, 0.050, 0.100, 0.150, 0.250 and 0.29 M respectively.

Figure 7.3: FN aqueous solutions where [MX] = 2-ethyl C_6H_4ONa containing 15 mM CTABr, 0.1 M Pip, 0.03 M NaOH and 0.2 mM PS^-. The [MX] increases from left to the right handside where [2-EtC_6H_4ONa] = 0.005, 0.020, 0.030, 0.050, 0.100, 0.150, 0.250 and 0.29 M respectively.

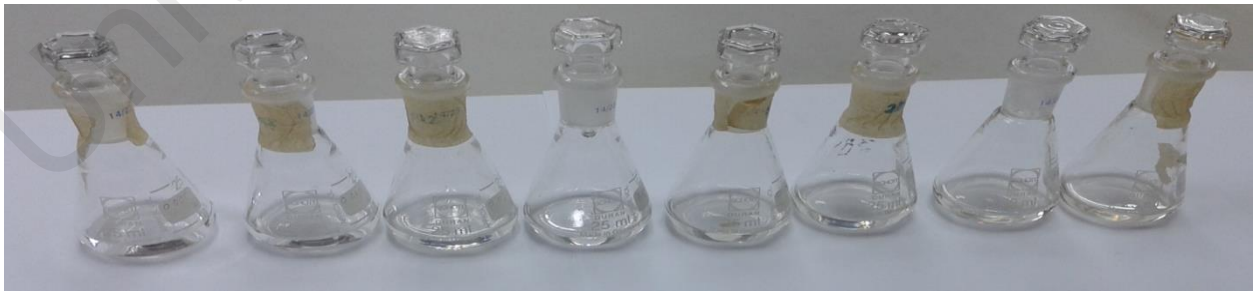

Figure 7.4: FN aqueous solutions where [MX] = 3- ethyl C_6H_4ONa containing 15 mM CTABr, 0.1 M Pip, 0.03 M NaOH and 0.2 mM PS^-. The [MX] increases from left to the right handside where [3-EtC_6H_4ONa] = 0.005, 0.020, 0.030, 0.050, 0.100, 0.150, 0.250 and 0.29 M respectively.

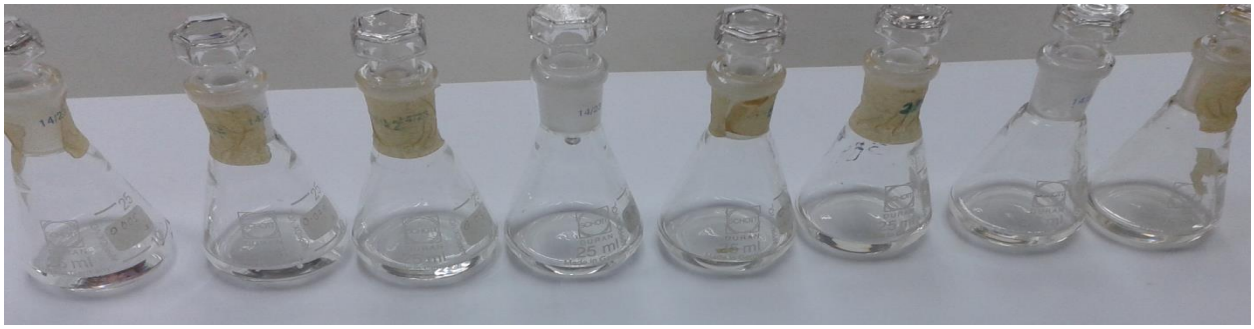

Figure 7.5: FN aqueous solutions where [MX] = 4- ethyl C_6H_4ONa containing 15 mM CTABr, 0.1 M Pip, 0.03 M NaOH and 0.2 mM PS^-. The [MX] increases from left to the right handside where [4-EtC_6H_4ONa] = 0.005, 0.020, 0.030, 0.050, 0.100, 0.150, 0.250 and 0.29 M respectively.

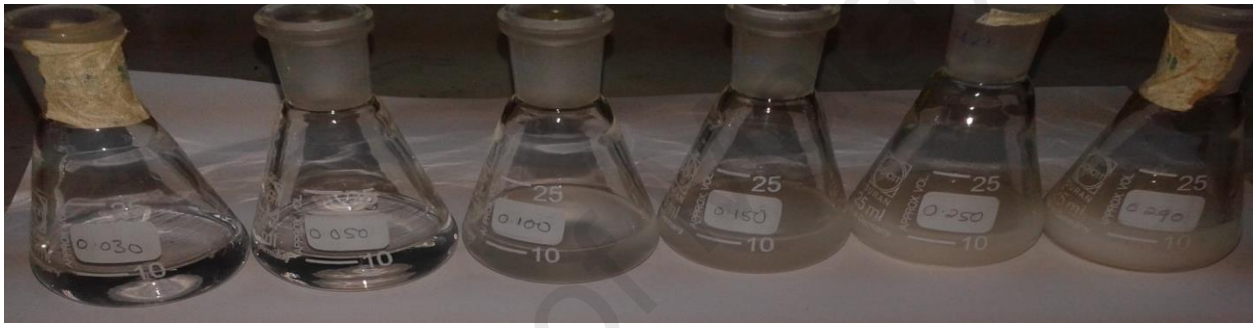

Figure 7.6: FN aqueous solutions where [MX] = 2-propyl C_6H_4ONa containing 15 mM CTABr, 0.1 M Pip, 0.03 M NaOH and 0.2 mM PS^-. The [MX] increases from left to the right handside where [2-$PropC_6H_4ONa$] = 0.030, 0.050, 0.100, 0.150, 0.250 and 0.29 M respectively.

Figure 7.7: FN aqueous solutions where [MX] = 4- propyl C_6H_4ONa containing 15 mM CTABr, 0.1 M Pip, 0.03 M NaOH and 0.2 mM PS^-. The [MX] increases from left to the right handside where [4-$PropC_6H_4ONa$] = 0.005, 0.020, 0.030, 0.050, 0.100, 0.150, 0.250 and 0.29 M respectively.

Figure 7.8: FN aqueous solutions where [MX] = 3-isopropyl C_6H_4ONa containing 15 mM CTABr, 0.1 M Pip, 0.03 M NaOH and 0.2 mM PS^-. The [MX] increases from left to the right handside where [3-IsopropC_6H_4ONa] = 0.005, 0.020, 0.030, 0.050, 0.100, 0.150, 0.250 and 0.29 M respectively.

Figure 7.9: FN aqueous solutions where [MX] = 4- isopropyl C_6H_4ONa containing 15 mM CTABr, 0.1 M Pip, 0.03 M NaOH and 0.2 mM PS^-. The [MX] increases from left to the right handside where [4-IsopropC_6H_4ONa] = 0.005, 0.020, 0.030, 0.050, 0.100, 0.150, 0.250 and 0.29 M respectively.

FN aqueous solutions containing [MX] = C_6H_5ONa (Figure 7.2), 2-ethyl C_6H_4ONa (Figure 7.3), 3-ethyl C_6H_4ONa (Figure 7.4) and 4-ethyl C_6H_4ONa (Figure 7.5) shows relatively no turbidity as the [MX] increases. However, for FN aqueous solutions containing [MX] =2-propyl C_6H_4ONa (Figure 7.6), 4- propyl C_6H_4ONa (Figure 7.7), 3-isopropyl C_6H_4ONa (Figure 7.8) and 4-isopropyl C_6H_4ONa (Figure 7.9), the turbidity are increases by the observation through the real presentations. All the findings coincide with Figure 7.1 where [MX] = 2-propyl C_6H_4ONa , 4- propyl C_6H_4ONa , 3-isopropyl C_6H_4ONa and 4- isopropyl C_6H_4ONa shown relative corrected absorbance (A_{ob}^{corr}) vs [MX].

7.3.2 Effects of [MX] on the particle size of FN

Due to the intriguing findings, the particle size of FN for [MX] = C_6H_5ONa, 2-ethyl C_6H_4ONa, 3-ethyl C_6H_4ONa, 4-ethyl C_6H_4ONa, 2-propyl C_6H_4ONa, 4-propyl C_6H_4ONa, 3-isopropyl C_6H_4ONa and 4- isopropyl C_6H_4ONa at 0.1 M Pip, 0.03 M NaOH, 0.2 mM PSaH, 15 mM CTABr and 35 ± 1°C are investigated through particle size analysis. Figure 7.10 depict the tabulated particle size (nm) of FN at respective [MX].

The particle size of micelles distribution in the FN system containing C_6H_5ONa, 2-ethyl C_6H_4ONa, 3-ethyl C_6H_4ONa, 4-ethyl C_6H_4ONa, 4-propyl C_6H_4ONa and 4-isopropyl C_6H_4ONa were less than 1 µm respectively. The average values of particle size distributions for micelles at respective [MX] are relatively insignificant in the Figure 7.10. Since the particle size of MX = 2-propyl C_6H_4ONa and 3-isopropyl C_6H_4ONa at 0.1 M shown in Figure 7.10 were 78100 nm (78.1 µm) and 57600 nm (57.6 µm) respectively, the determination of micellar structure was analyzed by Optical Polarization Microscope, OPM (micrometer size) where 15 mM CTABr, 0.1 M Pip, 0.03 M NaOH and 0.2 mM PS^- is kept constant. The samples are freshly prepared to prevent the effect of time on the micellar growth.

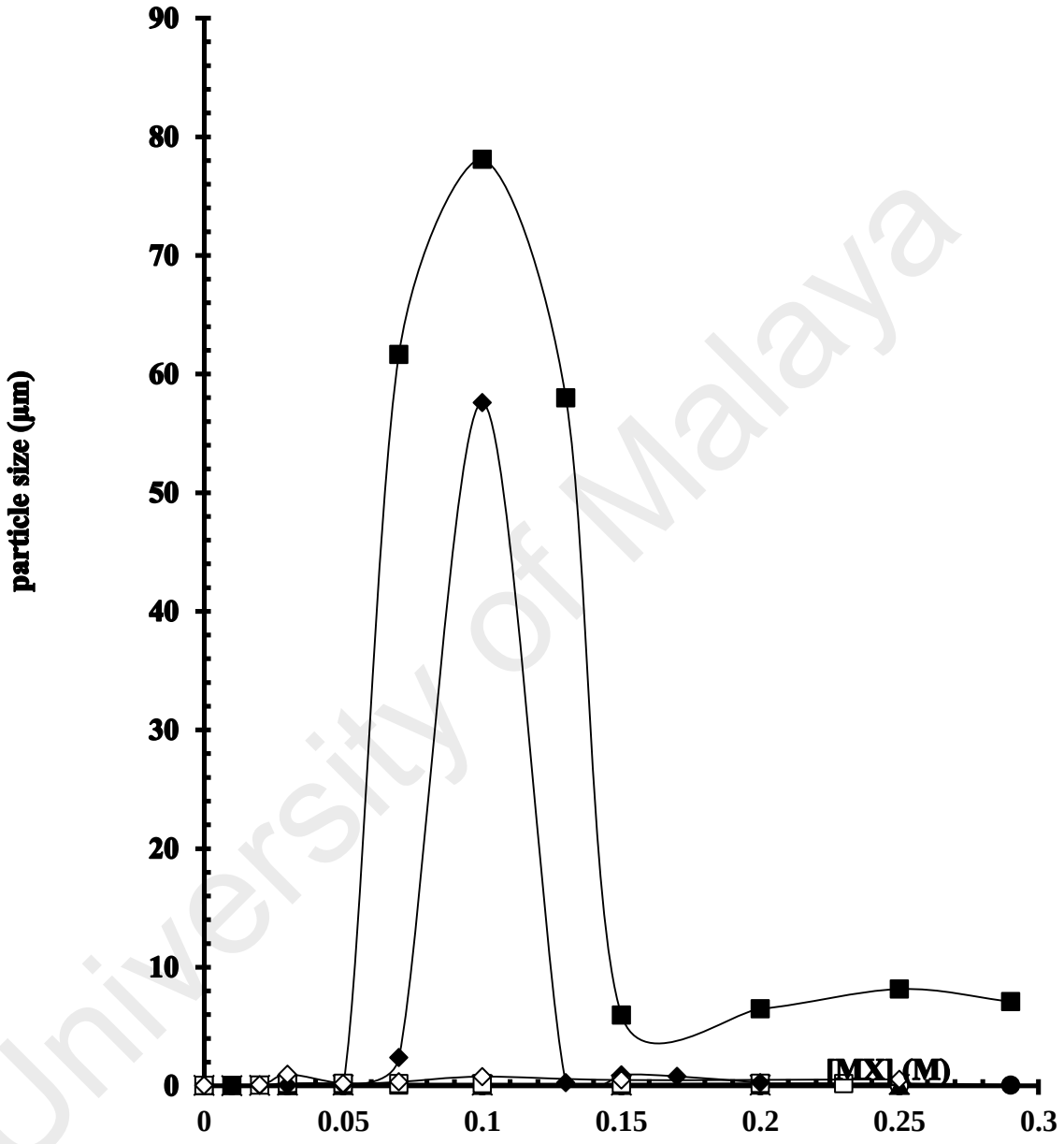

Figure 7.10: Effects of [MX] = C_6H_5ONa (●), 2-ethyl C_6H_4ONa (o), 3-ethyl C_6H_4ONa (▲), 4-ethyl C_6H_4ONa (×), 2-propyl C_6H_4ONa (■), 4- propyl C_6H_4ONa (□), 3-isopropyl C_6H_4ONa (♦) and 4- isopropyl C_6H_4ONa (◊) on particle size (µm) of aqueous containing 15 mM CTABr, 0.1 M Pip, 0.03 M NaOH and 0.2 mM PS^-.

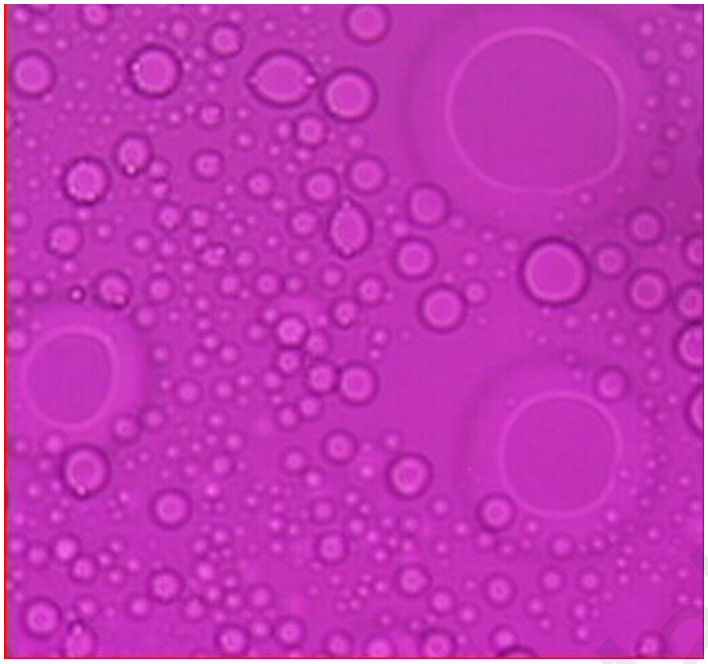

Figure 7.11: A GUV in the FN at [PSH] = 0.2mM, [NaOH] = 0.03M, [Pip] = 0.1M, [CTABr] = 0.015M and [MX] = 0.10 M where X = 2-propyl $C_6H_5O^-$ taken by OPM (100x lenset).

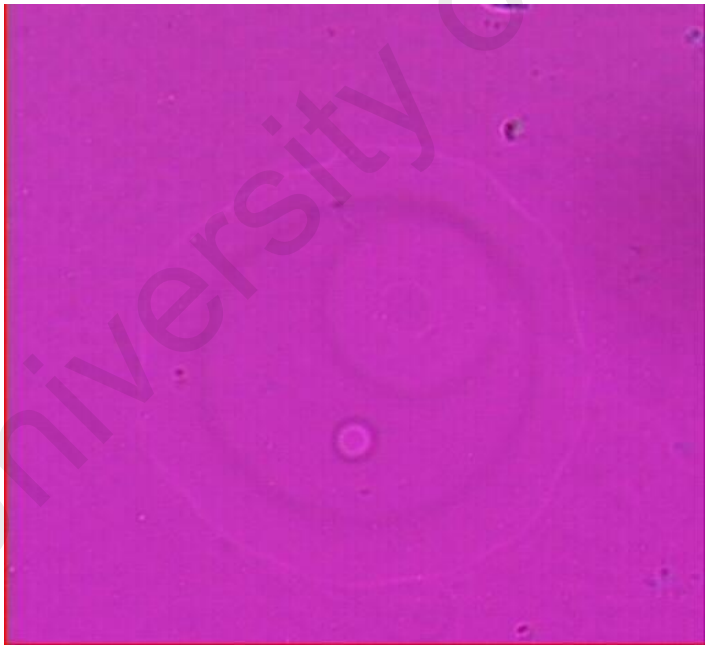

Figure 7.12: A GUV in the FN at [PSH] = 0.2mM, [NaOH] = 0.03M, [Pip] = 0.1M, [CTABr] = 0.015M and [MX] = 0.10 M where X = 3-isopropyl $C_6H_5O^-$ taken by OPM (100x lenset).

The use of OPM with an integration of particle size analysis was rationalized due to its ability to determine the presence of giant unilamellar vesicles (GUV) in aqueous solutions at the range of micrometer size (Moscho et al., 1996). OPM is an option to determine the micellar structure of the FN for the following reasons; i) the rheological analysis would be an advantageous tool to determine the presence of wormlike micelles (Davies et al., 2006), ii) TEM would be better analyzed within the nanoscale regions.

Based on the tabulated data depicted from Figure 7.10, the maximum increase of micellar size at 78.1 µm and 57.6 µm for MX = 2-propyl C_6H_4ONa and 3-isopropyl C_6H_4ONa or known as swelling phenomena (where the micellar size increase) were due development of giant unilamellar vesicle (GUV) micelles (Agarwal et al, 2006). 2-Prop$C_6H_4O^-$ and 3-isoprop$C_6H_4O^-$ are well known for its high hydrophobicity, prone to penetrate into the micellar system where these substituted phenolates counterions, X- expel out the less hydrobhobic counterions, i.e PS^-, Br^- at the head group and swelled the micelle into growth (Marques et al., 2003).

The micellar self-assembly structures for X = 2-propyl $C_6H_4O^-$ and 3-isopropyl $C_6H_5O^-$ at 0.10 M are shown in Figure 7.11 and 7.12 respectively. The findings are coincides with the previous article published elsewhere (Alexander et al., 1996).

CHAPTER 8

MICROSCOPIC EVIDENCE OF THE MICELLAR STRUCTURE FOR THE EFFECTS OF PHENOLATE AND ITS SUBSTITUTED IONS ON CATIONIC MICELLAR GROWTH

8.1 Introduction

Cetyltrimethylammonium bromide (CTABr) surfactants have commercial applications in the industries (Sauerová et al., 2015; Ferrer-Tasies et al., 2013; El-Sheikh et al., 2013; Lu et al., 2010; Chaudhuri & Paria, 2010; Tang et al., 2010). It contains both hydrophilic regions (polar head groups) as well as hydrophobic regions (the long hydrophobic chain). The aggregates of the surfactants which is called micelle could be spherical, worm-like or vesicle in shape. The self-aggregation of surfactant molecules is influenced by many factors, such as counterions, pH and temperatures (Toernblom & Henriksson, 1997; Hedin et al., 1999; Akhter & Alawi, 2002; Forland et al., 1994).

The influence of counterions on the growth of micelles is reported in many papers (Kunz et al., 2004; Kunz et al., 2004; Missel et al., 1989; Lu et al., 1993; He et al., 1989). Therefore, counterion binding efficiency studies are carried out to determine the effects of structure and dynamics of micelles (Oelshlaeger et al., 2010). Also known as dopants, the effect of counterion structure for the transition of spherical micelle to wormlike micelle; which theoretically justified through the chemistry of the substituent was published in previous literature (Bijma et al., 1998; Martín et al., 2012).

This research has the application potential in many areas (Kim et al., 2005; Kim et al., 2006). Micellar-enhanced ultra filtration (MEUF) process is a successful concept adapted from this study. MEUF has been used for the removal of organics substances like

phenol and *o*-cresol in aqueous phase (Syamal et al., 1997; Tung et al., 2002; Witek et al., 2006; Zeng et al., 2007). The principle of MEUF dictated that the micelles are too large to pass through the membranes and retain highly concentrated surfactant micelles containing soluble contaminants (Purkait et al., 2005). The applications of the research also encompass the study of drug delivery system. The micelles have been used as skin permeation enhancers for transdermal drug delivery coordination (Karande et al., 2007; Karande et al., 2004). Micelles are usually applied with a solvent system and their motion depends on the charge and hydrophobicity of tail lengths. Ethosomes are relatively new types of vesicle systems and composed of water, ethanol and micelles (Dayan & Touitou, 2000; Touitou & Godin, 2007). Ethosomes were also reported as the effective method at delivering salicylates to and through the skin towards the systemic circulation (Mustafa et al., 2007).

Due to the importance of the research (Giorgio et al., 2016; Can et al., 2016; Tian et al., 2016; Misbah et al., 2015; Sharma et al., 2015) this chapter will discuss the effect of counterions to the self-assembly structure of micelle (Yusof & Khan, 2011; Khan et al., 2010; Khan & Ismail, 2010; Khan et al., 2000; Khan et al., 1997). In the present study, the microscopic evidence for the self-assembly micelle under the influenced of flexible nanoparticle (FN)-catalyzed piperidinolysis of phenyl salicylate ions (PS^-) are reported in correlation with some related data and references from previous chapters and studies.

8.2 Experimental

8.2.1 Chemicals

Commercial products of highest available purity such as cetyltrimethylammonium bromide, $C_{16}H_{33}NMe_3Br$, phenyl salicylate, C_6H_5OH, 2-ethyl C_6H_4OH, 3-ethyl C_6H_4OH, 4-ethyl C_6H_4OH, 2-propyl C_6H_4OH, 4- propyl C_6H_4OH, 3-isopropyl C_6H_4OH and 4-isopropyl C_6H_4OH, piperidine (Pip) and all other common chemicals used were of reagent grade. The

stock solutions of PSaH=0.01M were prepared in acetonitrile because of its low aqueous solubility. The stock solutions (w M) of nonionic substituted phenols were prepared by adding (w + 0.05 M) sodium hydroxide so that wM XH solutions become wM NaX.

8.2.2 High Resolution-Transmission Electron Microscopy (TEM)

Morphological structure of the micelles were observed via computer controlled TEM Leo Libra 120 equipped with SIViewer in Department of Medicine, University of Malaya which was operated at accelerating voltage of 120 kV for imaging and analysis purposes. A day old sample was dropped on to a 400 mesh copper-coated carbon grid using a disposable pipette and a clean filter paper was used to remove excess solution. A drop of 3% phosphotungstic acid as a negative staining agent was added on to the grid and the excess liquid was removed. The micrograph was taken immediately after the satisfactory replica was observed at low kV of energy source (Mosho et al., 1996; Tan & Misni, 2013, Eh Suk & Misni, 2017).

8.3 Results and Discussions

8.3.1 Determination of micellar self-assembly structure (X = $C_6H_5O^-$, 2-ethyl $C_6H_4O^-$, 3-ethyl $C_6H_4O^-$, 4-ethyl $C_6H_4O^-$, 2-propyl $C_6H_4O^-$, 4-propyl $C_6H_4O^-$, 3-isopropyl $C_6H_4O^-$ and 4-isopropyl $C_6H_4O^-$)

In this study, the phenolate ions ($C_6H_5O^-$) act as a probe to verify the findings of all experimental data. The reason of the selection was due to the report published on this organic dopant (Agarwal et al., 2006). The spherical (also known as globular) nanoparticle was reported for the growth of self-assembly micelles in the presence of CTABr and phenolate ions through cryo-TEM technique which coincides with the findings of the presence experimental data (Agarwal et al., 2006). The spherical self-assembly micelles for

NaX = C_6H_5ONa were observed at 0.29 M as depicted in Figure 8.1 by TEM. The observation was strongly supported with the evidence of previous literature (Agarwal et al., 2006). This result corresponds with published literature correlating the R_X^{Br} values and micellar structures through the semi empirical kinetic (SEK) technique (Khalid et al., 2016). The kinetic experimental findings showed the R_X^{Br} = 6.3 ± 1.0 for X^- = $C_6H_5O^-$ in [CTAB] = 15 mM, PS^- = 0.2 mM, piperidine = 100 mM, NaOH = 30 mM at 35 °C (Khalid et al., 2016). The value coincides with the study of 2,6-$Cl_2Bz'^-$ which suggests the nanoparticle self-assembly structure for respective R_X^{Br} = 5.0 was spherical micelle (Magid et al., 1997). The interest concentration of phenol as doping were analyzed at 0.29 M since the kinetic data showed the monotonic increase up to [NaX] = 0.29 M of nonlinear plot of k_{obs} with the increase of [NaX] where the graph become plato/ flat region. The amount of PS^- expelled out from the micelles increase up to the plato region due to the effects of counterions phenolates, where the affinity of phenolates ion to the headspace of micelles is greater than phenyl salicylate ions (PS^-) ($k_{obs} \cong k_W = 31.1\times10^{-3}\ s^{-1}$) (Khalid et al., 2016).

The spherical self-assembly micelles were observed at 0.20 M for X = 2-ethyl $C_6H_4O^-$ and 3-ethyl $C_6H_4O^-$, depicted in Figure 8.2 and Figure 8.3 by TEM. However, Figure 8.2 and Figure 8.3 showed an obvious spherical self-assembly micelles along with the present of wormlike micelles dictated by the arrow (the curvature were indistinctive maybe due to high concentration of sample dropped onto the carbon grid during the sample preparation). The addition of respective substituted phenolate salts may lead to the morphological changes to the homogenous wormlike or rodlike micelles (Singh et al., 2004). This results were also coincides with predetermined structure of micellar self-assembly through the kinetic experimental work where R_X^{Br} = 24.0 ± 1.1 (Khalid et al., 2016).

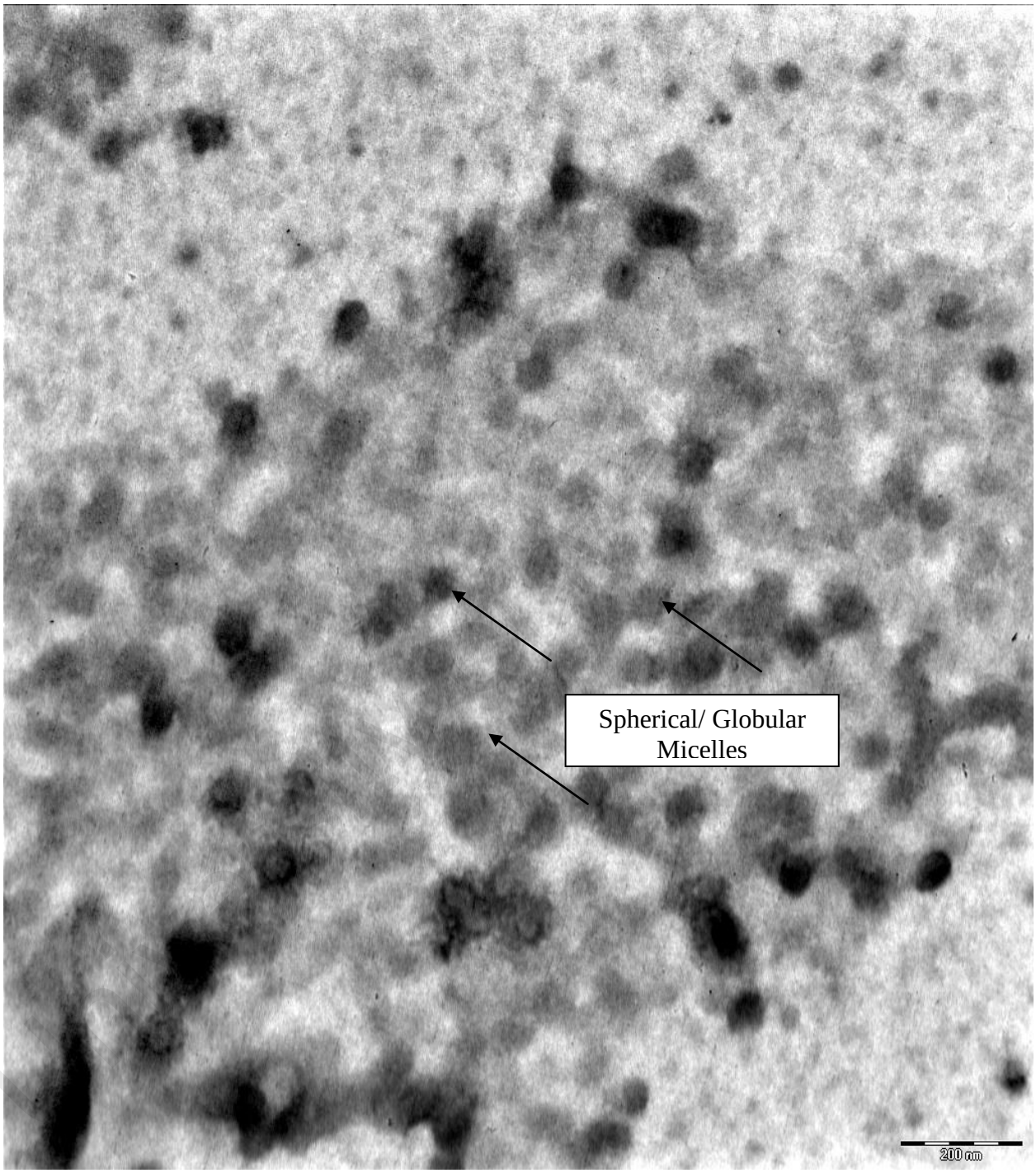

Figure 8.1 Electron Micrograph (TEM) image of spherical micelle at the concentrations of MX = 0.29 M (MX = C_6H_5ONa), [CTAB] = 15 mM, PS^- = 0.2 mM, piperidine = 100 mM, NaOH = 30 mM at 35 °C and the arrow indicates the presence of globular micelles. The scale bar corresponds to 200 nm.

The study on X = 4-$CH_3C_6H_4SO_3^-$ for R_X^{Br} = 20 reported the presence of wormlike micelles in CTABr mixtures (Gamboa et al., 1989). These additional information support the verification of the findings for the presence study where spherical and wormlike micelles are present in the flexible nanoparticle (FN)-catalyzed piperidinolysis of phenyl salicylate ions (PS^-) at [2-ethyl C_6H_4ONa] = 0.20 M. The findings of the 2-ethyl phenolate ions (2-ethyl $C_6H_4O^-$) were also verified by the experimental data of phenolates ion, which coincides with kinetic evidence and literatures (Khalid et al., 2016). The amount of PS^- expelled out from the micelles increased up to the plato region due to the effects of counterions ($k_{obs} \cong k_W = 31.1\times10^{-3}\ s^{-1}$) in Figure 5.5 and Figure 5.7 for 2-propyl C_6H_4ONa and 3-isopropyl C_6H_4ONa respectively. In view to this reasons, the [2-propyl C_6H_4ONa] = 0.2 M and [3-isopropyl C_6H_4ONa] = 0.1 M are investigated in terms of microscopic evidence to determine the micellar self-assembly structure of FN-catalyzed piperidinolysis of PS^-. The microscopic observations showed [2-propyl C_6H_4ONa] = 0.2 M and [3-isopropyl C_6H_4ONa] = 0.1 M representing vesicle micelles in Figure 8.5 and Figure 8.7 respectively. Shear thinning is observed at [4-ethyl C_6H_4ONa] = 0.05 M with η_0 = 7.66 m Pa.s (Figure 6.12). The findings relatively indicate the presence of wormlike/ rodlike micelles. In confirmation of these findings, Figure 8.4 rationalized the microscopic evidence of [4-ethyl C_6H_4ONa] = 0.05 for the existence of homogenous wormlike micelles in FN aqueous solution. The previous assumptions in Chapter 6 that's shear thinning representing the presence of wormlike/ rodlike micelles with supporting indications of η_0 is proven by the findings of [4-propyl C_6H_4ONa] = 0.02 M and [4-isopropyl C_6H_4ONa] = 0.02 M in Figure 8.6 and Figure 8.8. The microscopic evidence of micellar self-assembly structure of [4-propyl C_6H_4ONa] = 0.02 M and [4-isopropyl C_6H_4ONa] = 0.02 M shows lumpy rodlike micelles and wormlike micelles respectively.

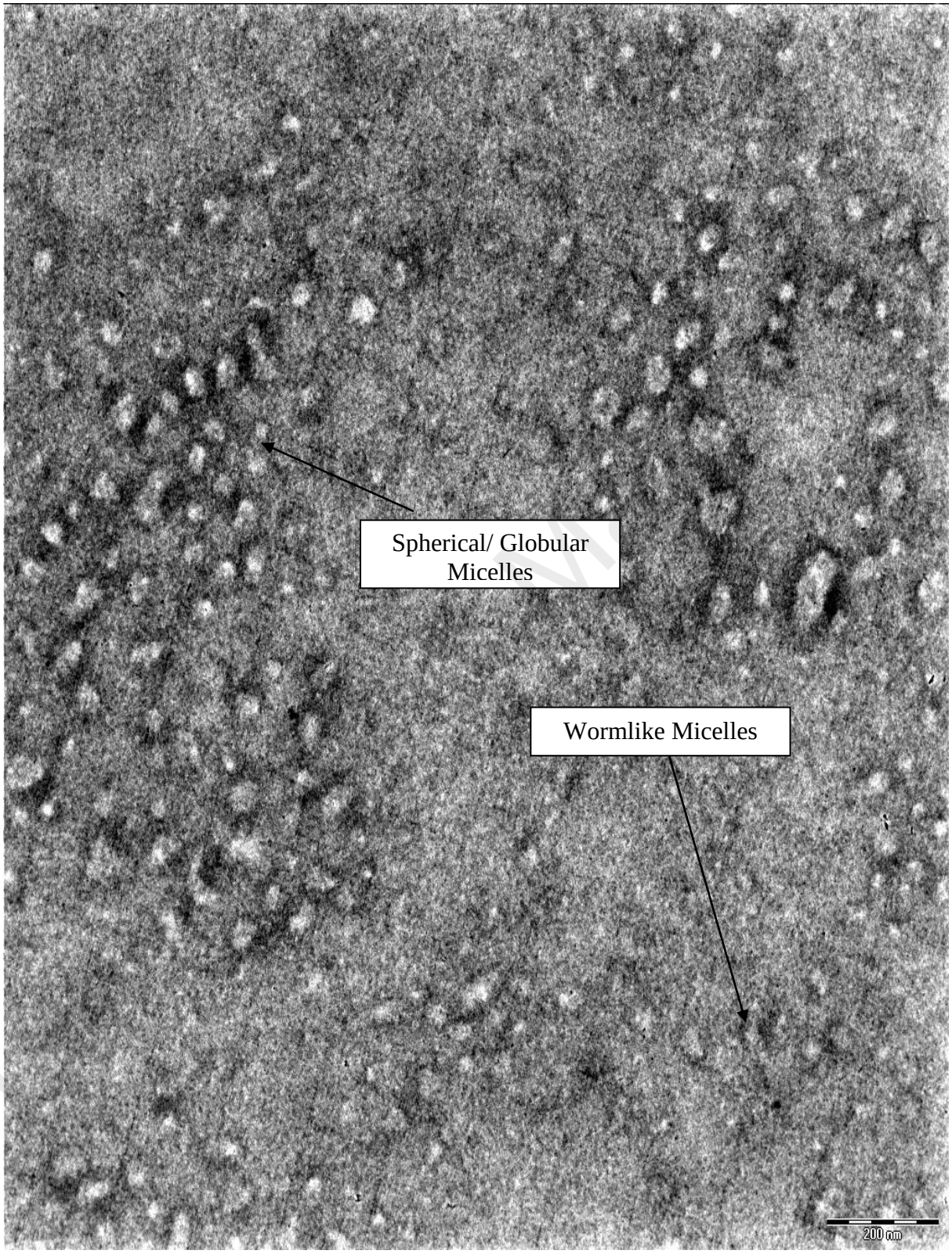

Figure 8.2 Electron Micrograph (TEM) image of micellar aggregates at the concentrations of NaX = 0.20 M (NaX = 2-ethyl C_6H_4ONa), [CTAB] = 15 mM, PS^- = 0.2 mM, piperidine = 100 mM, NaOH = 30 mM at 35 °C and the arrow indicates the presence of globular and indistinctive wormlike micelles. The scale bar corresponds to 200 nm.

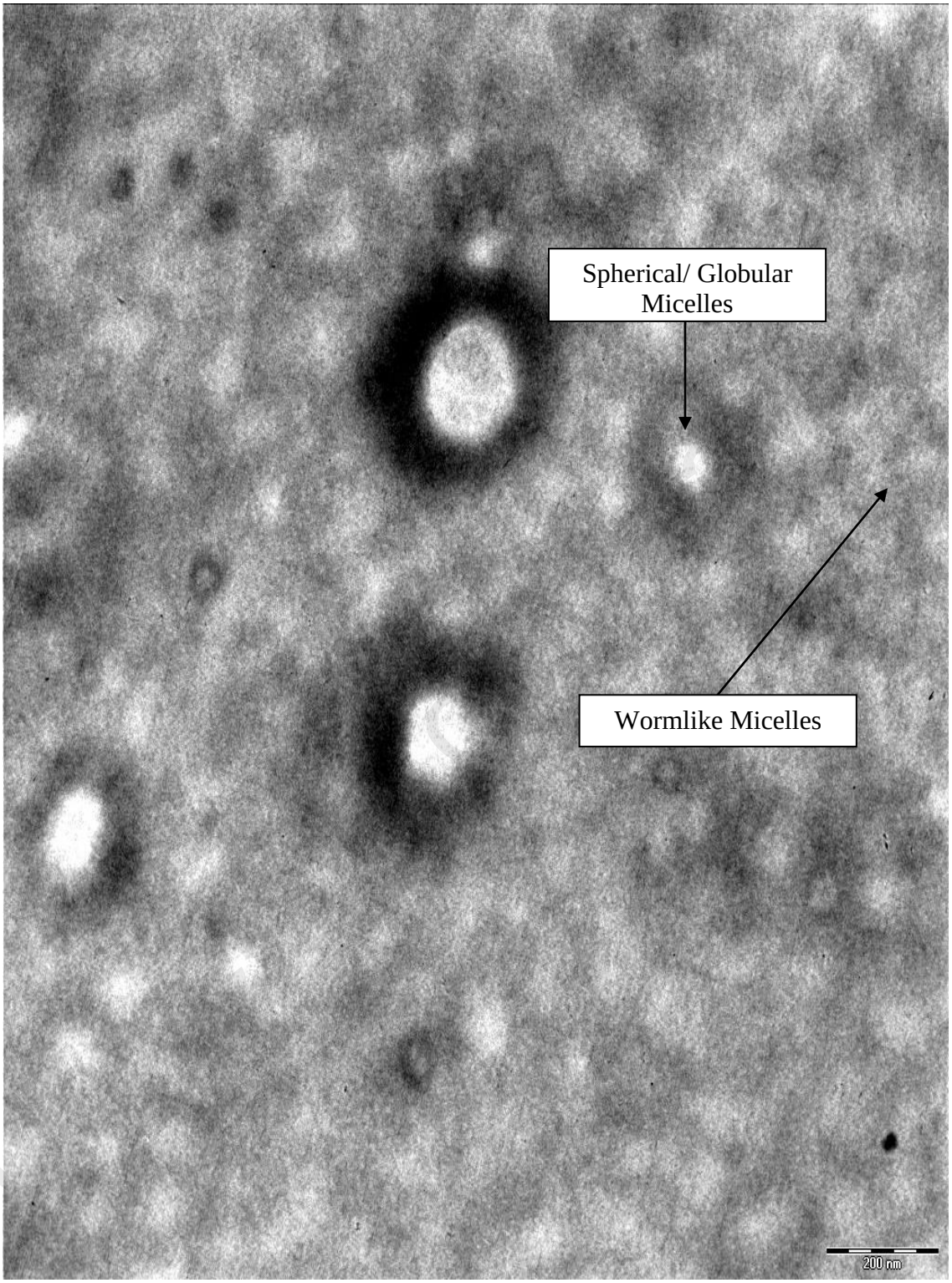

Figure 8.3 Electron Micrograph (TEM) image of micellar aggregates at the concentrations of NaX = 0.20 M (NaX = 3-ethyl C_6H_4ONa), [CTAB] = 15 mM, PS^- = 0.2 mM, piperidine = 100 mM, NaOH = 30 mM at 35 °C and the arrow indicates the presence of globular and indistinctive wormlike micelles. The scale bar corresponds to 200 nm.

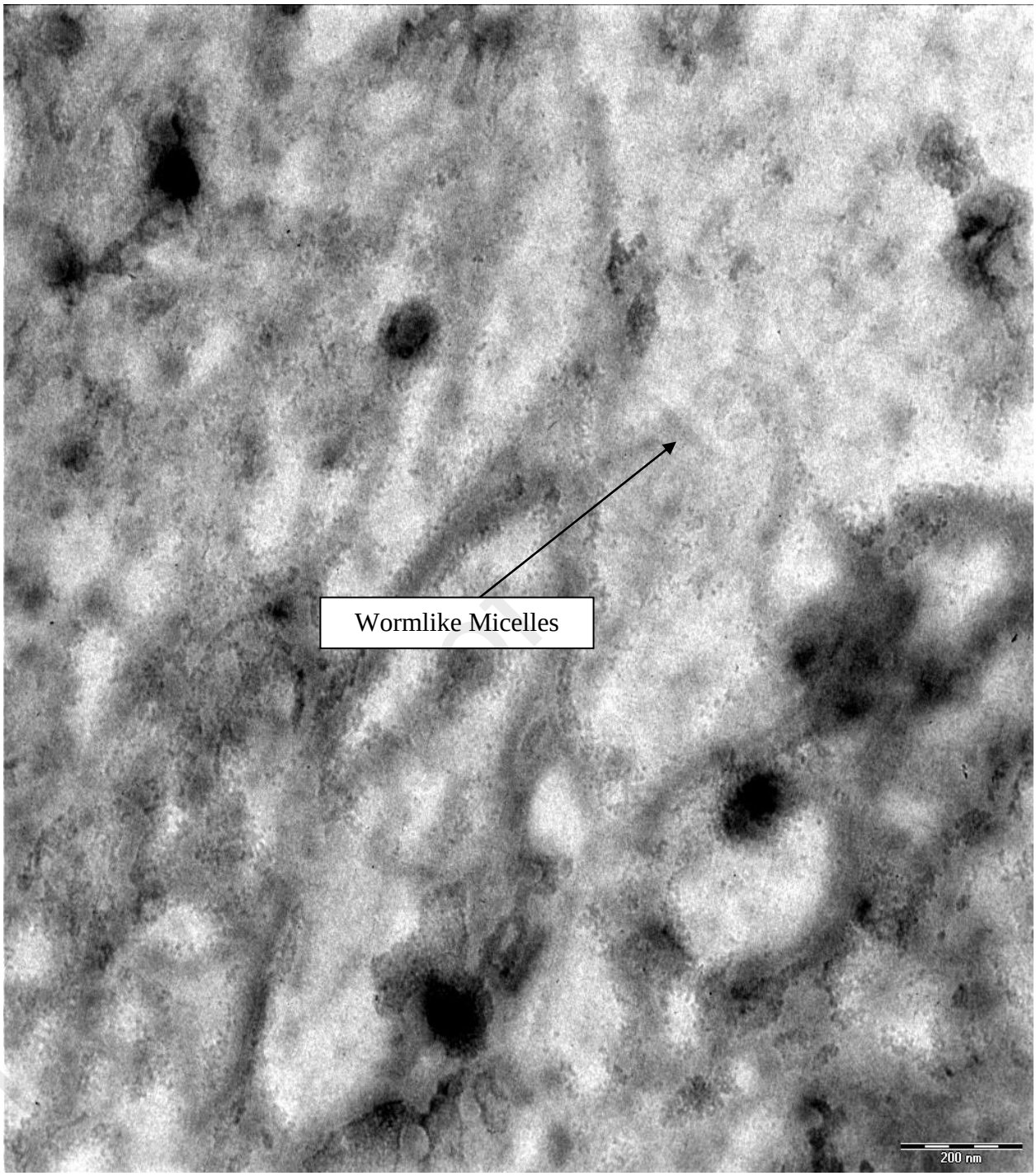

Figure 8.4 Electron Micrograph (TEM) image of micellar aggregates at the concentrations of NaX = 0.05 M (NaX = 4-ethyl C_6H_4ONa), [CTAB] = 15 mM, PS^- = 0.2 mM, piperidine = 100 mM, NaOH = 30 mM at 35 °C and the arrow indicates the presence of wormlike micelles. The scale bar corresponds to 200 nm.

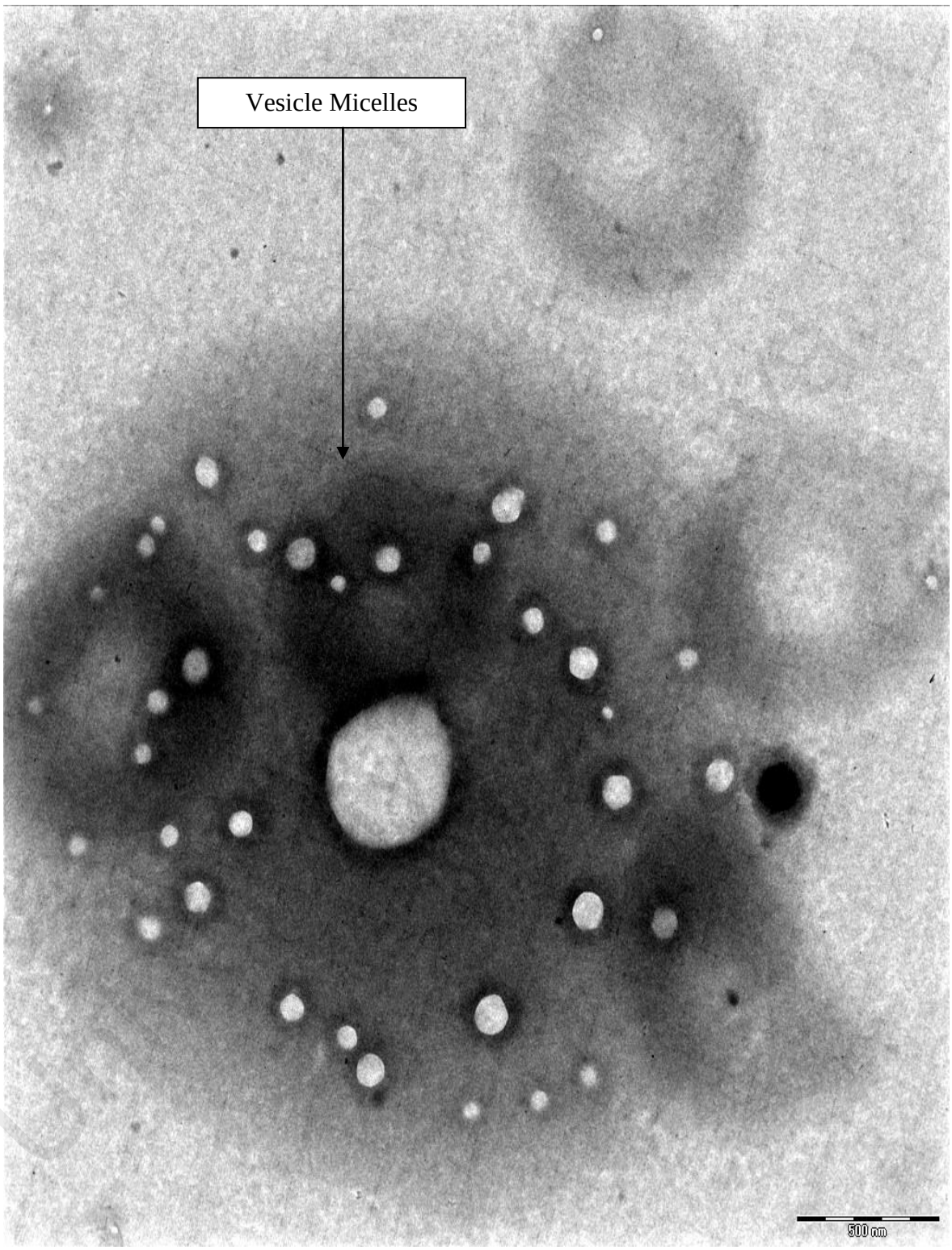

Figure 8.5 Electron Micrograph (TEM) image of micellar aggregates at the concentrations of NaX = 0.20 M (NaX = 2-propyl C_6H_4ONa), [CTAB] = 15 mM, PS^- = 0.2 mM, piperidine = 100 mM, NaOH = 30 mM at 35 °C and the arrow indicates the presence of vesicle micelles. The scale bar corresponds to 500 nm.

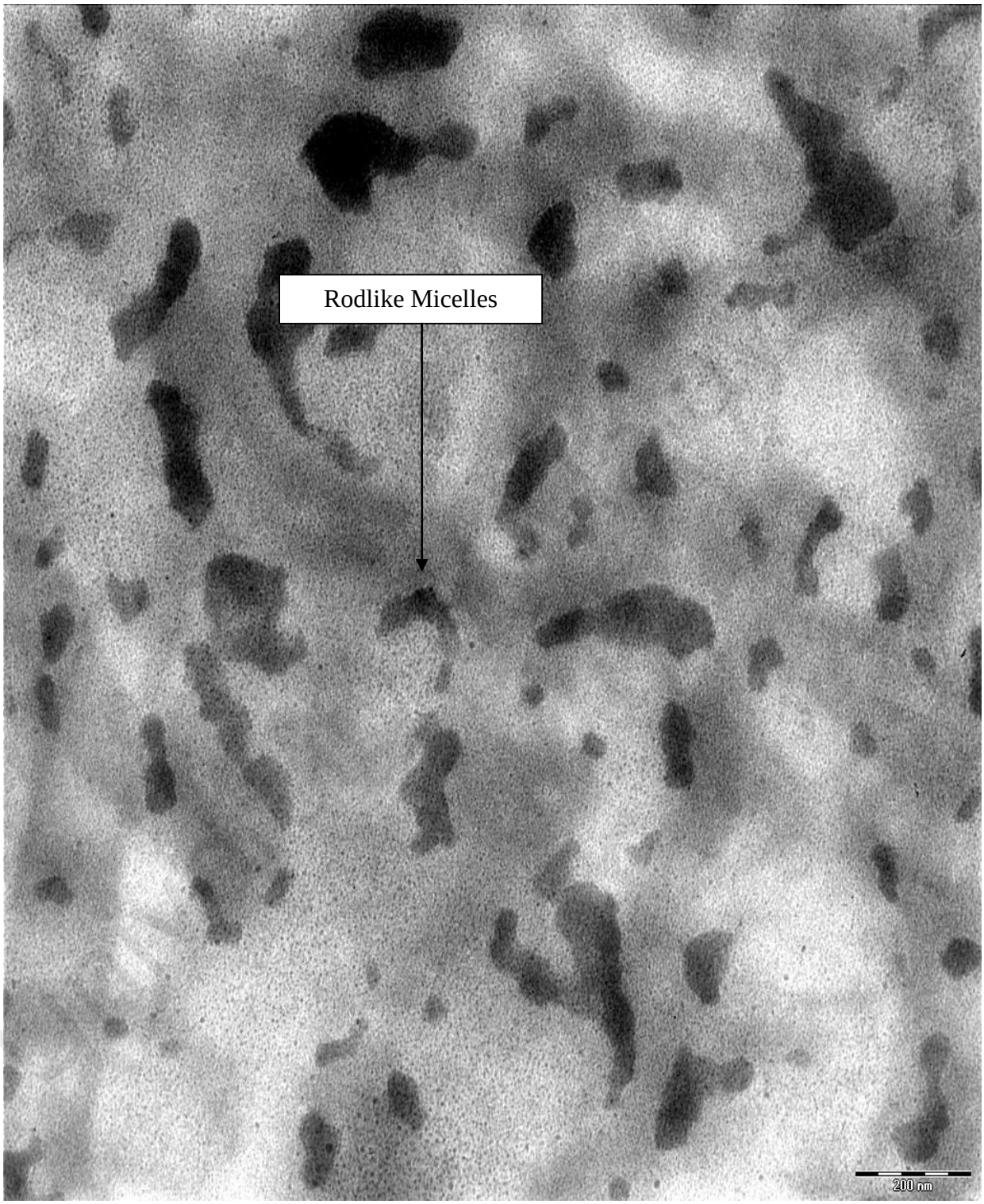

Figure 8.6 Electron Micrograph (TEM) image of micellar aggregates at the concentrations of NaX = 0.02 M (NaX = 4-propyl C_6H_4ONa), [CTAB] = 15 mM, PS^- = 0.2 mM, piperidine = 100 mM, NaOH = 30 mM at 35 °C and the arrow indicates the presence of lumpy rodlike micelles. The scale bar corresponds to 200 nm.

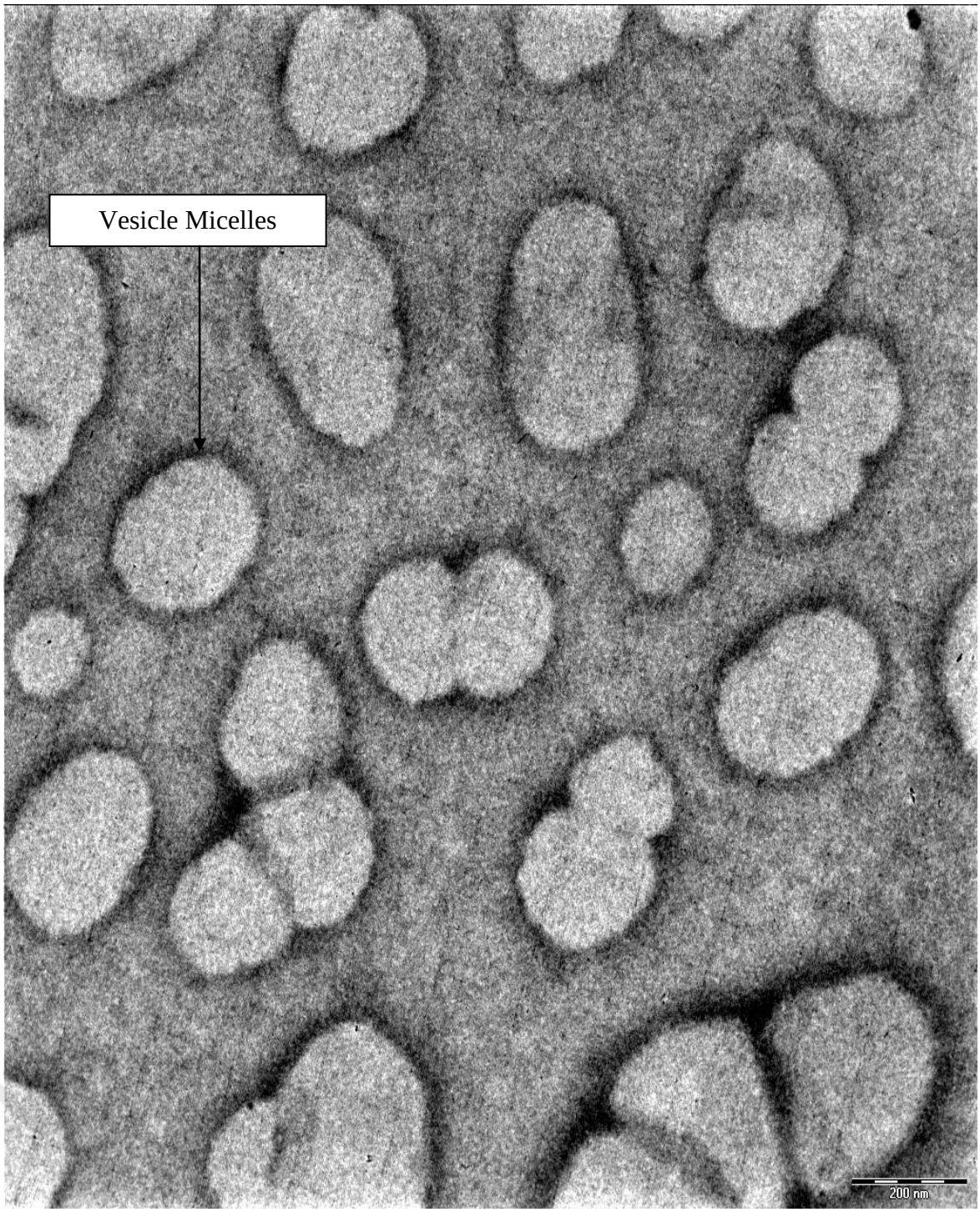

Figure 8.7 Electron Micrograph (TEM) image of micellar aggregates at the concentrations of NaX = 0.10 M (NaX = 3-isopropyl C_6H_4ONa), [CTAB] = 15 mM, PS^- = 0.2 mM, piperidine = 100 mM, NaOH = 30 mM at 35 °C and the arrow indicates the presence of vesicle micelles. The scale bar corresponds to 200 nm.

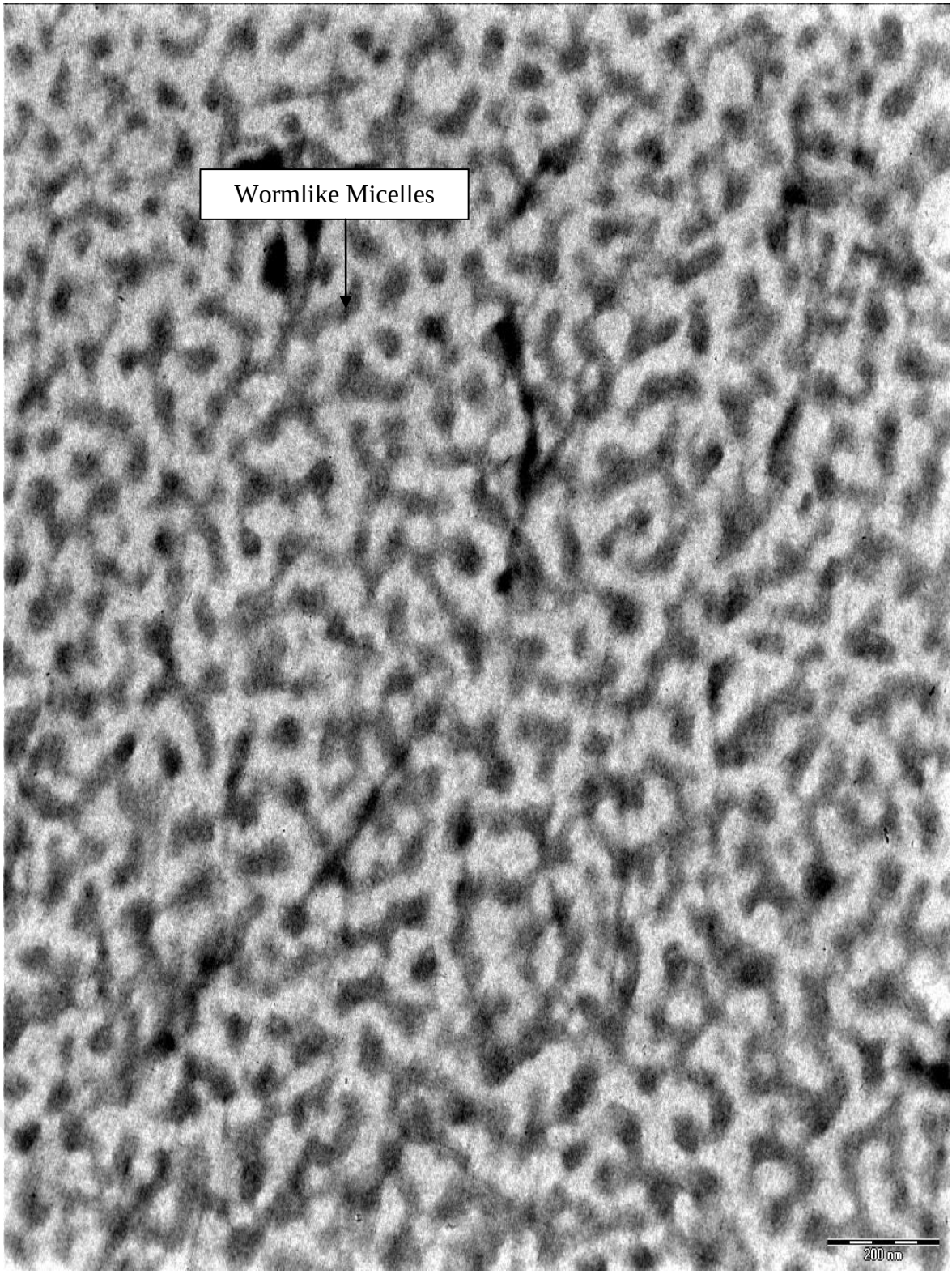

Figure 8.8 Electron Micrograph (TEM) image of micellar aggregates at the concentrations of NaX = 0.02 M (NaX = 4-isopropyl C_6H_4ONa), [CTAB] = 15 mM, PS^- = 0.2 mM, piperidine = 100 mM, NaOH = 30 mM at 35 °C and the arrow indicates the presence of wormlike micelles. The scale bar corresponds to 200 nm.

CHAPTER 9

CONCLUSION AND RECOMMENDATION

9.1 Conclusion

The use of semi empirical methods, SESp and SEK, in the calculation of the values of R_X^{Br} or K_X^{Br}, involves an inherent assumption that the values of R_X^{Br} or K_X^{Br} should be independent of the physicochemical characteristics of probe molecules. This assumption appears to be appropriate in the use of SEK method where many different probe molecules have been used. The first study on use of SESp method involved *N*- (2-methoxyphenyl)phthalamate ion as a probe and the values of R_X^{Br} or K_X^{Br} have been determined for many counterions including 2,6-dichlorobenzoate ion (Khan et al., 2013). The study described in the present chapter uses PSa^- as a probe and the mean value of R_X^{Br} or K_X^{Br} is found to be 4.8 ± 0.3 which is comparable with the reported values obtained by the use of different probe and SEK method as well as different physical methods (Magid et al., 1997). These observations are in favour of the assumption mentioned above.

The validity of Equation (4.8) within the wide range of R_X^{Br} values (2.4-210) provided a nanoparticle catalytic kinetic method to determine the value of R_X^{Br} from the relationship $R_X^{Br} = k_X/k_{Br}$, in which the value of k_X was determined from Equation (4.2) under the experimental conditions used for the determination of k_{Br}. Use of this relationship gave the value of K_{Br}^{Cl} (=2.7), which was comparable to most of the reported values of K_{Br}^{Cl} obtained by using various physicochemical techniques (Romsted, 1984; Khan, 2002; Khan et al., 2010; Khan & Ismail, 2010; Khan et al., 2008; Cuccovia et al., 1997; Bartet et al., 1980; Morgan et al., 1994).

Almost the entire catalytic effect of the nanoparticles was found to be due to 1) the ability of nonreactive counter ions, X^-, to expel reactive counter ions, phenyl salicylate

(PSa^-), from the nanoparticles to the bulk water phase and 2) the much larger value of the second-order rate constant for the nucleophilic reaction of piperidine with PSa^- in the bulk water phase compared with that in the less polar reaction environment of the cetyltrimethylammonium bromide/NaX/H_2O nanoparticles (X=Br, Cl). Notably, Romsted and Cordes (Romsted & Cordes, 1968) emphasized that the anion inhibitions of alkaline hydrolysis of *p*-nitrophenyl hexanoate in the presence of TTACl/MX/H_2O micelles (MX=NaF, NaCl, NaBr, $NaNO_3$, Na_2SO_4; TTACl=tetradecyltrimethylammonium chloride) have many parallels in protein and enzyme chemistry.

More than 4- to 10-fold (Table 5.1) larger values of R_X^{Br} for X = 2-ethyl $C_6H_4O^-$, 3-ethyl $C_6H_4O^-$, 4-ethyl $C_6H_4O^-$, 2-propyl $C_6H_4O^-$, 4-propyl $C_6H_4O^-$, 3-isopropyl $C_6H_4O^-$ and 4-isopropyl C_6H_4O compared with that for X = $C_6H_5O^-$ (as shown in Scheme 9.1) are attributed to the positional attachment of hydrophobic substituent (ethyl , propyl , isopropyl) to phenolic benzene ring. It's also observed that the values of catalytic constants (k_{cat}) are decrease with the increases of $[CTABr]_T$.

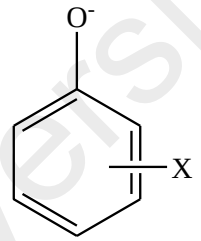

X = H, Phenolate ion
= 2-Et, 2-ethyl phenolate ion
= 3-Et, 3-ethyl phenolate ion
= 4-Et, 4-ethyl phenolate ion
= 2-Prop, 2-propyl phenolate ion
= 4-Prop, 4-propyl phenolate ion
= 3-Isoprop, 3-isopropyl phenolate ion
= 4-Isoprop, 4-isopropyl phenolate ion

Scheme 9.1: Schematic diagram for phenolate and its substituted ions

The shear thinning of rheological measurements indicate the possibility of the presence of nonspherical micelles in the samples (Razak & Khan, 2013, Razak et al., 2014). This might be a usefull probe to determine the nonspherical micelles for samples. The plot of ln (η_0) vs. 1/T is expected to be linear only if the value of E_a^F remains constant under specific temperature range at a constant [MX] and [CTABr] (Razak et al., 2014). However,

the plot of ln (η_0) vs. 1/T for MX = 4-propyl C_6H_4ONa is found to be nonlinear within temperature range 20-55°C which is because the value of E_a^F do not remain constant under such temperature range despite the values of K_X^{Br} or R_X^{Br} for these salt are higher compared to other salts. The change in value of E_a^F from 20 to 55°C is probably because of possible phase transition of CTABr/MX/H_2O nanoparticles to another structure.

The unprecedented findings of GUV in FN at [PSH] = 0.2mM, [NaOH] = 0.03M, [Pip] = 0.1M, [CTABr] = 0.015M, [MX] = 0.10 where X = 2-propyl $C_6H_4O^-$ and 3-isopropyl $C_6H_5O^-$ proved the technique involved is also considered a rapid method. The study also found the possibility of counterions (X= $C_6H_5O^-$, 2-ethyl $C_6H_4O^-$, 3-ethyl $C_6H_4O^-$, 4-ethyl $C_6H_4O^-$, 2-propyl $C_6H_4O^-$, 4-propyl $C_6H_4O^-$, 3-isopropyl $C_6H_4O^-$, 4-isopropyl $C_6H_4O^-$) act as swelling agents for the micellar evolution in the future study.

In correlation of kinetic and rheological data for flexible nanoparticle catalysis in the reaction of piperidine with PS^-, Table 9.1 tabulates the findings described in all chapters for X = $C_6H_5O^-$, 2-ethyl $C_6H_4O^-$, 3-ethyl $C_6H_4O^-$, 4-ethyl $C_6H_4O^-$, 2-propyl $C_6H_4O^-$, 4-propyl $C_6H_4O^-$, 3-isopropyl $C_6H_4O^-$ and 4-isopropyl $C_6H_4O^-$ with references of previous literatures. The assumption that the higher values of counterion binding constants, R_X^{Br} induce the micellar structural transition from spherical to wormlike/rodlike micelles or vesicles (Khan, 2010), seems to be coherent with the experimental data shown in Table 9.1. The higher values of R_X^{Br} representing a strong counterion binding to micellar pseudophase which caused the transition of spherical micelles to rod/ wormlike micelles and vesicles. This justification is supported with the present findings where the values of $R_X^{Br} > 30$ for [MX] = 4-ethyl C_6H_4ONa, 2-propyl C_6H_4ONa, 4-propyl C_6H_4ONa, 3-isopropyl C_6H_4ONa and 4-isopropyl C_6H_4ONa were found to be wormlike/rodlike and vesicles. These

assumptions of micellar aggregates for different [MX] at 35°C are coherent with microscopic evidence, rheological and turbidity measurements.

Table 9.1 $F_{X/S}$ values and R_X^{Br} for different X in the presence of flexible nanoparticles (CTABr micelles)[a]

X	$[MX]_o^{op}$	$10^2 F_{X/S}$	R_X^{Br}	$10^3 k_{cat}$ $[M^{-1}]$	Micelles [b]	η_0 at 25°C [m Pa.s]	η_0 at 35°C [m Pa.s]
4- $^-OBz_1^-$			2.7[i]		SM [l]		
2,6-Cl_2Bz^- [g]	Nonzero	63	4.7 ± 0.6		SM[d]		
2-$CH_3Bz_1^-$	Nonzero	43	4.9 [m]		SM [n]		
3- $^-OBz_1^-$			4.9[i]		SM[j,l]		
2,6-Cl_2Bz^-			5.0[h]		SM [h]		
$C_6H_5CO_2^-$	Zero	70	5.8 [e]		SM [f]		
$C_6H_5O^-$	**Nonzero**	**58**	**6.3 ± 1.0**	**74.7 ± 5.1**	**SM**	**0.95[0.29]**[o]	**0.78[0.29]**
4- $CH_3Bz_1^-$	Nonzero	48	16.7 [m]		WM [n]		
(2,3-Cl_2Bz^-)	Zero	83 ± 8	17 ± 2				
3-$CH_3Bz_1^-$	Nonzero	50	17.7[m]		WM [n]		
2-$HOBz_1^-$			20 [k]		WM [j]		
2-ethyl $C_6H_4O^-$	**Nonzero**	**99**	**24.0 ± 1.1**	**308.4 ± 22.8**	**SM**	**1.43[0.20]**	**1.01[0.20]**
3-ethyl $C_6H_4O^-$	**Nonzero**	**96**	**24.4 ± 0.8**	**311.0 ± 22.3**	**SM**	**1.64[0.20]**	**1.02[0.20]**
2,3-Cl_2Bz^-	Nonzero	70 ± 4[c]	25 ± 2[c]		SWM [d]		
4-ethyl $C_6H_4O^-$	**Nonzero**	**107**	**32.3 ±0.8**	**415.5 ± 31.3**	**WM**	**16.24[0.05]**	**7.66[0.05]**
2- $^-OBz_1^-$			44[i]		WM [j]		
3-isoprop$C_6H_4O^-$	**Nonzero**	**71**	**60.8 ± 0.8**	**471.3 ± 7.2**	**V_S**	**5.43[0.10]**	**1.09[0.10]**
2-propyl $C_6H_4O^-$	**Nonzero**	**67**	**66.3 ± 1.3**	**505.2 ± 94.5**	**V_S**	**1.45[0.20]**	**1.18[0.20]**
4-isoprop$C_6H_4O^-$	**Nonzero**	**48**	**66.6 ± 4.2**	**531.4 ± 68.8**	**WM**	**18.70[0.02]**	**5.80[0.02]**
(3,5-Cl_2Bz^-)	Zero	111 ± 2	111 ± 4				
4-propyl $C_6H_4O^-$	**Nonzero**	**108** ± 1	**145.9 ± 1.3**	**1219 ± 66.8**	**RM**	**190[0.02]**	**25.5[0.02]**
3,5-Cl_2Bz^-	Nonzero	95 ± 3	206 ± 4				
2,6-Cl_2Bz^-		**99**	**4.3 ± 0.5**		**SM**		

[a]Unless otherwise noted 15 mM flexible nanoparticle is used, Bz^- = $C_6H_3CO_2^-$, Bz_1^- = $C_6H_4CO_2^-$, SM = spherical aggregates, WM = wormlike aggregates (long linear, entangled and branched), RM = rodlike micelles, V_S = vesicle aggregates and SWM = short wormlike aggregates. [b]Structure CTABr-MX aggregates where [MX] is generally < 100 mM.[c] Error limits are standard deviations. [d] The micellar structure derived from rheological measurements. [e]Ref. (Khan, 2010) [f]Ref. (Yusof et al., 2013), [g]Ref. (Ali & Makhloufi, 1991), [h]Ref. (Magid et al., 1997), [i]Ref. (Khan et al., 2010), [j]Ref (Rao et al., 1987),[k]Ref. (Bachofer & Simonis, 1996), [l]Ref. (Lin et al., 1994),[m]Ref. (Khan, 2010), [n]Ref.(Rehage & Hoffmann, 1991), [o]Values in brackets represent the concentration for the maximum zero shear viscosity, η_0

9.2 Recommendation

The current studies emphasized the correlation of the kinetic data and rheological behavior for micellar aggregates. This research can also predict the phase transitions of micellar microstructures. However, an extensive research is required to determine the exact transitional point of the micellar structure. The studies may requires various concentrations of FN in the presence of [MX] followed by the microscopic analysis such as TEM.

The present studies used the fresh FN sample for the understanding of the reactions and analytical investigations. It is also recommended that the effects of time on micellar growth will be studied in the future research.

Since the micelle/ surfactant is widely used in the industries, the recent work also contributes to the references in polymer study, micellar-enhanced ultrafiltration system (MEUF), drug delivery research and lipid-protein studies.

REFERENCES

Abdel-Raouf, M. E., Maysour, N. E., Abdul-Raheim, A. M., El-Saeed, S. M., & Farag, R. K. (2011). Synthesis and study of the surface properties of alkylnaphthalene and alkylphenanthrene sulfonates. *Journal of Surfactants and Detergents, 14*(1), 23-30.

Agarwal, V., Singh, M., McPherson, G., John, V., & Bose, A. (2006). Microstructure evolution in aqueous solutions of cetyl trimethylammonium bromide (CTAB) and phenol derivatives. *Colloids and Surfaces A: Physicochemical and Engineering Aspects, 281*(1-3), 246-253.

Akhter, M. S., & Alawi, S. M. (2002). Micellar behaviour of cetyltrimethylammonium bromide in *N*-methyl acetamide—alkanol and *N, N*-dimethyl acetamide—alkanol mixtures. *Colloids and Surfaces A: Physicochemical and Engineering Aspects, 196*(2), 163-174.

Akram, M., Saeed, A. A. M., & Kabir Ud, D. (2015). Micellar, salt, and organic solvent effects on the rate of [Cu(II)-Gly-$_L$-Ala]$^+$ complex-ninhydrin reaction. *Journal of Molecular Liquids, 209*, 367-373.

Alam, M. S., Kamely, N., Siddiq, A. M., Madhavan, K., Vijayakumar, N., Nareshkumar, V., & Mandal, A. B. (2015). Effect of dextrose and temperature on the micellization of cationic gemini surfactant (16-6-16). *Journal of Dispersion Science and Technology, 36*(7), 1029-1035.

Alam, M. S., Siddiq, A. M., Kamely, N., Keerthi, M., Maeshwari, R. U., & Mandal, A. B. (2015). Micellization behavior of a cationic gemini surfactant, pentanediyl-1, 5-bis (dimethylcetylammonium bromide): effect of asparagine and temperature. *Journal of Dispersion Science and Technology, 36*(8), 1134-1139.

Alam, M. S., Siddiq, A. M., Mythili, V., Priyadharshini, M., Kamely, N., & Mandal, A. B. (2014). Effect of organic additives and temperature on the micellization of cationic surfactant cetyltrimethylammonium chloride: evaluation of thermodynamics. *Journal of Molecular Liquids, 199*, 511-517.

Allijn, I. E., Schiffelers, R. M., & Storm, G. (2016). Comparison of pharmaceutical nanoformulations for curcumin: Enhancement of aqueous solubility and carrier retention. *International Journal of Pharmaceutics, 506*(1-2), 407-413.

Ali, A. A., & Makhloufi, R. (1999). Effect of organic salts on micellar growth and structure studied by rheology. *Colloid and Polymer Science, 277*(2-3), 270-275.

Anderson, M. T., Martin, J. E., Odinek, J. G., & Newcomer, P. P. (1998). Effect of Methanol Concentration on CTAB Micellization and on the Formation of Surfactant-Templated Silica (STS). *Chemistry of Materials, 10*(6), 1490-1500.

Andreozzi, P., Funari, S. S., La Mesa, C., Mariani, P., Ortore, M. G., Sinibaldi, R., & Spinozzi, F. (2010). Multi-to unilamellar transitions in catanionic vesicles. *The Journal of Physical Chemistry B, 114*(24), 8056-8060.

Antheunis, H., van der Meer, J.-C., de Geus, M., Heise, A., & Koning, C. E. (2010). Autocatalytic equation describing the change in molecular weight during hydrolytic degradation of aliphatic polyesters. *Biomacromolecules, 11*(4), 1118-1124.

Aoun, B., Sharma, V. K., Pellegrini, E., Mitra, S., Johnson, M., & Mukhopadhyay, R. (2015). Structure and dynamics of ionic micelles: MD simulation and neutron scattering study. *Journal of Physical Chemistry B, 119*(15), 5079-5086.

Arranja, A., Waton, G., Schosseler, F., & Mendes, E. (2016). Lack of a unique kinetic pathway in the growth and decay of Pluronic micelles. *Soft Matter, 12*(3), 769-778.

Azizi Namaghi, H., & Mousavi, S. M. (2016). Factorial experimental design for treatment of an industrial wastewater using micellar-enhanced ultrafiltration. *Desalination and Water Treatment, 57*(12), 5416-5424.

Bachofer, S. J., & Simonis, U. (1996). Determination of the ion exchange constants of four aromatic organic anions competing for a cationic micellar interface. *Langmuir, 12*(7), 1744-1754.

Baccile, N., Babonneau, F., Jestin, J., Pehau-Arnaudet, G., & Van Bogaert, I. (2012). Unusual, pH-induced, self-assembly of sophorolipid biosurfactants. *ACS nano, 6*(6), 4763-4776.

Bahrami, K., Khodaei, M. M., & Abbasi, J. (2012). Synthesis of sulfonyl chlorides and sulfonic acids in SDS micelles. *Synthesis, 2012*(2), 316-322.

Bahri, M. A., Hoebeke, M., Grammenos, A., Delanaye, L., Vandewalle, N., & Seret, A. (2006). Investigation of SDS, DTAB and CTAB micelle microviscosities by electron spin resonance. *Colloids and Surfaces A: Physicochemical and Engineering Aspects, 290*(1-3), 206-212.

Bailey, R. E., & Cady, G. H. (1969). Nuclear magnetic resonance studies of heptafluorobutyric acid micelle formation. *Journal of Physical Chemistry, 73*(5), 1612-1614.

Bales, B. L. (2001). A definition of the degree of ionization of a micelle based on its aggregation number. *Journal of Physical Chemistry B, 105*(29), 6798-6804.

Bartet, D., Gamboa, C., & Sepulveda, L. (1980). Association of anions to cationic micelles. *The Journal of Physical Chemistry, 84*(3), 272-275.

Bharadwaj, S., & Sar, S. K. (2014). micellization of some bile salts in binary aqueous solvent mixtures. *Journal of Surfactants and Detergents, 17*(1), 143-150.

Bijma, K., & Engberts, J. B. (1997). Effect of counterions on properties of micelles formed by alkylpyridinium surfactants. 1. Conductometry and 1H-NMR chemical shifts. *Langmuir, 13*(18), 4843-4849.

Bijma, K., Rank, E., & Engberts, J. B. (1998). Effect of counterion structure on micellar growth of alkylpyridinium surfactants in aqueous solution. *Journal of Colloid and Interface Science, 205*(2), 245-256.

Bossev, D. P., Matsumoto, M., & Nakahara, M. (1999). 1H and 19F NMR Study of the Counterion Effect on the Micellar Structures Formed by Tetraethylammonium and Lithium Perfluorooctylsulfonates. 1. Neat Systems. *Journal of Physical Chemistry B, 103*(39), 8251-8258.

Briganti, G., D'Archivio, A. A., Galantini, L., & Giglio, E. (1996). Structural study of the micellar aggregates of sodium and rubidium Glyco- and taurodeoxycholate. *Langmuir, 12*(5), 1180-1187.

Briggs, D. (1928). *Surface conductance.* Paper presented at the Colloid Symposium Monograph at University of Toronto, Canada

Broxton, T. J., Christie, J. R., & Chung, R. P. T. (1988). Micellar catalysis of organic reactions. 23. Effect of micellar orientation of the substrate on the magnitude of micellar catalysis. *Journal of Organic Chemistry, 53*(13), 3081-3084.

Broxton, T. J., Christie, J. R., & Dole, A. J. (1994). Micellar catalysis of organic reactions. Part 35. Kinetic determination of the critical micelle concentration of cationic micelles in the presence of additives. *Journal of Physical Organic Chemistry, 7*(8), 437-441.

Bunton, C. A., & Robinson, L. (1968). Micellar effects upon nucleophilic aromatic and aliphatic substitution. *Journal of the American Chemical Society, 90*(22), 5972-5979.

Bunton, C. A. (1979). Reaction Kinetics in Aqueous Surfactant Solutions. *Catalysis Reviews - Science and Engineering, 20*(1), 1-56.

Bunton, C. A., Romsted, L. S. & Thamavit, C. (1980) The pseudophase model of micellar catalysis. Addition of cyanide ion to N-alkylpyridium ions. *Journal of American Chemical Society 102*(11), 3900-3903.

Bunton, C. A., Gan, L. H., Moffatt, J. R., Romsted, L. S., & Savelll, G. (1981). Reactions in micelles of cetyltrimethylammonium hydroxide. Test of the pseudophase model for kinetics. *Journal of Physical Chemistry, 85*(26), 4118-4125.

Bunton, C. A., & Savelli, G. (1987) Organic Reactivity in Aqueous Micelles and Similar Assemblies. *Vol. 22. Advances in Physical Organic Chemistry* (pp. 213-309).

Bunton, C. A. (1991). Micellar rate effects: what we know and what we think we know *Surfactants in Solution* (pp. 17-40) New York, NY: Springer.

Bunton, C. A. (1997). Reactivity in aqueous association colloids. Descriptive utility of the pseudophase model. *Journal of Molecular Liquids, 72*(1-3), 231-249.

Bunton, C. A. (2006). The dependence of micellar rate effects upon reaction mechanism. *Advances in Colloid and Interface Science, 123*, 333-343.

Butler, H. (2013). *Poucher's perfumes, cosmetics and soaps*. New York, NY: Springer Science & Business Media.

Can, V., Kochovski, Z., Reiter, V., Severin, N., Siebenbürger, M., Kent, B., Justus, J., Jurgen, P. R., Matthias, B., Okay, O. (2016). Nanostructural Evolution and Self-Healing Mechanism of Micellar Hydrogels. *Macromolecules, 49*(6), 2281-2287.

Carpena, P., Aguiar, J., Bernaola-Galván, P., & Carnero Ruiz, C. (2002). Problems associated with the treatment of conductivity-concentration data in surfactant solutions: Simulations and experiments. *Langmuir, 18*(16), 6054-6058.

Chang, W. S., Chen, S. S., Sie, C. H., Nguyen, N. C., Cheng, H. H., & Hsu, H. T. (2015). Recovery of chromium from plastic plating wastewater by cetyltrimethylammonium bromide MEUF and electrodialysis. *Desalination and Water Treatment, 55*(9), 2408-2415.

Chapman, D., & Morrison, A. (1966). Physical studies of phospholipids. IV. High resolution nuclear magnetic resonance spectra of phospholipids and related substances. *Journal of Biological Chemistry, 241*(21), 5044-5052.

Chaudhuri, R. G., & Paria, S. (2010). Synthesis of sulfur nanoparticles in aqueous surfactant solutions. *Journal of Colloid and Interface Science, 343*(2), 439-446.

Chen, L. G., Strassburg, S. H., & Bermudez, H. (2016). Micelle co-assembly in surfactant/ionic liquid mixtures. *Journal of Colloid and Interface Science, 477*, 40-45.

Chen, W.-J., Zhai, L.-M., Li, G.-Z., Li, B.-Q., & Xu, J. (2004). Spontaneous vesicle formation and vesicle–tubular microstructure transition in aqueous solution of a poly-tailed cationic and anionic surfactants mixture. *Journal of Colloid and Interface Science, 278*(2), 447-452.

Clifford, J., & Pethica, B. A. (1964). Properties of micellar solutions. Part 2. - N.m.r. chemical shift of water protons in solutions of sodium alkyl sulphates. *Transactions of the Faraday Society, 60*, 1483-1490.

Clint, J. H. (2012). *Surfactant aggregation*. New York, NY: Springer Science & Business Media.

Codari, F., Lazzari, S., Soos, M., Storti, G., Morbidelli, M., & Moscatelli, D. (2012). Kinetics of the hydrolytic degradation of poly (lactic acid). *Polymer degradation and stability, 97*(11), 2460-2466.

Cognigni, A., Gaertner, P., Zirbs, R., Peterlik, H., Prochazka, K., Schröder, C., & Bica, K. (2016). Surface-active ionic liquids in micellar catalysis: Impact of anion selection on reaction rates in nucleophilic substitutions. *Physical Chemistry Chemical Physics, 18*(19), 13375-13384.

Cuccovia, I. M., da Silva, I. N., Chaimovich, H., & Romsted, L. S. (1997). New method for estimating the degree of ionization and counterion selectivity of cetyltrimethylammonium halide micelles: chemical trapping of free counterions by a water soluble arenediazonium ion. *Langmuir, 13*(4), 647-652.

Cullum, D. (1994). *Introduction to surfactant analysis*. New York, NY: Springer.

Dai, Z., Tu, Y., & Zhu, L. (2016). Multifunctional micellar nanocarriers for tumor-targeted delivery of hydrophobic drugs. *Journal of Biomedical Nanotechnology, 12*(6), 1199-1210.

Davies, T. S., Ketner, A. M., & Raghavan, S. R. (2006). Self-assembly of surfactant vesicles that transform into viscoelastic wormlike micelles upon heating. *Journal of the American Chemical Society, 128*(20), 6669-6675.

Dayan, N., & Touitou, E. (2000). Carriers for skin delivery of trihexyphenidyl HCl: ethosomes vs. liposomes. *Biomaterials, 21*(18), 1879-1885.

De Lisi, R., Inglese, A., Milioto, S., & Pellerito, A. (1997). Demixing of mixed micelles. Thermodynamics of sodium perfluorooctanoate-sodium dodecanoate mixtures in water. *Langmuir, 13*(2), 192-202.

Deda, D. K., & Araki, K. (2015). Nanotechnology, light and chemical action: An effective combination to kill cancer cells. *Journal of the Brazilian Chemical Society, 26*(12), 2448-2470.

Delle, S. A. (2001). Factors affecting sorption of organic compounds in natural sorbent/water systems and sorption coefficients for selected pollutants. A review. *Journal of Physical and Chemical Reference Data, 30*(1), 187-439.

Dey, J., Saha, M., Pal, A. K., & Ismail, K. (2013). Regioselective nitration of aromatic compounds in an aqueous sodium dodecylsulfate and nitric acid medium. *RSC Advances, 3*(40), 18609-18613.

Doehlert, D. C., Moreau, R. A., Welti, R., Roth, M. R., & McMullen, M. S. (2010). Polar lipids from oat kernels. *Cereal Chemistry, 87*(5), 467-474.

Domínguez, A., Fernández, A., Gonzalez, N., Iglesias, E., & Montenegro, L. (1997). Determination of critical micelle concentration of some surfactants by three techniques. *Journal of Chemical Education, 74*(10), 1227-1231.

Duynstee, E. F. J., & Grunwald, E. (1959). Organic reactions occurring in or on micelles. I. Reaction rate studies of the alkaline fading of triphenylmethane dyes and sulfonphthalein indicators in the presence of detergent salts. *Journal of the American Chemical Society, 81*(17), 4540-4542.

Eh Suk, V. R., & Misran, M. (2017). Development and characterization of DOPEPEG2000 coated oleic acid liposomes encapsulating anticancer drugs. *Journal of Surfactants and Detergents, 20*(2) 1-9

Elsayed, M. M., Abdallah, O. Y., Naggar, V. F., & Khalafallah, N. M. (2007). Lipid vesicles for skin delivery of drugs: reviewing three decades of research. *International Journal of Pharmaceutics, 332*(1), 1-16.

El-Sheikh, S., El-Sherbiny, S., Barhoum, A., & Deng, Y. (2013). Effects of cationic surfactant during the precipitation of calcium carbonate nano-particles on their size, morphology, and other characteristics. *Colloids and Surfaces A: Physicochemical and Engineering Aspects, 422*, 44-49.

Evans, D. F. (1988). Self-organization of amphiphiles. *Langmuir, 4*(1), 3-12.

Fan, C., Zhu, Y. A., Zhou, X. G., & Liu, Z. P. (2011). Catalytic hydrogenation of benzene to cyclohexene on Ru(0001) from density functional theory investigations. *Catalysis Today, 160*(1), 234-241.

Farn, R. J. (2008). *Chemistry and technology of surfactants*. New York, NY: John Wiley & Sons, 32-45

Fendler, J., & Fendler, E. (1975). *Catalysis in Micellar and Macromolecular Systems*. London, UK: Academic Press, 43-65

Fendler, J. H. (1982). *Membrane mimetic chemistry: characterizations and applications of micelles, microemulsions, monolayers, bilayers, vesicles, host-guest systems, and polyions*. New York, NY: John Wiley & Sons Inc, 5-83

Feitosa, E., Karlsson, G., & Edwards, K. (2006). Unilamellar vesicles obtained by simply mixing dioctadecyldimethylammonium chloride and bromide with water. *Chemistry and Physics of Lipids, 140*(1), 66-74.

Ferreira, A. R. V., Torres, C. A. V., Freitas, F., Sevrin, C., Grandfils, C., Reis, M. A. M., Coelhoso, I. M. (2016). Development and characterization of bilayer films of FucoPol and chitosan. *Carbohydrate Polymers, 147*, 8-15.

Ferrer-Tasies, L., Moreno-Calvo, E., Cano-Sarabia, M., Aguilella-Arzo, M., Angelova, A., Lesieur, S., Ricart, S., Faraudo, J., Ventosa, N., Veciana, J. (2013). Quatsomes: Vesicles formed by self-assembly of sterols and quaternary ammonium surfactants. *Langmuir, 29*(22), 6519-6528.

Fischer, P., & Rehage, H. (1997). Rheological master curves of viscoelastic surfactant solutions by varying the solvent viscosity and temperature. *Langmuir, 13*(26), 7012-7020.

Fischer, A., Hebrant, M., & Tondre, C. (2002). Glucose encapsulation in catanionic vesicles and kinetic study of the entrapment/release processes in the sodium dodecyl benzene sulfonate/cetyltrimethylammonium tosylate/water system. *Journal of Colloid and Interface Science, 248*(1), 163-168.

Foley, P., Kermanshahi P. A., Beach, E. S., & Zimmerman, J. B. (2012). Derivation and synthesis of renewable surfactants. *Chemical Society Reviews, 41*(4), 1499-1518.

Førland, G., Samseth, J., Høiland, H., & Mortensen, K. (1994). The effect of medium chain length alcohols on the micellar properties of sodium dodecyl sulfate in sodium chloride solutions. *Journal of Colloid and Interface Science, 164*(1), 163-167.

Fuangswasdi, A., Charoensaeng, A., Sabatini, D., Scamehorn, J., Acosta, E., Osathaphan, K., & Khaodhiar, S. (2006). Mixtures of anionic and cationic surfactants with single and twin head groups: adsorption and precipitation studies. *Journal of Surfactants and Detergents, 9*(1), 21-28.

Gamboa, C., Ríos, H., & Sepúlveda, L. (1989). Effect of the nature of counterions on the sphere-to-rod transition in cetyltrimethylammonium micelles. *Journal of Physical Chemistry, 93*(14), 5540-5543.

Geng, Y., Romsted, L. S., & Menger, F. (2006). Specific ion pairing and interfacial hydration as controlling factors in gemini micelle morphology. Chemical trapping studies. *Journal of the American Chemical Society, 128*(2), 492-501.

Germani, R., Savelli, G., Romeo, T., Spreti, N., Cerichelli, G., & Bunton, C. A. (1993). Micellar head group size and reactivity in aromatic nucleophilic substitution. *Langmuir, 9*(1), 55-60.

Gibhardt, H., Haramagatti, C. R., Islamov, A. K., Ivankov, O. I., Kuklin, A. I., & Eckold, G. (2014). Universal Behaviour of the structure and dynamics of micelles formed from cationic surfactants. *Zeitschrift fur Physikalische Chemie, 228*(6-7), 769-791.

Ginley, M., & Henriksson, U. (1992). Self-diffusion study of counterion complexation in aqueous micellar lithium dodecyl sulfate solutions. *Journal of Colloid and Interface Science, 150*(1), 281-284.

Giorgio, G., Colafemmina, G., Mavelli, F., Murgia, S., & Palazzo, G. (2016). The impact of alkanes on the structure of Triton X100 micelles. *RSC Advances, 6*(1), 825-836.

Gnezdilov, O. I., Zuev, Y. F., Zueva, O. S., Potarikina, K. S., & Us'yarov, O. G. (2011). Self-diffusion of ionic surfactants and counterions in premicellar and micellar solutions of sodium, lithium and cesium dodecyl sulfates as studied by NMR-diffusometry. *Applied Magnetic Resonance, 40*(1), 91-103.

Gogoi, P., Hazarika, P., & Konwar, D. (2005). Surfactant/I2/water: An efficient system for deprotection of oximes and imines to carbonyls under neutral conditions in water. *Journal of Organic Chemistry, 70*(5), 1934-1936.

Goswami, M. M., Dey, C., Bandyopadhyay, A., Sarkar, D., & Ahir, M. (2016). Micelles driven magnetite (Fe_3O_4) hollow spheres and a study on AC magnetic properties for hyperthermia application. *Journal of Magnetism and Magnetic Materials, 417*, 376-381.

Handa, S., Slack, E. D., & Lipshutz, B. H. (2015). Nanonickel-Catalyzed Suzuki-Miyaura Cross-Couplings in Water. *Angewandte Chemie - International Edition, 54*(41), 11994-11998.

Haque, R., Tinsley, I. J., & Schmedding, D. (1973). Lipid binding and mode of action of compounds of the dichlorodiphenyltrichloroethane type: a proton magnetic resonance study. *Molecular Pharmacology, 9*(1), 17-22.

Hartley, G. S. (1936). *Aqueous solutions of paraffin-chain salts: a study in micelle formation*. New York, NY: Hermann & Cie, 19-23.

Harvey, C. E., & Weckhuysen, B. M. (2015). Surface-and Tip-Enhanced Raman Spectroscopy as Operando Probes for Monitoring and Understanding Heterogeneous Catalysis. *Catalysis Letters, 145*(1), 40-57.

Hassan, P. A., Fritz, G., & Kaler, E. W. (2003). Small angle neutron scattering study of sodium dodecyl sulfate micellar growth driven by addition of a hydrotropic salt. *Journal of Colloid and Interface Science, 257*(1), 154-162.

He, Z. M., O'Connor, P. J., Romsted, L. S., & Zanette, D. (1989). Specific counterion effects on indicator equilibria in micellar solutions of decyl phosphate and lauryl sulfate surfactants. *The Journal of Physical Chemistry, 93*(10), 4219-4226.

Hedin, N., Sitnikov, R., Furo, I., Henriksson, U., & Regev, O. (1999). Shape changes of C16TABr micelles on benzene solubilization. *The Journal of Physical Chemistry B, 103*(44), 9631-9639.

Helgeson, M. E., Hodgdon, T. K., Kaler, E. W., & Wagner, N. J. (2010). A systematic study of equilibrium structure, thermodynamics, and rheology of aqueous CTAB/$NaNO_3$ wormlike micelles. *Journal of Colloid and Interface Science, 349*(1), 1-12.

Holmberg, K., Jönsson, B., Kronberg, B., & Lindman, B. (2002). Surfactant–Polymer Systems. *Surfactants and Polymers in Aqueous Solution, Second Edition*, 277-303.

Hooshyar, H., & Sadeghi, R. (2015). Influence of Sodium Salts on the Micellization and Interfacial Behavior of Cationic Surfactant Dodecyltrimethylammonium Bromide in Aqueous Solution. *Journal of Chemical & Engineering Data, 60*(4), 983-992.

Iijima, H., Kato, T., & Söderman, O. (2000). Variation in degree of counterion binding to cesium perfluorooctanoate micelles with surfactant concentration studied by 133Cs and 19F NMR. *Langmuir, 16*(2), 318-323.

Iyer, J., & Blankschtein, D. (2012). Are ellipsoids feasible micelle shapes? An answer based on a molecular-thermodynamic model of nonionic surfactant micelles. *Journal of Physical Chemistry B, 116*(22), 6443-6454.

Jan, R., Bhat, M. A., Islam, N., & Khan, B. (2015). Micellar Effect of Ammonium Based Cationic Surfactants on Kinetics of Methylene Blue-Assisted Ru (III) and Cu (II) Catalyzed Cysteine/Cystine Transformation in Acidic Aqueous Media. *Journal of Surfactants and Detergents, 18*(5), 855-862.

Jansson, M., & Stilbs, P. (1985). A comparative study of organic counterion binding to micelles with the Fourier transform NMR self-diffusion technique. *Journal of Physical Chemistry, 89*(22), 4868-4873.

Javadian, S., Ruhi, V., Heydari, A., Asadzadeh Shahir, A., Yousefi, A., & Akbari, J. (2013). Self-assembled CTAB nanostructures in aqueous/ionic liquid systems: Effects of hydrogen bonding. *Industrial and Engineering Chemistry Research, 52*(12), 4517-4526

Jia, K., Hu, J., Dong, J., & Li, X. (2016). Light-responsive multillamellar vesicles in coumaric acid/alkyldimethylamine oxide binary systems: Effects of surfactant and hydrotrope structures. *Journal of Colloid and Interface Science, 477*, 156-165.

Jiao, T., Liu, X., Wang, X., Wang, Y., & Niu, J. (2016). Synthesis and aggregation behaviors of disulfonate gemini surfactant with double hexadecyl tails. *Colloids and Surfaces A: Physicochemical and Engineering Aspects, 498*, 30-41.

Jungwirth, P., & Tobias, D. J. (2006). Specific ion effects at the air/water interface. *Chemical Reviews, 106*(4), 1259-1281.

Kaler, E. W., Murthy, A. K., Rodriguez, B. E., & Zasadzinski, J. (1989). Spontaneous vesicle formation in aqueous mixtures of single-tailed surfactants. *Science, 245*(4924), 1371-1374.

Karande, P., Jain, A., Arora, A., Ho, M. J., & Mitragotri, S. (2007). Synergistic effects of chemical enhancers on skin permeability: a case study of sodium lauroylsarcosinate and sorbitan monolaurate. *European Journal of Pharmaceutical Sciences, 31*(1), 1-7.

Karande, P., Jain, A., & Mitragotri, S. (2004). Discovery of transdermal penetration enhancers by high-throughput screening. *Nature Biotechnology, 22*(2), 192-197.

Kellermann, M., Bauer, W., Hirsch, A., Schade, B., Ludwig, K., & Böttcher, C. (2004). The first account of a structurally persistent micelle. *Angewandte Chemie - International Edition, 43*(22), 2959-2962.

Khalid, K., Noh, M. A. M., Zain, S. M., & Niyaz Khan, M. (2016). Correlation of Kinetic and Rheological Data for Flexible Nanoparticle Catalysis in the Reaction of Piperidine with PS. *Catalysis Letters, 146*(5), 960-967.

Khan, M. N., & Gambo, S. (1985). Intramolecular catalysis and the rate-determining step in the alkaline hydrolysis of ethyl salicylate. *International Journal of Chemical Kinetics, 17*(4), 419-428.

Khan, M. N., & Arifin, Z. (1996). Kinetics and mechanism of intramolecular general base-catalyzed methanolysis of ionized phenyl salicylate in the presence of cationic micelles. *Langmuir, 12*(2), 261-268.

Khan, M. N. (1997). Effects of hydroxide ion, salts and temperature on the hydrolytic cleavage of ionized N-hydroxyphthalimide (NHPH) in the presence of cationic micelles. *Colloids and Surfaces A: Physicochemical and Engineering Aspects, 127*(1-3), 211-219.

Khan, M. N., Arifin, Z., Lasidek, M. N., Hanifiah, M. A. M., & Alex, G. (1997). Effects of cationic micelles on rate of intramolecular general base-catalyzed aminolysis of ionized phenyl salicylate. *Langmuir, 13*(15), 3959-3964.

Khan, M. N., Arifin, Z., Ismail, E., & Ali, S. F. (2000). Effects of [NaBr] on the rates of intramolecular general base-catalyzed reactions of ionized phenyl salicylate (PS-) with n-butylamine and piperidine in the presence of cationic micelles. *The Journal of Organic Chemistry, 65*(5), 1331-1334.

Khan, M. N., & Hubbard, A. (2002). Encyclopedia of surface and colloid science. *Hubbard, AT (Ed.)*, 3178-3179.

Khan, M. N. (2006). *Micellar catalysis*. Boca Raton, US:CRC Press-Taylor&Francis, 19-99

Khan, M. N., Cheong, M. Y., & Ariffin, A. (2008). *Kinetic and mechanism of large rate enhancement in an acidic aqueous cleavage of the tertiary amide bond of N-(2-methoxyphenyl)-N-morpholinophthalamide*. Paper presented at the NANO-SciTech, Shah Alam, Selangor, Malaysia.

Khan, M. N., & Ismail, E. (2009). Kinetic evidence for the occurrence of independent ion-exchange processes in the cationic micellar-mediated reaction of piperidine with anionic phenyl salicylate. *The Journal of Physical Chemistry A, 113*(23), 6484-6488.

Khan, M. N. (2010). A new semi-empirical kinetic method for the determination of ion exchange constants for the counterions of cationic micelles. *Advances in Colloid and Interface Science, 159*(2), 160-179.

Khan, M. N., & Ismail, E. (2010). Kinetic study on the effects of sodium benzoate on piperidinolysis of phenyl salicylate in alkaline pure cationic and mixed cationic-nonionic micelles. *Journal of Dispersion Science and Technology, 31*(3), 314-320.

Khan, M. N., Ismail, E., & Yusof, N. S. M. (2010). A new empirical kinetic method for the determination of ion-exchange constants for the counterions of cationic micelles: The rate of piperidinolysis and hydrolysis of anionic phenyl salicylate as the kinetic probes. *Colloids and Surfaces A: Physicochemical and Engineering Aspects, 361*(1-3), 150-161.

Khan, M. N., & Sinasamy, S. (2011). A new semiempirical kinetic method for the determination of ion exchange constants for counterions of cationic micelles: Study of the rate of pH-independent hydrolysis of phthalimide as the kinetic probe. *International Journal of Chemical Kinetics, 43*(1), 9-20.

Khan, M. N., Yusof, N. S. M., & Razak, N. A. (2013). A semi-empirical spectrophotometric (SESp) method for the indirect determination of the ratio of cationic micellar binding constants of counterions X- and Br-. *Journal of Oleo Science, 62*(9), 695-708.

Kim, H., Baek, K., Lee, J., Iqbal, J., & Yang, J.-W. (2006). Comparison of separation methods of heavy metal from surfactant micellar solutions for the recovery of surfactant. *Desalination, 191*(1), 186-192.

Kim, H.-J., Baek, K., Kim, B.-K., & Yang, J.-W. (2005). Humic substance-enhanced ultrafiltration for removal of cobalt. *Journal of Hazardous Materials, 122*(1), 31-36.

Kondo, Y., Uchiyama, H., Yoshino, N., Nishiyama, K., & Abe, M. (1995). Spontaneous vesicle formation from aqueous solutions of didodecyldimethylammonium bromide and sodium dodecyl sulfate mixtures. *Langmuir, 11*(7), 2380-2384.

Koya, P. A., Wagay, T. A., & Ismail, K. (2015). Conductometric Studies on Micellization of Cationic Surfactants in the Presence of Glycine. *Journal of Solution Chemistry, 44*(1), 100-111.

Kreke, P. J., Magid, L. J., & Gee, J. C. (1996). 1H and 13C NMR studies of mixed counterion, cetyltrimethylammonium bromide/ cetyltrimethylammonium dichlorobenzoate, surfactant solutions: The intercalation of aromatic counterions. *Langmuir, 12*(3), 699-705.

Kumar, S., Khan, Z. A., & Kabir ud, D. (2002). Micellar association in simultaneous presence of organic salts/additives. *Journal of Surfactants and Detergents, 5*(1), 55-59.

Kunz, W., Henle, J., & Ninham, B. W. (2004). 'Zur Lehre von der Wirkung der Salze'(about the science of the effect of salts): Franz Hofmeister's historical papers. *Current Opinion in Colloid & Interface Science, 9*(1), 19-37.

Kunz, W., Nostro, P. L., & Ninham, B. W. (2004). The present state of affairs with Hofmeister effects. *Current Opinion in Colloid & Interface Science, 9*(1), 1-18.

Kunitake, T., Okahata, Y., Ando, R., Shinkai, S., & Hirakawa, S. (1980). Decarboxylation of 6-nitrobenzisoxazole-3-carboxylate catalyzed by ammonium bilayer membranes. A comparison of the catalytic behavior of micelles, bilayer membranes, and other aqueous aggregates. *Journal of the American Chemical Society, 102*(27), 7877-7881.

Kuperkar, K. C., Mata, J. P., & Bahadur, P. (2011). Effect of 1-alkanols/salt on the cationic surfactant micellar aqueous solutions-A dynamic light scattering study. *Colloids and Surfaces A: Physicochemical and Engineering Aspects, 380*(1-3), 60-65.

Kusano, T., Akutsu, K., Iwase, H., Yoshimura, T., & Shibayama, M. (2016). Structural study on aggregation behavior of star-type trimeric surfactant in the presence of sodium salicylate. *Colloids and Surfaces A: Physicochemical and Engineering Aspects, 497*, 109-116.

La Sorella, G., Strukul, G., & Scarso, A. (2015). Recent advances in catalysis in micellar media. *Green Chemistry, 17*(2), 644-683.

Lawson, K. D., & Flautt, T. J. (1965). Measurement of the spin-lattice relaxation times of dimethyloctylamine oxide through the critical micelle concentration. *Journal of Physical Chemistry, 69*(9), 3204-3205.

Lebarron, J., & London, E. (2016). Effect of lipid composition and amino acid sequence upon transmembrane peptide-accelerated lipid transleaflet diffusion (flip-flop). *Biochimica et Biophysica Acta - Biomembranes, 1858*(8), 1812-1820.

Langevin, D. (1992). Micelles and microemulsions. *Annual Review of Physical Chemistry, 43*(1), 341-369.

Li, Z. Q., Gong, Q. T., Luo, L., Zhang, L., Zhao, S., & Yu, J. Y. (2011). Aggregation of sodium 2,4,5-(tri-n-Alkyl)-benzene sulfonates in aqueous solution: Micellization and microenvironment characteristics studied by electron paramagnetic resonance and steady-state fluorescence quenching. *Journal of Dispersion Science and Technology, 32*(2), 167-173.

Lin, I. J., Moudgil, B. M., & Somasundaran, P. (1974). Estimation of the effective number of - CH2 - groups in long-chain surface active agents. *Colloid and Polymer Science Kolloid Zeitschrift & Zeitschrift für Polymere, 252*(5), 407-414.

Lin, Z., Cai, J. J., Scriven, L. E., & Davis, H. T. (1994). Spherical-to-wormlike micelle transition in CTAB solutions. *Journal of Physical Chemistry, 98*(23), 5984-5993.

Lindemuth, P. M., & Bertrand, G. L. (1993). Calorimetric observations of the transition of spherical to rodlike micelles with solubilized organic additives. *Journal of Physical Chemistry, 97*(29), 7769-7773.

Lipfert, J., Columbus, L., Chu, V. B., Lesley, S. A., & Doniach, S. (2007). Size and shape of detergent micelles determined by small-angle X-ray scattering. *Journal of Physical Chemistry B, 111*(43), 12427-12438.

Loppinet, B., & Monteux, C. (2016) Dynamics of surfactants and polymers at liquid interfaces. *Lecture Notes in Physics, 917,* 137-157.

Lu, B., Li, X., Scriven, L., Davis, H., Talmon, Y., & Zakin, J. (1998). Effect of chemical structure on viscoelasticity and extensional viscosity of drag-reducing cationic surfactant solutions. *Langmuir, 14*(1), 8-16.

Lu, J. R., Marrocco, A., Su, T. J., Thomas, R. K., & Penfold, J. (1993). Adsorption of dodecyl sulfate surfactants with monovalent metal counterions at the air-water interface studied by neutron reflection and surface tension. *Journal of Colloid and Interface Science, 158*(2), 303-316.

Lu, K., Zhang, X.-L., Zhao, Y.-L., & Wu, Z.-L. (2010). Removal of color from textile dyeing wastewater by foam separation. *Journal of Hazardous Materials, 182*(1), 928-932.

Magid, L. J., Han, Z., Warr, G. G., Cassidy, M. A., Butler, P. D., & Hamilton, W. A. (1997). Effect of counterion competition on micellar growth horizons for cetyltrimethylammonium micellar surfaces: Electrostatics and specific binding. *Journal of Physical Chemistry B, 101*(40), 7919-7927.

Magid, L. (1998). The surfactant-polyelectrolyte analogy. *The Journal of Physical Chemistry B, 102*(21), 4064-4074.

Magid, L. J., Li, Z., & Butler, P. D. (2000). Flexibility of elongated sodium dodecyl sulfate micelles in aqueous sodium chloride: A small-angle neutron scattering study. *Langmuir, 16*(26), 10028-10036.

Maiti, K., Mitra, D., Guha, S., & Moulik, S. P. (2009). Salt effect on self-aggregation of sodium dodecylsulfate (SDS) and tetradecyltrimethylammonium bromide (TTAB): Physicochemical correlation and assessment in the light of Hofmeister (lyotropic) effect. *Journal of Molecular Liquids, 146*(1), 44-51.

Manabe, K., Iimura, S., Sun, X. M., & Kobayashi, S. (2002). Dehydration reactions in water. Brønsted acid-surfactant-combined catalyst for ester, ether, thioether, and dithioacetal formation in water. *Journal of the American Chemical Society, 124*(40), 11971-11978.

Marques, E. F., Regev, O., Khan, A., da Graca Miguel, M., & Lindman, B. (1998). Vesicle formation and general phase behavior in the catanionic mixture SDS-DDAB-water. The anionic-rich side. *The Journal of Physical Chemistry B, 102*(35), 6746-6758.

Marques, E., Regev, O., Khan, A., & Lindman, B. (2003). Self-organization of double-chained and pseudodouble-chained surfactants: counterion and geometry effects. *Advances in Colloid and Interface Science, 100*, 83-104.

Martín, V. I., del Mar Graciani, M., Rodríguez, A., & Moyá, M. L. (2012). Kinetic studies in micellar solutions of novel bromide mono-and dimeric surfactants with phenyl and cyclohexyl rings in the head group. *Colloids and Surfaces A: Physicochemical and Engineering Aspects, 409*, 52-60.

Mata, J., Varade, D., Ghosh, G., & Bahadur, P. (2004). Effect of tetrabutylammonium bromide on the micelles of sodium dodecyl sulfate. *Colloids and Surfaces A: Physicochemical and Engineering Aspects, 245*(1-3), 69-73.

McBain, J., & Taylor, M. (1910). *Ber. deutsche Chem*. Berlin, German: Ges.

McBain, J. W., & Taylor, M. (1911). Zur Kenntnis der Konstitution von Seifenlosungen Losungen von" Natriumpalmitaten,". *Z. physik. Chem, 76*, 179-185.

McBain, J. (1913). Mobility of highly-charged micelles. *Trans. Faraday Soc, 9*(99), 107-109.

McBain, J. W., & Salmon, C. (1920). Colloidal Electrolytes. Soap solutions and their constitution. 2. *Journal of the American Chemical Society, 42*(3), 426-460.

McBain, J. W. (1944). Solutions of soaps and detergents as colloidal electrolytes. *Colloid Chemistry: Theoretical and Applied, 5*, 102-109.

Meenakshi, G., Ritsuko, N., & Mitsuru, U. (1999). Direct synthesis of diphenyl carbonate by oxidative carbonylation of phenol using Pd-Cu based redox catalyst. *Journal of Molecular Catalysis A: Chemistry 137*(2), 147-154.

Menger, F. M., & Portnoy, C. E. (1967). On the chemistry of reactions proceeding inside molecular aggregates. *Journal of the American Chemical Society, 89*(18), 4698-4703.

Menger, F. M. (1979). The structure of micelles. *Accounts of Chemical Research, 12*(4), 111-117.

Menger, F. M., & Bonicamp, J. M. (1981). Experimental test for micelle porosity. *Journal of the American Chemical Society, 103*(8), 2140-2141.

Miqan, S. N., Tabrizi, F. F., & Abedini, H. (2015). Study of several approaches for predicting electrical conductivity of sodium-dodecyl-sulfate solution in the presence of Na_2CO_3 and KPS. *Journal of Molecular Liquids, 201*, 59-67.

Misbah, M. H., Quintanilla, L., Alonso, M., & Rodríguez-Cabello, J. C. (2015). Evolution of amphiphilic elastin-like co-recombinamer morphologies from micelles to a lyotropic hydrogel. *Polymer (United Kingdom), 81*, 37-44.

Mishra, B., Samant, S., Pradhan, P., Mishra, S. B., & Manohar, C. (1993). A new strongly flow birefringent surfactant system. *Langmuir, 9*(4), 894-898.

Missel, P. J., Mazer, N. A., Carey, M. C., & Benedek, G. B. (1989). Influence of alkali-metal counterion identity on the sphere-to-rod transition in alkyl sulfate micelles. *The Journal of Physical Chemistry, 93*(26), 8354-8366.

Moghassemi, S., & Hadjizadeh, A. (2014). Nano-niosomes as nanoscale drug delivery systems: An illustrated review. *Journal of Controlled Release, 185*(1), 22-36.

Mondal, M. H., Malik, S., Roy, A., Saha, R., & Saha, B. (2015). Modernization of surfactant chemistry in the age of gemini and bio-surfactants: A review. *RSC Advances, 5*(112), 92707-92718.

Morgan, J. D., Napper, D. H., Warr, G. G., & Nicol, S. K. (1994). Measurement of the selective adsorption of ions at air/surfactant solution interfaces. *Langmuir, 10*(3), 797-801.

Moscho, A., Orwar, O., Chiu, D. T., Modi, B. P., & Zare, R. N. (1996). Rapid preparation of giant unilamellar vesicles. *Proceedings of the National Academy of Sciences, 93*(21), 11443-11447.

Muller, N., & Birkhahn, R. H. (1965). 14N-H and13C-H coupling constants in deuterated ammonium ion and toluene. *The Journal of Chemical Physics, 43*(12), 4540-4541.

Muller, N., & Birkhahn, R. H. (1968). Investigation of micelle structure by fluorine magnetic resonance. II. Effects of temperature changes, added electrolyte, and counterion size. *Journal of Physical Chemistry, 72*(2), 583-588.

Mustafina, A. R., Zakharova, L. Y., Elistratova, J. G., Voronin, M. A., Syakaev, V. V., & Konovalov, A. I. (2009). Counterion effect in SDS–calix [4] resorcinarene micelles. *Journal of Colloid and Interface Science, 333*(2), 613-618.

Myers, D. (2005). *Surfactant science and technology*. New York, NY: John Wiley & Sons.

Nairoukh, Z., Avnir, D., & Blum, J. (2013). Acid-catalyzed hydration of alkynes in aqueous microemulsions. *ChemSusChem, 6*(3), 430-432.

Naskar, B., Dey, A., & Moulik, S. P. (2013). Counter-ion effect on micellization of ionic surfactants: A comprehensive understanding with two representatives, sodium dodecyl sulfate (SDS) and dodecyltrimethylammonium bromide (DTAB). *Journal of Surfactants and Detergents, 16*(5), 785-794.

Nguyen, L. A. T., Schwarze, M., & Schomäcker, R. (2015). Adsorption of non-ionic surfactant from aqueous solution onto various ultrafiltration membranes. *Journal of Membrane Science, 493*, 120-133.

Oelschlaeger, C., Suwita, P., & Willenbacher, N. (2010). Effect of counterion binding efficiency on structure and dynamics of wormlike micelles. *Langmuir, 26*(10), 7045-7053.

Olkowska, E., Polkowska, Z., & Namieśnik, J. (2012). Analytical procedures for the determination of surfactants in environmental samples. *Talanta, 88*, 1-13.

Otzen, D. E. (2015). Proteins in a brave new surfactant world. *Current Opinion in Colloid and Interface Science, 20*(3), 161-169.

Pan, A., Sil, P., Dutta, S., Das, P. K., Bhattacharya, S. C., Rakshit, A. K., Moulik, S. P. (2014). Micellization of cetyltrimethylammonium bromide: Effect of small chain bola electrolytes. *Journal of Physical Chemistry B, 118*(11), 3041-3052.

Papaioannou, A. I., Papiris, S., Papadaki, G., Manali, E. D., Roussou, A., Spathis, A., Kostikas, K. (2016). Surfactant proteins in smoking-related lung disease. *Current Topics in Medicinal Chemistry, 16*(14), 1574-1581.

Park, K. H., Berrier, C., Lebaupain, F., Pucci, B., Popot, J. L., Ghazi, A., & Zito, F. (2007). Fluorinated and hemifluorinated surfactants as alternatives to detergents for membrane protein cell-free synthesis. *Biochemical Journal, 403*(1), 183-187.

Patil, V. K., Gawali, I. T., & Usmani, G. A. (2016). Synthesis and Properties of Novel Cationic Triazolium Gemini Surfactants. *Journal of Dispersion Science and Technology, 37*(11), 1630-1637.

Patist, A., Oh, S. G., Leung, R., & Shah, D. O. (2001). Kinetics of micellization: Its significance to technological processes. *Colloids and Surfaces A: Physicochemical and Engineering Aspects, 176*(1), 3-16.

Pottage, M. J., Greaves, T. L., Garvey, C. J., & Tabor, R. F. (2016). The effects of alkylammonium counterions on the aggregation of fluorinated surfactants and surfactant ionic liquids. *Journal of Colloid and Interface Science, 475*, 72-81.

Purkait, M., DasGupta, S., & De, S. (2005). Separation of aromatic alcohols using micellar-enhanced ultrafiltration and recovery of surfactant. *Journal of Membrane Science, 250*(1), 47-59.

Quina, F. H., & Chaimovich, H. (1979). Ion exchange in micellar solutions. 1. Conceptual framework for ion exchange in micellar solutions. *Journal of Physical Chemistry, 83*(14), 1844-1850.

Rafique, R. F., Min, Z., Son, G., & Lee, S. H. (2016). Removal of cadmium ion using micellar-enhanced ultrafiltration (MEUF) and activated carbon fiber (ACF) hybrid processes: adsorption isotherm study for micelle onto ACF. *Desalination and Water Treatment, 57*(17), 7780-7788.

Rajendar Reddy, K., Rajanna, K. C., & Uppalaiah, K. (2013). Environmentally benign contemporary Friedel-Crafts acylation of 1-halo-2-methoxynaphthalenes and its related compounds under conventional and nonconventional conditions. *Tetrahedron Letters, 54*(26), 3431-3436.

Rakitin, A. R., & Pack, G. R. (2005). Necessity of aromatic carboxylate anions to be planar to induce growth of cationic micelles. *Langmuir, 21*(3), 837-840.

Rao, U. R. K., Manohar, C., Valaulikar, B. S., & Iyer, R. M. (1987). Micellar chain model for the origin of the viscoelasticity in dilute surfactant solutions. *Journal of Physical Chemistry, 91*(12), 3286-3291.

Razak, N. A., & Khan, M. N. (2013). Determination of flow activation energy at viscosity maximum for spherical and wormlike micelles of different lengths and flexibility. *Rheologica Acta, 52*(10-12), 927-937.

Razak, N. A., Yusof, N. S. M., & Khan, M. N. (2014). Kinetics and mechanism of nanoparticles (CTABr/MX/H 2 O)-catalyzed piperidinolysis of ionized phenyl salicylate. 1. *Journal of the Taiwan Institute of Chemical Engineers, 45*(5), 2777-2785.

Rehage, H., & Hoffmann, H. (1991). Viscoelastic surfactant solutions:Model systems for theological research. *Molecular Physics, 74*(5), 933-973.

Roca, M., Andrés, J., Moliner, V., Tuñón, I., & Bertrán, J. (2005). On the nature of the transition state in catechol O-methyltransferase. A complementary study based on molecular dynamics and potential energy surface explorations. *Journal of the American Chemical Society, 127*(30), 10648-10655.

Romsted, L., & Cordes, E. (1968). Secondary valence force catalysis. VII. Catalysis of hydrolysis of p-nitrophenyl hexanoate by micelle-forming cationic detergents. *Journal of the American Chemical Society, 90*(16), 4404-4409.

Romsted, L. S. (1977). A general kinetic theory of rate enhancements for reactions between organic substrates and hydrophilic ions in micellar systems *Micellization, solubilization, and microemulsions* Springer. 509-530

Romsted, L. (1984). *Micellar Effects on Reaction Rates and Equilibria*, vol. 2, Plenum Press, New York. 32-45

Romsted, L. S. (2007). Do amphiphile aggregate morphologies and interfacial compositions depend primarily on interfacial hydration and ion-specific interactions? The evidence from chemical trapping. *Langmuir, 23*(2), 414-424.

Roschat, W., Siritanon, T., Kaewpuang, T., Yoosuk, B., & Promarak, V. (2016). Economical and green biodiesel production process using river snail shells-derived heterogeneous catalyst and co-solvent method. *Bioresource Technology, 209*, 343-350.

Rosen, M. J. (2004). Micelle formation by surfactants. *Surfactants and Interfacial Phenomena, Third Edition*, 105-177.

Ruiz, C. C. (1999). Thermodynamics of micellization of tetradecyltrimethylammonium bromide in ethylene glycol–water binary mixtures. *Colloid and Polymer Science, 277*(7), 701-707.

Sabatino, P., Szczygiel, A., Sinnaeve, D., Hakimhashemi, M., Saveyn, H., Martins, J. C., & Van der Meeren, P. (2010). NMR study of the influence of pH on phenol sorption in cationic CTAB micellar solutions. *Colloids and Surfaces A: Physicochemical and Engineering Aspects, 370*(1-3), 42-48.

Sadegh, F., & Naghash, H. J. (2015). Synthesis of monoallyl-end-capped polydimethylsiloxane-based polymerizable surfactant. *Progress in Organic Coatings, 78*, 381-386.

Šarac, B., Mériguet, G., Ancian, B., & Bešter-Rogač, M. (2013). Salicylate isomer-specific effect on the micellization of dodecyltrimethylammonium chloride: Large effects from small changes. *Langmuir, 29*(14), 4460-4469.

Sato, A., Kinoshita, H., Shinokubo, H., & Oshima, K. (2004). Hydrosilylation of alkynes with a cationic rhodium species formed in an anionic micellar system. *Organic Letters, 6*(13), 2217-2220.

Sauerová, P., Verdánová, M., Mravec, F., Pilgrová, T., Venerová, T., Kalbáčová, M. H., & Pekař, M. (2015). Hyaluronic acid as a modulator of the cytotoxic effects of cationic surfactants. *Colloids and Surfaces A: Physicochemical and Engineering Aspects, 483*, 155-161.

Savaroglu, G., & Yurt, A. (2011). Determination of the second critical micelle concentration of benzyldimethyltridecylazanium chloride in aqueous solution by acoustic and conductometric measurements. *The Journal of Chemical Thermodynamics, 43*(10), 1552-1556.

Schindler, T., Kröner, D., & Steinhauser, M. O. (2016). On the dynamics of molecular self-assembly and the structural analysis of bilayer membranes using coarse-grained molecular dynamics simulations. *Biochimica et Biophysica Acta - Biomembranes, 1858*(9), 1955-1963.

Schramm, L. L., Stasiuk, E. N., & Marangoni, D. G. (2003). Surfactants and their applications. *Annual Reports on the Progress of Chemistry - Section C, 99*, 3-48.

Sehgal, P., Wimmer, R., Mogensen, J. E., & Doe, H. (2007). Interactions between the cationic surfactants bearing different polar head groups: Interfacial, conductivity, NMR, and fluorescence studies. *Journal of Dispersion Science and Technology, 28*(8), 1262-1271. doi: 10.1080/01932690701528266

Sen, P. K., Chatterjee, P., & Pal, B. (2015). Evidence of co-operativity in the pre-micellar region in the hydrolytic cleavage of phenyl salicylate in the presence of cationic surfactants of CTAB, TTAB and CPC. *Journal of Molecular Catalysis A: Chemical, 396*, 23-30.

Seo, D.-J., Fujita, H., & Sakoda, A. (2011). Effects of a non-ionic surfactant, Tween 20, on adsorption/desorption of saccharification enzymes onto/from lignocelluloses and saccharification rate. *Adsorption, 17*(5), 813-822.

Shah, A., Shahzad, S., Munir, A., Nadagouda, M. N., Khan, G. S., Shams, D. F., Rana, U. A. (2016). Micelles as soil and water decontamination agents. *Chemical Reviews, 116*(10), 6042-6074.

Sharma, V. K., Mitra, S., Verma, G., Hassan, P. A., Sakai, V. G., & Mukhopadhyay, R. (2010). Internal dynamics in SDS micelles: Neutron scattering study. *Journal of Physical Chemistry B, 114*(51), 17049-17056.

Sharma, S., Yadav, N., Chowdhury, P. K., & Ganguli, A. K. (2015). Controlling the microstructure of reverse micelles and their templating effect on shaping nanostructures. *Journal of Physical Chemistry B, 119*(34), 11295-11306.

Sigoillot, J. C., & Nguyen, M. H. (1992). Complete oxidation of linear alkylbenzene sulfonate by bacterial communities selected from coastal seawater. *Applied and Environmental Microbiology, 58*(4), 1308-1312.

Sim, Y. L., Damit, E. F., Ariffin, A., & Khan, M. N. (2009). Kinetics and mechanism of hydrolysis of *N*-(2′-hydroxyphenyl) phthalamic acid (1) and *N*-(2′-methoxyphenyl) phthalamic Acid (2) in a highly alkaline medium. *International Journal of Chemical Kinetics, 41*(1), 1-11.

Singh, R. (2012). Micellar effects on nucleophilic addition reaction and applicability of enzyme catalysis model. *Journal of Chemistry, 9*(3), 1181-1187.

Singh, M., Ford, C., Agarwal, V., Fritz, G., Bose, A., John, V. T., & McPherson, G. L. (2004). Structural evolution in cationic micelles upon incorporation of a polar organic dopant. *Langmuir, 20*(23), 9931-9937.

Song, S., Song, A., & Hao, J. (2014). Self-assembled structures of amphiphiles regulated via implanting external stimuli. *RSC Advances, 4*(79), 41864-41875.

Stang, P. J. (2012). Abiological self-assembly via coordination: formation of 2D metallacycles and 3D metallacages with well-defined shapes and sizes and their chemistry. *Journal of the American Chemical Society, 134*(29), 11829-11830.

Stefani, S., Sharma, S. K., Haag, R., & Servin, P. (2016). Core-shell nanocarriers based on PEGylated hydrophobic hyperbranched polyesters. *European Polymer Journal, 80*, 158-168.

Stilbs, P., & Lindman, B. (1981). Determination of organic counterion binding to micelles through Fourier transform NMR self-diffusion measurements. *Journal of Physical Chemistry, 85*(18), 2587-2589.

Suárez-Suárez, S., Carriedo, G. A., & PresaSoto, A. (2016). Reversible Morphological Evolution of Responsive Giant Vesicles to Nanospheres by the Self-assembly of Crystalline-b-Coil Polyphosphazene Block Copolymers. *Chemistry - A European Journal*, 22(13), 4483-4491

Syamal, M., De, S., & Bhattacharya, P. (1997). Phenol solubilization by cetyl pyridinium chloride micelles in micellar enhanced ultrafiltration. *Journal of Membrane Science, 137*(1), 99-107.

Tan, H. W. & Misni, M (2013) Polysaccharide-anchored fatty acid liposomes. *International Journal of Pharmaceutics, 441*, 414-423

Tang, X.-F., Yang, Z.-G., & Wang, W.-J. (2010). A simple way of preparing high-concentration and high-purity nano copper colloid for conductive ink in inkjet printing technology. *Colloids and Surfaces A: Physicochemical and Engineering Aspects, 360*(1), 99-104.

Techen, A., Hille, C., Dosche, C., & Kumke, M. U. (2012). Fluorescence study of drug-carrier interactions in CTAB/PBS buffer model systems. *Journal of Colloid and Interface Science, 377*(1), 251-261.

Tian, J. N., Ge, B. Q., Shen, Y. F., He, Y. X., & Chen, Z. X. (2016). Thermodynamics and structural evolution during a reversible vesicle-micelle transition of a vitamin-derived bolaamphiphile induced by sodium cholate. *Journal of Agricultural and Food Chemistry, 64*(9), 1977-1988.

Tondre, C., & Caillet, C. (2001). Properties of the amphiphilic films in mixed cationic/anionic vesicles: a comprehensive view from a literature analysis. *Advances in Colloid and Interface Science, 93*(1), 115-134.

Törnblom, M., & Henriksson, U. (1997). Effect of solubilization of aliphatic hydrocarbons on size and shape of rodlike C16TABr micelles studied by 2H NMR relaxation. *The Journal of Physical Chemistry B, 101*(31), 6028-6035.

Touitou, E., & Godin, B. (2007). Ethosomes for skin delivery. *Journal of Drug Delivery Science and Technology, 17*(5), 303-308.

Tsujii, K. (1998). *Surface activity: principles, phenomena, and applications*. Cambridge, UK: Academic Press, 23-92

Tung, C.-C., Yang, Y.-M., Chang, C.-H., & Maa, J.-R. (2002). Removal of copper ions and dissolved phenol from water using micellar-enhanced ultrafiltration with mixed surfactants. *Waste Management, 22*(7), 695-701.

Tyagi, S., & Tyagi, V. K. (2014). Novel cationic Gemini surfactants and methods for determination of their antimicrobial activity - Review. *Tenside, Surfactants, Detergents, 51*(5), 379-386.

Ulmius, J., Wennerstroem, H., Johansson, L. B., Lindblom, G., & Gravsholt, S. (1979). Viscoelasticity in surfactant solutions. Characteristics of the micellar aggregates and the formation of periodic colloidal structures. *Journal of Physical Chemistry, 83*(17), 2232-2236.

Upadhyay, R. K., Waghmare, P. R., & Roy, S. S. (2016). Application of oil-swollen surfactant gels as a growth medium for metal nanoparticle synthesis, and as an exfoliation medium for preparation of graphene. *Journal of Colloid and Interface Science, 474*, 41-50.

Vance, J. E., & Vance, D. E. (2008). *Biochemistry of lipids, lipoproteins and membranes*. New York, NY: Elsevier.

Velázquez, M. M., Valero, M., Ortega, F., & González, J. B. R. (2007). Structure and size of spontaneously formed aggregates in Aerosol OT/PEG mixtures: Effects of polymer size and composition. *Journal of Colloid and Interface Science, 316*(2), 762-770.

Vera, S., & Rodenas, E. (1986). Influence of N-cetyl-N,N,N-trimethylammonium bromide counterions in the basic hydrolysis of negatively charged aromatic esters. *Journal of Physical Chemistry, 90*(15), 3414-3417.

Vermathen, M., Stiles, P., Bachofer, S. J., & Simonis, U. (2002). Investigations of monofluoro-substituted benzoates at the tetradecyltrimethylammonium micellar interface. *Langmuir, 18*(4), 1030-1042.

Vincent, B. (2014). McBain and the centenary of the micelle. *Advances in Colloid and Interface Science, 203*, 51-54.

Walker, L. M. (2001) Rheology and Structure of Worm-like Micelles, *Current Opinion in Colloid and Interface Science, 6*, 451 - 456.

Wasserman, A. M., Motyakin, M. V., Yasina, L. L., Zakharova, Y. A., Matveenko, V. N., Shulevich, Y. V., & Rogovina, L. Z. (2010). EPR spin probe study of new micellar systems. *Applied Magnetic Resonance, 38*(1), 117-135.

Witek, A., Kołtuniewicz, A., Kurczewski, B., Radziejowska, M., & Hatalski, M. (2006). Simultaneous removal of phenols and Cr 3+ using micellar-enhanced ultrafiltration process. *Desalination, 191*(1), 111-116.

Wong, T. C. (2006). Micelles and Bicelles as Membrane Mimics for Nuclear Magnetic Resonance Studies of Peptides and Proteins *Encyclopedia of Surface and Colloid Science, Second Edition* (pp. 3809-3824).

Wu, S., Yan, Z., Wen, X., Xu, C., & Pan, Q. (2014). Conductometric and fluorescence probe investigations of molecular interactions between dodecyltrimethylammonium bromide and dipeptides. *Colloid and Polymer Science, 292*(11), 2775-2783.

Xia, Y., Goldmints, I., Johnson, P. W., Hatton, T. A., & Bose, A. (2002). Temporal evolution of microstructures in aqueous CTAB/SOS and CTAB/HDBS solutions. *Langmuir, 18*(10), 3822-3828.

Xin, X., Zhang, H., Xu, G., Tan, Y., Zhang, J., & Lv, X. (2013). Influence of CTAB and SDS on the properties of oil-in-water nano-emulsion with paraffin and span 20/Tween 20. *Colloids and Surfaces A: Physicochemical and Engineering Aspects, 418*, 60-67.

Xu, W., Zhang, Q., Wei, H., Qin, J., & Yu, L. (2015). Self-Aggregation of Catanionic Surface Active Ionic Liquids in Aqueous Solutions. *Journal of Surfactants and Detergents, 18*(3), 421-428.

Yang, J. (2002) Viscoelastic wormlike micelles and their applications, *Current Opinion in Colloid and Interface Science 7*, 276 - 281.

Yang, Q., Zhou, Q., & Somasundaran, P. (2008). NMR study of micellar microstructures of cationic single-chain and gemini surfactants and their mixtures with nonionic surfactant n-dodecyl-β-d-maltoside. *Colloids and Surfaces A: Physicochemical and Engineering Aspects, 322*(1-3), 40-46.

Yang, Y., Guo, Y., Sun, R., & Wang, X. (2016). Self-assembly and β-carotene loading capacity of hydroxyethyl cellulose-graft-linoleic acid nanomicelles. *Carbohydrate Polymers, 145*, 56-63.

Yusof, N. S. M., & Khan, M. N. (2010). Determination of an ion exchange constant by the use of a kinetic probe: A new semiempirical kinetic approach involving the effects of 3-F- and 4-F-substituted benzoates on the rate of piperidinolysis of anionic phenyl salicylate in aqueous cationic micelles. *Langmuir, 26*(13), 10627-10635.

Yusof, N. S. M., & Niyaz Khan, M. (2011). Kinetic and rheological measurements of the effects of inert 2-, 3- and 4-bromobenzoate ions on the cationic micellar-mediated rate of piperidinolysis of ionized phenyl salicylate. *Journal of Colloid and Interface Science, 357*(1), 121-128.

Yusof, N. S. M., Razak, N. A., & Niyaz Khan, M. (2013). Quantitative correlation between counterion (X) affinity to cationic micelles and X-induced micellar growth for X = 2,4-; 2,5-; 2,6- and 3,4-dichlorobenzoate ions. *Journal of Oleo Science, 62*(5), 257-269.

Yusof, N. S. M., & Khan, M. N. (2013). Quantitative correlation between counterion-affinity to cationic micelles and counterion-induced micellar growth. *Advances in Colloid and Interface Science, 193*, 12-23.

Zaheer, Z., Aazam, E. S., & Kosa, S. A. (2016). Effects of cationic and anionic micelles on the morphology of biogenic silver nanoparticles, and their catalytic activity for congo red. *Journal of Molecular Liquids, 220*, 364-369.

Zana, R., Lévy, H., Danino, D., Talmon, Y., & Kwetkat, K. (1997). Mixed micellization of cetyltrimethylammonium bromide and an anionic dimeric (gemini) surfactant in aqueous solution. *Langmuir, 13*(3), 402-408.

Zeng, G.-M., Xu, K., Huang, J.-H., Li, X., Fang, Y.-Y., & Qu, Y.-H. (2008). Micellar enhanced ultrafiltration of phenol in synthetic wastewater using polysulfone spiral membrane. *Journal of Membrane Science, 310*(1), 149-160.

Zeng, J., & Liu, P. (2016). Facile synthesis of amphiphilic poly(ethylene glycol) conjugate and its micellization as injectable targeted vehicle for DOX. *Reactive and Functional Polymers, 103*, 54-62.

Zhang, Y., Li, Y., Song, Y., & Li, J. (2016). Synthesis and aggregation behaviors of tail-branched surfactant Guerbet-cetyl trimethyl ammonium chloride. *Colloid and Polymer Science, 294*(2), 271-279.

Zhao, Y., Cheung, P., & Shen, A. Q. (2014). Microfluidic flows of wormlike micellar solutions. *Advances in Colloid and Interface Science, 211*, 34-46.

APPENDICES

LIST OF PUBLICATIONS AND PAPER PRESENTED

JOURNALS

1. **KHALISANNI KHALID***, MUHAMMAD AZRI MOHD NOH, SHARIFUDDIN MD. ZAIN, M. NIYAZ KHAN* (2017) Determination of Relative Counterion Binding Constant to Cationic Micelles. *Topics in Current Chemistry* **375(45)**, 1-18
2. **KHALISANNI KHALID***, MUHAMMAD AZRI MOHD NOH, IBRAHIM ISAH FAGGE, SHARIFUDDIN MD. ZAIN, M. NIYAZ KHAN* (2016) Effects of Cationic Nanoparticles (CNP) on Counterion Binding Constant (R_X^{Br}) and Catalytic Constant (k_{cat}) in Micellar System. *Journal of Molecular Catalysis A: Chemical* **423**, 365-370
3. **KHALISANNI KHALID***, MUHAMMAD AZRI MOHD. NOH, SHARIFUDDIN MD. ZAIN, MOHAMMAD NIYAZ KHAN* (2016) Correlation of Kinetic and Rheological Data for Flexible Nanoparticle Catalysis in the Reaction of Piperidine with PS^-. *Catalysis Letters* **146(5)**, 960-967
4. **KHALISANNI KHALID***, M. NIYAZ KHAN, M. Z. SHARIFUDDIN, R. P. T. KIM, M. N. MUHAMMAD AZRI (2016) Determination of the Ratio of Cationic Flexible Nanoparticles Binding Constant of Counterions X^- and Br^- (K_X/K_{Br}) using the Semi-Empirical Spectrophotometric (SESp) Technique. *AIP Conference Proceedings* **1733**, 020017
5. M. AZRI MOHD NOH, **KHALISANNI KHALID**, AZHAR ARIFFIN, M. NIYAZ KHAN* (2016) Kinetics and mechanism of cationic flexible nanoparticles (CFN) – catalyzed piperidinolysis of anionic phenyl salicylate: CFN = TTABr/MX/H2O

with MX = NaCl, NaBr; $C_nH_{2n+1}CO_2Na$, n = 4, 5, 6 and 7. *Journal of Oleo Science* **165(9),** 749-758

6. IBRAHIM ISAH FAGGE, **KHALISANNI KHALID**, MUHAMMAD AZRI MOHD NOH, NOR SAADAH MOHD YUSOFF, SHARIFUDDIN MD. ZAIN, M. NIYAZ KHAN* (2016) Influence of Mixed CTABr-$C_{16}E_{20}$ Nanoparticles on Relative Counterion Binding Constants in Solutions of Inert Salts (2-$HOC_6H_4CO_2Na$ and NaBr): Kinetic and Rheometric Study. *RSC Advances* **6**, 95504-95511

ORAL PRESENTATION

1. Determination of relative Counterion binding constant (R_X^{Br}) in Cationic Flexible Nanoparticles (FN) using Semi-Emperical Kinetic (SEK)/ Semi-Emperical Spectrophotometric (SESp) Techniques. *4th International Congress on Nano Science and Nanotechnology 2016 (ICNT 2016)*, Kuala Lumpur, Malaysia

2. Catalytic effect of cationic flexible nanoparticles (CFN)-TTABr/MX/H_20 towards the piperidinolysis of ionized phenyl salicylate. *4th International Congress on Nano Science and Nanotechnology 2016 (ICNT 2016)*, Kuala Lumpur, Malaysia

3. Determination of The Ratio of cationic Flexible nanoparticles Binding Constants if Counterion X^- and Br^- (K_X/K_{Br}) using The Semi-Emperical Spectrophotometric (SESp) Technique. *International Conference on Nano-Electronic Technology Devices and Materials 2015* (*IC-NET 2015*), Shah Alam, Selangor, Malaysia